Department of Electrical and Computer Engineering

Villanova University

TECHNICAL REPORT

(10/1/98 - 9/30/99)

BLIND TIME-FREQUENCY ANALYSIS FOR SOURCE DISCRIMINATION IN MULTISENSOR ARRAY PROCESSING

Submitted to

Office of Naval Research

Grant No. N00014-98-1-0176

Principle Investigator

Moeness G. Amin

October 1999

Table of Contents

1. Executive Summary

Bilinear Time-Frequency Analysis for Source Discrimination in Multisensor Array Processing

Moeness Amin (PI)

This report presents the results of the research work performed under the ONR funding, grant number N00014-98-1-0176 over the period of October 1st, 1998 to September 30th, 1999. The research project is titled "Bilinear Time-Frequency Analysis for Source Discrimination in Multisensor Array Processing." The research team members working on this grant at Villanova University consisted of: Professor Moeness Amin (Principle Investigator), Dr. Yimin Zhang (Postdoctoral Fellow), Mr. Weifeng Mu (Graduate Student), Mr. Govind Mandapati (Graduate Student), and Mr. Ce Zhang (Graduate Student). We have also collaborated with Prof. Miguel Lagunas (Spain), Dr. Salim Kayhan (Turkey), and Dr. Alex Gershman (Canada). We are pleased to report that the ONR research funding this year has produced five journal papers under review, three journal papers accepted, and ten conference papers, of a total of eighteen paper submissions. Copies of all papers are included in the appendix.

The research efforts over 1998/1999 phase focused on nonstationary signals and the applications of time-frequency signal representations to multi-antenna receivers. We have clearly demonstrated, through analysis and simulations, the offerings of time-frequency distributions in solving key problems in sensor array processing, including direction finding, source discrimination, and blind signal recovery. Significant progress has been made in understanding how the time-frequency signatures of the signals impinging on an array of sensors can be utilized to improve array performance.

The major contributions over the fiscal year ending September 30th 1999 are: 1) Regress analysis of eignestructure methods employing time-frequency distributions which has demonstrated their superiority over those used in conventional high resolution methods based on data covariance matrices, 2) Evaluating the performance of the spatial time-frequency distributions in low SNR and coherent signal environments, and introducing maximum likelihood techniques based on the sources' time-frequency signatures, 3) Identifying the role of time-frequency cross-terms in spatial signal processing, and presenting a prudent way to use those terms for enhanced performance, 4) Providing a novel approach for incorporating the revolutionary power spectra into source discrimination and angle of arrival estimation, and examining their advantages over quadratic time-frequency distributions. We have also made significant advances in the solutions of the problem of suppressing nonstationary jammers in broadband signal environment, using both projection techniques and frequency diversity methods. In the following, we summarize the above key contributions, leaving the details to the appendix, which also includes other contributions we have made from the research funding of this project.

1.1 Spatial Averaging of Time-Frequency Distribution for Source Separation

Symmetric spatial averaging of spatial time-frequency distributions has been introduced. The spatial averaging of the spatial time-frequency distributions of the data across an antenna array removes the undesired effect of crossterms between the impinging signals. These terms reside along the off-diagonal entries of the source time-frequency distribution matrix, and consequently impede the source separation performance, which is based on pre-assumed diagonal matrix structure. Spatial averaging amounts to forming a spatial Hermitian Toeplitze matrix using the auto- and cross-time-frequency distributions of the data over one half of the array. This matrix is then added to the spatial matrix corresponding to the other half of the array. The desired effect of this averaging is reallocating the interaction between the source signals in the time-frequency domain from the off diagonal to the diagonal elements of the source TFD matrix. In this respect, cross-terms, due to their potential high values, are regarded as useful components that could be employed for improved performance. Without spatial-averaging, array performance is very sensitive to whether only auto-term or cross-term points or their mix are incorporated in the source separation procedure. With spatial averaging, this is no longer a concern, and as such, a major burden is using bilinear time-frequency distributions has been alleviated.

1.2 Subspace Analysis of Spatial Time-Frequency Distribution Matrices

Subspace analysis of spatial time-frequency distribution (STFD) matrices have been developed. It has been shown that for signals with clearly defined time-frequency signatures, such as FM signals, smaller estimation errors in the signal and noise subspaces can be achieved by using spatial time-frequency matrices over the subspace estimates obtained from using the data covariance matrix approach. This improvement in subspace estimation is the result of incorporating the time-frequency points along the instantaneous frequencies of the impinging signals on the array into the subspace estimation procedure. These points belong to autoterm regions of high power concentrations, and as such, when used in constructing STFDs, they provide high SNR matrices with improved eigen-decompositions. The advantages of STFD-based direction finding over traditional direction finding methods using data covariance matrices were demonstrated using the MUSIC algorithm. It was shown that the time-frequency MUSIC outperforms conventional MUSIC in the two situations of low SNR and closely spaced sources. Unlike conventional array processing techniques, which are nondiscriminatory, and must therefore spatially localize all signals incident on the array, the STFD-based array processing provides the flexibility of dealing with all signal arrivals, or a subset of them. In this respect, it does not suffer from the drawback of requiring higher number of sensors than sources. The ability to select fewer sources depends on the distinction of their time-frequency signatures from those of other source signals. The eigenstructure of the STFD matrix constructed from the time-frequency points that belong to the autoterm regions of a number of sources will only yield the signal subspace of these sources. It was shown that the maximum improvement in subspace estimation using STFD over data covariance matrices is achieved when constructing the STFD from only one source signal.

1.3 Time-Frequency Maximum Likelihood Methods for Direction Finding

We have introduced a novel time-frequency maximum likelihood (t-f ML) method for direction-of-arrival (DOA) estimation for non-stationary signals impinging on a multi-sensor array receiver. We have shown the superiority of this method over conventional maximum likelihood DOA estimation techniques. Time-frequency distributions localize the signal power in the time-frequency domain, and as such enhance the effective SNR, leading to improved DOA estimation. The localization of signals with different time-frequency signatures permits the division of the time-frequency domain into smaller regions; each contains smaller number of signals than those incident on the array. The reduction of the number of signals within different time-frequency regions not only reduces the required number of sensors, but also decreases the computational load in multi-dimensional optimizations. Compared to the recently proposed time-frequency MUSIC (t-f MUSIC), the proposed t-f ML method can be applied in coherent environments, without the need to perform any type of preprocessing that is subject to both array geometry and array aperture.

1.4 Spatial evolutionary Spectrum for DOA Estimation and Blind Source Separation

The evolutionary spectrum (ES) was introduced in the sixties by Priestly. This spectrum is based on the modeling of nonstationary signal as a collection of uncorrelated sinusoids with random time-varying amplitudes. The work in this area has lead to the generalization, estimation, and the linkage of ES to TFDs. For processes with restricted time-frequency correlation, referred to as underspread nonstationary random processes, it has already been shown that major definitions of time-varying spectra, such as the generalized Wigner-Ville spectrum and generalized evolutionary spectrum, yield effectively equivalent results. We have successfully combined the concepts of the evolutionary spectrum and array processing. The nonstationary signals received by each sensor of the array will be modeled as a sum of complex sinusoids with time-varying amplitudes. These amplitudes carry information about the direction of arrival. The time-varying amplitudes using linear estimators based on mean-squared error minimization are first estimated. These estimates are then used to generate the time-varying cross-power distributions between the data across the array. Proceeding similar to spatial joint-variable distributions, the time-varying cross-power estimates computed at high SNR time-frequency points are used for angle estimation. Further, we have shown that the spatial evolutionary spectrum can be directly used for blind source separation. Due to their attractive cross-terms properties, the spatial evolutionary spectrum performance for direction finding and signal recovery compares and potentially exceeds that of TFDs. The same argument applies to positive time-frequency distributions. Next year, we aim to develop positive spatial joint-distributions and examine the offering of positive spectra in angle estimations.

2. **Appendix** (Publications)

- Spatial Averaging of Time-Frequency Distributions for Source Separations
- Subspace analysis of spatial time-frequency distributions matrices
- The spatial ambiguity function and its applications
- Direction finding based on spatial time-frequency distribution matrices
- Time-frequency maximum Likelihood methods for direction finding
- Spatial evolutionary spectrum for DOA estimation and blind signal separation
- Spatial averaging of time-frequency distributions
- Maximum Likelihood methods for array processing based on TFDs
- Spatial evolutionary spectrum for DOA estimation and blind source separation
- Direction finding based on spatial time-frequency distribution matrices
- Spatial bilinear distributions for direction finding and source separation
- A Subband MUSIC technique for direction finding
- Beamspace time-frequency MUSIC with application to airborne antenna array
- Nonstationary interference excision in spread communications using projection filtering methods
- Spatial time frequency distributions for direction finding and blind source separation
- Adaptive blind spatial processing for frequency diversity spread spectrum Communications
- Time-frequency MUSIC

SPATIAL AVERAGING OF TIME-FREQUENCY DISTRIBUTIONS FOR SOURCE SEPARATIONS

Yimin Zhang and *Moeness G. Amin**

Department of Electrical and Computer Engineering
Villanova University, Villanova, PA 19085, USA
Phone: (610) 519-7305 Fax : (610) 519-4436
e-mail: zhang,moeness@ece.vill.edu

ABSTRACT

This paper presents a novel approach based on time-frequency distributions (TFDs) for separating signals received by a multiple antenna array. This approach provides a significant improvement in performance over the recently introduced spatial time-frequency distributions, specifically for signals with close or highly overlapping time-frequency signatures. In this approach, symmetric spatial averaging of the time-frequency distributions of the sensor data is performed at multiple time-frequency points. This averaging restores the realness property and the diagonal structure of the source TFD matrix necessary for source separation. With symmetric spatial averaging, crossterms move from their off-diagonal positions in the source TFD matrix to become part of the matrix diagonal entries. It is shown that the proposed approach yields improved performance over the case when no spatial averaging is performed. Further, we demonstrate that, in the context of source separation, the spatially-averaged Wigner-Ville distribution outperforms the combined spatial-time-frequency averaged distributions, such as the one obtained by using the Choi-Williams distribution. Simulation examples involving the separation of two sources with close AM and FM modulations are presented.

EDICS : 2.TIFR

* Corresponding author

This work is supported by ONR under Grant #N00014-98-1-0176.

I. INTRODUCTION

Recently, time-frequency distributions (TFD) have been employed for direction finding and blind source separation problems in sensor array processing [1-5]. The spatial time-frequency distributions (STFDs) were introduced in [1] and represented by a spatial matrix whose elements are the auto- and cross-time-frequency distributions of the data received at the different array sensors.

The application of STFDs to separating sources with distinct time-frequency (t-f) signatures is presented in [2]. In this reference, it is shown that the source TFD matrix, whose elements are the auto- and cross-TFD of the source signals, and the sensor data STFD have the same relationship as the one between the source and the data correlation matrices. This relationship is defined by the mixing, or the array manifold matrix. The steps applied in blind source separation based on second order statistics (the SOBI technique) outlined in [9] could therefore be used in the time-frequency formulation of the problem. The spatial time-frequency distribution matrices evaluated at several time-frequency points are incorporated into a joint-diagonalization technique based on generalized Jacobi transform to estimate the mixing matrix. This matrix is then used, through pseudo matrix inversion, to estimate the source signals up to a multiplicative complex scalar and the order of the sources. The general theory of solving blind source separation problems using spatial arbitrary joint-variable distributions, including those of time and frequency, is given in [3]. In [4], the two arbitrary variables are chosen as the time-lag and frequency-lag, and the source separation was performed using spatial ambiguity functions. The use of STFDs as an eigenstructure-based approach for direction finding is given in [5], where the time-frequency MUSIC technique is proposed to estimate the signal and noise subspaces.

Although blind source separations based on time-frequency distribution outperform the SOBI method, specifically under time-varying environments, the fundamental problem with the bilinear time-frequency approach is the need for the incorporation of STFD matrices computed only at source autoterm points. Crossterms impede performance, as they reside on the off-diagonal

elements of the source TFD matrix, and as such, violate its diagonal structure necessary for source separation. Identification of autoterm regions are often difficult for a large class of multi-component nonstationary signals, and even if properly identified, due to the complexity of the impinging signal and the use of finite data records, autoterm regions cannot be entirely free from crossterm mainlobe or/and sidelobe contamination.

In this paper, we overcome the drawbacks of the recently introduced approach for source separation based on time-frequency distributions [2]. By performing symmetric spatial averaging on the spatial time-frequency distribution matrices at any given time-frequency point, we set the off-diagonal elements of the corresponding source TFD matrix to zero. This is achieved by moving the crossterms from their off-diagonal positions to join the autoterms as diagonal entries of the source TFD matrix. In this respect, performance of the source separation technique becomes much less dependent on the selection of the time-frequency points at which the STFD matrices are computed. Moreover, due to their potential high values, specifically in the Wigner-Ville distribution, the presence of the crossterms along the matrix diagonal can increase the effective signal-to-noise ratio (SNR), and thus be used for improved performance. It is shown that the symmetric spatially-averaged STFDs outperforms the case where no spatial averaging is performed, even when only autoterm points are involved in both cases.

Symmetric spatial averaging is a simple and well-known technique in conventional array processing [6]. It employs additional array sensors to reduce cross-correlation in coherent and correlated signal environments, and thereby permits proper angle-of-arrival (AOA) estimations and source separations. In this paper, we show that spatial averaging plays a key role in the underlying TFD-based source separation problem and its application leads to matrix diagonalization and crossterm mitigation. Spatial averaging gives robustness to time-frequency point selections and yields to improved performance over other TFD-based techniques, specifically for sources whose signatures are closely separated in the time-frequency domain.

The restoration of the diagonal structure of the source TFD is only part of the problem. Source separation using spatially-averaged TFD evaluated at a single (t, f) point can still lead to noisy and non-unique results. Since the power distribution of the signals impinging on the array varies over

the time-frequency plane, then different (t, f) points may exhibit different SNRs. The main two advantages of incorporating several spatially-averaged TFD matrices evaluated at different time-frequency points into a joint-diagonalization scheme are to avoid having degenerate eigenvalues and to reduce the possibility of choosing a point with high noise contamination.

It is noted that, unlike the method in [2], the proposed approach requires the information on the array manifold. In this case, conventional AOA finding methods, such as the maximum likelihood [11] and MUSIC [12] techniques, can also be used to estimate the mixing matrix, and further to separate the source signals. The advantage of using source separation approaches over the conventional AOA finding methods for known array geometry and manifold lies in the fact that the proposed method is similar to ESPRIT [13], in the sense that both methods do not require angular search [14].

This paper is organized as follows. In Section II, the source separation approach based on spatial time-frequency distribution is briefly summarized. In Section III, we introduce the spatially averaged time-frequency distributions, and discuss the difference between spatial averaging and kernel methods in handling the crossterm problem. Simulation results demonstrating the usefulness of the proposed technique are given in Section IV.

II. SOURCE SEPARATION BASED ON SPATIAL TIME-FREQUENCY DISTRIBUTIONS

A. Spatial Time-Frequency Distributions

In many practical situations, the data vector $\mathbf{x}(t)$ for an N-element array follows an instantaneous mixture model and is given by

$$\mathbf{x}(t) = \mathbf{y}(t)+\mathbf{n}(t) = \mathbf{A}\mathbf{s}(t)+\mathbf{n}(t), \tag{1}$$

where $\mathbf{x}(t)=[x_0(t), \ldots, x_{N-1}(t)]^T$ is the data snapshot vector at time t. The vector $\mathbf{s}(t)=[s_1(t), \ldots, s_n(t)]^T$ contains n source signals at the same time, and $\mathbf{n}(t)$ is the additive noise. This model is commonly used in the field of narrowband array processing. The vector $\mathbf{y}(t)=[y_0(t), \ldots, y_{N-1}(t)]^T$ contains the noise-free array output. The mixing matrix $\mathbf{A}$ is the transfer function between the

source signals and the data at the array sensors. We assume that the mixing matrix **A** has full column rank.

The source signal vector $\mathbf{s}(t)$ is assumed to be a nonstationary multivariate process with

$$\mathbf{R}_{ss} = \lim_{T\to\infty} \frac{1}{T}\sum_{t=1}^{T} \mathbf{s}(t+\tau)\mathbf{s}^H(t) \tag{2}$$

where superscript ^{H} denotes the conjugate transpose of a matrix or a vector. In reference [2], it is assumed that $\mathbf{R}_{ss} = \text{diag}\,[r_{11}(\tau), ..., r_{nn}(\tau)]$, where diag[.] is the diagonal matrix formed with the elements of its vector valued argument, and $r_{ii}(\tau) = \lim_{T\to\infty} \frac{1}{T}\sum_{t=1}^{T} s_i(t+\tau)s_i^*(t)$ denotes the autocorrelation of $s_i(t)$. This assumption implies that the components $s_i(t)$, $1\le i\le n$ are mutually uncorrelated. However, in our proposed method, this assumption is no longer necessary.

The additive noise $\mathbf{n}(t)$ is modeled as a stationary, temporally white, zero-mean complex random process independent of the source signals. For simplicity, we also require $\mathbf{n}(t)$ to be spatially white, i.e.,

$$E[\mathbf{n}(t+\tau)\mathbf{n}^H(t)] = \sigma_n^2\delta(\tau)\mathbf{I} \tag{3}$$

where $\delta(\tau)$ is the Kronecker delta and **I** denotes the identity matrix. Since the signal power and the signal ordering are indeterminable in source separations [3], we simplify the problem by treating the source signals as if they have unit power. Accordingly

$$\mathbf{R}_{ss}=\mathbf{I} \text{ and } \mathbf{R}_{yy} = \lim_{T\to\infty} \frac{1}{T}\sum_{t=1}^{T} \mathbf{y}(t)\mathbf{y}^H(t) = \mathbf{A}\mathbf{A}^H. \tag{4}$$

The discrete-time form of Cohen's class of TFD for signal $x(t)$ is given by [7]

$$D_{xx}(t,f) = \sum_{l=-\infty}^{\infty}\sum_{m=-\infty}^{\infty} \phi(m,l)x(t+m+l)x^*(t+m-l)e^{-j4\pi fl} \tag{5}$$

where t and f represent the time index and the frequency index, respectively. The kernel $\phi(m,l)$ characterizes the TFD and is a function of both the time and lag variables. The cross-TFD of two signals $x_i(t)$ and $x_j(t)$ is defined by [7]

$$D_{x_ix_j}(t,f) = \sum_{l=-\infty}^{\infty}\sum_{m=-\infty}^{\infty} \phi(m,l)x_i(t+m+l)x_j^*(t+m-l)e^{-j4\pi fl} \tag{6}$$

One possible definition of spatial time-frequency distribution (STFD) is given in [2] and incorporates both equations (5) and (6),

$$\mathbf{D}_{\mathbf{xx}}(t,f) = \sum_{l=-\infty}^{\infty}\sum_{m=-\infty}^{\infty}\phi(m,l)\mathbf{x}(t+m+l)\mathbf{x}^{H}(t+m-l)e^{-j4\pi fl} \tag{7}$$

where $[\mathbf{D}_{\mathbf{xx}}(t,f)]_{i,j} = D_{x_i x_j}(t,f)$, for i, j=0, ..., N-1. It is shown in the next section that other forms of STFD can be more useful in the context of source separation. Under the linear data model of Eq. (1), and assuming noise-free environment, the STFD matrix in (7) takes the following simple structure

$$\mathbf{D}_{\mathbf{xx}}(t,f) = \mathbf{A}\mathbf{D}_{\mathbf{ss}}(t,f)\mathbf{A}^{H} \tag{8}$$

where $\mathbf{D}_{\mathbf{ss}}(t,f)$ is the signal TFD matrix whose entries are the auto- and cross-TFDs of the sources. Eq. (8) is similar to the formula that is commonly used in conventional blind source separation and direction-of-arrival (DOA) estimation problems [8,9], relating the signal correlation matrix to the data spatial correlation matrix. If $\mathbf{D}_{\mathbf{ss}}(t,f)$ is a full-rank matrix, the two subspaces spanned by the principle eigenvectors of $\mathbf{D}_{\mathbf{xx}}(t,f)$ and the columns of $\mathbf{A}$ become identical. In this case, directional finding techniques based on eigenstructures can be applied. If $\mathbf{D}_{\mathbf{ss}}(t,f)$ is diagonal, i.e., the signal cross-TFDs at the time-frequency point (t, f) are zeros, the mixture matrix and the signal waveforms can be recovered using blind source separation methods [1,2].

B. Source Separation based on Spatial Time-Frequency Distributions

The source separation algorithm based on spatial time-frequency distributions is an essential part of the proposed method. The algorithm is given in details in reference [2] and summarized below.

The first step is the whitening of the signal part $\mathbf{y}(t)$ of the observation. This is achieved by applying a whitening matrix $\mathbf{W}$ to $\mathbf{y}(t)$, i.e., an n x N matrix satisfying:

$$\lim_{T\to\infty}\frac{1}{T}\sum_{t=1}^{T}\mathbf{W}\mathbf{y}(t)\mathbf{y}^{H}(t)\mathbf{W}^{H} = \mathbf{W}\mathbf{R}_{\mathbf{y}}\mathbf{W}^{H} = \mathbf{W}\mathbf{A}\mathbf{A}^{H}\mathbf{W}^{H} = \mathbf{I}. \tag{9}$$

$\mathbf{WA}$ is an n x n unitary matrix $\mathbf{U}$, and matrix $\mathbf{A}$ can be written as

$$\mathbf{A} = \mathbf{W}^{\#}\mathbf{U} \tag{10}$$

where superscript # denotes pseudo-inverse. The whitened process $\mathbf{z}(t)=\mathbf{W}\mathbf{x}(t)$ still obeys a linear model,

$$\mathbf{z}(t) = \mathbf{W}\mathbf{x}(t) = \mathbf{W}[\mathbf{A}\mathbf{s}(t) + \mathbf{n}(t)] = \mathbf{U}\mathbf{s}(t) + \mathbf{W}\mathbf{n}(t). \tag{11}$$

By pre- and post-multiplying the STFD matrices $\mathbf{D}_{xx}(t,f)$ by $\mathbf{W}$, we obtain

$$\mathbf{D}_{zz}(t,f) = \mathbf{W}\mathbf{D}_{xx}(t,f)\mathbf{W}^H \tag{12}$$

which is, in essence, the STFD of the whitened data vector $\mathbf{z}(t)$. From the definitions of $\mathbf{W}$ and $\mathbf{U}$,

$$\mathbf{D}_{zz}(t,f) = \mathbf{U}\mathbf{D}_{ss}(t,f)\mathbf{U}^H. \tag{13}$$

Equation (13) shows that if $\mathbf{D}_{ss}(t,f)$ is diagonal, then any whitened data STFD matrix is diagonal in the basis of the columns of the matrix $\mathbf{U}$, and the eigenvalues of $\mathbf{D}_{zz}(t,f)$ are the diagonal entries of $\mathbf{D}_{ss}(t,f)$. An estimate $\hat{\mathbf{U}}$ of the unitary matrix $\mathbf{U}$ may be obtained as a signal subspace of a whitened STFD matrix evaluated at a time-frequency point corresponding to the signal autoterm. The source signals can then be estimated as $\hat{\mathbf{s}}(t) = \hat{\mathbf{U}}\hat{\mathbf{W}}\mathbf{x}(t)$, and the mixing matrix $\mathbf{A}$ is estimated by $\hat{\mathbf{A}} = \hat{\mathbf{W}}^{\#}\hat{\mathbf{U}}$.

Although the unitary matrix can be obtained from a single time-frequency point, STFDs corresponding to different (t, f) points should be incorporated, so as to reduce the possibility of having degenerate eigenvalues and subsequently non-unique solutions. The joint-diagonalization (JD) scheme can be used to incorporate multiple time-frequency points [2]. This scheme forms K STFD matrices $\{\mathbf{D}_{zz}(t_i,f_i) \mid i=1,...,K\}$ at a set of preferable K (t, f) autoterm points. The unitary matrix $\hat{\mathbf{U}}$ is then obtained as the joint diagonalizer of the set $\{\mathbf{D}_{zz}(t_i,f_i) \mid i=1,...,K\}$.

III. SPATIAL AVERAGING TIME-FREQUENCY DISTRIBUTIONS

A. Spatial Averaging Methods

Symmetric spatial averaging method was introduced by Pillai [6] to restore the full-rank property of the signal covariance matrix in the presence of coherent signals. Unlike other spatial smoothing methods [15-18], which only restore the full rank property of the mixing matrix when the impinging signals are coherent, the symmetric spatial averaging method enforces the diagonal

structure of the signal correlation matrix. This diagonal matrix property is essential to perform source separation, as previously discussed. Here, we present the role of spatial averaging in the context of TFD analysis, and propose signal separation using joint diagonalization based on spatial averaging of spatial TFD matrices.

The basic idea of symmetric spatial averaging is to use a symmetric subarray to obtain an averaged covariance matrix, or in the underlying problem, an averaged STFD matrix, with the off-diagonal elements set to zero.

Without loss of generality, we consider a simple example of n=2, i.e., there are only two sources, $s_1(t)$ and $s_2(t)$. The result is generally true for n sources and N sensors, as long as $n<N$.

By ignoring the effect of noise, the received signal at the i-th array sensor (i= 0, 1, 2, ..., N-1) is represented by

$$x_i(t) = x_i^{(1)}(t) + x_i^{(2)}(t) = s_1(t)e^{-jd_i\omega_1} + s_2(t)e^{-jd_i\omega_2} \tag{14}$$

where $\omega_k=2\pi\sin\phi_k/\lambda$ (k =1,2) is the spatial radian frequency, ϕ_k is the angle-of-arrival, λ is the RF wavelength, and d_i is the distance between 0-th and i-th array sensors. The cross-TFD of $x_i(t)$ and $x_j(t)$, assuming uniform linear array, is

$$\begin{aligned} D_{x_i x_j}(t,f) &= D_{x_i^{(1)}x_j^{(1)}}(t,f) + D_{x_i^{(2)}x_j^{(1)}}(t,f) + D_{x_i^{(2)}x_j^{(2)}}(t,f) + D_{x_i^{(1)}x_j^{(2)}}(t,f) \\ &= \left[D_{s_1 s_1}(t,f) + D_{s_2 s_1}(t,f)e^{-jd_i(\omega_2-\omega_1)} \right] e^{-j(d_i-d_j)\omega_1} \\ &\quad + \left[D_{s_2 s_2}(t,f) + D_{s_1 s_2}(t,f)e^{jd_i(\omega_2-\omega_1)} \right] e^{-j(d_i-d_j)\omega_2} \end{aligned} \tag{15}$$

Due to the presence of the cross-terms (second term in each bracket in (15)), the TFD matrix $\mathbf{D}_{\mathbf{xx}}(t,f)$ does not provide the proper information to carry out source separations.

The auto- and cross-TFD of the data $x_0(t)$ and $x_i(t)$, i= 0, 1, 2, ..., N-1, is

$$D_{x_0 x_i}(t,f) = \left[D_{s_1 s_1}(t,f) + D_{s_2 s_1}(t,f) \right] e^{jd_i\omega_1} + \left[D_{s_2 s_2}(t,f) + D_{s_1 s_2}(t,f) \right] e^{jd_i\omega_2} \tag{16}$$

where we used the sensor receiving $x_0(t)$ as the reference sensor and set d_0=0. Denote $b_1 = D_{s_1 s_1}(t,f) + D_{s_2 s_1}(t,f)$ and $b_1 = D_{s_2 s_2}(t,f) + D_{s_1 s_2}(t,f)$. The values of b_1 and b_2 are generally complex. If b_1 and b_2 are real, then the Hermitian Toeplitz spatial time-frequency matrix

$$\overline{\mathbf{D}}_{\mathbf{xx}}(t,f)=\begin{bmatrix} D_{x_0x_0}(t,f) & D_{x_0x_1}(t,f) & \cdots & D_{x_0x_{N-1}}(t,f) \\ D^*_{x_0x_1}(t,f) & D_{x_0x_0}(t,f) & \cdots & D_{x_0x_{N-2}}(t,f) \\ \vdots & \vdots & \ddots & \vdots \\ D^*_{x_0x_{n-1}}(t,f) & D^*_{x_0x_{N-2}}(t,f) & \cdots & D_{x_0x_0}(t,f) \end{bmatrix} \tag{17}$$

generated from the cross-TFD $D_{x_0x_0}(t,f), D_{x_0x_1}(t,f), ..., D_{x_0x_{N-1}}(t,f)$ between the data samples at the reference sensor and those at other sensors of the array can be expressed as [19]

$$\overline{\mathbf{D}}_{\mathbf{xx}}(t,f)=\mathbf{A}\overline{\mathbf{D}}_{\mathbf{ss}}(t,f)\mathbf{A}^H \tag{18}$$

where $\mathbf{A}$ is a Vandermonde matrix, and

$$\overline{\mathbf{D}}_{\mathbf{ss}}(t,f)=diag[b_1 \quad b_2] \tag{19}$$

is the corresponding source TFD matrix. Note that $\overline{\mathbf{D}}_{\mathbf{xx}}(t,f)$ has a different structure from that of the STFD matrix defined in (7), and was used in reference [2] for blind source separation. Clearly, (18) has the same form as (8), but $\overline{\mathbf{D}}_{\mathbf{ss}}(t,f)$ here is diagonal, even if the selected (t,f) point corresponds to a crossterm.

In the case of complex signal waveforms, the realness and the diagonal structure of $\overline{\mathbf{D}}_{\mathbf{ss}}(t,f)$ can be restored by spatial averaging. We add N-1 array sensors symmetrically about the reference point, as shown in Fig.1. The received signal at i-th sensor of the new set is,

$$x_{-i}(t)=x^{(1)}_{-i}(t)+x^{(2)}_{-i}(t)=s_1(t)e^{jd_i\omega_1}+s_2(t)e^{jd_i\omega_2} \tag{20}$$

The new cross-TFD of $x_0(t)$ and $x_{-i}(t)$ is,

$$D_{x_0x_{-i}}(t,f)=\left[D_{s_1s_1}(t,f)+D_{s_2s_1}(t,f)\right]e^{-jd_i\omega_1}+\left[D_{s_2s_2}(t,f)+D_{s_1s_2}(t,f)\right]e^{-jd_i\omega_2} \tag{21}$$

The spatial averaging of (16) and (21) is given by

$$\tilde{D}^{(i)}_{xx}(t,f)=\left\{D_{x_0x_i}(t,f)+D^*_{x_0x_{-i}}(t,f)\right\}/2=c_1e^{jd_i\omega_1}+c_2e^{jd_i\omega_2} \tag{22}$$

where

$$c_1=D_{s_1s_1}(t,f)+\mathrm{Re}\left(D_{s_2s_1}(t,f)\right), \qquad c_2=D_{s_2s_2}(t,f)+\mathrm{Re}\left(D_{s_1s_2}(t,f)\right).$$

Since the terms in the brackets in (21) are all real, the matrix formed from the TFDs (22)

$$\tilde{\mathbf{D}}_{\mathbf{xx}}(t,f)=\begin{bmatrix} \tilde{D}^{(0)}_{xx}(t,f) & \tilde{D}^{(1)}_{xx}(t,f) & \cdots & \tilde{D}^{(N-1)}_{xx}(t,f) \\ \tilde{D}^{(1)*}_{xx}(t,f) & \tilde{D}^{(0)}_{xx}(t,f) & \cdots & \tilde{D}^{(N-2)}_{xx}(t,f) \\ \vdots & \vdots & \ddots & \vdots \\ \tilde{D}^{(N-1)*}_{xx}(t,f) & \tilde{D}^{(N-2)*}_{xx}(t,f) & \cdots & \tilde{D}^{(0)}_{xx}(t,f) \end{bmatrix} \tag{23}$$

is Hermitian and Toeplitz. This matrix is referred to as the spatially-averaged TFD (SATFD) matrix. Similar to the real TFD case, in the noise-free environment, the SATFD matrix in (23) can be expressed as

$$\tilde{\mathbf{D}}_{xx}(t,f) = \mathbf{A}\tilde{\mathbf{D}}_{ss}\mathbf{A}^{H} \tag{24}$$

where

$$\tilde{\mathbf{D}}_{ss}(t,f) = diag[c_1 \quad c_2]. \tag{25}$$

The off-diagonal elements of the $\tilde{\mathbf{D}}_{ss}(t,f)$ are zeros, where as the matrix diagonal entries are now made up of both autoterms and crossterms of the impinging source signals. By enforcing the diagonal structure of the source TFD matrix $\tilde{\mathbf{D}}_{ss}(t,f)$, spatial averaging of the Hermitian Toeplitz STFD matrices extends the validity of the TFD-based signal separation in the presence of cross-TFDs.

The steps for source separation used in [2] and summarized in Section II can be applied to the SATFD $\tilde{\mathbf{D}}_{xx}(t,f)$ instead of the STFD $\mathbf{D}_{xx}(t,f)$. With spatial averaging, the incorporation of STFDs at only autoterm points into the joint-diagonalization scheme is no longer crucial to achieve good performance.

B. Comparison between spatial averaging and kernel methods

There are two sources of crossterms in the underlying source separation problem. The first type are the crossterms that are the results of the interactions between the components of the same source signal. Whether we use the STFD defined in (7) or in (17), those crossterms are not harmful to the blind source separation problem, since they always reside, along with the autoterms, on the main diagonal of the source TFD matrix. The other type of crossterms are those generated from the interactions between two signal components belonging to two different sources. These crossterms are associated with cross-TFDs of the source signals and, at any given time-frequency point, they constitute the off-diagonal entries of the source TFD matrices. The crossterms generated from the data cross-TFDs violate the basic assumption in the problem of source separation regarding the diagonal structure of the source TFD matrix. We must therefore select the t-f points that belong to autoterm regions where crossterm contributions are at minimum.

However, the selection of autoterm points is often difficult in the absence of *a priori* information of the source signals, specifically for low SNR or when the signals have highly overlapping time-frequency signatures. The later case can be encountered in radar echoes and acoustic signal processing.

The use of smoothing time-frequency kernel for crossterm reduction is a candidate solution of the above problem. The main function of this kernel in the context of source separation is to prevent the selection and incorporation of crossterm points in the joint-diagonalization scheme, as well as to reduce the contribution of crossterms at selected autoterm points. In essence, the fundamental role of the t-f kernel is to make the source TFD matrices as close to a diagonal structure as possible. The t-f kernel can be applied to both forms of STFDs in (7) and (23). It is noteworthy that the smoothing kernel does not distinguish between the aforementioned two types of crossterms, and accordingly it reduces all entries of the source TFD matrix, including the diagonal elements.

The problem with the smoothing kernel is fourfold. First, for sources with closely separated time-frequency signatures, the effectiveness of the smoothing kernel in reducing crossterms is highly impaired. Second, reduction of crossterms depends on their time-frequency locations, specially when fixed shape kernels are used. For example, t-f kernels satisfying the marginal properties are not suitable for removing the crossterms which lie on the time-lag and frequency-lag axes in the ambiguity domain. Third, depending on the employed t-f kernel, part or all of the crossterms may be displaced to mount on the selected autoterm points. The situation can make the source TFD matrix to further deviate from a diagonal structure, cause performance deterioration from the case when no smoothing is applied. We refer to this undesired property as the smoothing problem. Fourth, since source separation is often performed incorporating a finite number of data samples, the intrusion of crossterms on autoterm regions cannot be prevented or entirely removed. This is because the window spreads out the crossterms in the time-frequency domain so that the mainlobe or/and the sidelobes of the crossterms are deemed to overlap with the signal autoterms. We refer to this undesired property as the leakage problem in STFDs. In addition to the above drawbacks, the t-f kernel ignores the fact that the first type of crossterms need not be smoothed, as its appearance along the diagonal elements can improve the effective signal to noise ratio.

The spatial averaging of the STFD defined in (23) at a given (t, f) point does not smooth or reduce the crossterms at that point, but rather move them from their residence on the off-diagonal matrix entries to be part of the matrix diagonal elements. The other part represents the contribution of the autoterms at the same point. Therefore, not only we are able to set the off-diagonal elements of the source TFD matrix to zeros, but also we can improve performance by selecting the (t,f) points of peak values, irrespective of whether these points belong to autoterm or crossterm regions.

IV. PERFORMANCE EVALUATION

A. Performance index

We use a slightly modified version of the performance index applied in [2] to evaluate the performance of the proposed source separation technique. The estimate of the source signal vector is computed by applying the pseudo-inverse of the estimated mixing matrix $\hat{\mathbf{A}}$ to the received signal vector $\mathbf{x}(t)$, i.e.,

$$\hat{\mathbf{s}}(t) = \hat{\mathbf{A}}^{\#}\mathbf{x}(t) = \hat{\mathbf{A}}^{\#}\mathbf{A}\mathbf{s}(t) + \hat{\mathbf{A}}^{\#}\mathbf{n}(t) \tag{26}$$

where $\hat{\mathbf{A}} = \hat{\mathbf{W}}^{\#}\hat{\mathbf{U}}$. We stress that in general, this procedure is not optimal for recovering the source signals based on an estimate $\hat{\mathbf{A}}$. For large enough sample size, matrix $\hat{\mathbf{A}}$ should be close to the true one **A**, so that $\hat{\mathbf{A}}^{\#}\mathbf{A}$ well approximates the identity matrix. We normalize matrix $\hat{\mathbf{A}}$ by

$$\hat{\mathbf{A}}_e = \hat{\mathbf{A}}\,\mathrm{diagonal}(\hat{\mathbf{A}}^{\#}\mathbf{A}) \tag{27}$$

where diagonal(**F**) denotes the matrix formed by the diagonal elements of **F**. As such, the diagonal elements of $\hat{\mathbf{A}}_e^{\#}\mathbf{A}$ become exactly one, giving more meaning to the performance index

$$I_{pq} = E\left|(\hat{\mathbf{A}}_e^{\#}\mathbf{A})_{pq}\right|^2 \tag{28}$$

which defines the interference-to-signal ratio (ISR). Thus, I_{pq} measures the ratio of the power of the interference of qth source signal to the power of the pth source signal. As the measure of the global quality of the separation process, we also apply the global rejection level to evaluate the overall performance of the proposed method

$$I_{perf} = \sum_{q \neq p} I_{pq} \tag{29}$$

B. Effect of crossterms between source signals

In this section, we examine the effect of the time-frequency crossterms on source separation performance when spatial averaging is not applied. To simplify the problem, we assume that $\mathbf{R}_{ss}$ is an identity matrix. When crossterms are present at the off-diagonal elements of the TFD matrix $\mathbf{D}_{ss}(t,f)$, then

$$\mathbf{D}_{ss}(t,f) = \mathbf{P}(t,f)\mathbf{G}(t,f)\mathbf{P}^H(t,f) \tag{30}$$

where $\mathbf{G}(t,f)$ is the diagonal matrix with the eigenvalues at the diagonal elements, and $\mathbf{P}(t,f)$ is the matrix whose columns are the corresponding eigenvectors. Note that all the above matrices depend on the selected (t, f) point. Substituting (30) in (8), the STFD matrix of the data vector under noise-free conditions becomes

$$\mathbf{D}_{xx}(t,f) = \mathbf{A}\mathbf{D}_{ss}(t,f)\mathbf{A}^H = \mathbf{A}\mathbf{P}(t,f)\mathbf{G}(t,f)\mathbf{P}^H(t,f)\mathbf{A}^H \tag{31}$$

and the STFD matrix of the whitened array signal vector is

$$\mathbf{D}_{zz}(t,f) = \mathbf{W}\mathbf{A}\mathbf{D}_{ss}(t,f)\mathbf{A}^H\mathbf{W}^H = \mathbf{W}\mathbf{A}\mathbf{P}(t,f)\mathbf{G}(t,f)\mathbf{P}^H(t,f)\mathbf{A}^H\mathbf{W}^H \tag{32}$$

Since $\mathbf{G}(t,f)$ is diagonal, $\mathbf{WAP}(t,f)$ is unitary. If the estimated mixing matrix $\hat{\mathbf{A}}$ is provided based on a single (t,f) point, then from (32),

$$\hat{\mathbf{A}} = \mathbf{W}^{\#}\mathbf{W}\mathbf{A}\mathbf{P}(t,f) = \mathbf{A}\mathbf{P}(t,f) \tag{33}$$

which is dependent on the unitary matrix $\mathbf{P}(t,f)$. Furthermore,

$$\hat{\mathbf{A}}^{\#}\mathbf{A} = \{\mathbf{A}\mathbf{P}(t,f)\}^{\#}\mathbf{A} = \mathbf{P}^H(t,f) \tag{34}$$

and

$$\begin{aligned}
\hat{\mathbf{A}}_e^{\#}\mathbf{A} &= \left\{\text{diagonal}(\hat{\mathbf{A}}^{\#}\mathbf{A})\right\}^{-1}\hat{\mathbf{A}}^{\#}\mathbf{A} \\
&= \left\{\text{diagonal}(\mathbf{P}^H(t,f))\right\}^{-1}\mathbf{P}^H(t,f) \\
&= \begin{bmatrix} p_{11}^{-1}(t,f) & & & \mathbf{O} \\ & p_{22}^{-1}(t,f) & & \\ & \vdots & \ddots & \vdots \\ \mathbf{O} & & & p_{nn}^{-1}(t,f) \end{bmatrix}^* \begin{bmatrix} p_{11}(t,f) & p_{21}(t,f) & \cdots & p_{n1}(t,f) \\ p_{12}(t,f) & p_{22}(t,f) & \cdots & p_{n2}(t,f) \\ \vdots & \vdots & \ddots & \vdots \\ p_{1n}(t,f) & p_{2n}(t,f) & \cdots & p_{nn}(t,f) \end{bmatrix}^*
\end{aligned}$$

$$= \begin{bmatrix} 1 & p_{22}^{-1}(t,f)p_{21}(t,f) & \cdots & p_{nn}^{-1}(t,f)p_{n1}(t,f) \\ p_{11}^{-1}(t,f)p_{12}(t,f) & 1 & \cdots & p_{nn}^{-1}(t,f)p_{n2}(t,f) \\ \vdots & \vdots & \ddots & \vdots \\ p_{11}^{-1}(t,f)p_{1n}(t,f) & p_{22}^{-1}(t,f)p_{2n}(t,f) & \cdots & 1 \end{bmatrix}^{*}. \tag{35}$$

where $p_{ij}(t,f) = [\mathbf{P}(t,f)]_{i,j}$. Accordingly, the performance index becomes

$$I_{pq} = \left| p_{qq}^{-1}(t,f)p_{qp}(t,f) \right|^2 \tag{36}$$

and the global rejection level is given by

$$I_{perf} = \sum_{p \neq q} I_{pq} = \sum_{q=1}^{n} \left| p_{qq}(t,f) \right|^{-2} \sum_{\substack{p=1 \\ p \neq q}}^{n} \left| p_{qp}(t,f) \right|^2 = \sum_{q=1}^{n} \left| p_{qq}(t,f) \right|^{-2} - n \tag{37}$$

In general, since the absolute values of $p_{qq}(t,f)$ are always equal to or smaller than 1, the global rejection level I_{perf} takes a positive value. It is clear that I_{perf}=0 only when $p_{qq}(t,f)$=1 holds true for all q. That is, $\mathbf{P}$ is an identity matrix, which implies that there is no off-diagonal non-zero elements in matrix $\mathbf{D}_{ss}(t,f)$.

Consider the specific case of n=2. If we select a (t, f) point where the contributions of the two sources to the source TFD matrix are the same, i.e., $D_{s_1 s_1}(t,f) = D_{s_2 s_2}(t,f)$, and since $D_{s_1 s_2}(t,f) = D_{s_2 s_1}^{*}(t,f)$ by definition, then it is straightforward to show that $\left| p_{qq}(t,f) \right| = 1/\sqrt{2}$. In this case, I_{perf} is constant equal to 2. The (t, f) points having such property include all crossterms at which the autoterms have equal contributions.

C. Simulation results

In this section we demonstrate the effectiveness of the spatially-averaged time-frequency distributions in source separations. The whitening joint-diagonalization scheme [2] is used for incorporating multiple time-frequency points into the proposed spatial averaging method. In all simulations, two sources with the chirp signals

$$s_1(t) = e^{-j\mu\frac{t^2}{2}}, \quad s_2(t) = e^{-j\mu\frac{t^2}{2}-(\alpha+j\omega)t} \tag{38}$$

are used, where μ is chosen as 0.008π. Different values of ω and α are considered. These values control the frequency offset and amplitude variation between the two signals and can be chosen to

yield closely or widely separated source signatures in the time-frequency domain. 128 data samples are considered, from which a time-frequency matrix of 128 x 128 is formed. The DOAs of the two signals $s_1(t)$ and $s_2(t)$ are set equal to 30° and 60°, respectively, from the broadside direction. Furthermore, we assume an equi-spaced 5-element linear array with the interelement spacing 0.5λ, where λ is the wavelength. Subsequently, when the spatial averaging method is used, two sub-arrays are formed, each with 3 elements.

In the first set of simulations, we choose α=0, i.e., neither signal is amplitude modulated. The Wigner-Ville (WV) distribution of each signal is shown in Fig.2, where δf (=$\omega/2\pi$) is set equal to 0.05. Fig.3 shows the time-frequency distribution of the mixed signals at the center array sensor. No noise is present for this case. It is clear that the crossterms lie in the middle of the two chirps, and their amplitude change periodically. Fig.4(a) shows the time-frequency distributions of the separated signals using the technique in [2], where joint diagonalization is used without the utilization of the proposed spatial averaging method. Three time-frequency (t, f) points are used at t = 32, 64, and 96. The frequency f is chosen so that the TFD computed using the data at the center array sensor is the largest at each t. Peak values of the WV distribution may either correspond to autoterms or crossterms. In this case, out of three (t, f) points, one crossterm point and two autoterm peaks were selected. The obtained $\hat{\mathbf{A}}_e^{\#}\mathbf{A}$ matrix is

$$\hat{\mathbf{A}}_e^{\#}\mathbf{A} = \begin{bmatrix} 1.00 + j0.00 & 0.19 + j0.65 \\ -0.21 + j0.63 & 1.00 + j0.00 \end{bmatrix}$$

and the computed global rejection level I_{perf} is –0.43 dB. The result is clearly unsatisfactory, as the matrix $\hat{\mathbf{A}}_e^{\#}\mathbf{A}$ is far from the identity matrix and crossterms appear in the separated signals.

Next, we force the selection of autoterm peaks by only considering the (t, f) points along the instantaneous frequencies of the two input signals at the same above time instants. Although no crossterm point is selected, yet as discussed in Section III, because of the finite data record, the crossterms leak into autoterm regions, causing the source TFD matrix to deviate from a diagonal structure. We show in Fig.4(b) the result of source separation when only the autoterm points are considered. The obtained $\hat{\mathbf{A}}_e^{\#}\mathbf{A}$ matrix becomes

$$\hat{\mathbf{A}}_e^{\#}\mathbf{A} = \begin{bmatrix} 1.00 + j0.00 & 0.00 - j0.06 \\ -0.01 - j0.01 & 1.00 + j0.00 \end{bmatrix}$$

and the respective global rejection level I_{perf} is –23.96 dB. It is clear that the source separation performance is greatly improved. This good performance implies that the contributions of crossterms at the three selected autoterm points were insignificant, implying that the corresponding source TFD matrices in this case were close to diagonal.

Fig.5 shows the time-frequency distributions of the separated signals at the same condition as Fig.4(a), except with the utilization of the proposed spatial averaging method. Spatial averaging entirely mitigates the effect of crossterms. It is clear that the time-frequency distributions of the separated signals are the same as those of the original source signals, and $\hat{\mathbf{A}}_e^{\#}\mathbf{A}$ are exactly identity matrices. Similar results can be obtained when all three (t, f) points are autoterms.

Fig.6 shows the global rejection level I_{perf} versus the frequency difference δf between the two chirps, where the input SNR is 20dB. When the proposed spatial averaging method is used, the global rejection level maintains low values. On the other hand, without spatial averaging, the global rejection levels become very high. The main reason of the large fluctuation of the I_{perf} without spatial averaging is that the influence as well as the number of crossterm points incorporated in the joint-diagonalization scheme varies with the frequency difference δf (when δf =0.1, no crossterm points were selected). Note that the crossterms of the Wigner-Ville distribution remain high even when the frequency difference is large. When selected, these terms put large values along the off-diagonal terms of the source TFD matrix, and subsequently cause considerable error, as evident from the figure. However, when only autoterm (t, f) points are used, the global rejection level decreases as δf increases. In this case, the matrix off-diagonal elements are the crossterm values at the autoterm points which become smaller for higher values of δf.

Next we show the effect of using time-frequency smoothing kernels for reduced interference terms. The Choi-Williams (CW) distribution [10] is considered with σ=1. Fig.7 shows the CW distribution of each signal separately, whereas the CW distribution of the mixed signals at the center array sensor is depicted in Fig.8. The signals are the same as the ones used in the WV distribution simulations with δf=0.05. Fig.9(a) shows the CW distributions of the separated signals. The obtained $\hat{\mathbf{A}}_e^{\#}\mathbf{A}$ matrix is

$$\hat{\mathbf{A}}_e^{\#}\mathbf{A} = \begin{bmatrix} 1.00 + j0.00 & 0.03 + j0.70 \\ -0.05 + j0.67 & 1.00 + j0.00 \end{bmatrix}$$

and the respective global rejection level I_{perf} is –0.26 dB. At this small frequency offset, effective smoothing of crossterms is difficult, and as a result, even with the use of time-frequency kernel, one crossterm (t, f) point was still selected out of the three (t, f) points. When only the autoterm (t, f) points are used, the $\hat{\mathbf{A}}_e^{\#}\mathbf{A}$ matrix becomes

$$\hat{\mathbf{A}}_e^{\#}\mathbf{A} = \begin{bmatrix} 1.00 + j0.00 & -0.02 + j0.18 \\ 0.01 + j0.14 & 1.00 + j0.00 \end{bmatrix}$$

and the global rejection level I_{perf} is reduced to –12.86 dB. The CW distributions of the separated signals are shown in Fig.9(b).

Fig.10 shows the CW distributions of the separated signals under the same condition as Fig.9(a), with the utilization of the spatial averaging method. Again, it is clear that the time-frequency distributions of both cases are the same as the source signals, and $\hat{\mathbf{A}}_e^{\#}\mathbf{A}$ are exactly an identity matrix. The same results can be obtained when only the autoterm (t, f) points are used.

Fig.11 shows the global rejection level I_{perf} versus the frequency difference δf between the two chirps, where the input SNR is 20dB. It is evident from this figure that the kernel method fails when the two signals have close time-frequency signatures. Using the proposed spatial averaging method outperforms the case when no spatial averaging is applied. Three important observations on the difference between the WV distribution and the CW distribution in the context of source separation are in order. First, the CW kernel effectively reduces the crossterms, particularly when δf is large. Accordingly, crossterms are not as large as the autoterms, and as such, it is unlikely for the crossterms to be selected and incorporated in the joint-diagonalization scheme. Second, when δf is large enough, the global rejection level is significantly reduced for the CW distribution, even when spatial averaging is not applied. Third, when the spatial averaging method is used, the performance at small frequency offset from the CW distribution is worse than that obtained from the WV distribution. The reason is, source separation is perturbed by the presence of noise, and the performance nevertheless is sensitive to the input SNR. When comparing the WV distribution and the CW distribution, the noise floor relative to peak values is lower in WV distribution than CW for the underlying chirp signal example.

To show the effect of the input SNR on the source separation performance, Fig.12 and Fig.13 depict the global rejection level versus the input SNR, where the frequency difference is 0.01.

Increasing the SNR certainly improves the source separation performance when spatial averaging is applied. On the other hand, without spatial averaging, the source separation performance holds an almost constant high level. Such performance demonstrates that crossterms are more of a fundamental problem than noise in TFD-based source separation problems.

In the second set of simulations, ω is set to zero in equation (38), rendering the two source signals identical in terms of their instantaneous frequency characteristic. However, one of the two source signals is amplitude modulated, caused by a nonzero positive value of α.

Fig.14 shows the global rejection level versus α, where the WV distribution is considered, and the input SNR is 20dB. It is clear that, the two signals cannot be separated without spatial averaging, but when applying spatial averaging, satisfactory performance of source separation can be achieved. For α=0.002, the proposed technique yields a global rejection level –26.72dB.

V. CONCLUSIONS

Symmetric spatial averaging of spatial time-frequency distributions was introduced. The spatial averaging of the spatial time-frequency distributions of the data across an antenna array removes the undesired effect of crossterms between the impinging signals. These terms reside along the off-diagonal entries of the source time-frequency distribution matrix, and consequently impede the source separation performance, which is based on preassumed diagonal matrix structure. Spatial averaging amounts to forming a spatial Hermitian Toeplitze matrix using the auto- and cross-time-frequency distributions of the data over one half of the array. This matrix is then added to the spatial matrix corresponding to the other half of the array. The desired effect of this averaging is reallocating the interaction between the source signals in the time-frequency domain from the off-diagonal to the diagonal elements of the source TFD matrix. In this respect, unlike the method proposed in [2], cross-terms, due to their potential high values, are regarded as useful components that could be used for improved performance. Spatial averaging can be applied to all members of Cohen's class of TFDs, irrespective of the employed smoothing kernel. When using a time-

frequency kernel, the problem amounts to averaging in all three dimensions of time, frequency, and space.

Joint-diagonalization (JD) is applied to include multiple spatially averaged time-frequency distributions at different time-frequency points. With cross-terms moved to the diagonal entries of the TFD matrix, the prime task of the source separation based on the JD scheme is to avoid degenerate eigenvalues which are responsible for non-uniqueness solution of the problem.

Simulation examples were presented to illustrate the effectiveness of the new approach. The two performance measures used were the global rejection level and the values of the off-diagonal elements of the product of the mixing matrix and the Pseudo inverse of its estimate. Two sources and five sensors were considered. The source signals were chirp signals with the same sweeping frequency, but their corresponding constant frequencies and amplitudes were offset by different values. Both Wigner-Ville and Choi-Williams distributions were considered. It was shown that the spatial averaging method significantly improves the performance measures over the non-spatially averaging method, specifically when the two signals have close time-frequency signatures.

Without spatial-averaging, performance is very sensitive to whether only auto-term or cross-term points or their mix are incorporated in the source separation procedure. With spatial averaging, this is no longer a concern, since both terms appear along the diagonal. It is also shown that the Choi-Williams distribution provides better results than the Wigner-Ville distribution when no spatial averaging is applied, since it lowers the likelihood of selecting crossterm points. With spatial averaging, the issue becomes merely SNR, and in this respect, the Wigner-Ville distribution, due to its high peak values, yields better performance than the Choi-Williams distribution.

REFERENCES

[1] A. Belouchrani and M. Amin, "Source separation based on the diagonalization of a combined set of spatial time-frequency distribution matrices," in *Proc. IEEE ICASSP'97*, Germany, April 1997.

[2] A. Belouchrani and M. Amin, "Blind source separation based on time-frequency signal representation," *IEEE Trans. Signal Processing*, vol. 46, no. 11, pp. 2888-2897, Nov. 1998.

[3] A. Belouchrani and M. Amin, "Blind source separation using joint signal representations," in *Proc. SPIE Conf. on Advanced Algorithms and Architectures for Signal Processing*, San Diego, CA, Aug. 1997.

[4] M. Amin and A. Belouchrani, "Blind source separation using the spatial ambiguity functions," in *Proc. IEEE Int. Symp. on Time-Frequency and Time-Scale Analysis*, Pittsburgh, PA, pp. 413-416, Oct. 1998.

[5] M. Amin and A. Belouchrani, "Time-frequency MUSIC: an array signal processing method based on time-frequency signal representation," in *Proc. SPIE Conf. on Radar Processing, Technology and Applications*, San Diego, CA, pp. 186-194, July 1997.

[6] S. U. Pillai, *Array Signal Processing*, Springer-Verlog, 1989.

[7] L. Cohen, *Time-frequency Analysis*, Prentice Hall, 1995.

[8] L. Tong, Y. Inouye, and R-W. Liu, "Waveform-preserving blind estimation of multiple independent sources," *IEEE Trans. Signal Processing*, vol, 41, no. 7, pp. 2461-2470, July 1993.

[9] A. Belouchrani, K. A. Meraim, H.-F. Cardoso, and E. Muylines, "A blind source separation techniques using second order statistics," *IEEE Trans. Signal Processing*, vol. 45, no. 2, pp. 434-444, Feb. 1997.

[10] H. I. Choi and W. J. Williams, "Improved time-frequency representation of multicomponent signals using exponential kernels," *IEEE Trans. Acoust., Speech, Signal Processing*, vol. 37, no. 6, pp. 862-871, June 1989.

[11] P. Stoica and K. Sharman, "Maximum likelihood methods for direction-of-arrival estimation," *IEEE Trans. Acoust., Speech, Signal Processing*, vol. 38, no. 7, pp. 1132-1143, July 1990.

[12] R. O. Schmidt, "Multiple emitter location and signal parameter estimation," *IEEE Trans. Antennas Propagat.*, vol. 34, no. 3, pp. 276-280, March 1986.

[13] R. Roy and T. Kailath, "ESPRIT – estimation of signal parameters via rotational invariance techniques," *IEEE Trans. Acoust., Speech, Signal Processing*, vol. 37, no. 7, pp. 984-995, July 1989.

[14] A. J. Weiss and B. Friedlander, "Direction finding via joint diagonalization," in *Proc. 8th IEEE Signal Processing Workshop on Statistical Signal and Array Processing*, Corfu, Greece, pp. 66-69, June 1996.

[15] J. E. Evans, J. R. Johnson, D. F. Sun, "High resolution angular spectrum estimation techniques for terrain scattering analysis and angle of arrival estimation," in *Proc. 1st ASSP Workshop on Spectral Estimation*, Hamilton, Canada, Aug. 1981.

[16] T. J. Shan and T. Kailath, "On spatial smoothing for DOA estimation of coherent sources," *IEEE Trans. Acoust., Speech, Signal Processing*, vol. 33, no. 4, pp. 806-811, 1985.

[17] R. T. Williams, S. Prasad, A. K. Mahalanabis, and L. H. Sibul, "An improved spatial smoothing technique for bearing estimation in multipath environment," *IEEE Trans. Acoust., Speech, Signal Processing*, vol. 36, no. 4, pp. 425-432, 1988.

[18] S. U. Pillai and B. H. Kwon, "Forward/backward spatial smoothing techniques for coherent signal identification," *IEEE Trans. Acoust., Speech, Signal Processing*, vol. 37, no. 1, pp. 8-15, Jan. 1989.

[19] S. U. Pillai, Y. Barness, and F. Haber, "A new approach to array geometry for improved spatial spectrum estimation," *Proc. IEEE*, vol. 73, pp. 1522-1524, Oct. 1985.

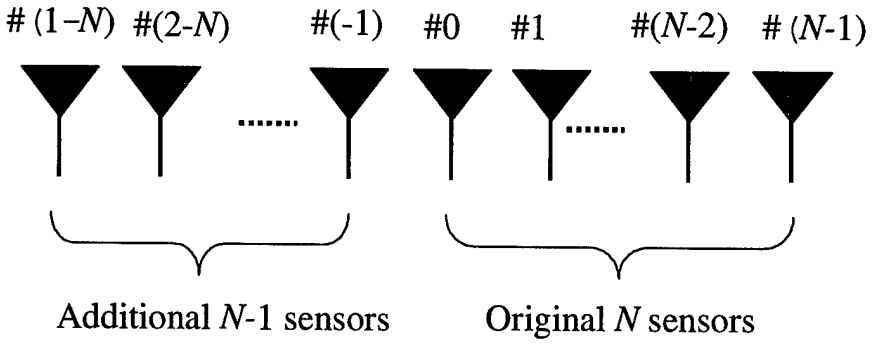

Fig.1 Array configuration for spatial averaging

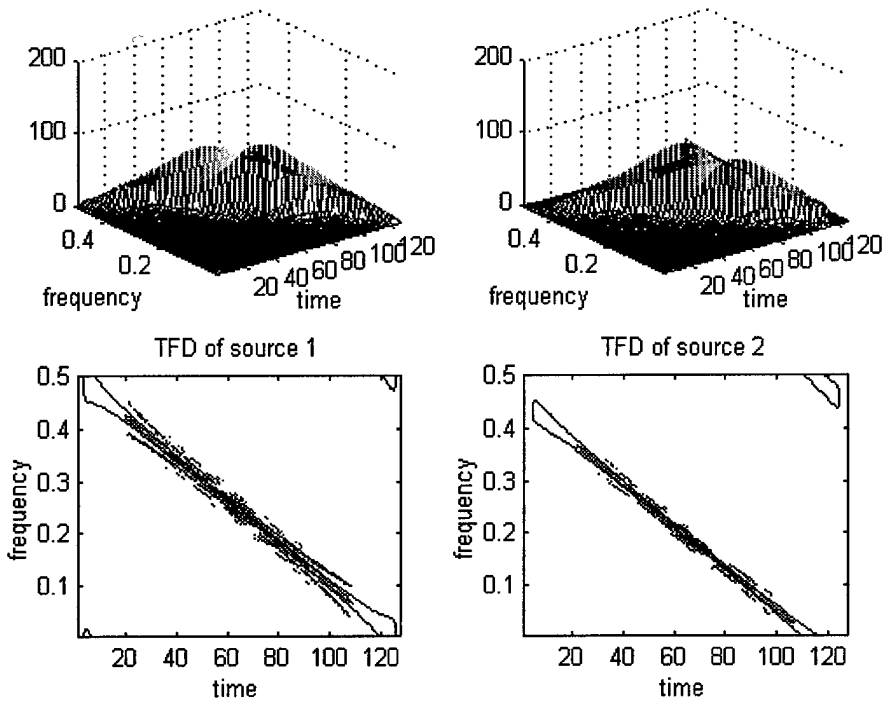

Fig.2 TFD of the source signals (Wigner-Ville distribution)

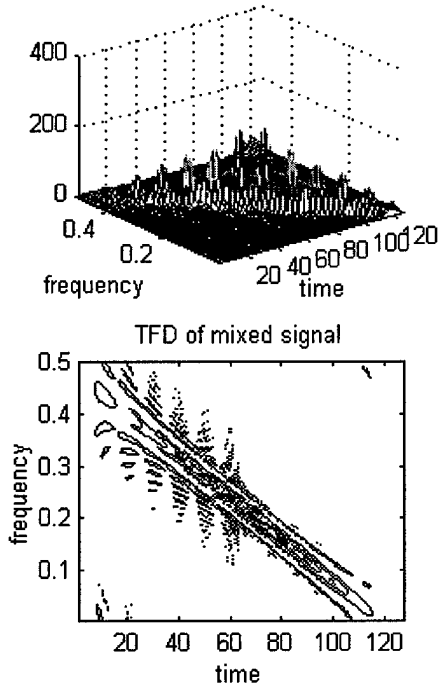

Fig.3 TFD of the mixed signal (Wigner-Ville distribution)

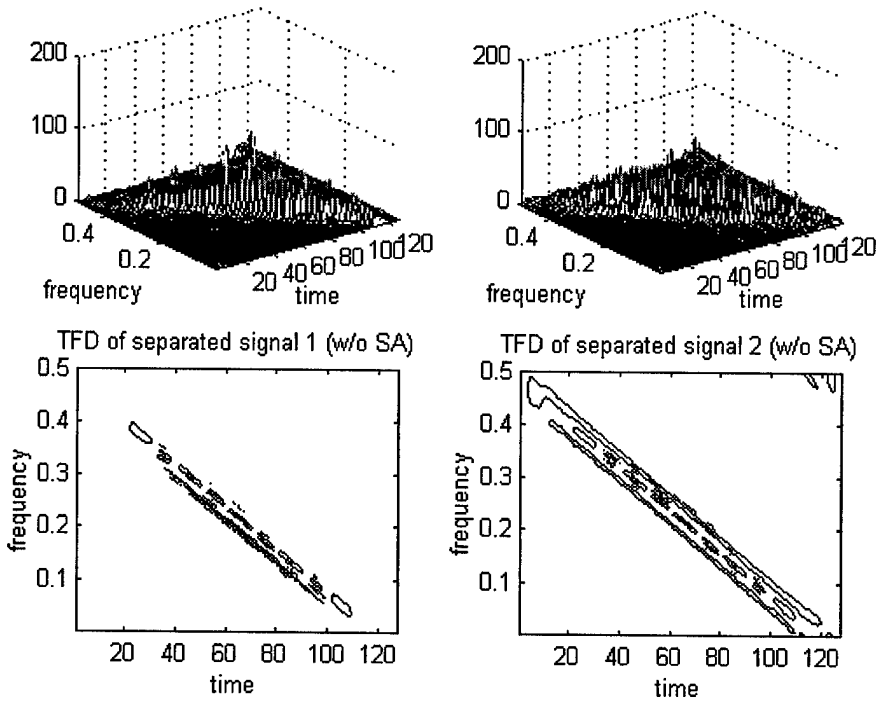

(a) Using peak time-frequency points

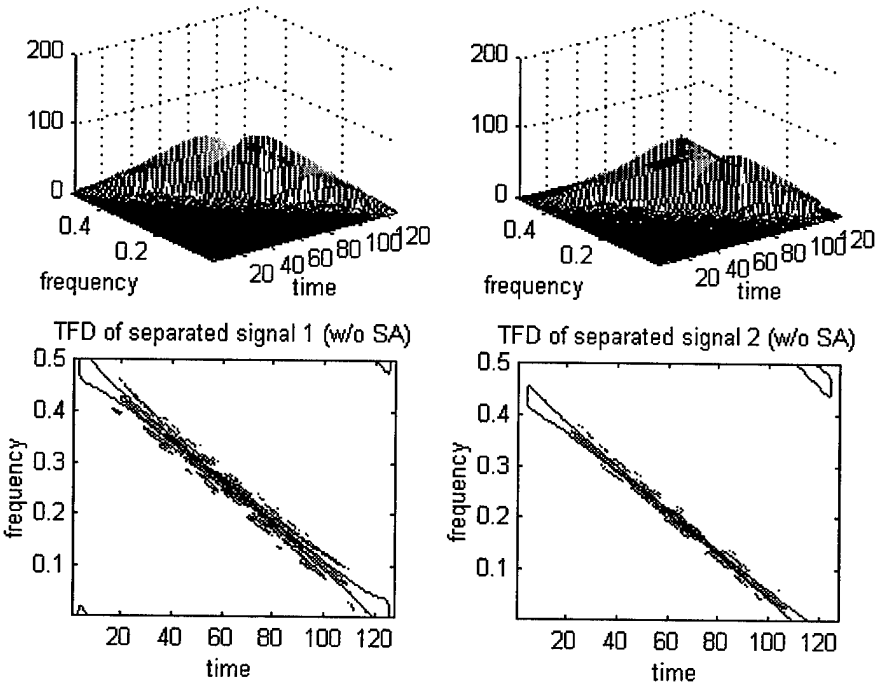

(b) Using autoterm points

Fig.4 TFD of the separated signals without spatial averaging (Wigner-Ville distribution)

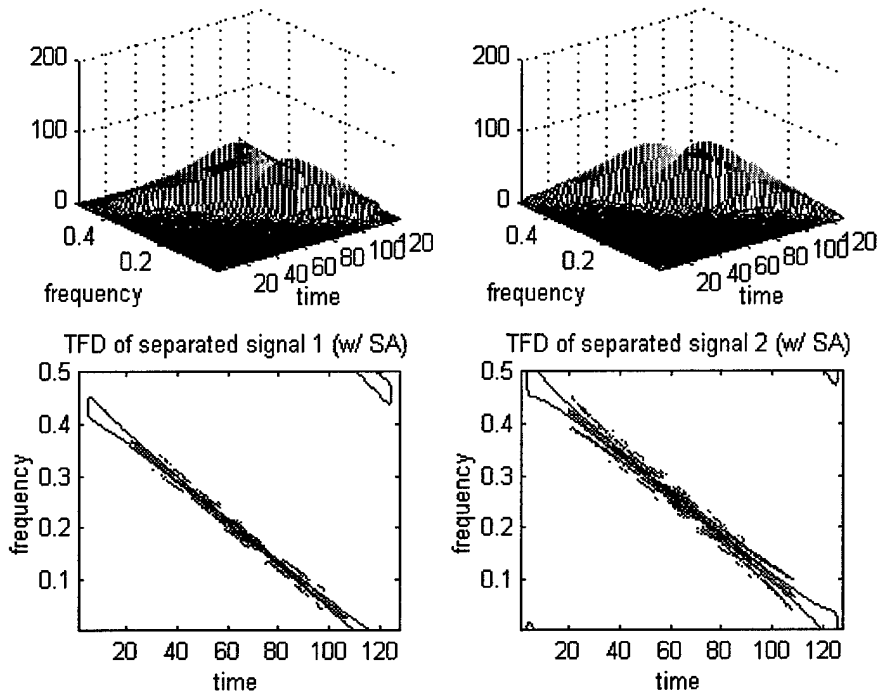

Fig.5 TFD of the separated signals with spatial averaging (Wigner-Ville distribution)

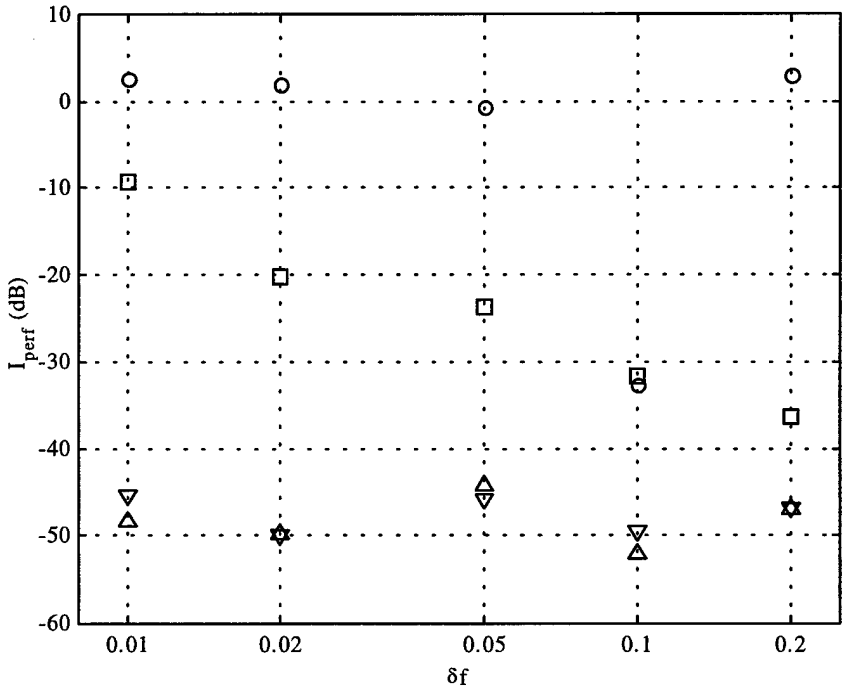

Fig.6 Global rejection level versus frequency difference δf (Wigner-Ville distribution)
(input SNR=20 dB, o: without spatial averaging, Δ: with spatial averaging,
□: without spatial averaging using autoterm points, ∇ : with spatial averaging using autoterm points)

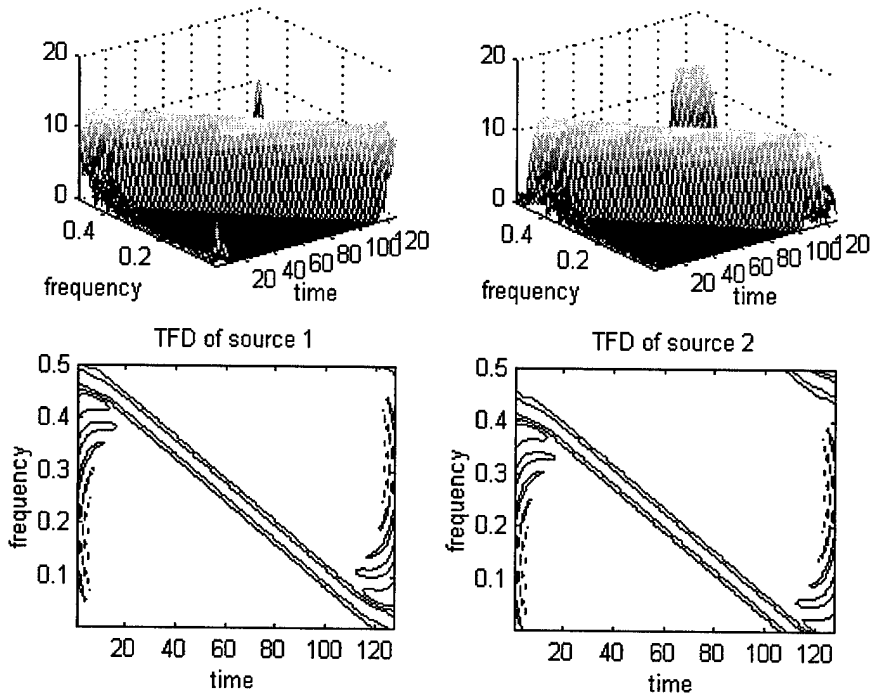

Fig.7 TFD of the source signals (Choi-Williams distribution)

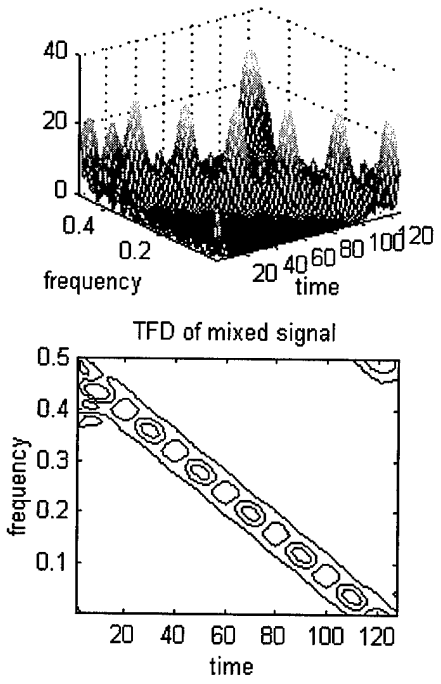

Fig.8 TFD of the mixed signal (Choi-Williams distribution)

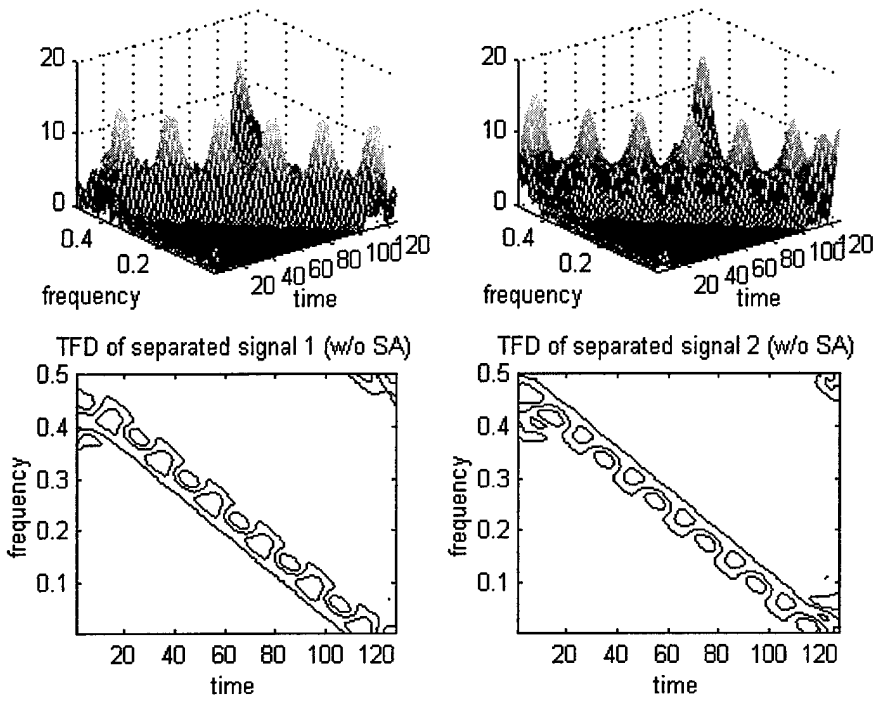

(a) Using peak time-frequency points

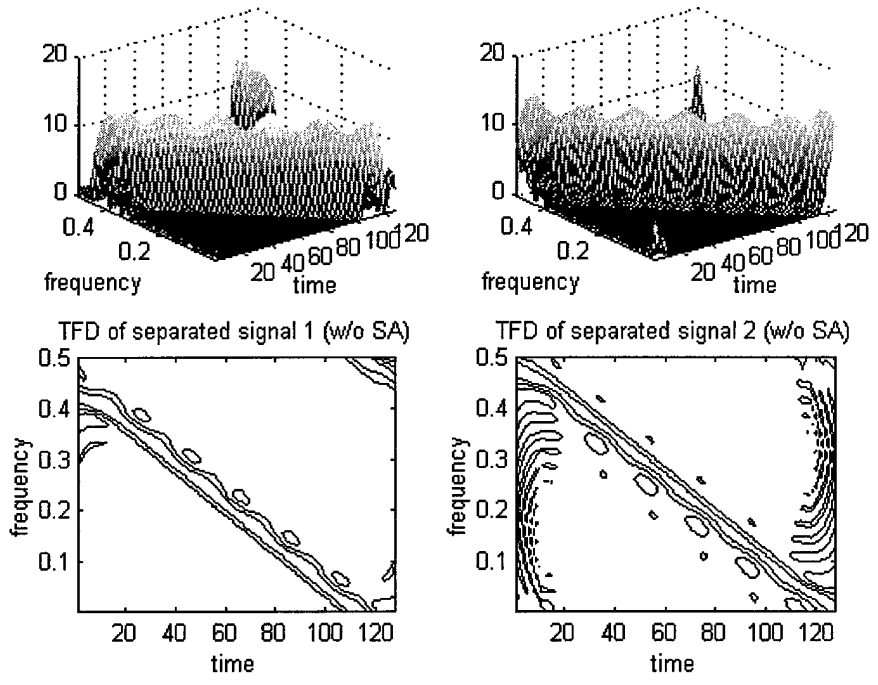

(b) Using autoterm points

Fig.9 TFD of the separated signals without spatial averaging (Choi-Williams distribution)

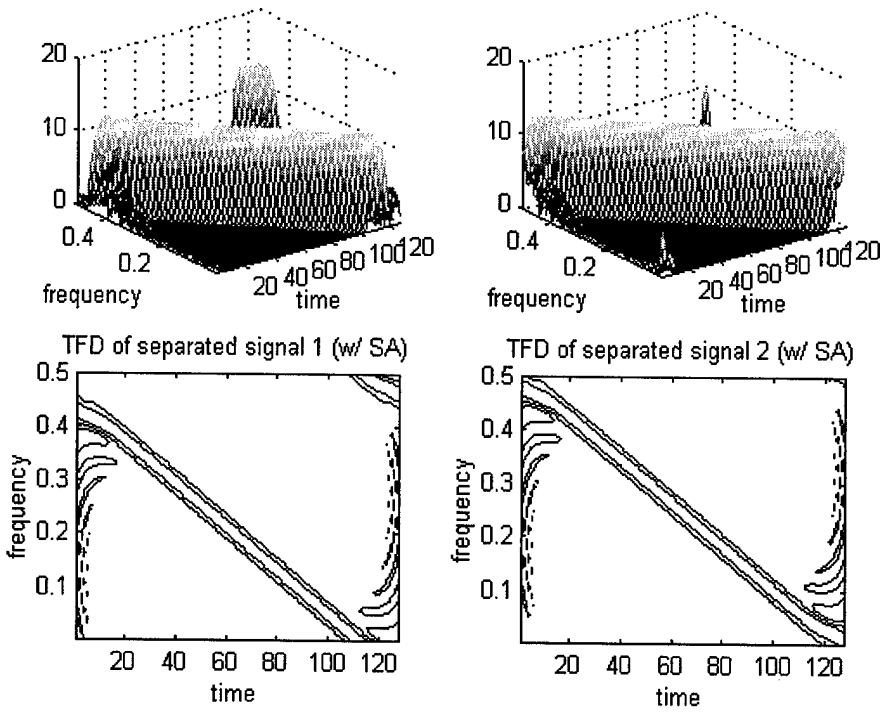

Fig.10 TFD of the separated signals with spatial averaging (Choi-Williams distribution)

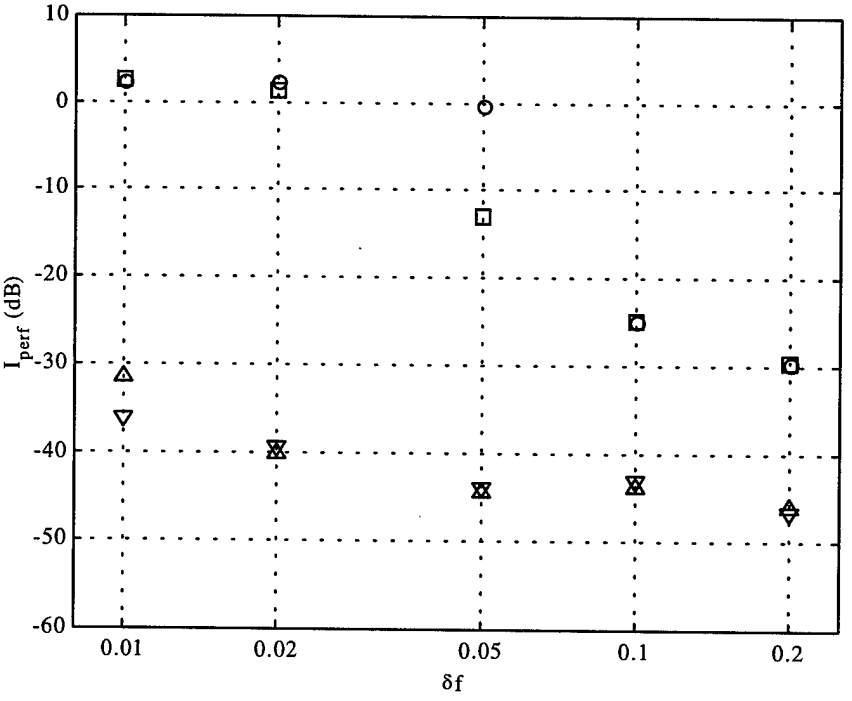

Fig.11 Global rejection level versus frequency difference δf (Choi-Williams distribution)
(input SNR=20 dB, o: without spatial averaging, Δ: with spatial averaging,
□: without spatial averaging using autoterm points, ∇ : with spatial averaging using autoterm points)

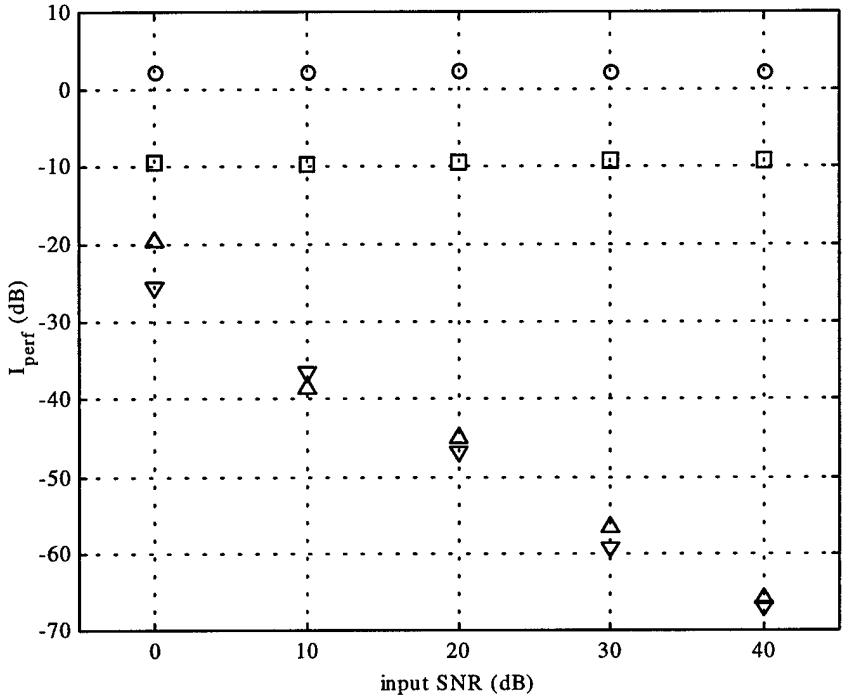

Fig.12 Global rejection level versus input SNR (Wigner-Ville distribution)
(δf=0.01, o: without spatial averaging, Δ: with spatial averaging,
□: without spatial averaging using autoterm points, ∇ : with spatial averaging using autoterm points)

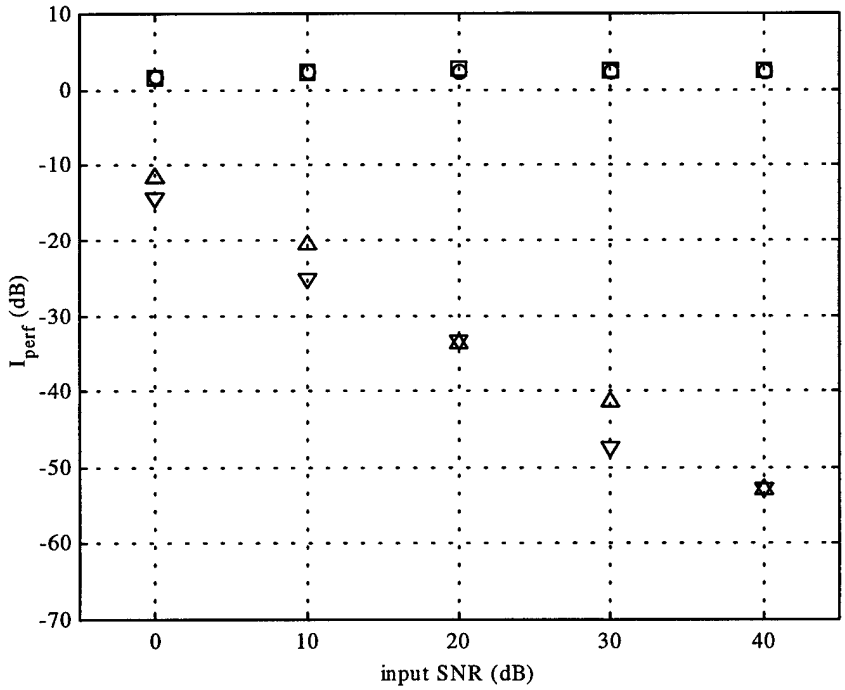

Fig.13 Global rejection level versus input SNR (Choi-Williams distribution)
(δf=0.01, o: without spatial averaging, Δ: with spatial averaging,
□: without spatial averaging using autoterm points, ∇ : with spatial averaging using autoterm points)

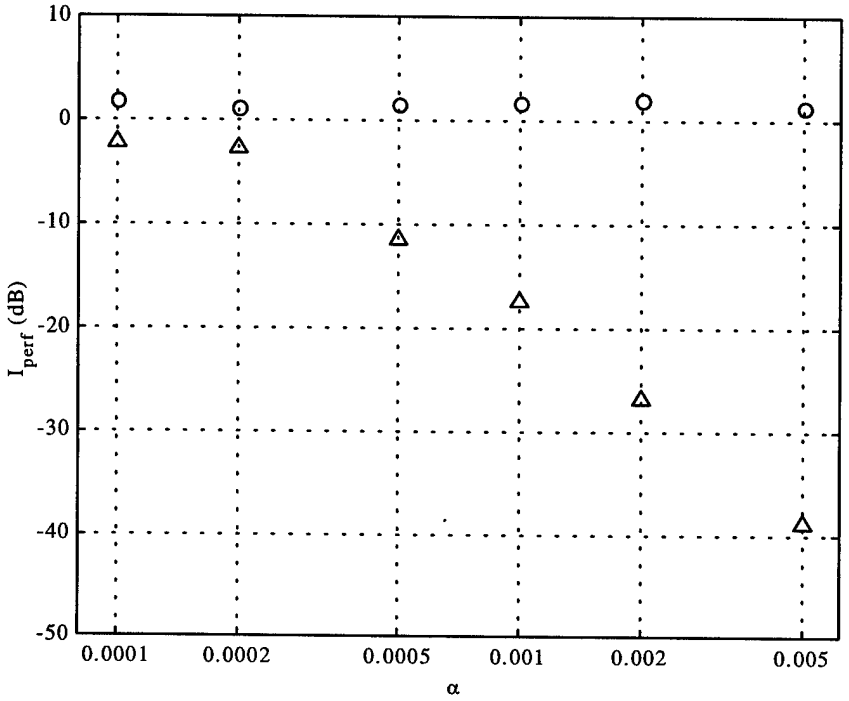

Fig.14 Global rejection level versus α (Wigner-Ville distribution)
(input SNR=20 dB, o: without spatial averaging, Δ: with spatial averaging)

Subspace Analysis of Spatial Time-Frequency Distribution Matrices

Yimin Zhang, Weifeng Mu, and Moeness G. Amin*

Department of Electrical and Computer Engineering,

Villanova University, Villanova, PA 19085

Phone: (610)519-7305 Fax: (610)519-4436

E-mail: moeness@ece.vill.edu

Abstract

Spatial time-frequency distributions (STFDs) have been recently introduced as the natural means to deal with source signals that are localizable in the time-frequency domain. Previous work in the area has not provided the eigen analysis of STFD matrices which is key to understand their role in solving direction finding and blind source separation problems for multi-sensor array receivers. This paper examines the eigenstructure of the spatial time-frequency distribution matrices and develops the analysis and statistical properties of the subspace estimates based on STFDs. It is shown that improved estimates of the signal and noise subspaces are achieved by constructing the subspaces from the time-frequency signatures of the signal arrivals rather than from the data covariance matrices, which is commonly used in conventional subspace estimation methods. This improvement is clearly evident in low signal-to-noise ratio (SNR) environment and in the cases of closely spaced sources. The paper considers the MUSIC technique to demonstrate the advantages of STFDs and uses it as grounds for comparison between time-frequency and conventional subspace estimates.

Keywords

Time-frequency distribution, subspace analysis, time-frequency MUSIC, spatial time-frequency distribution, array signal processing.

Permission to publish this abstract separately is granted.

EDIS: 2.TIFR

* Corresponding author

This work is supported by ONR under Grant #N00014-98-1-0176.

I. Introduction

While time-frequency distributions have been sought out and successfully used in the areas of speech, biomedicine, automotive industry, and machine monitoring, their use in sensor and spatial signal processing has not been properly investigated. The evaluation of quadratic time frequency distributions of the data snapshots across the array yields what we have defined as spatial time-frequency distributions (STFDs) [1], [2]. These spatial distributions permit the application of eigenstructure subspace techniques to solving a large class of channel estimation and equalization, blind source separation, and high-resolution direction-of-arrival (DOA) estimation problems. Spatial time-frequency distribution techniques are most appropriate to handle sources of nonstationary waveforms that are localized in the time-frequency domain, or any other domain of a different joint variable signal representations. In the area of blind source separation, the spatial time-frequency distributions allow the separation of Gaussian sources with identical spectral shape, but with different time frequency localization properties, i.e., different signatures in the time-frequency domain. For direction of arrival estimation problems, the construction of the signal and noise subspaces using the source time-frequency signatures improves angular resolution performance.

Although the applications of the spatial time-frequency distributions to blind source separation and DOA problems using multiple antenna arrays in nonstationary environments have been introduced in [1], [3], yet so far there has not been sufficient analysis that explains their offerings and justify their performance. The aim of this paper is to examine the eigenstructure of the spatial time-frequency distribution matrices and provide statistical analysis of their respective signal and noise subspaces. The paper shows that the subspaces obtained from the STFDs are robust to both noise and angular separation of the waveforms incident on the array. This robustness is primarily due to spreading the noise power while localizing the source energy in the time-frequency domain. By forming the STFD matrices from the points residing on the source time-frequency signatures, we in essence, increase the input signal to noise ratio, and hence improve subspace estimates.

This paper is organized as follows. Section II presents the signal model and gives a brief review of the definition and basic properties of the spatial time-frequency distribu-

tions. In Section III, we consider nonstationary environments characterized by frequency-modulation (FM) source signals. The statistical properties of signal and noise subspace estimates for uncorrelated FM signals over the observation period are delineated. In Section IV, we derive the signal and noise subspaces using STFD matrices for the general class of FM signals. We demonstrate the robustness of the STFD-based subspace estimates to both noise and angular source separation compared to those obtained in Section III, using covariance matrices. The analytical results of Sections III and IV are used in Section V to examine the performance of the direction finding MUSIC technique based on the covariance and STFD noise subspace estimates. Numerical simulations are given in Section VI.

II. Background

A. Signal Model

In narrowband array processing, when n signals arrive at an m-element array, the linear data model

$$\mathbf{x}(t) = \mathbf{y}(t) + \mathbf{n}(t) = \mathbf{A}(\boldsymbol{\Theta})\mathbf{d}(t) + \mathbf{n}(t) \tag{1}$$

is commonly assumed, where the $m \times n$ spatial matrix $\mathbf{A}(\boldsymbol{\Theta}) = [\mathbf{a}(\theta_1)...\mathbf{a}(\theta_n)]$ represents the mixing matrix or the steering matrix, and $\mathbf{a}(\theta_i)$ are the steering vectors. Due to the mixture of the signals at each sensor, the elements of the $m \times 1$ data vector $\mathbf{x}(t)$ are multicomponent signals, whereas each source signal $d_i(t)$ of the $n \times 1$ signal vector $\mathbf{d}(t)$ is often a monocomponent signal. $\mathbf{n}(t)$ is an additive noise vector whose elements are modeled as stationary, spatially and temporally white, zero-mean complex random processes, independent of the source signals. That is,

$$E[\mathbf{n}(t+\tau)\mathbf{n}^H(t)] = \sigma\delta(\tau)\mathbf{I} \text{ and } E[\mathbf{n}(t+\tau)\mathbf{n}^T(t)] = \mathbf{0} \text{ for any } \tau \tag{2}$$

where $\delta(\tau)$ is the Kronecker delta function, $\mathbf{I}$ denotes the identity matrix, σ is the noise power at each sensor, superscript ^{H} and ^{T} respectively denote conjugate transpose and transpose, and $E(\cdot)$ is the statistical expectation operator.

In equation (1), it is assumed that the number of sensors is higher than the number of sources, i.e., $m > n$. Further, matrix $\mathbf{A}(\boldsymbol{\Theta})$ is full column rank, which implies that the

steering vectors corresponding to n different angles of arrival are linearly independent. We further assume that the correlation matrix

$$\mathbf{R}_{\mathbf{xx}} = E[\mathbf{x}(t)\mathbf{x}^H(t)] \tag{3}$$

is nonsingular, and the observation period consists of N snapshots with $N > m$.

Under the above assumptions, the correlation matrix is given by

$$\mathbf{R}_{\mathbf{xx}} = E[\mathbf{x}(t)\mathbf{x}^H(t)] = \mathbf{A}(\boldsymbol{\Theta})\mathbf{R}_{\mathbf{dd}}\mathbf{A}^H(\boldsymbol{\Theta}) + \sigma\mathbf{I}, \tag{4}$$

where $\mathbf{R}_{\mathbf{dd}} = E[\mathbf{d}(t)\mathbf{d}^H(t)]$ is the signal correlation matrix. For notational convenience, we drop the argument $\boldsymbol{\Theta}$ in equation (1) and simply use $\mathbf{A}$ instead of $\mathbf{A}(\boldsymbol{\Theta})$. If $\hat{\boldsymbol{\Theta}}$ is an estimate of $\boldsymbol{\Theta}$, then we also use $\hat{\mathbf{A}}$ instead of $\mathbf{A}(\hat{\boldsymbol{\Theta}})$.

Let $\lambda_1 > \lambda_2 > \cdots > \lambda_n > \lambda_{n+1} = \lambda_{n+2} = \cdots = \lambda_m = \sigma$ denote the eigenvalues of $\mathbf{R}_{\mathbf{xx}}$. It is assumed that λ_i, $i = 1, \cdots, n$, are distinct. The unit-norm eigenvectors associated with $\lambda_1, ..., \lambda_n$ constitute the columns of matrix $\mathbf{S} = [\mathbf{s}_1, ..., \mathbf{s}_n]$, and those corresponding to $\lambda_{n+1}, ..., \lambda_m$ make up matrix $\mathbf{G} = [\mathbf{g}_1, ..., \mathbf{g}_{m-n}]$. Since the columns of $\mathbf{A}$ and $\mathbf{S}$ span the same subspace, then $\mathbf{A}^H\mathbf{G} = \mathbf{0}$.

In practice, $\mathbf{R}_{\mathbf{xx}}$ is unknown, and therefore should be estimated from the available data samples (snapshots) $\mathbf{x}(i)$, $i = 1, 2, ..., N$. The estimated correlation matrix is given by

$$\hat{\mathbf{R}}_{\mathbf{xx}} = \frac{1}{N}\sum_{i=1}^{N}\mathbf{x}(i)\mathbf{x}^H(i). \tag{5}$$

Let $\{\hat{\mathbf{s}}_1, ..., \hat{\mathbf{s}}_n, \hat{\mathbf{g}}_1, ..., \hat{\mathbf{g}}_{m-n}\}$ denote the unit-norm eigenvectors of $\hat{\mathbf{R}}_{\mathbf{xx}}$, arranged in the descending order of the associated eigenvalues, and let $\hat{\mathbf{S}}$ and $\hat{\mathbf{G}}$ denote the matrices defined by the set of vectors $\{\hat{\mathbf{s}}_i\}$ and $\{\hat{\mathbf{g}}_i\}$, respectively. The statistical properties of the eigenvectors of the sample covariance matrix $\hat{\mathbf{R}}_{\mathbf{xx}}$ for signals modeled as independent processes with additive white noise is given in [4].

B. Spatial Time-Frequency Distributions

The spatial time-frequency distributions (STFDs) based on Cohen's class of time-frequency distribution were introduced in [1] and its applications to direction finding and blind source separation have been discussed in [3] and [1], respectively. In this paper,

we focus one key member of Cohen's class, namely the pseudo Wigner-Ville distribution (PWVD) [5] and its respective spatial distribution. Only the time-frequency (t-f) points in the autoterm regions of PWVD are considered for STFD matrix construction. In these regions, it is assumed that the crossterms are negligible.

The discrete form of pseudo Wigner-Ville distribution of a signal $x(t)$, using a rectangular window of odd length L, is given by

$$D_{xx}(t,f) = \sum_{\tau=-\frac{L-1}{2}}^{\frac{L-1}{2}} x(t+\tau)x^*(t-\tau)e^{-j4\pi f\tau}, \tag{6}$$

where * denotes complex conjugate. The spatial pseudo Wigner-Ville distribution (SPWVD) matrix is obtained by replacing $x(t)$ by the data snapshot vector $\mathbf{x}(t)$,

$$\mathbf{D_{xx}}(t,f) = \sum_{\tau=-\frac{L-1}{2}}^{\frac{L-1}{2}} \mathbf{x}(t+\tau)\mathbf{x}^H(t-\tau)e^{-j4\pi f\tau}. \tag{7}$$

Substitute (1) into (7), we obtain

$$\begin{aligned} \mathbf{D_{xx}}(t,f) &= \mathbf{D_{yy}}(t,f) + \mathbf{D_{yn}}(t,f) + \mathbf{D_{ny}}(t,f) + \mathbf{D_{nn}}(t,f) \\ &= \mathbf{D_{yy}}(t,f) + 2\mathrm{Re}\left[\mathbf{D_{yn}}(t,f)\right] + \mathbf{D_{nn}}(t,f). \end{aligned} \tag{8}$$

We note that $\mathbf{D_{xx}}(t,f)$, $\mathbf{D_{yy}}(t,f)$, $\mathbf{D_{yn}}(t,f)$, $\mathbf{D_{ny}}(t,f)$, and $\mathbf{D_{nn}}(t,f)$ are matrices of dimension $m \times m$, whereas the source TFD matrix $\mathbf{D_{dd}}(t,f)$ is of dimension $n \times n$. Under the uncorrelated signal and noise assumption and the zero-mean noise property, the expectation of the crossterm TFD matrices between the signal and noise vectors is zero, i.e., $E\left[\mathbf{D_{yn}}(t,f)\right] = E\left[\mathbf{D_{ny}}(t,f)\right] = \mathbf{0}$, and it follows

$$\begin{aligned} E\left[\mathbf{D_{xx}}(t,f)\right] &= \mathbf{D_{yy}}(t,f) + E\left[\mathbf{D_{nn}}(t,f)\right] \\ &= \mathbf{A}\mathbf{D_{dd}}(t,f)\mathbf{A}^H + E\left[\mathbf{D_{nn}}(t,f)\right]. \end{aligned} \tag{9}$$

For narrowband array signal processing applications, the mixing matrix $\mathbf{A}$ holds the spatial information and maps the auto- and cross-TFDs of the source signals into auto- and cross-TFDs of the data.

Equation (9) is similar to that which has been commonly used in DOA estimation and blind source separation problems, relating the signal correlation matrix to the data spatial

correlation matrix. In the above formulation, however, the correlation matrices are replaced by the spatial time-frequency distribution matrices. This implies that key problems in various applications of array processing, specifically those dealing with nonstationary signal environments, can be approached using bilinear transformations.

It is noted that the relationship (9) holds true for every (t, f) points. In order to reduce the effect of noise and ensure the full column rank property of the STFD matrix, we consider multiple time-frequency points, instead of a single one. That is, the signal and noise subspaces are constructed using as many (t, f) points in the source autoterm regions as possible. This allows more information of the source signal time-frequency signatures to be included into their respective subspace formulation, and as such enhances direction finding and source separation performance. Joint-diagonalization [6] and time-frequency averaging are the two main approaches that have been used for this purpose [1], [3], [7]. In this paper, however, we only consider averaging over multiple time-frequency points.

III. Subspace Analysis for FM Signals

In this paper, we focus on frequency modulation (FM) signals, modeled as

$$\mathbf{d}(t) = [d_1(t), ..., d_n(t)]^T = [D_1 e^{j\psi_1(t)}, ..., D_n e^{j\psi_n(t)}]^T, \tag{10}$$

where D_i and $\psi_i(t)$ are the fixed amplitude and time-varying phase of ith source signal. For each sampling time t, $d_i(t)$ has an instantaneous frequency $f_i(t) = \frac{1}{2\pi}\frac{d\psi_i(t)}{dt}$.

FM signals are often encountered in applications such as radar and sonar [11]. The consideration of FM signals in this paper is motivated by the fact that these signals are uniquely characterized by their instantaneous frequencies, and therefore, they have clear time-frequency signatures that can be utilized by the STFD approach. Also, FM signals have constant amplitudes and, subsequently, yield time-independent covariance matrices. This property makes them amenable to conventional array processing based on second-order statistics.

To simplify the analysis, we assume that the FM signals are mutually uncorrelated over the observation period. That is,

$$\frac{1}{N}\sum_{k=1}^{N} d_i(k) d_j^*(k) = 0 \qquad \text{for } i \neq j,\ i, j = 1, ..., n. \tag{11}$$

In this case, the signal correlation matrix in (4) is

$$\mathbf{R_{dd}} = diag\left[D_i^2,\ i = 1, 2, ..., n\right]$$

where $diag[\cdot]$ is the diagonal matrix formed with the elements of its vector valued arguments.

From the above assumptions, we have the following Lemma.

Lemma 1: For uncorrelated FM signals with white additive noise,

a) The estimated errors $(\hat{\mathbf{s}}_i - \mathbf{s}_i)$ are asymptotically (for large N) jointly Gaussian distributed with zero means and covariance matrices given by (see Appendix A)

$$\begin{aligned} &E\left[(\hat{\mathbf{s}}_i - \mathbf{s}_i)(\hat{\mathbf{s}}_j - \mathbf{s}_j)^H\right] \\ &= \frac{\sigma}{N}\left[\sum_{\substack{k=1 \\ k\neq i}}^{n} \frac{\lambda_i + \lambda_k - \sigma}{(\lambda_k - \lambda_i)^2}\mathbf{s}_k\mathbf{s}_k^H + \sum_{k=1}^{m-n} \frac{\lambda_i}{(\sigma - \lambda_i)^2}\mathbf{g}_k\mathbf{g}_k^H\right]\delta_{i,j} \triangleq \mathbf{W}_i'\delta_{i,j}, \end{aligned} \tag{12}$$

$$E\left[(\hat{\mathbf{s}}_i - \mathbf{s}_i)(\hat{\mathbf{s}}_j - \mathbf{s}_j)^T\right] = -\frac{\sigma}{N}\frac{(\lambda_i + \lambda_j - \sigma)}{(\lambda_j - \lambda_i)^2}\mathbf{s}_j\mathbf{s}_i^T(1 - \delta_{i,j}) \triangleq \mathbf{V}_{i,j}'. \tag{13}$$

b) The orthogonal projections of $\{\hat{\mathbf{g}}_i\}$ onto the column space of $\mathbf{S}$ are asymptotically (for large N) jointly Gaussian distributed with zero means and covariance matrices given by

$$E\left[\left(\mathbf{S}\mathbf{S}^H\hat{\mathbf{g}}_i\right)\left(\mathbf{S}\mathbf{S}^H\hat{\mathbf{g}}_j\right)^H\right] = \frac{\sigma}{N}\left[\sum_{k=1}^{n}\frac{\lambda_k}{(\sigma - \lambda_k)^2}\mathbf{s}_k\mathbf{s}_k^H\right]\delta_{i,j} \triangleq \frac{1}{N}\mathbf{U}'\delta_{i,j}, \tag{14}$$

$$E\left[\left(\mathbf{S}\mathbf{S}^H\hat{\mathbf{g}}_i\right)\left(\mathbf{S}\mathbf{S}^H\hat{\mathbf{g}}_j\right)^T\right] = 0 \ \text{ for all } i,\ j. \tag{15}$$

Equations (12) and (13) are similar to those of [4]. The only difference is that the term $(\lambda_i\lambda_k)$ in equations (3.8a) and (3.8b) in reference [4] is replaced by $\sigma(\lambda_i + \lambda_k - \sigma)$ in (12) and (13), due to the uncorrelation property (11). Accordingly, for high input SNR $(\lambda_k \gg \sigma, k = 1, 2, ..., n)$, the estimated error of $(\hat{\mathbf{s}}_i - \mathbf{s}_i)$ can be greatly reduced. From (12) and (13), each column of the signal subspace will be perfectly estimated when $\sigma = 0$. This is in contrast with the estimation error that would result under the same noise-free condition, if we use the temporally-independent signal characteristics considered in [4].

Equations (14) and (15) are identical to (3.9) and (3.10) derived in reference [4]. The reason of such identity is that, despite the difference in the eigenvectors, the signal subspaces in both cases are the same, defined by the mixing matrix **A**. Accordingly, the projection of the estimated noise subspace basis vectors on the true signal subspace for both FM signals and white random processes yield equal results.

IV. Subspace Analysis for STFD Matrices

The purpose of this section is to show that the signal and noise subspaces based on time-frequency distributions for nonstationary signals are more robust than those obtained from conventional array processing.

A. SNR Enhancement

The time-frequency distribution (TFD) maps one-dimensional signals in the time domain into two-dimensional signals in the time-frequency domain. The TFD property of concentrating the input signal around its instantaneous frequency (IF), while spreading the noise over the entire time-frequency domain increases the effective SNR and proves valuable in the underlying problem.

The ith diagonal element of TFD matrix $\mathbf{D_{dd}}(t,f)$ is given by

$$D_{d_i d_i}(t,f) = \sum_{\tau=-\frac{L-1}{2}}^{\frac{L-1}{2}} D_i^2 e^{j[\psi_i(t+\tau)-\psi_i(t-\tau)]-j4\pi f\tau}. \tag{16}$$

Assume that the third-order derivative of the phase is negligible over the window length L, then along the true time-frequency points of ith signal, $f_i = \frac{1}{2\pi}\frac{d\psi_i(t)}{dt}$, and $\psi_i(t+\tau) - \psi_i(t-\tau) - 4\pi f_i\tau = 0$. Accordingly,

$$D_{d_i d_i}(t,f_i) = \sum_{\tau=-\frac{L-1}{2}}^{\frac{L-1}{2}} D_i^2 = LD_i^2. \tag{17}$$

Similarly, the noise STFD matrix $\mathbf{D_{nn}}(t,f)$ is

$$\mathbf{D_{nn}}(t,f) = \sum_{\tau=-\frac{L-1}{2}}^{\frac{L-1}{2}} \mathbf{n}(t+\tau)\mathbf{n}^H(t-\tau)e^{-j4\pi f\tau}. \tag{18}$$

Under the spatial white and temporal white assumptions, the statistical expectation of $\mathbf{D}_{\mathbf{nn}}(t,f)$ is given by

$$E\left[\mathbf{D}_{\mathbf{nn}}(t,f)\right] = \sum_{\tau=-\frac{L-1}{2}}^{\frac{L-1}{2}} E\left[\mathbf{n}(t+\tau)\mathbf{n}^H(t-\tau)\right] e^{-j4\pi f\tau} = \sigma\mathbf{I}. \tag{19}$$

Therefore, when we select the time-frequency points along the time-frequency signature or the IF of an FM signal, the SNR in model (9) is LD_i^2/σ, which has an improved factor L over the one associated with model (4).

The pseudo Wigner-Ville distribution of each FM source has a constant value over the observation period, providing that we leave out the rising and falling power distributions at both ends of the data record. For convenience of analysis, we select those $N-L+1$ time-frequency points of constant distribution value for each source signal. Therefore, the averaged STFD over the time-frequency signatures of n_o sources, i.e., a total of $n_o(N-L+1)$ time-frequency points, is given by

$$\hat{\mathbf{D}} = \frac{1}{n_o(N-L+1)} \sum_{q=1}^{n_o} \sum_{i=1}^{N-L+1} \mathbf{D}_{\mathbf{xx}}(t_i, f_{q,i}), \tag{20}$$

where $f_{q,i}$ is the instantaneous frequency of the qth signal at the ith time sample. The expectation of the averaged STFD matrix is

$$\begin{aligned} \mathbf{D} &= E\left[\hat{\mathbf{D}}\right] = \frac{1}{n_o(N-L+1)} \sum_{q=1}^{n_o} \sum_{i=1}^{N-L+1} E\left[\mathbf{D}_{\mathbf{xx}}(t_i, f_{q,i})\right] \\ &= \frac{1}{n_o} \sum_{p=1}^{n_o} \left[LD_p^2 \mathbf{a}(\theta_p)\mathbf{a}^H(\theta_p) + \sigma\mathbf{I}\right] = \frac{L}{n_o} \mathbf{A}^o \mathbf{R}_{\mathbf{dd}}^o (\mathbf{A}^o)^H + \sigma\mathbf{I}, \end{aligned} \tag{21}$$

where $\mathbf{R}_{\mathbf{dd}}^o$ and $\mathbf{A}^o$, respectively, represent the signal correlation matrix and the mixing matrix formulated by only considering n_o signals out of the total number of signal arrivals n.

It is clear from (21) that the SNR improvement $G = L/n_o$ (we assume $L > n_o$ throughout this paper) is inversely proportional to the number of sources contributing matrix $\mathbf{D}$. Therefore, from the SNR perspective, it is best to set $n_o = 1$, i.e., to select the sets of $N-L+1$ (t,f) points that belong to individual signals one set at a time, and then separately evaluate the respective STFD matrices.

This procedure is made possible by the fact that STFD-based direction finding is, in essence, a discriminatory technique in the sense that it does not require simultaneous

localization and extraction of all unknown signals received by the array. With STFDs, direction finding can be performed using STFDs of a subclass of the impinging signals with specific time-frequency signatures. In this respect, the proposed direction finding technique acts as a spatial filter, removing all other signals from consideration and, subsequently, saves any downstream processing that is required to separate interference and signals of interest. It is also important to note that with the ability to construct the STFD matrix from one or few signal arrivals, the well known $m > n$ condition on source localization using arrays can be relaxed, i.e., we can perform direction finding or source separation with the number of array sensors smaller than the number of impinging signals [2]. From the angular resolution perspective, closely spaced sources with different time-frequency signatures can be resolved by constructing two separate STFDs, each corresponds to one source, and then proceed with subspace decomposition for each STFD matrix, followed by an appropriate source localization method (MUSIC, for example). The drawback of performing several direction finding using different STFD matrices is of course the need for repeated computations of eigen-decompositions and source localizations.

In all the analysis and simulations provided herein, when considering STFDs, we only use those (t, f) points on the signal time-frequency signatures. In case of FM signals, we choose the (t, f) points along the signal IFs.

B. Signal and Noise Subspaces Using STFDs

The following Lemma provides the relationship between the eigen-decompositions of the STFD matrices and the data covariance matrices used in conventional array processing.

Lemma 2: Let $\lambda_1^o > \lambda_2^o > \cdots > \lambda_{n_o}^o > \lambda_{n_o+1}^o = \lambda_{n_o+2}^o = \cdots = \lambda_m^o = \sigma$ denote the eigenvalues of $\mathbf{R}_{\mathbf{xx}}^o$, which is defined from a data record of a mixture of the n_o selected FM signals. Denote the unit-norm eigenvectors associated with $\lambda_1^o, ..., \lambda_{n_o}^o$ by the columns of $\mathbf{S}^o = [\mathbf{s}_1^o, ..., \mathbf{s}_{n_o}^o]$, and those corresponding to $\lambda_{n_o+1}^o, ..., \lambda_m^o$ by the columns of $\mathbf{G}^o = [\mathbf{g}_1^o, ..., \mathbf{g}_{m-n_o}^o]$. We also denote $\lambda_1^{tf} > \lambda_2^{tf} > \cdots > \lambda_{n_o}^{tf} > \lambda_{n_o+1}^{tf} = \lambda_{n_o+2}^{tf} = \cdots = \lambda_m^{tf} = \sigma^{tf}$ as the eigenvalues of $\mathbf{D}$ defined in (21). The unit-norm eigenvectors associated with $\lambda_1^{tf}, ..., \lambda_{n_o}^{tf}$ are represented by the columns of $\mathbf{S}^{tf} = [\mathbf{s}_1^{tf}, ..., \mathbf{s}_{n_o}^{tf}]$, and those corresponding to $\lambda_{n_o+1}^{tf}, ..., \lambda_m^{tf}$ are represented by the columns of $\mathbf{G}^{tf} = [\mathbf{g}_1^{tf}, ..., \mathbf{g}_{m-n_o}^{tf}]$. Then,

a) The signal and noise subspaces of $\mathbf{S}^{tf}$ and $\mathbf{G}^{tf}$ are the same as $\mathbf{S}^o$ and $\mathbf{G}^o$, respectively.

b) The eigenvalues have the following relationship:

$$\lambda_i^{tf} = \begin{cases} \frac{L}{n_o}(\lambda_i^o - \sigma) + \sigma = \frac{L}{n_o}\lambda_i^o + \left(1 - \frac{L}{n_o}\right)\sigma & i \le n_o \\ \sigma^{tf} = \sigma & n_o < i \le m. \end{cases} \tag{22}$$

Both parts of the above equations are direct results of (21).

An important conclusion from Lemma 2 is that, the largest n_o eigenvalues are amplified using STFD analysis. Fig. 1 shows the eigenvalues λ_i^o and λ_i^{tf} (for $L = 33$ and $L = 129$), where a uniform linear array of 8 sensors ($m = 8$) separated by half a wavelength and receiving signal from 2 sources ($n_o = n = 2$) is used. The two signals are of equal power($D_1 = D_2 = D$), and their angular separation $\Delta\theta$ is defined as $\theta_2 - \theta_1$. We choose $\theta_1 + \theta_2 = 0$, that is, the two signals are symmetric with respect to the broadside direction. Denote

$$\beta = \frac{\mathbf{a}^H(\theta_1)\mathbf{a}(\theta_2)}{[||\mathbf{a}(\theta_1)||\mathbf{a}(\theta_2)||]^{1/2}}$$

as the spatial correlation coefficient between angles θ_1 and θ_2 where $|\mathbf{a}|$ is the norm of a vector $\mathbf{a}$. The two largest eigenvalues for uncorrelated signals are given by [10]

$$\lambda_{1,2}^o = mD^2\left[1 \pm |\beta|\right] + \sigma \qquad \lambda_{1,2}^{tf} = \frac{mL}{n_o}D^2\left[1 \pm |\beta|\right] + \sigma. \tag{23}$$

The amplification of the largest n_o eigenvalues improves detection of the number of the impinging signals on the array, as it widens the separation between dominant and noise-level eigenvalues. Determination of the number of signals is key to establishing the proper signal and noise subspaces, and subsequently plays a fundamental role in subspace-based applications [13]. When the input SNR is low, or the signals are closely spaced, the number of signals may often be underdetermined. Fig. 2 shows, for the same signal scenario of Fig. 1, the threshold level of the input SNR required to determine the correct number of signals $\hat{n} = 2$ according to the Akaike Information Criterion (AIC) [14]

$$\min_{\hat{n}} N(m - \hat{n})log\left(\frac{f_1\hat{n}}{f_2\hat{n}}\right) + f_3(\hat{n}), \tag{24}$$

where

$$f_1(\hat{n}) \triangleq \frac{1}{m - \hat{n}}\sum_{i=\hat{n}+1}^{m}\lambda_i, \quad f_2(\hat{n}) \triangleq \left(\prod_{i=\hat{n}+1}^{m}\lambda_i\right)^{\frac{1}{m-\hat{n}}}, \quad f_3(\hat{n}) \triangleq \hat{n}(2m - \hat{n}). \tag{25}$$

It is clear from Fig. 2 that, when the STFD is applied, the SNR threshold level necessary for the correct determination of the number of signals is greatly reduced.

Next we consider the signal and noise subspace estimates from a finite number of data samples. When we form the STFD matrix based on the true (t, f) points along the n_o FM signals, if we assume that their third-order derivatives are negligibly small during each window, we have the following Lemma.

Lemma 3: If the third-order derivative of the phase of the FM signals is negligible over the time-period $[t-L+1, t+L-1]$, then

a) The estimated errors in the signal vectors are asymptotically (for $N \gg L$) jointly Gaussian distributed with zero means and covariance matrices given by

$$\begin{aligned} & E\left(\hat{\mathbf{s}}_i^{tf}-\mathbf{s}_i^{tf}\right)\left(\hat{\mathbf{s}}_j^{tf}-\mathbf{s}_j^{tf}\right)^H \\ & =\frac{\sigma L}{n_o(N-L+1)}\left[\sum_{\substack{k=1 \\ k\neq i}}^{n_o}\frac{\lambda_i^{tf}+\lambda_k^{tf}-\sigma}{(\lambda_k^{tf}-\lambda_i^{tf})^2}\mathbf{s}_k^{tf}\left(\mathbf{s}_k^{tf}\right)^H+\sum_{k=1}^{m-n_o}\frac{\lambda_i^{tf}}{(\sigma-\lambda_i^{tf})^2}\mathbf{g}_k^{tf}\left(\mathbf{g}_k^{tf}\right)^H\right]\delta_{i,j} \qquad (26) \\ & \triangleq \mathbf{W}_i^{tf}\delta_{i,j}, \end{aligned}$$

$$\begin{aligned} & E\left(\hat{\mathbf{s}}_i^{tf}-\mathbf{s}_i^{tf}\right)\left(\hat{\mathbf{s}}_j^{tf}-\mathbf{s}_j^{tf}\right)^T \\ & =-\frac{\sigma L}{n_o(N-L+1)}\frac{(\lambda_i^{tf}+\lambda_j^{tf}-\sigma)}{(\lambda_j^{tf}-\lambda_i^{tf})^2}\mathbf{s}_j^{tf}\left(\mathbf{s}_i^{tf}\right)^T(1-\delta_{i,j}) \triangleq \mathbf{V}_{i,j}^{tf}. \end{aligned} \qquad (27)$$

b) The orthogonal projections of $\left\{\hat{\mathbf{g}}_i^{tf}\right\}$ onto the column space of $\mathbf{S}^{tf}$ are asymptotically (for $N \gg L$) jointly Gaussian distributed with zero means and covariance matrices given by

$$\begin{aligned} & E\left(\mathbf{S}^{tf}\left(\mathbf{S}^{tf}\right)^H\hat{\mathbf{g}}_i^{tf}\right)\left(\mathbf{S}^{tf}\left(\mathbf{S}^{tf}\right)^H\hat{\mathbf{g}}_j^{tf}\right)^H \\ & =\frac{\sigma L}{n_o(N-L+1)}\left[\sum_{k=1}^{n_o}\frac{\lambda_k^{tf}}{(\sigma-\lambda_k^{tf})^2}\mathbf{s}_k^{tf}\left(\mathbf{s}_k^{tf}\right)^H\right]\delta_{i,j} \triangleq \frac{1}{(N-L+1)}\mathbf{U}^{tf}\delta_{i,j}, \end{aligned} \qquad (28)$$

$$E\left(\mathbf{S}^{tf}\left(\mathbf{S}^{tf}\right)^H\hat{\mathbf{g}}_i^{tf}\right)\left(\mathbf{S}^{tf}\left(\mathbf{S}^{tf}\right)^H\hat{\mathbf{g}}_j^{tf}\right)^T=\mathbf{0} \text{ for all } i,\ j. \qquad (29)$$

The proof of (26)-(27) is given in Appendix B, and the proof of (28)-(29) is given in Appendix C.

To demonstrate the performance advantage of using STFDs, we substitute (22) into (26)-(28),

$$
\begin{aligned}
&E\left(\hat{\mathbf{s}}_i^{tf}-\mathbf{s}_i^{tf}\right)\left(\hat{\mathbf{s}}_j^{tf}-\mathbf{s}_j^{tf}\right)^H \\
&=\frac{\sigma}{N-L+1}\times \\
&\left[\sum_{\substack{k=1\\k\neq i}}^{n_o}\frac{(\lambda_i^o-\sigma)+(\lambda_k^o-\sigma)+\frac{n_o}{L}\sigma}{(\lambda_k^o-\lambda_i^o)^2}\mathbf{s}_k^o\left(\mathbf{s}_k^o\right)^H+\sum_{k=1}^{m-n_o}\frac{(\lambda_i^o-\sigma)+\frac{n_o}{L}\sigma}{(\sigma-\lambda_i^o)^2}\mathbf{g}_k^o\left(\mathbf{g}_k^o\right)^H\right]\delta_{i,j},
\end{aligned}
\tag{30}
$$

$$
\begin{aligned}
&E\left(\hat{\mathbf{s}}_i^{tf}-\mathbf{s}_i^{tf}\right)\left(\hat{\mathbf{s}}_j^{tf}-\mathbf{s}_j^{tf}\right)^T \\
&=-\frac{\sigma}{N-L+1}\frac{(\lambda_k^o-\sigma)+(\lambda_i^o-\sigma)+\frac{n_o}{L}\sigma}{(\lambda_k^o-\lambda_i^o)^2}\mathbf{s}_j^o\left(\mathbf{s}_i^o\right)^T(1-\delta_{i,j}),
\end{aligned}
\tag{31}
$$

and

$$
\begin{aligned}
&E\left(\mathbf{S}^{tf}\left(\mathbf{S}^{tf}\right)^H\hat{\mathbf{g}}_i^{tf}\right)\left(\mathbf{S}^{tf}\left(\mathbf{S}^{tf}\right)^H\hat{\mathbf{g}}_j^{tf}\right)^H \\
&=\frac{\sigma}{N-L+1}\left[\sum_{k=1}^{n_o}\frac{(\lambda_k^o-\sigma)+\frac{n_o}{L}\sigma}{(\sigma-\lambda_k^o)^2}\mathbf{s}_k^o\left(\mathbf{s}_k^o\right)^H\right]\delta_{i,j}.
\end{aligned}
\tag{32}
$$

From (30)-(32), two important observations are in order. First, if the signals are both localizable and separable in the time-frequency domain, then the reduction of the number of signals from n to n_o greatly reduces the estimation error, specifically when the signals are closely spaced. The examples, given in the following section, show the advantages of using t-f MUSIC with partially selected signals. The second observation relates to SNR enhancements. The above equations show that error reductions using STFDs are more pronounced for the cases of low SNR and/or closely spaced signals. It is clear from (30)-(32) that, when $\lambda_k^o \gg \sigma$ for all $k = 1, 2, ..., n_o$, the results are almost independent of L (suppose $N \gg L$ so that $N - L + 1 \simeq N$), and therefore there would be no obvious improvement in using the STFD over conventional array processing. On the other hand, when some of the eigenvalues are close to σ ($\lambda_k^o \simeq \sigma$, for some $k = 1, 2, ..., n_o$), which is the case of weak or closely spaced signals, all the results of above three equations are reduced by a factor of up to $G = \frac{L}{n_o}$, respectively. This factor represents, in essence, the gain achieved from using STFD processing.

V. The Time-Frequency MUSIC

To demonstrate the robustness of the eigen-decomposition of the STFDs when used in practical applications, we consider in this section the recently proposed time-frequency MUSIC (t-f MUSIC) algorithm [6]. We first recall that the DOAs are estimated in the

MUSIC technique by determining the n values of θ for which the following spatial spectrum is maximized [15],

$$f_{MU}(\theta) = \left[\mathbf{a}^H(\theta)\hat{\mathbf{G}}\hat{\mathbf{G}}^H\mathbf{a}(\theta)\right]^{-1} = \left[\mathbf{a}^H(\theta)\left(\mathbf{I} - \hat{\mathbf{S}}\hat{\mathbf{S}}^H\right)\mathbf{a}(\theta)\right]^{-1}. \tag{33}$$

The variance of those estimates in the conventional MUSIC technique, assuming white noise processes, is given by [4]

$$E\left(\hat{\omega}_i - \omega_i\right)^2 = \frac{1}{2N}\frac{\mathbf{a}^H(\theta_i)\mathbf{U}\mathbf{a}(\theta_i)}{h(\theta_i)} \tag{34}$$

where ω is the spatial frequency associated with DOA θ, and $\hat{\omega}$ is its estimate obtained by the conventional MUSIC. In the above equation

$$\mathbf{U} = \sigma\left[\sum_{k=1}^{n}\frac{\lambda_k}{(\sigma-\lambda_k)^2}\mathbf{s}_k\mathbf{s}_k^H\right], \quad \mathbf{d}(\theta) = d\mathbf{a}(\theta)/d\omega, \quad h(\theta) = \mathbf{d}^H(\theta)\mathbf{G}\mathbf{G}^H\mathbf{d}(\theta). \tag{35}$$

From the results of Lemma 1, part (b), $\mathbf{U}' = \mathbf{U}$, which implies that (34) also holds true when the conventional MUSIC algorithm is applied to FM signals in white noise environment.

Similarly, for t-f MUSIC, when n_o signals are selected, the angles of the n_o signals are determined by locating the n_o peaks of the spatial spectrum defined from the n_o signals' respective time-frequency regions.

$$f_{MU}^{tf}(\theta) = \left[\mathbf{a}^H(\theta)\hat{\mathbf{G}}^{tf}\left(\hat{\mathbf{G}}^{tf}\right)^H\mathbf{a}(\theta)\right]^{-1} = \left[\mathbf{a}^H(\theta)\left(\mathbf{I} - \hat{\mathbf{S}}^{tf}\left(\hat{\mathbf{S}}^{tf}\right)^H\right)\mathbf{a}(\theta)\right]^{-1}. \tag{36}$$

Following the same procedure in [4] and using the results of Lemmas 2 and 3, we obtain the variance of the DOA estimates based on t-f MUSIC,

$$E\left(\hat{\omega}_i^{tf} - \omega_i^{tf}\right)^2 = \frac{1}{2(N-L+1)}\frac{\mathbf{a}^H(\theta_i)\mathbf{U}^{tf}\mathbf{a}(\theta_i)}{h^{tf}(\theta_i)} \tag{37}$$

where $\mathbf{U}^{tf}$ is defined in (28), and

$$h^{tf}(\theta) = \mathbf{d}^H(\theta)\mathbf{G}^{tf}\left(\mathbf{G}^{tf}\right)^H\mathbf{d}(\theta) \tag{38}$$

which is equal to $h(\theta)$ if $n_o = n$.

VI. Simulation Results

Consider a uniform linear array of 8 sensors separated by half a wavelength. Two chirp signals emitted from two sources positioned at angle θ_1 and θ_2. The start and end frequencies of the chirp signal of the source at θ_1 are $\omega_{s1} = 0$ and $\omega_{e1} = \pi$, while the corresponding two frequencies for the signal of the other source at θ_2 are $\omega_{s2} = \pi$ and $\omega_{e2} = 0$, respectively. The noise used in this simulation is zero-mean, Gaussian distributed, and temporally white. The noise power, σ, is adjusted to give the desired $SNR = -10log(\sigma)$. Fig. 3 shows the PWVD of the mixed noise-free signals for $L = 129$.

Fig. 4 displays the variance of the estimated DOA $\hat{\theta}_1$ versus SNR for the case $(\theta_1, \theta_2) = (-10°, 10°)$. The curves in this figure show the theoretical and experimental results of the conventional MUSIC and t-f MUSIC (for L=33 and 129). The CRB is also shown in Fig. 4. Both signals are selected when performing t-f MUSIC ($n_o = n = 2$). We assume that the number of signals is correctly estimated for each case. Simulation results are averaged over 100 independent trials of Monte Carlo experiments. The advantages of t-f MUSIC in low SNR cases are evident from this figure. The experiment results deviate from the theoretical results for low SNR, since we only considered the lowest order of the coefficients of the perturbation expansion of $\check{\mathbf{v}}_i$ in deriving the theoretical results (see Appendix A). Fig 5 shows estimated spatial spectra at SNR=−20 dB based on t-f MUSIC ($L = 129$) and the conventional MUSIC. The t-f MUSIC spectral peaks are clearly resolved.

Fig. 6 shows examples of the estimated spatial spectrum based on t-f MUSIC ($L = 129$) and the conventional MUSIC where the angle separation is small ($\theta_1 = -2.5$ degrees, $\theta_2 = 2.5$ degrees). The input SNR is −5 dB and the number of samples is 1024. Two t-f MUSIC algorithms are performed using two sets of time-frequency points, each set belongs to the time-frequency signature of one source ($n_o = 1$). It is evident that the two signals cannot be resolved when MUSIC is applied, whereas by applying t-f MUSIC separately over the two signals, the two signals are clearly separated and reasonable DOA estimation is achieved. It is noted that there is a small bias in the estimated result of t-f MUSIC due to the imperfect separation of the two signals in the time-frequency domain.

VII. Conclusions

Subspace analyses of spatial time-frequency distribution (STFD) matrices have been presented. It has been shown that for signals with clearly defined time-frequency signatures, such as FM signals, smaller estimation errors in the signal and noise subspaces can be achieved by using spatial time-frequency matrices over the subspace estimates obtained from using the data covariance matrix approach. This improvement in subspace estimation is the result of incorporating the time-frequency points along the instantaneous frequencies of the impinging signals on the array into the subspace estimation procedure. These points belong to autoterm regions of high power concentrations, and as such, when used in constructing STFDs, they provide high SNR matrices with improved eigen-decompositions.

The advantages of STFD-based direction finding over traditional direction finding methods using data covariance matrices were demonstrated using the MUSIC algorithm. It was shown that the time-frequency MUSIC outperforms conventional MUSIC in the two situations of low SNR and closely spaced sources.

Unlike conventional array processing techniques, which are nondiscriminatory, and must therefore spatially localize all signals incident on the array, the STFD-based array processing provides the flexibility of dealing with all signal arrivals, or a subset of them. In this respect, it does not suffer from the drawback of requiring higher number of sensors than sources. The ability to select fewer source sources depends on the distribution of their time-frequency signatures from those of other source signals. The eigenstructure of the STFD matrix constructed from the time-frequency points that belong to the autoterm regions of a number of sources will only yield the signal subspace of theses sources. It was shown that the maximum improvement in subspace estimation using STFD over data covariance matrices is achieved when constructing the STFD from only one source signal.

Appendix A

For notation simplicity, we denote $\mathbf{v}_i$, $i = 1, 2, ..., m$, as the eigenvectors of the correlation matrix $\mathbf{R_{xx}}$, where the first n vectors form the signal subspace ($\mathbf{s}_i$, $i = 1, 2, ..., n$), and the last $m - n$ vectors form the noise subspace ($\mathbf{g}_i$, $i = 1, 2, ..., m - n$).

To derive the covariance matrices, we follow the same procedure in [4] and [8], but note

the fact that the underlying signals are deterministic rather than white random processes, which are considered in [4] and [8]. We define $\hat{\mathbf{R}}_{xx}$ in terms of a random perturbation to $\mathbf{R}_{xx}$ with a perturbation factor p, $0 < p \ll 1$. Thus,

$$\hat{\mathbf{R}}_{xx} = \mathbf{R}_{xx} + (\hat{\mathbf{R}}_{xx} - \mathbf{R}_{xx}) = \mathbf{R}_{xx} + p\mathbf{B}. \tag{A.1}$$

When the source signals are FM and the noise vector forms a multivariate white Gaussian process, then $\mathbf{B}$ is a Hermitian, zero-mean random matrix whose elements are asymptotically jointly Gaussian. Let $\check{\mathbf{v}}_i$ denote the unnormalized perturbed version of the eigenvector $\mathbf{v}_i$. According to [9],

$$\check{\mathbf{v}}_i = \mathbf{v}_i + \sum_{\substack{k=1 \\ k \neq i}}^{m} \left(\sum_{l=1}^{\infty} t_{lk}^{(i)} p^l \right) \mathbf{v}_k \tag{A.2}$$

where $t_{lk}^{(i)}$, $l = 1, 2, ...,$ are the coefficients of the perturbation expansion of $\check{\mathbf{v}}_i$ along $\mathbf{v}_k$. By keeping the term with the lowest order of p, then [8]

$$t_{1k}^{(i)} = \frac{\mathbf{v}_k^H \mathbf{B} \mathbf{v}_i}{\lambda_k - \lambda_i}, \; k \neq i. \tag{A.3}$$

The mean square value of $t_{1k}^{(i)}$ is given by

$$E\left[\left|t_{1k}^{(i)}\right|^2\right] = E\left[\frac{\mathbf{v}_k^H \mathbf{B} \mathbf{v}_i \mathbf{v}_i^H \mathbf{B} \mathbf{v}_k}{(\lambda_k - \lambda_i)^2}\right]. \tag{A.4}$$

To evaluate the numerator in the above equation, we consider the following general case.

$$\begin{aligned} E\left[\mathbf{v}_1^H \mathbf{B} \mathbf{v}_2 \mathbf{v}_3^H \mathbf{B} \mathbf{v}_4\right] &= \frac{1}{p^2} E\left[\mathbf{v}_1^H \left(\hat{\mathbf{R}}_{xx} - \mathbf{R}_{xx}\right) \mathbf{v}_2 \mathbf{v}_3^H \left(\hat{\mathbf{R}}_{xx} - \mathbf{R}_{xx}\right) \mathbf{v}_4\right] \\ &= \frac{1}{(Np)^2} E\left[\left(\sum_{r=1}^{N} \mathbf{v}_1^H \mathbf{x}(t_r) \mathbf{x}^H(t_r) \mathbf{v}_2\right) \left(\sum_{q=1}^{N} \mathbf{v}_3^H \mathbf{x}(t_q) \mathbf{x}^H(t_q) \mathbf{v}_4\right)\right] \\ &\quad - \frac{1}{p^2} \mathbf{v}_1^H \mathbf{R}_{xx} \mathbf{v}_2 \mathbf{v}_3^H \mathbf{R}_{xx} \mathbf{v}_4. \end{aligned} \tag{A.5}$$

It can be easily realized that the expected value in (A.5) is taken from a product of four non-zero mean Gaussian random variables. It is well known that for Gaussian random variable x_1, x_2, x_3, x_4 with non-zero means,

$$\begin{aligned} E[x_1 x_2 x_3 x_4] &= E[x_1 x_2] E[x_3 x_4] + E[x_1 x_3] E[x_2 x_4] \\ &\quad + E[x_1 x_4] E[x_2 x_3] - 2E[x_1] E[x_2] E[x_3] E[x_4]. \end{aligned} \tag{A.6}$$

Using the properties of the zero-mean circular complex Gaussian noise vector and the deterministic source signal vector, then

$$\begin{aligned} E[\mathbf{x}(t_r)] &= \mathbf{y}(t_r), \\ E\left[\mathbf{x}(t_r)\mathbf{x}^H(t_q)\right] &= \mathbf{y}(t_r)\mathbf{y}^H(t_q) + \sigma\mathbf{I}\delta_{r,q}, \\ E\left[\mathbf{x}(t_r)\mathbf{x}^T(t_q)\right] &= \mathbf{y}(t_r)\mathbf{y}^T(t_q). \end{aligned}$$

Accordingly, (A.5) can be written as

$$\begin{aligned} & E\left[\mathbf{v}_1^H\mathbf{B}\mathbf{v}_2\mathbf{v}_3^H\mathbf{B}\mathbf{v}_4\right] \\ &= \frac{1}{(Np)^2}\sum_{r=1}^{N}\sum_{q=1}^{N} E\left[\mathbf{v}_1^H\mathbf{x}(t_r)\mathbf{x}^H(t_r)\mathbf{v}_2\right] E\left[\mathbf{v}_3^H\mathbf{x}(t_q)\mathbf{x}^H(t_q)\mathbf{v}_4\right] \\ &\quad + \frac{1}{(Np)^2}\sum_{r=1}^{N}\sum_{q=1}^{N} E\left[\mathbf{v}_1^H\mathbf{x}(t_r)\mathbf{v}_3^H\mathbf{x}(t_q)\right] E\left[\mathbf{x}^H(t_r)\mathbf{v}_2\mathbf{x}^H(t_q)\mathbf{v}_4\right] \\ &\quad + \frac{1}{(Np)^2}\sum_{r=1}^{N}\sum_{q=1}^{N} E\left[\mathbf{v}_1^H\mathbf{x}(t_r)\mathbf{x}^H(t_q)\mathbf{v}_4\right] E\left[\mathbf{v}_3^H\mathbf{x}(t_q)\mathbf{x}^H(t_r)\mathbf{v}_2\right] \\ &\quad - 2\frac{1}{(Np)^2}\sum_{r=1}^{N}\sum_{q=1}^{N} E\left[\mathbf{v}_1^H\mathbf{x}(t_r)\right] E\left[\mathbf{x}^H(t_r)\mathbf{v}_2\right] E\left[\mathbf{v}_3^H\mathbf{x}(t_q)\right] E\left[\mathbf{x}^H(t_q)\mathbf{v}_4\right] \\ &\quad - \frac{1}{p^2}\mathbf{v}_1^H\mathbf{R}_{\mathbf{xx}}\mathbf{v}_2\mathbf{v}_3^H\mathbf{R}_{\mathbf{xx}}\mathbf{v}_4 \\ &= \frac{1}{(Np)^2}\sum_{r=1}^{N}\sum_{q=1}^{N}\left[\mathbf{v}_1^H\mathbf{v}_4\sigma\delta_{r,q}\mathbf{v}_3^H\mathbf{y}(t_q)\mathbf{y}^H(t_r)\mathbf{v}_2\right] \\ &\quad + \frac{1}{(Np)^2}\sum_{r=1}^{N}\sum_{q=1}^{N}\left[\mathbf{v}_1^H\mathbf{y}(t_r)\mathbf{y}^H(t_q)\mathbf{v}_4\mathbf{v}_3^H\mathbf{v}_2\sigma\delta_{r,q}\right] \\ &\quad + \frac{1}{(Np)^2}\sum_{r=1}^{N}\sum_{q=1}^{N}\left[\mathbf{v}_1^H\mathbf{v}_4\mathbf{v}_3^H\mathbf{v}_2\sigma^2\delta_{r,q}\right] \qquad (A.7) \\ &= \frac{1}{(Np)^2}\sum_{r=1}^{N}\left[\delta_{\mathbf{v}_1,\mathbf{v}_4}\sigma\mathbf{v}_3^H\mathbf{y}(t_r)\mathbf{y}^H(t_r)\mathbf{v}_2\right] \\ &\quad + \frac{1}{(Np)^2}\sum_{r=1}^{N}\left[\mathbf{v}_1^H\mathbf{y}(t_r)\mathbf{y}^H(t_r)\mathbf{v}_4\delta_{\mathbf{v}_2,\mathbf{v}_3}\sigma\right] + \frac{1}{(Np)^2}\sum_{r=1}^{N}\left[\delta_{\mathbf{v}_1,\mathbf{v}_4}\delta_{\mathbf{v}_2,\mathbf{v}_3}\sigma^2\right] \end{aligned}$$

where

$$\delta_{\mathbf{v}_i,\mathbf{v}_j} = \begin{cases} 0, & i \neq j \\ 1, & i = j. \end{cases}$$

By using the uncorrelation assumption (11),

$$\frac{1}{N}\sum_{r=1}^{N}\mathbf{y}(t_r)\mathbf{y}^H(t_r) = \mathbf{A}\left[\frac{1}{N}\sum_{r=1}^{N}\mathbf{d}(t_r)\mathbf{d}^H(t_r)\right]\mathbf{A}^H = \mathbf{A}\mathbf{R}_{\mathbf{dd}}\mathbf{A}^H = \mathbf{R}_{\mathbf{yy}}, \qquad (A.8)$$

and equation (A.7) simplifies to

$$\begin{aligned} & E\left[\mathbf{v}_1^H \mathbf{B}\mathbf{v}_2 \mathbf{v}_3^H \mathbf{B}\mathbf{v}_4\right] \\ &= \frac{\sigma}{Np^2}\left[\delta_{\mathbf{v}_1,\mathbf{v}_4}\mathbf{v}_3^H \mathbf{R}_{\mathbf{yy}}\mathbf{v}_2 + \mathbf{v}_1^H \mathbf{R}_{\mathbf{yy}}\mathbf{v}_4\delta_{\mathbf{v}_2,\mathbf{v}_3}\right] + \frac{\sigma^2}{Np^2}\delta_{\mathbf{v}_1,\mathbf{v}_4}\delta_{\mathbf{v}_2,\mathbf{v}_3} \\ &= \frac{\sigma}{Np^2}\left[\lambda_{\mathbf{v}_1} + \lambda_{\mathbf{v}_2} - \sigma\right]\delta_{\mathbf{v}_1,\mathbf{v}_4}\delta_{\mathbf{v}_2,\mathbf{v}_3}. \end{aligned} \tag{A.9}$$

Therefore,

$$E\left[\left|t_{1k}^{(i)}\right|^2\right] = E\left[\frac{\mathbf{v}_k^H \mathbf{B}\mathbf{v}_i \mathbf{v}_i^H \mathbf{B}\mathbf{v}_k}{(\lambda_k - \lambda_i)^2}\right] = \frac{\sigma}{Np^2}\frac{(\lambda_i + \lambda_k - \sigma)}{(\lambda_i - \lambda_k)^2},\ k \neq i, \tag{A.10}$$

and

$$E\left[t_{1k}^{(i)}(t_{1k}^{(j)})^*\right] = E\left[\frac{\mathbf{v}_k^H \mathbf{B}\mathbf{v}_i \mathbf{v}_j^H \mathbf{B}\mathbf{v}_k}{(\lambda_k - \lambda_i)(\lambda_k - \lambda_j)}\right] = 0,\ k \neq i,\ k \neq j. \tag{A.11}$$

It is shown in [13] that

$$cov\left(\hat{\mathbf{v}}_i, \hat{\mathbf{v}}_j\right) = cov\left(\check{\mathbf{v}}_i, \check{\mathbf{v}}_j\right) + o(N^{-2}).$$

By ignoring the terms of N^{-2}, then

$$\begin{aligned} cov\left(\hat{\mathbf{v}}_i, \hat{\mathbf{v}}_j\right) &\simeq cov\left(\check{\mathbf{v}}_i, \check{\mathbf{v}}_j\right) \simeq E\left[\left(\sum_{\substack{k=1 \\ k\neq i}}^{m} t_{1k}^{(i)} p\mathbf{v}_k\right)\left(\sum_{\substack{k=1 \\ k\neq j}}^{m} t_{1k}^{(j)} p\mathbf{v}_k\right)^H\right] \\ &= E\left[\sum_{\substack{k=1 \\ k\neq i}}^{m}\left|t_{1k}^{(i)}\right|^2 p^2 \mathbf{v}_k \mathbf{v}_k^H \delta_{i,j}\right] = \frac{\sigma}{N}\sum_{\substack{k=1 \\ k\neq i}}^{m}\frac{\lambda_i + \lambda_k - \sigma}{(\lambda_i - \lambda_k)^2}\mathbf{v}_k \mathbf{v}_k^H \delta_{i,j}. \end{aligned} \tag{A.12}$$

Equation (12) in Section III follows by replacing $\mathbf{v}_k$ by $\mathbf{s}_k$ or $\mathbf{g}_k$. Similarly,

$$\begin{aligned} cov\left(\hat{\mathbf{v}}_i, \hat{\mathbf{v}}_j^*\right) &\simeq cov\left(\check{\mathbf{v}}_i, \check{\mathbf{v}}_j^*\right) \simeq E\left[\left(\sum_{\substack{k=1 \\ k\neq i}}^{m} t_{1k}^{(i)} p\mathbf{v}_k\right)\left(\sum_{\substack{k=1 \\ k\neq j}}^{m} t_{1k}^{(j)} p\mathbf{v}_k\right)^T\right] \\ &= p^2 E\left[\sum_{\substack{k_1=1 \\ k_1\neq i}}^{m}\sum_{\substack{k_2=1 \\ k_2\neq j}}^{m} t_{1k_1}^{(i)} t_{1k_2}^{(j)} \mathbf{v}_{k_1}\mathbf{v}_{k_2}^T\right] = p^2 \sum_{\substack{k_1=1 \\ k_1\neq i}}^{m}\sum_{\substack{k_2=1 \\ k_2\neq j}}^{m} E\left[\frac{\mathbf{v}_{k_1}^H \mathbf{B}\mathbf{v}_i}{(\lambda_{k_1} - \lambda_i)}\frac{\mathbf{v}_{k_2}^H \mathbf{B}\mathbf{v}_j}{(\lambda_{k_2} - \lambda_j)}\mathbf{v}_{k_1}\mathbf{v}_{k_2}^T\right]. \end{aligned} \tag{A.13}$$

From (A.9), it is clear that the above equation has non-zero value only when $k_1 = j$ and $k_2 = i$. Noting the fact that $k_1 \neq i$ and $k_2 \neq j$, (A.13) becomes

$$\begin{aligned} cov\left(\hat{\mathbf{v}}_i, \hat{\mathbf{v}}_j^*\right) &\simeq -\frac{p^2}{(\lambda_j - \lambda_i)^2} E\left[\mathbf{v}_j^H \mathbf{B}\mathbf{v}_i \mathbf{v}_i^H \mathbf{B}\mathbf{v}_j\right]\mathbf{v}_j \mathbf{v}_i^T (1 - \delta_{i,j}) \\ &= -\frac{\sigma}{N}\frac{\lambda_i + \lambda_j - \sigma}{(\lambda_j - \lambda_i)^2}\mathbf{v}_j \mathbf{v}_i^T (1 - \delta_{i,j}). \end{aligned} \tag{A.14}$$

For the signal subspace, $\mathbf{v}_i$ is $\mathbf{s}_i$, $i = 1, ..., n$, and (A.14) yields (13).

Appendix B

Similar to Appendix A, we let $\mathbf{v}_i$, $i = 1, 2, ..., m$, represent the whole eigenvectors of the STFD matrix $\mathbf{D}$, where the first n_o vectors form the signal subspace ($\mathbf{s}_i^{tf}$, $i = 1, 2, ..., n_o$), while the last $m-n_o$ vectors form the noise subspace ($\mathbf{g}_i^{tf}$, $i = 1, 2, ..., m-n_o$). As discussed in Section III, we assume that the selected time-frequency points belong to regions where no crossterm components are present.

For an array mixture of FM signals, we select points from n_o signals at the time-frequency domain, where the pseudo Wigner-Ville distribution matrix is defined in (13). We define $\hat{\mathbf{D}}$ in terms of a random perturbation to $\mathbf{D}$ with a perturbation factor p, $0 < p \ll 1$. Thus,

$$\hat{\mathbf{D}} = \mathbf{D} + (\hat{\mathbf{D}} - \mathbf{D}) = \mathbf{D} + p\mathbf{B}. \tag{B.1}$$

Matrix $\mathbf{B}$ is a Hermitian, zero-mean random matrix whose elements are asymptotically Jointly Gaussian [12]. Similar to Appendix A, we derive

$$\begin{aligned} E\left[\mathbf{v}_1^H\mathbf{B}\mathbf{v}_2\mathbf{v}_3^H\mathbf{B}\mathbf{v}_4\right] &= \frac{1}{p^2}E\left[\mathbf{v}_1^H\left(\hat{\mathbf{D}}-\mathbf{D}\right)\mathbf{v}_2\mathbf{v}_3^H\left(\hat{\mathbf{D}}-\mathbf{D}\right)\mathbf{v}_4\right] \\ &= \frac{1}{\left(n_o p(N-L+1)\right)^2}E\left[\left(\sum_{q=1}^{n_o}\sum_{i=1}^{N-L+1}\mathbf{v}_1^H\mathbf{D}_{\mathbf{xx}}(t_i, f_{q,i})\mathbf{v}_2\right)\left(\sum_{q=1}^{n_o}\sum_{i=1}^{N-L+1}\mathbf{v}_3^H\mathbf{D}_{\mathbf{xx}}(t_i, f_{q,i})\mathbf{v}_4\right)\right] \\ &\quad -\frac{1}{p^2}\mathbf{v}_1^H\mathbf{D}\mathbf{v}_2\mathbf{v}_3^H\mathbf{D}\mathbf{v}_4. \end{aligned} \tag{B.2}$$

Substituting (20) and (A.7) into (B.2), we obtain

$$\begin{aligned} &E\left[\mathbf{v}_1^H\mathbf{B}\mathbf{v}_2\mathbf{v}_3^H\mathbf{B}\mathbf{v}_4\right] \\ &= \frac{1}{\left(n_o p(N-L+1)\right)^2}\sum_{q_1=1}^{n_o}\sum_{q_2=1}^{n_o}\sum_{i_1=1}^{N-L+1}\sum_{i_2=1}^{N-L+1}\sum_{\tau_1=-\frac{L-1}{2}}^{\frac{L-1}{2}}\sum_{\tau_2=-\frac{L-1}{2}}^{\frac{L-1}{2}} e^{-j4\pi\left[f_{q_1,i_1}\tau_1+f_{q_2,i_2}\tau_2\right]} \\ &\quad\times\Big\{E\left[\mathbf{v}_1^H\mathbf{x}(t_{i_1}+\tau_1)\mathbf{x}^H(t_{i_1}-\tau_1)\mathbf{v}_2\right]E\left[\mathbf{v}_3^H\mathbf{x}(t_{i_2}+\tau_2)\mathbf{x}^H(t_{i_2}-\tau_2)\mathbf{v}_4\right] \\ &\quad +E\left[\mathbf{v}_1^H\mathbf{x}(t_{i_1}+\tau_1)\mathbf{v}_3^H\mathbf{x}(t_{i_2}+\tau_2)\right]E\left[\mathbf{x}^H(t_{i_1}-\tau_1)\mathbf{v}_2\mathbf{x}^H(t_{i_2}-\tau_2)\mathbf{v}_4\right] \\ &\quad +E\left[\mathbf{v}_1^H\mathbf{x}(t_{i_1}+\tau_1)\mathbf{x}^H(t_{i_2}-\tau_2)\mathbf{v}_4\right]E\left[\mathbf{v}_3^H\mathbf{x}(t_{i_2}+\tau_2)\mathbf{x}^H(t_{i_1}-\tau_1)\mathbf{v}_2\right] \\ &\quad -2E\left[\mathbf{v}_1^H\mathbf{x}(t_{i_1}+\tau_1)\right]E\left[\mathbf{x}^H(t_{i_1}-\tau_1)\mathbf{v}_2\right]E\left[\mathbf{v}_3^H\mathbf{x}(t_{i_2}+\tau_2)\right]E\left[\mathbf{x}^H(t_{i_2}-\tau_2)\mathbf{v}_4\right]\Big\} \\ &\quad -\frac{1}{p^2}\mathbf{v}_1^H\mathbf{D}\mathbf{v}_2\mathbf{v}_3^H\mathbf{D}\mathbf{v}_4 \end{aligned}$$

$$
\begin{aligned}
&= \frac{1}{\left(n_o p(N-L+1)\right)^2} \sum_{q_1=1}^{n_o} \sum_{q_2=1}^{n_o} \sum_{i_1=1}^{N-L+1} \sum_{i_2=1}^{N-L+1} \sum_{\tau_1=-\frac{L-1}{2}}^{\frac{L-1}{2}} \sum_{\tau_2=-\frac{L-1}{2}}^{\frac{L-1}{2}} e^{-j4\pi\left[f_{q_1,i_1}\tau_1 + f_{q_2,i_2}\tau_2\right]} \\
&\times \Big[\mathbf{v}_1^H \mathbf{y}(t_{i_1}+\tau_1)\mathbf{y}^H(t_{i_2}-\tau_2)\mathbf{v}_4 \sigma \delta_{\mathbf{v}_2,\mathbf{v}_3}\delta_{t_{i_1}-\tau_1,t_{i_2}+\tau_2} \\
&\quad + \sigma \delta_{\mathbf{v}_1,\mathbf{v}_4}\delta_{t_{i_1}+\tau_1,t_{i_2}-\tau_2}\mathbf{v}_3^H \mathbf{y}(t_{i_2}+\tau_2)\mathbf{y}^H(t_{i_1}-\tau_1)\mathbf{v}_2 \\
&\quad + \sigma^2 \delta_{\mathbf{v}_1,\mathbf{v}_4}\delta_{\mathbf{v}_2,\mathbf{v}_3}\delta_{t_{i_1},t_{i_2}}\delta_{\tau_1,\tau_2} \Big].
\end{aligned} \tag{B.3}
$$

Under the assumption of no crossterms, q_1 should be equivalent to q_2 to have non-zero values, and in this case, $q_1 = q_2 = q$. Note that within the time-frequency region of the qth signal, $\mathbf{y}(t) = \mathbf{y}_q(t) \triangleq \mathbf{A}\mathbf{d}_q(t)$. When the third-order derivative of the phase is negligible over $[t-L+1, t+L-1]$ for any signal and any t, we have

$$
\begin{aligned}
&E\left[\mathbf{v}_1^H \mathbf{B}\mathbf{v}_2 \mathbf{v}_3^H \mathbf{B}\mathbf{v}_4\right] \\
&\simeq \frac{1}{\left(Np(N-L+1)\right)^2} \sum_{q=1}^{n_o} \sum_{i_1=1}^{N-L+1} \sum_{i_2=1}^{N-L+1} \sum_{\tau_1=-\frac{L-1}{2}}^{\frac{L-1}{2}} \sum_{\tau_2=-\frac{L-1}{2}}^{\frac{L-1}{2}} \\
&\quad \times \Big[\mathbf{v}_1^H \mathbf{y}(t_{i_1}+\tau_1)\mathbf{y}^H(t_{i_2}-\tau_2)\mathbf{v}_4 \sigma \delta_{\mathbf{v}_2,\mathbf{v}_3}\delta_{t_{i_1}-\tau_1,t_{i_2}+\tau_2} \\
&\quad + \sigma \delta_{\mathbf{v}_1,\mathbf{v}_4}\delta_{t_{i_1}+\tau_1,t_{i_1}-\tau_1}\mathbf{v}_3^H \mathbf{y}(t_{i_2}+\tau_2)\mathbf{y}^H(t_{i_1}-\tau_1)\mathbf{v}_2 \Big] \\
&\quad + \frac{\sigma^2 L}{n_o(N-L+1)p^2}\delta_{\mathbf{v}_1,\mathbf{v}_4}\delta_{\mathbf{v}_2,\mathbf{v}_3} \\
&\simeq \frac{\sigma L}{n_o(N-L+1)p^2}\left[\frac{L}{n_o}(\lambda_{\mathbf{v}_1}-\sigma) + (\lambda_{\mathbf{v}_2}-\sigma) + \sigma\right]\delta_{\mathbf{v}_1,\mathbf{v}_4}\delta_{\mathbf{v}_2,\mathbf{v}_3} \\
&= \frac{\sigma L}{n_o(N-L+1)p^2}\left[(\lambda_{\mathbf{v}_1}^{tf} + \lambda_{\mathbf{v}_2}^{tf} - \sigma)\right]\delta_{\mathbf{v}_1,\mathbf{v}_4}\delta_{\mathbf{v}_2,\mathbf{v}_3}.
\end{aligned} \tag{B.4}
$$

Let $\check{\mathbf{v}}_i$ denote the unnormalized eigenvector given in a perturbation expansions by

$$
\check{\mathbf{v}}_i = \mathbf{v}_i + \sum_{\substack{k=1 \\ k\neq i}}^{m} \left(\sum_{l=1}^{\infty} t_{lk}^{(i)} p^l\right)\mathbf{v}_k \tag{B.5}
$$

where $t_{lk}^{(i)}$, $l = 1, 2, ...,$ are the coefficients of the perturbation expansion of $\check{\mathbf{v}}_i$ along $\mathbf{v}_k$, and keeping the term with the lowest order of p, then

$$
t_{1k}^{(i)} = \frac{\mathbf{v}_k^H \mathbf{B}\mathbf{v}_i}{\lambda_k^{tf} - \lambda_i^{tf}}, \; k \neq i. \tag{B.6}
$$

Therefore,

$$E\left[\left|t_{1k}^{(i)}\right|^2\right] = E\left[\frac{\mathbf{v}_k^H \mathbf{B}\mathbf{v}_i \mathbf{v}_i^H \mathbf{B}\mathbf{v}_k}{(\lambda_k^{tf} - \lambda_i^{tf})^2}\right] = \frac{\sigma L}{n_o(N-L+1)p^2} \frac{(\lambda_i^{tf} + \lambda_k^{tf} - \sigma)}{\left(\lambda_i^{tf} - \lambda_k^{tf}\right)^2},\ k \neq i, \tag{B.7}$$

and

$$E\left[t_{1k}^{(i)}(t_{1k}^{(j)})^*\right] = E\left[\frac{\mathbf{v}_k^H \mathbf{B}\mathbf{v}_i \mathbf{v}_j^H \mathbf{B}\mathbf{v}_k}{(\lambda_k^{tf} - \lambda_i^{tf})(\lambda_k^{tf} - \lambda_j^{tf})}\right] = 0,\ k \neq i,\ k \neq j. \tag{B.8}$$

Similar to Appendix A, we follow

$$\begin{aligned} cov\left(\hat{\mathbf{v}}_i, \hat{\mathbf{v}}_j\right) &\simeq cov\left(\check{\mathbf{v}}_i, \check{\mathbf{v}}_j\right) \simeq E\left[\left(\sum_{\substack{k=1 \\ k\neq i}}^{m} t_{1k}^{(i)} p\mathbf{v}_k\right)\left(\sum_{\substack{k=1 \\ k\neq j}}^{m} t_{1k}^{(j)} p\mathbf{v}_k\right)^H\right] \\ &= E\left[\sum_{\substack{k=1 \\ k\neq i}}^{m} \left|t_{1k}^{(i)}\right|^2 p^2 \mathbf{v}_k \mathbf{v}_k^H \delta_{i,j}\right] = \frac{\sigma L}{n_o(N-L+1)} \sum_{\substack{k=1 \\ k\neq i}}^{m} \frac{\lambda_i^{tf} + \lambda_k^{tf} - \sigma}{(\lambda_i^{tf} - \lambda_k^{tf})^2} \mathbf{v}_k \mathbf{v}_k^H \delta_{i,j}. \end{aligned} \tag{B.9}$$

(26) follows by properly replacing $\mathbf{v}_k$ by $\mathbf{s}_k^{tf}$ or $\mathbf{g}_k^{tf}$.

Similarly,

$$\begin{aligned} cov\left(\hat{\mathbf{v}}_i, \hat{\mathbf{v}}_j^*\right) &\simeq cov\left(\check{\mathbf{v}}_i, \check{\mathbf{v}}_j^*\right) \simeq E\left[\left(\sum_{\substack{k=1 \\ k\neq i}}^{m} t_{1k}^{(i)} p\mathbf{v}_k\right)\left(\sum_{\substack{k=1 \\ k\neq j}}^{m} t_{1k}^{(j)} p\mathbf{v}_k\right)^T\right] \\ &= p^2 \sum_{\substack{k_1=1 \\ k_1\neq i}}^{m} \sum_{\substack{k_2=1 \\ k_2\neq j}}^{m} E\left[\frac{\mathbf{v}_{k_1}^H \mathbf{B}\mathbf{v}_i}{(\lambda_{k_1}^{tf} - \lambda_i^{tf})} \frac{\mathbf{v}_{k_2}^H \mathbf{B}\mathbf{v}_j}{(\lambda_{k_2}^{tf} - \lambda_j^{tf})} \mathbf{v}_{k_1} \mathbf{v}_{k_2}^T\right] \\ &= -\frac{p^2}{(\lambda_j^{tf} - \lambda_i^{tf})^2} E\left[\mathbf{v}_j^H \mathbf{B}\mathbf{v}_i \mathbf{v}_i^H \mathbf{B}\mathbf{v}_j\right] \mathbf{v}_j \mathbf{v}_i^T (1 - \delta_{i,j}) \\ &= -\frac{\sigma L}{n_o(N-L+1)} \frac{\lambda_i^{tf} + \lambda_j^{tf} - \sigma}{(\lambda_j^{tf} - \lambda_i^{tf})^2} \mathbf{v}_j \mathbf{v}_i^T (1 - \delta_{i,j}). \end{aligned} \tag{B.10}$$

For the columns of signal subspace, $\mathbf{v}_i$ becomes $\mathbf{s}_i^{tf}$, and (B.10) becomes (27).

Appendix C

This appendix follows the procedure of [4]. Denote

$$\mathbf{\Gamma} = \left(\mathbf{S}^{tf}\right)^H \hat{\mathbf{D}}\mathbf{G}^{tf},$$

and γ_i the $i$the column of $\mathbf{\Gamma}$. Using the results of (B.2) – (B.4), and the fact $\left(\mathbf{S}^{tf}\right)^H \mathbf{D}\mathbf{G}^{tf} = \mathbf{0}$, we have

$$E\left[\gamma_i\gamma_j^H\right]_{t,q} = E\left[\left(\left(\mathbf{s}_t^{tf}\right)^H \hat{\mathbf{D}}\mathbf{g}_i^{tf}\right)\left(\left(\mathbf{g}_j^{tf}\right)^H \hat{\mathbf{D}}\mathbf{s}_q^{tf}\right)\right] = \frac{\sigma L}{n_o(N-L+1)}\lambda_t^{tf}\delta_{t,q}\delta_{i,j}. \qquad (C.1)$$

Subsequently

$$E\left[\gamma_i\gamma_j^H\right] = E\left[\left(\left(\mathbf{S}^{tf}\right)^H \hat{\mathbf{D}}\mathbf{g}_i^{tf}\right)\left(\left(\mathbf{g}_j^{tf}\right)^H \hat{\mathbf{D}}\mathbf{S}^{tf}\right)\right] = \frac{\sigma L}{n_o(N-L+1)}\mathbf{\Lambda}^{tf}\delta_{i,j}, \qquad (C.2)$$

where $\mathbf{\Lambda}^{tf} = diag\left[\lambda_1^{tf}, ..., \lambda_{n_o}^{tf}\right]$. Similarly,

$$E\left[\gamma_i\gamma_j^T\right]_{t,q} = E\left[\left(\left(\mathbf{s}_t^{tf}\right)^H \hat{\mathbf{D}}\mathbf{g}_i^{tf}\right)\left(\left(\mathbf{s}_q^{tf}\right)^H \hat{\mathbf{D}}\mathbf{g}_j^{tf}\right)\right] = 0, \qquad (C.3)$$

and subsequently

$$E\left[\gamma_i\gamma_j^T\right] = \mathbf{0}. \qquad (C.4)$$

Since $\mathbf{S}^{tf}\left(\mathbf{S}^{tf}\right)^H \hat{\mathbf{g}}_i^{tf}$ has the same limiting distribution as that of $-\mathbf{S}^{tf}(\mathbf{\Gamma} - \sigma\mathbf{I})^{-1}\gamma_i$ [8], then it follows

$$\begin{aligned} & E\left(\mathbf{S}^{tf}\left(\mathbf{S}^{tf}\right)^H \hat{\mathbf{g}}_i^{tf}\right)\left(\mathbf{S}^{tf}\left(\mathbf{S}^{tf}\right)^H \hat{\mathbf{g}}_j^{tf}\right)^H \\ &= \frac{\sigma L}{n_o(N-L+1)}\left[\mathbf{S}(\mathbf{\Lambda}^{tf} - \sigma\mathbf{I})^{-1}\mathbf{\Lambda}^{tf}(\mathbf{\Lambda}^{tf} - \sigma\mathbf{I})^{-1}\mathbf{S}^H\right]\delta_{i,j} \\ &= \frac{\sigma L}{n_o(N-L+1)}\left[\sum_{k=1}^{n_o}\frac{\lambda_k^{tf}}{(\sigma - \lambda_k^{tf})^2}\mathbf{s}_k^{tf}\left(\mathbf{s}_k^{tf}\right)^H\right]\delta_{i,j}, \end{aligned} \qquad (C.5)$$

and

$$E\left(\mathbf{S}^{tf}\left(\mathbf{S}^{tf}\right)^H \hat{\mathbf{g}}_i^{tf}\right)\left(\mathbf{S}^{tf}\left(\mathbf{S}^{tf}\right)^H \hat{\mathbf{g}}_j^{tf}\right)^T = \mathbf{0} \text{ for all } i,\ j. \qquad (C.6)$$

Acknowledgment

The authors would like to thank Dr. Kehu Yang, ATR Adaptive Communications Research Laboratories, Japan, for his helpful discussions on this subject during his visit to Villanova University.

References

[1] A. Belouchrani and M. Amin, "Blind source separation based on time-frequency signal representation," *IEEE Trans. Signal Processing*, vol. 46, no. 11, pp. 2888-2898, Nov. 1998.

[2] M. G. Amin, "Spatial time-frequency distributions for direction finding and blind source separation," (invited paper) in *Proc. SPIE: Wavelet Applications IV*, vol.3723, pp.62-70, April 1999.

[3] A. Belouchrani and M. Amin, "Time-frequency MUSIC," *IEEE Signal Processing Letters*, vol. 6, no. 5, pp. 109-110, May 1999.

[4] P. Stoica and A. Nehorai, "MUSIC, maximum likelihood, and Cramer-Rao bound," *IEEE Trans. Acoust. Speech, Signal Processing*, vol.37, no.5, pp.720-741, May 1989.

[5] L. Cohen, *Time-Frequency Analysis*, Englewood Cliffs, NJ: Prentice Hall, 1995.

[6] G. H. Golub and C. F. Van Loan, *Matrix Computations*, 3rd edition. Baltimore, Maryland: Johns Hopkins University Press, 1996.

[7] K. Sekihara, S. Nagarajan, D. Poeppel, and Y. Miyashita, "Time-frequency MEG-MUSIC algorithm," *IEEE Trans. Medical Imaging*, vol. 18, no. 1, pp.92-97, Jan. 1999.

[8] M. Kaveh and A. J. Barabell, "The statistical performance of the MUSIC and the minimum-norm algorithms in resolving plane waves in noise," *IEEE Trans. Acoust., Speech, Signal Proc.*, vol. ASSP-34, no. 2, pp. 331-340, April 1986.

[9] J. H. Wilkinson, *The Algebraic Eigenvalue Problem.* New York: Oxford University Press, 1965.

[10] J. E. Hudson, *Adaptive Array Principles.* London: Peter Peregrinus Ltd., 1981.

[11] S. Qian and D. Chen, *Joint Time-Frequency Analysis.* Englewood Cliffs, NJ: Prentice-Hill, 1996.

[12] Y. Zhang, W. Mu, and M. G. Amin, "Maximum likelihood methods for array processing based on time-frequency analysis," in *Proc. SPIE: Advanced Signal Processing Algorithms, Archtectures, and Implementations IX*, vol. 3807, Denver, CO, July 1999.

[13] L. C. Godara, "Application of antenna arrays to mobile communications, part II: Beam-forming and direction-of-arrival considerations," *Proc. IEEE*, vol. 85, no. 8,

pp. 1195-1245, Aug. 1997.

[14] M. Wax and T. Kailath, "Detection of signals by information theoretic criteria," *IEEE Trans. Acoust., Speech, Signal Proc.*, vol. 33, no. 2, pp. 387-392, April 1985.

[15] R. O. Schmidt, "Multiple emitter location and signal parameter estimation," *IEEE Trans. Antennas and Propagation*, vol. 34, no. 3, pp. 276-280, March 1986.

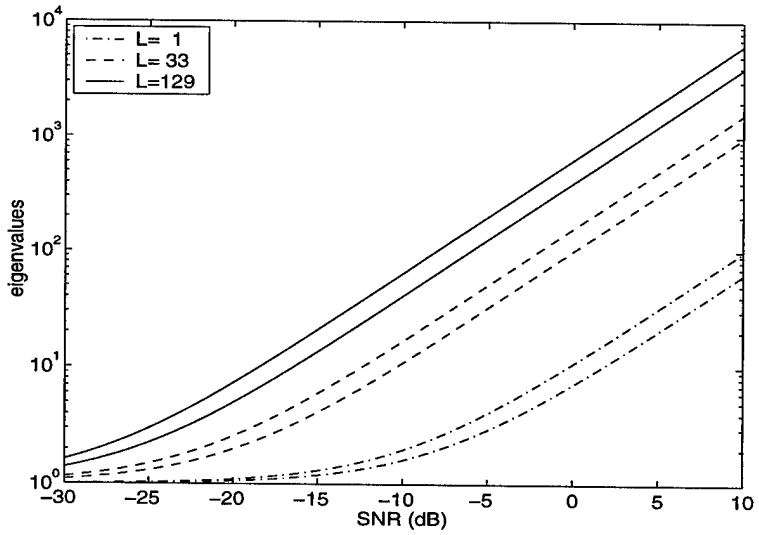

(a) $\theta_1 = -10^o, \theta_2 = 10^o$

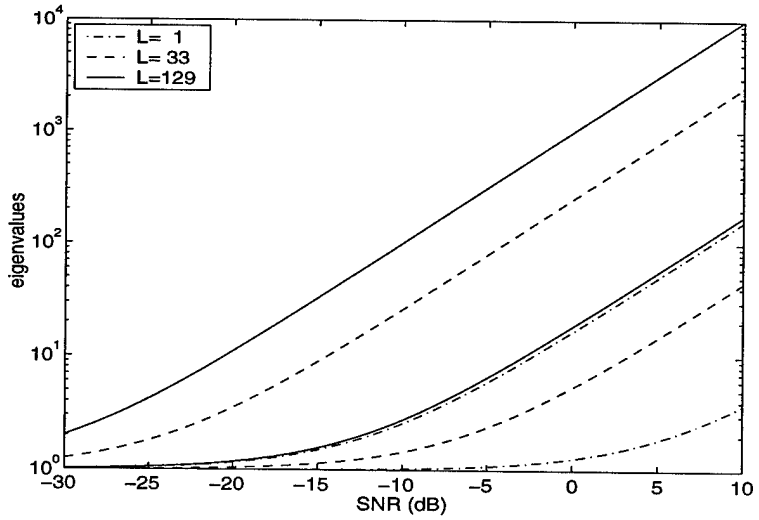

(b) $\theta_1 = -1^o, \theta_2 = 1^o$

Fig.1 The principal eigenvalues of correlation matrix and STFD matrix.

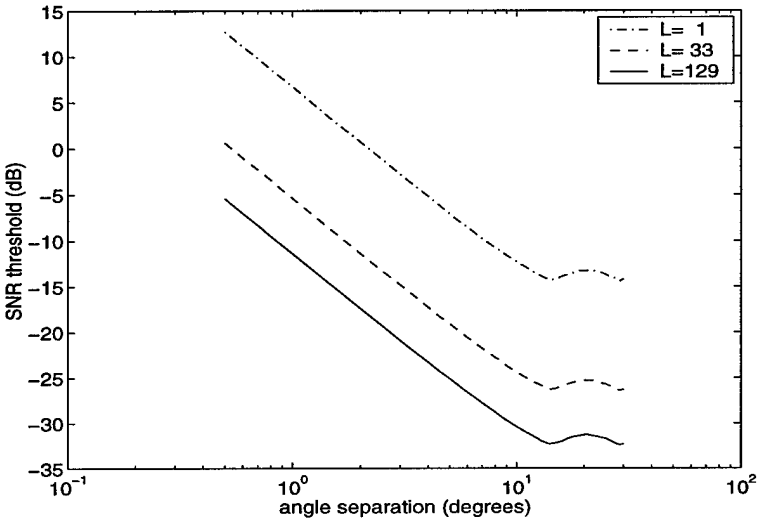

(a) SNR threshold vs. angle separation $N = 1024$

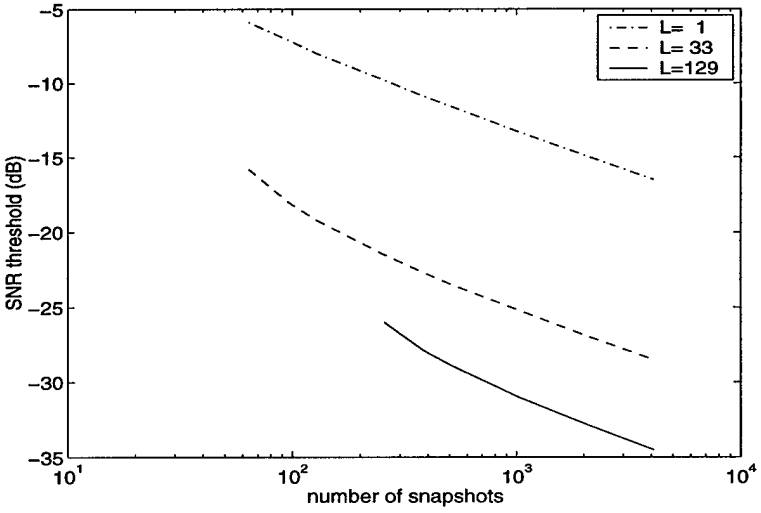

(b) SNR threshold vs. number of snapshots $\Delta\theta = 20°$

Fig.2 SNR thresholds to identify two signals ($m = 8$).

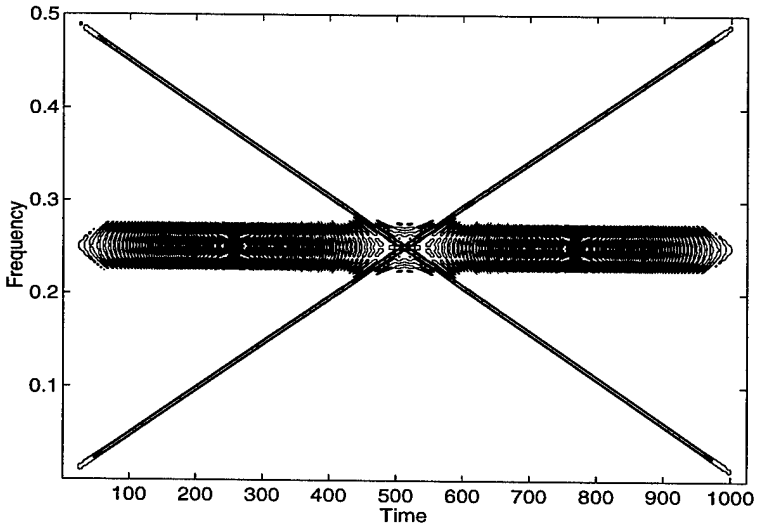

Fig.3 Pseudo Wigner-Ville distribution of the mixture of the two signals.

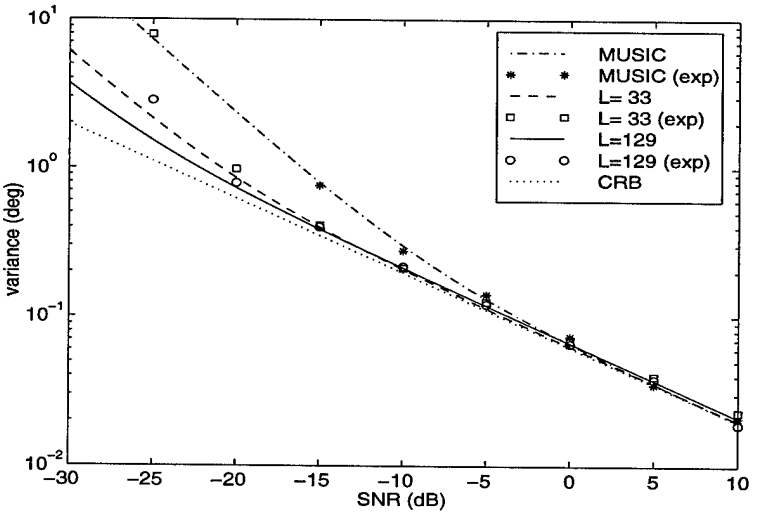

Fig.4 Variance of DOA estimation vs. SNR.

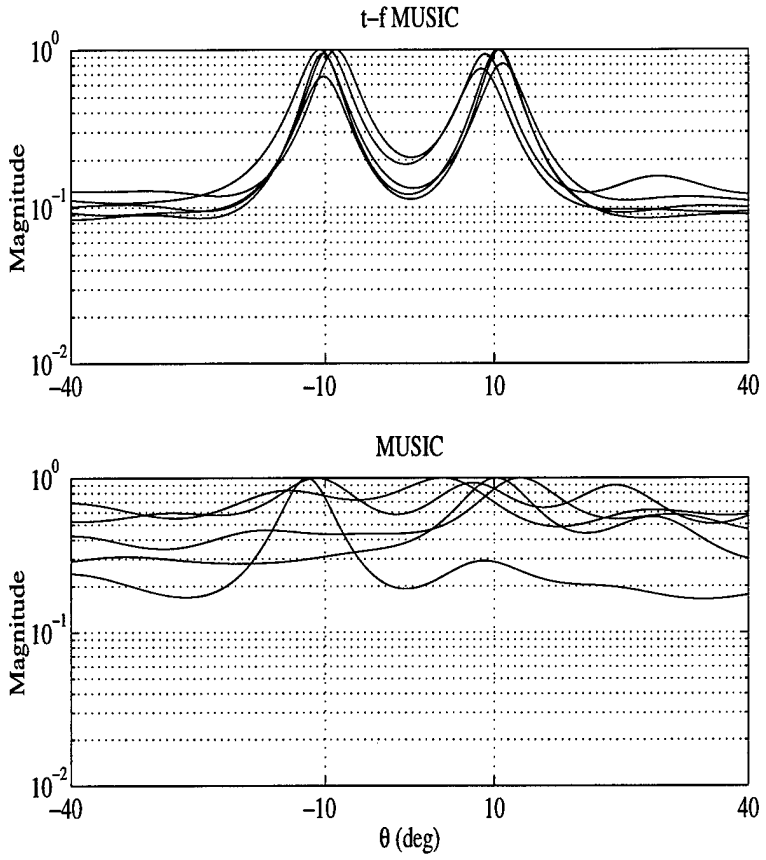

Fig.5 Estimated spatial spectra

($m = 8, N = 1024$,SNR= -20 dB,$L = 129$ for t-f MUSIC).

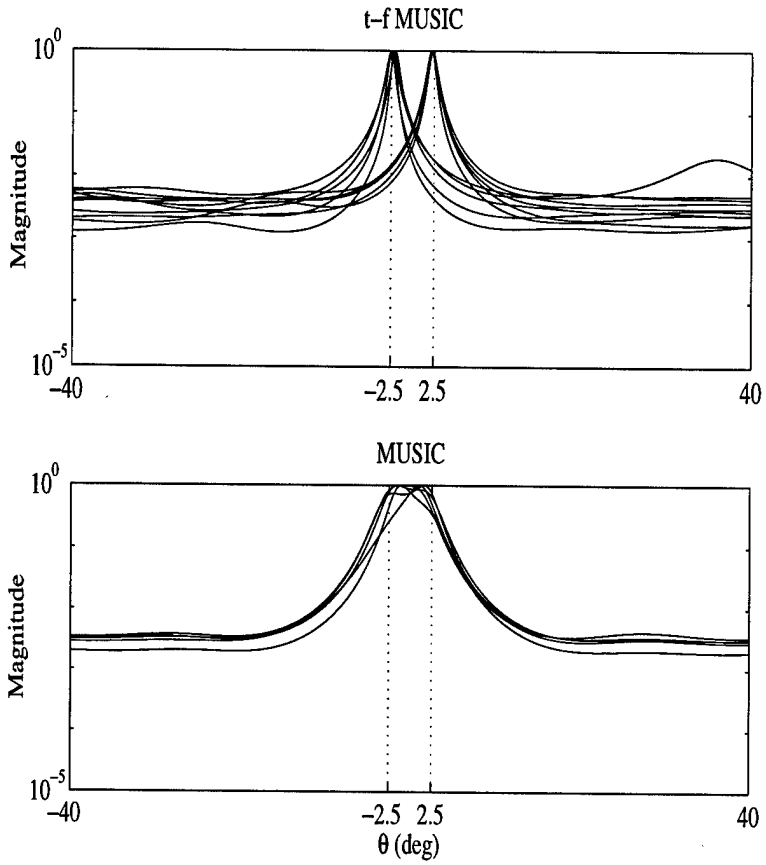

Fig.6 Estimated spatial spectra for closely spaced signals ($m = 8, N = 1024$,SNR= 5 dB,$L = 129$ for t-f MUSIC).

The Spatial Ambiguity Function and Its Applications

Moeness G. Amin[†*], Adel Belouchrani[‡], and Yimin Zhang[†]

[†] Department of Electrical and Computer Engineering,
Villanova University, Villanova, PA 19085

[‡] Department of Electrical Engineering,
Ecole National Polytechnique, Algiers, Algeria

Abstract

This letter introduces the spatial ambiguity functions (SAFs) and discusses their applications to direction finding and source separation problems. We emphasize two properties of the SAFs that make them an attractive tool for array signal processing.

Index Terms

Time-frequency distribution, spatial ambiguity function, joint-variable MUSIC, array signal processing, nonstationary signals.

SPL EDICS: SPL.SP.2.3 (TIME-FREQUENCY SIGNAL ANALYSIS)

* **Corresponding Author:**

Prof. Moeness G. Amin,

Department of Electrical and Computer Engineering,

Villanova University, Villanova, PA 19085

Phone: (610)519-7305 Fax: (610)519-4436 E-mail: moeness@ece.vill.edu

The work of M. G. Amin and Y. Zhang was supported by the Office of Naval Research under Grant N00014-98-1-0176.

I. Introduction

The evaluation of quadratic time-frequency distributions of the data snapshots across the array yields spatial time-frequency distributions (STFDs), which can be used to solve a large class of blind source separation and high-resolution direction-of-arrival (DOA) estimation problems [1], [2]. STFD techniques are appropriate to handle sources of nonstationary waveforms that are highly localized in the time-frequency domain.

The concept of STFD can been extended to arbitrary joint-variable domain [3], [4]. In this letter, the ambiguity functions are considered. Similar to STFDs, spatial ambiguity functions (SAFs) are descriminatory tools. The sources whose ambiguity domain signatures are used in constructing the SAF matrix are the only ones considered for signal separation and subspace estimation.

II. Analysis Model

The following linear data model

$$\mathbf{x}(t) = \mathbf{A}\mathbf{d}(t) + \mathbf{n}(t) \tag{1}$$

is commonly used in narrowband array processing, where $\mathbf{A}$ is the mixing matrix of dimension $m \times n$, $\mathbf{x}(t) = [x_1(t), ..., x_m(t)]^T$ is the sensor array output vector, and $\mathbf{d}(t) = [d_1(t), ..., d_n(t)]^T$ is the source signal vector. The superscript ^{T} denotes the transpose operator. $\mathbf{n}(t)$ is an additive noise vector. In direction finding problems, we require $\mathbf{A}$ to have a known structure.

The SAF matrix of a signal vector $\mathbf{x}(t)$ is defined as

$$\mathbf{D}_{\mathbf{xx}}(\theta, \tau) = \int_{-\infty}^{\infty} \mathbf{x}(u + \tau/2)\mathbf{x}^H(u - \tau/2)e^{j\theta u}du \tag{2}$$

where θ and τ are the frequency-lag and the time-lag, respectively, and ^{H} denotes conjugate transpose. In noise-free environment, $\mathbf{x}(t) = \mathbf{A}\mathbf{d}(t)$, then we have

$$\mathbf{D}_{\mathbf{xx}}(\theta, \tau) = \mathbf{A}\mathbf{D}_{\mathbf{dd}}(\theta, \tau)\mathbf{A}^H. \tag{3}$$

Equation (3) is similar to the formula that has been commonly used in blind source separation and DOA estimation problems, relating the data covariance correlation matrix to the signal correlation matrix [5], [6]. Here, these matrices are replaced by the data spatial ambiguity function and signal ambiguity function matrices, respectively. The two subspaces spanned by the principle eigenvectors of $\mathbf{D_{xx}}(\theta, \tau)$ and the columns of $\mathbf{A}$ are identical. This implies that array signal processing problems can be approached and solved based on the SAF.

III. Properties of Spatial Ambiguity Functions

The SAFs have the following two important offerings that distinguish them from other array spatial functions.

1) The crossterms in between source signals reside on the off-diagonal entries of matrix $\mathbf{D_{dd}}(\theta, \tau)$, violating its diagonal structure, which is necessary to perform blind source separation. In the ambiguity domain, the signal autoterms are positioned near and at the origin, making it easier to leave out crossterms from matrix construction.

2) The autoterms of all narrowband signals, regardless of their frequencies and phases, fall on the time-lag axis ($\theta = 0$), while those of the wideband signals fall on a different (θ, τ) region or spread over the entire ambiguity domain. Therefore, the SAF is a natural choice for recovering and spatially localizing narrowband sources in broadband signal platforms.

IV. Ambiguity-Domain MUSIC

Similar to time-frequency MUSIC [2], the signal and noise subspaces $\mathbf{E} = [\mathbf{E_s}\ \mathbf{E_n}]$ of the SAF matrix $\mathbf{D_{xx}}(\theta, \tau)$ can be obtained by the block joint-diagonalization of $\mathbf{D_{xx}}(\theta, \tau)$ obtained at different (θ, τ) points. Once the noise subspace $\mathbf{E_n}$ is estimated, the ambiguity-domain MUSIC (AD-MUSIC) technique estimates the DOAs by finding the n_o largest peaks of the localization function $f(\phi) = \left|\hat{\mathbf{E}}_\mathbf{n}^H \mathbf{a}(\phi)\right|^{-2}$.

Consider the scenario of a four-element equi-spaced linear array, where one chirp signal and two sinusoidal signals are received. The data record has 128 samples. All three signals have the same SNR of 20 dB. The DOAs of the chirp signal and the two sinusoidal signals are 15, 10, and 0 degrees, respectively. While the ambiguity function of the chirp signal sweeps the ambiguity domain with contribution at the origin, the exact autoterm ambiguity function of the narrowband arrivals $s_1(t)$ and $s_2(t)$ is zero for non-zero frequency-lags and may have non-zero values only along the vertical axis $\theta = 0$.

In this simulation example, we selected 24 points on the time-lag axis, excluding the origin, and as such emphasizing the narrowband components. Fig. 1 shows the ambiguity function where the two vertical lines represent the crossterms between the sinusoidal components. Fig. 2 shows the two estimated spatial spectra, one corresponds to the conventional method and the other corresponds to the AD-MUSIC. There are two dominant eigenvalues for the case of the AD-MUSIC, since we have not deliberately considered the chirp signal through our careful selection of the ambiguity-domain points. It is clear that the AD-MUSIC resolves the two sinusoidal signals, while the conventional MUSIC could not separate the three signals.

V. Ambiguity-Domain Source Separation

Analogous to blind source separation based on STFD [1], blind source separation based on SAF consists mainly of two steps. The first step is to whiten the array signal vector by an $m \times n$ matrix $\mathbf{W}$ such that $(\mathbf{WA})(\mathbf{WA})^H = \mathbf{UU}^H = \mathbf{I}$, i.e., $\mathbf{WA}$ is a unitary matrix. The whitening matrix $\mathbf{W}$ can be obtained, for example, from the covariance matrix [1]. The second step is to perform joint diagonalization to obtain the unitary matrix $\mathbf{U}$ [1], which is then used to provide $\mathbf{A} = \mathbf{W}^{\#}\mathbf{U}$, where $^{\#}$ denotes pseudo-inverse, and the source signal vector is recovered as $\mathbf{s}(t) = \mathbf{U}^H\mathbf{W}\mathbf{x}(t)$. All of the above matrices are replaced by their

estimates when dealing with one realization.

Assume that we have two sources and three equi-spaced sensors. One source is a sinusoid, whereas the other is a pulsed sinusoidal signal that extends over 8 samples. The SNR of both signals, defined in the total power, is 10 dB. In this example, the mixing matrix did not have a presumed structure and its columns were not complex exponential vectors.

The ambiguity function of the mixed signal at the first sensor is shown in Fig. 3. In this specific case, we select four points along the frequency-lag axis and the time-lag axis closest to the origin. Then, by using the spatial ambiguity functions, we are able to recover the original signals from only their observed mixture. Fig. 4 shows the waveforms of the original and the separated signals after multiplication by the proper complex scalar.

VI. Conclusions

The spatial ambiguity function and its application to direction finding and blind source separation have been discussed. Based on the spatial ambiguity functions, we have introduced the ambiguity-domain MUSIC and the ambiguity-domain blind source separation techniques.

References

[1] A. Belouchrani and M. G. Amin, "Blind source separation based on time-frequency signal representation," *IEEE Trans. Signal Processing*, vol. 46, no. 11, pp. 2888-2898, Nov. 1998.

[2] ——, "Time-frequency MUSIC," *IEEE Signal Processing Letters*, vol. 6, no. 5, pp. 109-110, May 1999.

[3] R. G. Baraniuk and L. Cohen, "On joint distributions for arbitrary variables," *IEEE Signal Processing Letters*, vol. 2, no. 1, pp. 10-12, Jan. 1995.

[4] R. G. Baraniuk and D. L. Jones, "Unitary equivalence: a new twist on signal processing," *IEEE Trans. Signal Processing*, vol. 43, no. 10, pp. 2269-2282, Oct. 1995.

[5] R. Schmidt, "Multiple emitter location and signal parameter estimation," *IEEE Trans. Antenna Propagat.*, vol. 34, no. 1, pp. 276-280, Jan. 1986.

[6] A. Belouchrani, K. Abed Meraim, J.-F. Cardoso, and E. Moulines, "A blind source separation technique using second order statistics," *IEEE Trans. Signal Processing*, vol. 45, no. 2, pp. 434-444, Feb. 1997.

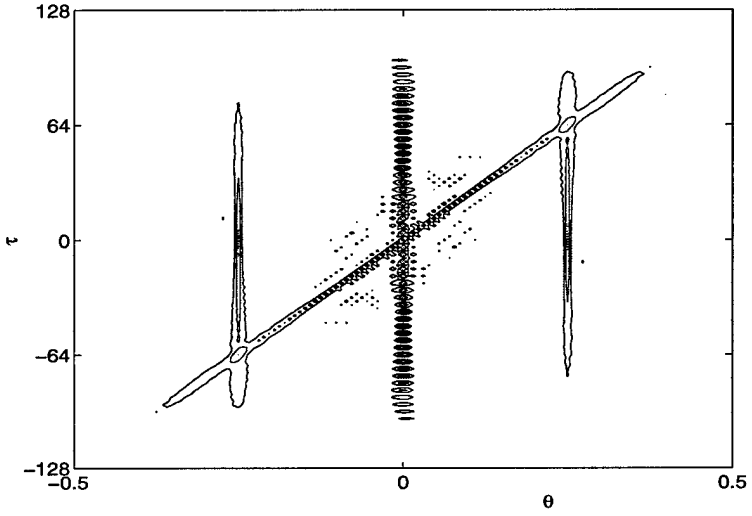

Fig. 1 The ambiguity functions of the chirp signal and two sinusoidal signals.

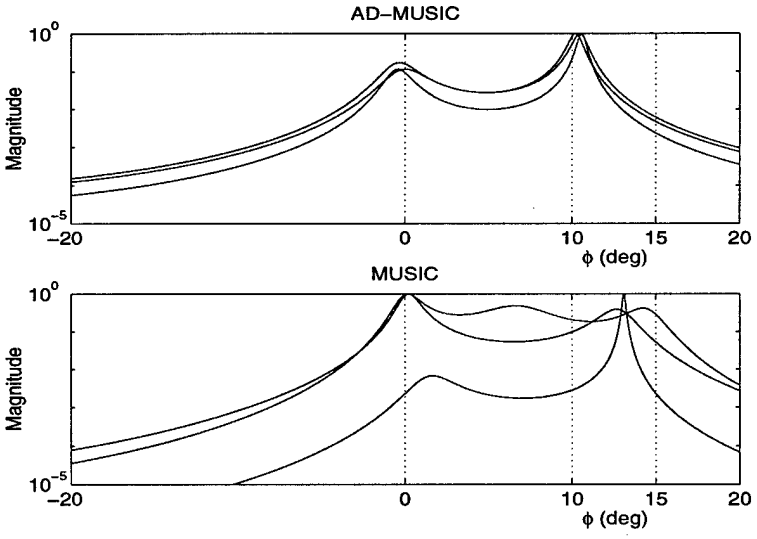

Fig. 2 The estimated spatial spectra of AD-MUSIC and conventional MUSIC.

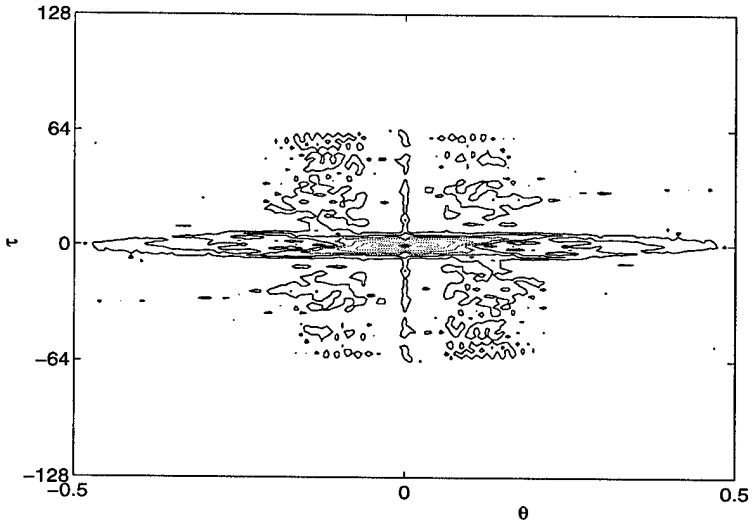

Fig. 3 The ambiguity functions of the mixed signal.

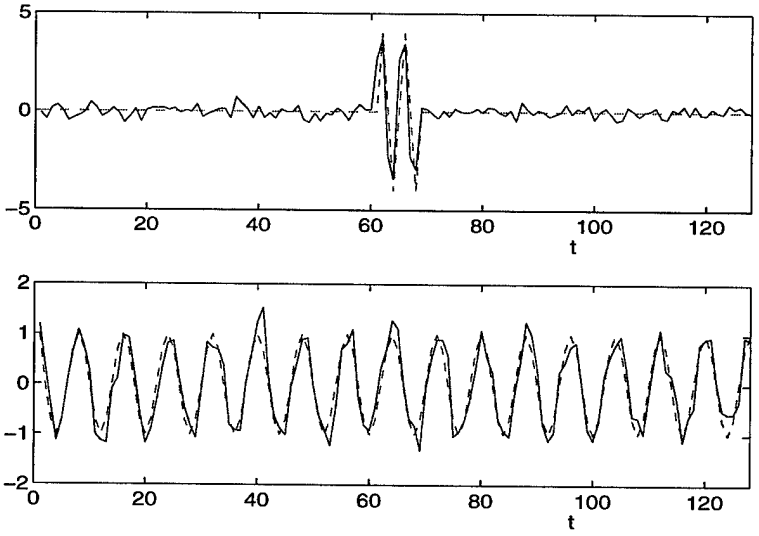

Fig. 4 Real part of the waveforms of the source signals (– – –) and the separated signals(——).

Direction Finding Based on Spatial Time-Frequency Distribution Matrices

Moeness G. Amin and Yimin Zhang
Department of Electrical and Computer Engineering,
Villanova University, Villanova, PA 19085
Phone: (610)519-7305 Fax: (610)519-4436
E-mail: moeness@ece.vill.edu, yimin@ieee.org

Spatial time-frequency distributions (STFDs) have been recently introduced as the natural means to deal with source signals that are localizable in the time-frequency domain. It has been shown that improved estimates of the signal and noise subspaces are achieved by constructing the subspaces from the time-frequency signatures of the signal arrivals rather than from the data covariance matrices, which are commonly used in conventional subspace estimation methods. This paper discusses the application of STFD to high-resolution direction finding. We focus on both the role and the effect of crossterms in angle estimation when multiple time-frequency points are incorporated. Simulation examples are presented to compare the performance of joint block-diagonalization and time-frequency averaging techniques for incorporating multiple autoterm and crossterm points in subspace estimation.

Key Words: Spatial time-frequency distribution, direction finding, crossterm distribution, array signal processing

1. INTRODUCTION

In many signal processing applications, the multidimensional signal is directly utilized to estimate some signal parameters, such as the number of sources and their directions of arrival [1, 2]. Subspace-based methods use a geometrical relation involving the exact moments of the data. The desired signal parameters are extracted by solving this relation in some approximate sense, and by using sample moments instead of the exact ones. The commonly applied eigenstructure subspace methods assume stationary signals. When the frequency content of the measured

This work was supported by the Office of Naval Research under Grant N00014-98-1-0176.

data is time-varying, the performance of these methods can be significantly improved by proper use of the data time-frequency characteristics.

The evaluation of quadratic time frequency distributions of the data snapshots across the array yields spatial time-frequency distributions, which are most appropriate to handle sources of nonstationary waveforms that are highly localized in the time-frequency domain [3, 4, 9]. Spreading the noise power while localizing the source energy in the time-frequency domain amounts to increasing the robustness of eigenstructure signal and noise subspace estimation methods with respect to channel and receiver noise, and hence improves resolution and signal separation performance.

In this paper, we consider the applications of spatial time-frequency distributions to the direction finding problem. In [4], the time-frequency MUSIC (t-f MUSIC) was introduced. In [9], the subspace analysis for the time-frequency distribution matrices is presented, and the performance of the time-frequency MUSIC is analyzed. The time-frequency maximum likelihood (t-f ML) also has been introduced and analyzed [8]. However, these results were obtained under the assumption that only the autoterms of STFDs are considered for STFD matrix construction. The effect of crossterms have not been made clear. In this paper, we focus on the performance of the t-f MUSIC when crossterms are incorporated.

This paper is organized as follows. Section 2 introduces the signal model, and gives a brief review of the definition and properties of the spatial time-frequency distributions. In Section 3, the time-frequency MUSIC algorithm is briefly discussed. In Section 4, we consider the effect of crossterms to direction finding. Simulation examples are presented to examine the effect of crossterms, and a comparison between joint block-diagonalization and time-frequency averaging is performed.

2. SPATIAL TIME-FREQUENCY DISTRIBUTIONS

2.1. Signal Model

In narrowband array processing, when n signals arrive at an m-element array, the linear data model

$$\mathbf{x}(t) = \mathbf{y}(t) + \mathbf{n}(t) = \mathbf{A}\mathbf{d}(t) + \mathbf{n}(t) \tag{1}$$

is commonly used, where $\mathbf{A}$ is the mixing matrix of dimension $m \times n$, $\mathbf{x}(t) = [x_1(t), ..., x_m(t)]^T$ is the sensor array output vector, and $\mathbf{d}(t) = [d_1(t), ..., d_n(t)]^T$ is the source signal vector. The superscript ^{T} denotes the transpose operator. In direction finding problems, the DOAs of the source signals $\mathbf{\Theta} = [\theta_1, ..., \theta_n]^T$ are of interest, and the mixing matrix takes the form of $\mathbf{A}(\mathbf{\Theta}) = [\mathbf{a}(\theta_1)...\mathbf{a}(\theta_n)]$, where $\mathbf{a}(\theta_i)$ is the ith steering vector with known structure. On the other hand, in blind source separation application, it is often assumed that the array manifold is unknown, and the mixing matrix is not finitely parameterized. $\mathbf{n}(t)$ is an additive noise vector whose elements are modeled as stationary, spatially and temporally white, zero-mean complex random processes, independent of the source signals. That is,

$$E[\mathbf{n}(t+\tau)\mathbf{n}^H(t)] = \sigma\delta(\tau)\mathbf{I} \text{ and } E[\mathbf{n}(t+\tau)\mathbf{n}^T(t)] = \mathbf{0} \text{ for any } \tau \tag{2}$$

where $\delta(\tau)$ is the Dirac delta function, $\mathbf{I}$ denotes the identity matrix, σ is the noise power at each sensor, and the superscript ^{H} denotes conjugate transpose, and $E(\cdot)$ is the statistical expectation operator.

In equation (1), it is assumed that the number of sensors is higher than the number of sources, i.e., $m > n$. Further, matrix $\mathbf{A}$ is full column rank, which implies that the steering vectors corresponding to n different angles of arrival are linearly independent. The correlation matrix is given by

$$\mathbf{R_{xx}} = E[\mathbf{x}(t)\mathbf{x}^H(t)] = \mathbf{A}\mathbf{R_{dd}}\mathbf{A}^H + \sigma\mathbf{I}, \tag{3}$$

where $\mathbf{R_{dd}} = E[\mathbf{d}(t)\mathbf{d}^H(t)]$ is the signal correlation matrix. We assume that $\mathbf{R_{xx}}$ is nonsingular, and the observation period consists of N snapshots with $N > m$.

2.2. Concept of Spatial Time-Frequency Distribution

The spatial time-frequency distributions (STFDs) based on Cohen's class of time-frequency distribution were introduced in [3]. The discrete form of Cohen's class of time-frequency distribution of a signal $x(t)$ is given by [5]

$$D_{xx}(t,f) = \sum_{m=-\infty}^{\infty}\sum_{\tau=-\infty}^{\infty} \phi(m,\tau)x(t+m+\tau)x^*(t+m-\tau)e^{-j4\pi f\tau}, \tag{4}$$

where $\phi(m,\tau)$ is a kernel and the superscript * denotes complex conjugate. The spatial time-frequency distribution matrix is obtained by replacing $x(t)$ by the data snapshot vector $\mathbf{x}(t)$,

$$\mathbf{D_{xx}}(t,f) = \sum_{m=-\infty}^{\infty}\sum_{\tau=-\infty}^{\infty} \phi(m,\tau)\mathbf{x}(t+m+\tau)\mathbf{x}^H(t+m-\tau)e^{-j4\pi f\tau}. \tag{5}$$

Substitute (1) into (5), we can extend $\mathbf{D_{xx}}$ to the following form

$$\mathbf{D_{xx}}(t,f) = \mathbf{D_{yy}}(t,f) + \mathbf{D_{yn}}(t,f) + \mathbf{D_{ny}}(t,f) + \mathbf{D_{nn}}(t,f) \tag{6}$$

Under the uncorrelated signal and noise assumption and the zero-mean noise property, it is obvious that $E[\mathbf{D_{yn}}(t,f)] = E[\mathbf{D_{ny}}(t,f)] = \mathbf{0}$, and it follows

$$\begin{aligned} E[\mathbf{D_{xx}}(t,f)] &= \mathbf{D_{yy}}(t,f) + E[\mathbf{D_{nn}}(t,f)] \\ &= \mathbf{A}\mathbf{D_{dd}}(t,f)\mathbf{A}^H + E[\mathbf{D_{nn}}(t,f)]. \end{aligned} \tag{7}$$

Equation (7) is similar to equation (3) that has been commonly used in DOA estimation and blind source separation problems, relating the signal correlation matrix to the data spatial correlation matrix. In the above formulation, however, the correlation matrices are replaced by the spatial time-frequency distribution matrices. This implies that key problems in various applications of array processing, specifically those dealing with nonstationary signal environments, can be approached using bilinear transformations.

It is noted that the relationship (7) holds true for every (t,f) point. In order to reduce the effect of noise and ensure the full column rank property of the STFD

matrix, we consider multiple time-frequency points. Joint block-diagonalization [6, 14] and time-frequency averaging [7, 9] are the two main approaches that have been used for this purpose.

The aforementioned fact of incorporating multiple time-frequency points allows us to choose specific time-frequency regions, and as such perform array processing for a subclass of signals. For example, two sources A and B are incident on a multisensor array. As shown in Fig. 1, we assume that source A occupies the time-frequency region R_a, where source B occupies the time-frequency region R_b. The time-frequency signatures of the two sources overlap, but each source still has a time-frequency region that is not intruded over by the other source. Therefore, when we select (t, f) points of the region $R_a \cap \bar{R}_b$, only signal A will be involved. The performance improvement is specially significant for closely spaced signals [10].

When n_o source signals are selected out of the n signals based on their time-frequency signatures, (7) becomes

$$E\left[\mathbf{D_{xx}}(t,f)\right] = \mathbf{A}^o \mathbf{D}^o_{\mathbf{dd}}(t,f)(\mathbf{A}^o)^H + E\left[\mathbf{D_{nn}}(t,f)\right]. \tag{8}$$

where $\mathbf{A}^o$ and $\mathbf{D}^o_{\mathbf{dd}}(t,f)$, respectively, denote the mixing matrix and the source signal TFD matrix defined using the selected n_o signals.

It is important to note that with the ability to construct the STFD matrix from one or few signal arrivals, the well known $m > n$ condition on source localization using arrays can be relaxed to $m > n_o$. That is to say, we can perform direction finding or source separation with the number of array sensors smaller than the number of impinging signals.

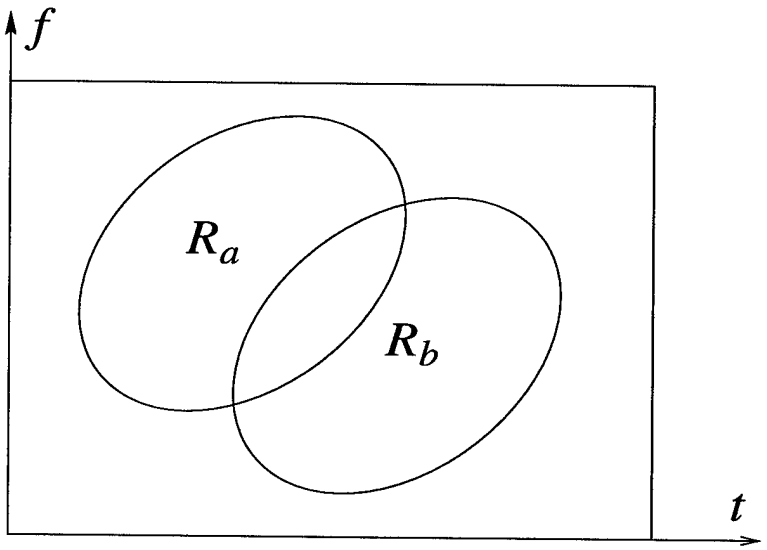

Fig. 1 Signals with different time-frequency signatures.

2.3. Properties

We focus here on frequency modulation (FM) signals, modeled as

$$\mathbf{d}(t) = [d_1(t), ..., d_n(t)]^T = [D_1 e^{j\psi_1(t)}, ..., D_n e^{j\psi_n(t)}]^T, \tag{9}$$

where D_i and $\psi_i(t)$ are the fixed amplitude and time-varying phase of ith source signal. For each sampling time t, $d_i(t)$ has an instantaneous frequency (IF) $f_i(t) = \frac{1}{2\pi}\frac{d\psi_i(t)}{dt}$.

The consideration of FM signals is motivated by their simplicity as well as the fact that these signals are uniquely characterized by their instantaneous frequencies, and therefore, they have clear time-frequency signatures that can be utilized by the STFD approach.

Consider a simple case that the FM signals are mutually uncorrelated over the observation period, and the time-frequency signatures do not overlap, i.e.,

$$\frac{1}{N}\sum_{k=1}^{N} d_i(k)d_j^*(k) = 0 \qquad \text{for } i \neq j,\ i,j = 1, ..., n. \tag{10}$$

then the signal correlation matrix in (3) is

$$\mathbf{R_{dd}} = diag\left[D_1^2, D_2^2, ..., D_n^2\right]$$

where $diag[\cdot]$ is the diagonal matrix formed with the elements of its vector valued arguments.

We consider pseudo Wigner-Ville distribution (PWVD) as an example of Cohen's class here. The spatial pseudo Wigner-Ville distribution (SPWVD) matrix, using a rectangular window of odd length L, is

$$\mathbf{D_{xx}}(t,f) = \sum_{\tau=-\frac{L-1}{2}}^{\frac{L-1}{2}} \mathbf{x}(t+\tau)\mathbf{x}^H(t-\tau)e^{-j4\pi f\tau}. \tag{11}$$

Assuming that the third-order derivative of the phase is negligible over the window length L, then along the true time-frequency points of ith signal, $f_i = \frac{1}{2\pi}\frac{d\psi_i(t)}{dt}$, and $\psi_i(t+\tau) - \psi_i(t-\tau) - 4\pi f_i\tau = 0$. Accordingly, the ith diagonal element of PWVD matrix $\mathbf{D_{dd}}(t,f)$ becomes

$$D_{d_i d_i}(t, f_i) = \sum_{\tau=-\frac{L-1}{2}}^{\frac{L-1}{2}} D_i^2 = LD_i^2. \tag{12}$$

On the other hand, under the spatial white and temporal white assumptions, the statistical expectation of the noise STFD matrix $\mathbf{D_{nn}}(t,f)$ is

$$E\left[\mathbf{D_{nn}}(t,f)\right] = \sum_{\tau=-\frac{L-1}{2}}^{\frac{L-1}{2}} E\left[\mathbf{n}(t+\tau)\mathbf{n}^H(t-\tau)\right] e^{-j4\pi f\tau} = \sigma\mathbf{I}. \tag{13}$$

Therefore, when selecting the time-frequency points along the time-frequency signature or the IF of an FM signal, the SNR of model (7) is LD_i^2/σ, which has an improved factor L over the one associated with model (3).

The PWVD of each FM source has a constant value over the observation period, providing that we leave out the rising and falling power distributions at both ends of the data record. For convenience of analysis, we select those $N-L+1$ time-frequency points of constant distribution value for each source signal. Therefore, the averaged STFD over the time-frequency signatures of n_o sources, i.e., a total of $n_o(N-L+1)$ time-frequency points, is given by

$$\hat{\mathbf{D}} = \frac{1}{n_o(N-L+1)} \sum_{q=1}^{n_o} \sum_{i=1}^{N-L+1} \mathbf{D}_{\mathbf{xx}}(t_i, f_{q,i}), \tag{14}$$

where $f_{q,i}$ is the instantaneous frequency of the qth signal at the ith time sample. The expectation of the averaged STFD matrix is

$$\mathbf{D} = E\left[\hat{\mathbf{D}}\right] = \frac{L}{n_o} \mathbf{A}^o \mathbf{R}^o_{\mathbf{dd}} (\mathbf{A}^o)^H + \sigma \mathbf{I}, \tag{15}$$

where $\mathbf{R}^o_{\mathbf{dd}}$ represents the signal correlation matrix formulated by only considering n_o signals out of the total number of signal arrivals n.

Let $\lambda^o_1 > \lambda^o_2 > \cdots > \lambda^o_{n_o} > \lambda^o_{n_o+1} = \lambda^o_{n_o+2} = \cdots = \lambda^o_m = \sigma$ denote the eigenvalues of the correlation matrix defined from a data record of a mixture of the n_o selected FM signals, $\mathbf{R}^o_{\mathbf{xx}} = \mathbf{A}^o \mathbf{R}^o_{\mathbf{dd}} (\mathbf{A}^o)^H + \sigma \mathbf{I}$. We also denote $\lambda^{tf}_1 > \lambda^{tf}_2 > \cdots > \lambda^{tf}_{n_o} > \lambda^{tf}_{n_o+1} = \lambda^{tf}_{n_o+2} = \cdots = \lambda^{tf}_m = \sigma^{tf}$ as the eigenvalues of $\mathbf{D}$ defined in (15). From (15), we have

$$\lambda^{tf}_i = \begin{cases} \dfrac{L}{n_o}(\lambda^o_i - \sigma) + \sigma = \dfrac{L}{n_o}\tilde{\lambda}^o_i + \sigma & i \le n_o \\ \sigma^{tf} = \sigma & n_o < i \le m. \end{cases} \tag{16}$$

where $\tilde{\lambda}^o_i \triangleq \lambda^o_i - \sigma$.

3. TIME-FREQUENCY MUSIC

When n_o signals are selected, the t-f MUSIC determines the angles of the n_o signals by locating the n_o peaks of the spatial spectrum defined from the n_o signals' respective time-frequency regions [4].

$$\begin{aligned} f^{tf}_{MU}(\theta) &= \left[\mathbf{a}^H(\theta) \hat{\mathbf{G}}^{tf} \left(\hat{\mathbf{G}}^{tf}\right)^H \mathbf{a}(\theta)\right]^{-1} \\ &= \left[\mathbf{a}^H(\theta) \left(\mathbf{I} - \hat{\mathbf{S}}^{tf} \left(\hat{\mathbf{S}}^{tf}\right)^H\right) \mathbf{a}(\theta)\right]^{-1} \end{aligned} \tag{17}$$

where $\mathbf{G}^{tf}$ and $\mathbf{S}^{tf}$ are the noise and signal subspace estimates obtained from the eigenstructure of matrix $\mathbf{D}$. When $N-L+1$ points for each of the n_o FM signals are used in the time-frequency averaging, the variance of the DOA estimates based on t-f MUSIC is given by [9]

$$E\left(\hat{\omega}^{tf}_i - \omega^{tf}_i\right)^2 = \frac{1}{2(N-L+1)} \frac{\mathbf{a}^H(\theta_i) \mathbf{U}^{tf} \mathbf{a}(\theta_i)}{h^{tf}(\theta_i)} \tag{18}$$

where ω is the spatial frequency associated to DOA θ, and $\hat{\omega}^{tf}$ is its estimate obtained by the t-f MUSIC. Moreover,

$$\begin{aligned}\mathbf{U}^{tf} &= \frac{\sigma L}{n_o(N-L+1)}\left[\sum_{k=1}^{n_o}\frac{\lambda_k^{tf}}{(\sigma-\lambda_k^{tf})^2}\mathbf{s}_k^{tf}\left(\mathbf{s}_k^{tf}\right)^H\right]\delta_{i,j} \\ &= \frac{\sigma}{N-L+1}\left[\sum_{k=1}^{n_o}\frac{\tilde{\lambda}_k^o+\frac{n_o}{L}\sigma}{(\tilde{\lambda}_k^o)^2}\mathbf{s}_k^o\left(\mathbf{s}_k^o\right)^H\right]\delta_{i,j}.\end{aligned} \tag{19}$$

and

$$h^{tf}(\theta) = \mathbf{c}^H(\theta)\mathbf{G}^{tf}\left(\mathbf{G}^{tf}\right)^H\mathbf{c}(\theta), \tag{20}$$

with

$$\mathbf{c}(\theta) = d\mathbf{a}(\theta)/d\omega. \tag{21}$$

From (18) and (19), two important observations are in order. First, if the signals are both localizable and separable in the time-frequency domain, then the reduction of the number of signals from n to n_o greatly reduces the estimation error, specifically when the signals are closely spaced. The second observation relates to SNR enhancements. The above equations show that error reductions using STFDs are more pronounced for the cases of low SNR and/or closely spaced signals. It is clear from (19) that, when $\lambda_k^o \gg \sigma$ for $k = 1, 2, ..., n_o$, the results are almost independent of L (assume $N \gg L$ so that $N - L + 1 \simeq N$), and therefore there would be no obvious improvement in using the STFD over conventional array processing. On the other hand, when some of the eigenvalues are close to σ ($\lambda_k^o \simeq \sigma$, for some $k = 1, 2, ..., n_o$), which is the case of weak or closely spaced signals, all the results of above three equations are reduced by a factor of up to $G = \frac{L}{n_o}$, respectively. This factor represents, in essence, the gain achieved by using STFD processing. To numerically demonstrate the effect of the SNR enhancement, Fig. 2 shows the following normalized factor that is obtained using the kth term in the summation (19) and its respective value in conventional MUSIC

$$\eta_k = \frac{L}{n_o}\frac{\lambda_k^{tf}}{(\sigma-\lambda_k^{tf})^2}\Bigg/\frac{\lambda_k^o}{(\sigma-\lambda_k^o)^2} = \frac{\tilde{\lambda}_k^o+\frac{n_o}{L}\sigma}{\tilde{\lambda}_k^o+\sigma}$$

versus $\tilde{\lambda}_k^o/\sigma$ for different gain factor $G = L/n_o$. This is a key factor in determining the DOA variance of the t-f MUSIC estimates (18). It is evident from this figure that the effect of the gain factor becomes significant at low SNR.

4. EFFECT OF CROSSTERM DISTRIBUTION

4.1. Crossterm Distribution

Crossterms are a byproduct of the time-frequency distribution due to its bilinearity. Although different kernels have different ways of mitigating crossterms [15], nevertheless complete removal of crossterms are very difficult to achieve.

There are two sources of crossterms in the underlying direction finding problems. The first type is due to the interactions between the components of the same source

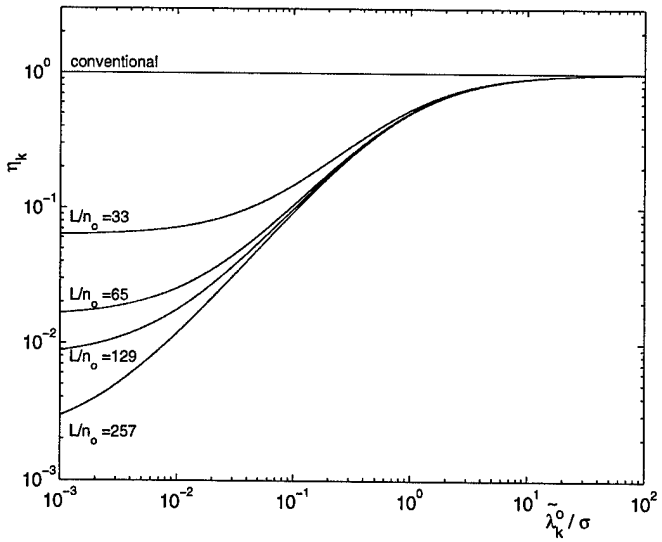

Fig. 2 Normalized factor η_k vs. $\tilde{\lambda}_k^o/\sigma$.

signal. These crossterms, always reside, along with the autoterms, on the main diagonal of the source TFD matrix. The other type of crossterms are those generated from the interactions between two signal components belonging to two different sources, These crossterms are associated with cross-TFD of the source signals and, at any given time-frequency point, they constitute the off-diagonal entries of the source TFD matrices.

Here we consider the second type of crossterms. When crossterms are present at the selected time-frequency point, the source TFD takes the following general form

$$\mathbf{D_{dd}}(t,f) = \begin{bmatrix} D_{d_1d_1}(t,f) & D_{d_1d_2}(t,f) & \cdots & D_{d_1d_n}(t,f) \\ D_{d_2d_1}(t,f) & D_{d_2d_2}(t,f) & \cdots & D_{d_2d_n}(t,f) \\ \vdots & \vdots & \ddots & \vdots \\ D_{d_nd_1}(t,f) & D_{d_nd_2}(t,f) & \cdots & D_{d_nd_n}(t,f) \end{bmatrix} \tag{22}$$

where the off-diagonal element

$$D_{d_id_j}(t,f) = \sum_{m=-\infty}^{\infty} \sum_{\tau=-\infty}^{\infty} \phi(m,\tau) d_i(t+m+\tau) d_j^*(t+m-\tau) e^{-j4\pi f\tau},$$

is the crossterm of source signals $d_i(t)$ and $d_j(t)$ at the point (t,f).

4.2. Comparison to Cross-Correlation

Here we compare the crossterms to the cross-correlation between signals in conventional array processing, whose properties are familiar. When signals are corre-

lated, the covariance matrix of the source signals is given at the form

$$\mathbf{R_{dd}} = \begin{bmatrix} R_{d_1d_1} & R_{d_1d_2} & \cdots & R_{d_1d_n} \\ R_{d_2d_1} & R_{d_2d_2} & \cdots & R_{d_2d_n} \\ \vdots & \vdots & \ddots & \vdots \\ R_{d_nd_1} & R_{d_nd_2} & \cdots & R_{d_nd_n} \end{bmatrix} \tag{23}$$

where the off-diagonal element

$$R_{d_id_j} = E[d_i(t)d_j^*(t)]$$

represents the correlation between source signals d_i and d_j. Direction finding problems can usually be solved when the signals are partially correlation, however, full rank property of the covariance matrix $\mathbf{R_{dd}}$ is a necessary condition.

Comparing equations (22) and (23), it is clear that the cross-correlation terms and the crossterms have analogous form and similar function. However, (23) is the correlation matrix that is constant in stationary signal environments, whereas (22) is defined at a (t, f) point and its value usually varies with respect to time t and frequency f under both stationary and nonstationary signal conditions. When multiple (t, f) points are incorporated, the effect of crossterm may be reduced, since the crossterm usually oscillates with respect to time. In the next subsection, we demonstrate this property by using simulation examples.

4.3. Examples

Consider a six-element linear array with half-wavelength inter-element spacing, and two chirp signals arrive. The start and end frequencies of the first signal $d_1(t)$ are $f_{1s} = 0.1$ and $f_{1e} = 0.5$, and those for the second signal $d_2(t)$ are $f_{2s} = 0$ and $f_{2e} = 0.4$, respectively. The SNR is 10 dB for each signal, and the DOAs of the two signals are $\theta_1 = -10°$ and $\theta_2 = 10°$, respectively. The number of samples is 256. PWVD is used and the window length is $N = 129$. Fig. 3 shows the PWVD of the mixed signals at the first sensor.

The expressions of the signals at the reference array element are given by

$$d_1(t) = \exp[j(0.1t + 0.2t^2/N)] \quad \text{and} \quad d_2(t) = \exp[j0.2t^2/N] \tag{24}$$

The autoterms and the crossterms are obtained as

$$D_{d_1d_1}(t,f) = \begin{cases} L & f(t) = 0.1 + 0.4t/N \\ \dfrac{\sin[2\pi L(0.1 + 0.4t/N - f)]}{\sin[2\pi(0.1 + 0.4t/N - f)]} & \text{otherwise} \end{cases} \tag{25}$$

$$D_{d_2d_2}(t,f) = \begin{cases} L & f(t) = 0.4t/N \\ \dfrac{\sin[2\pi L(0.4t/N - f)]}{\sin[2\pi(0.4t/N - f)]} & \text{otherwise} \end{cases} \tag{26}$$

$$D_{d_1d_2}(t,f) = \begin{cases} L\exp[j0.2\pi t] & f(t) = 0.05 + 0.4t/N \\ \dfrac{\sin[2\pi L(0.05 + 0.4t/N - f)]}{\sin[2\pi(0.05 + 0.4t/N - f)]}\exp[j0.2\pi t] & \text{otherwise} \end{cases} \tag{27}$$

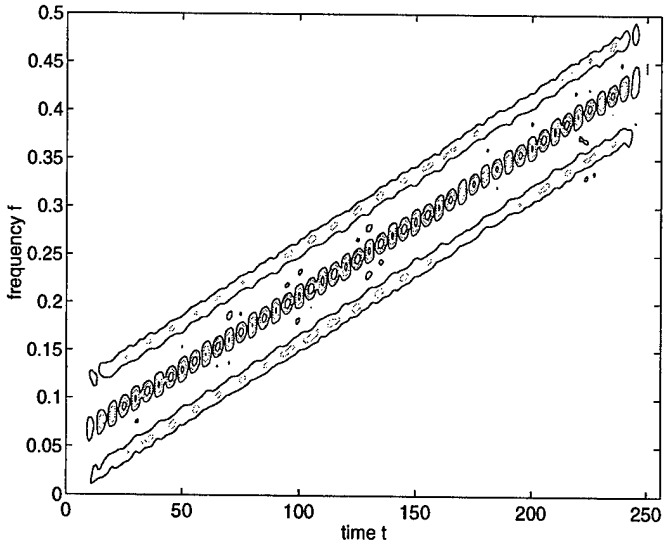

Fig. 3 PWVD of two chirp signals.

and

$$D_{d_2d_1}(t,f) = D^*_{d_1d_2}(t,f). \tag{28}$$

Specially, we consider the autorerms and the crossterms at the following two regions: i) autoterm regions (t, f_1) with $f_1(t) = 0.1 + 0.4t/N$ and (t, f_2) with $f_2(t) = 0.4t/N$, where the autoterms are dominant; and ii) crossterm region (t, f_c) with $f_c(t) = [f_1(t) + f_2(t)]/2 = 0.05 + 0.4t/N$, where the crossterm is dominant. Both the autoterm and crossterm regions have large peak values and are most likely to be selected.

i) *Autoterm regions.* In the autoterm region of $d_1(t)$, (t, f_1), the autoterm of $d_1(t)$ is constant. The autoterm of $d_2(t)$ and the crossterm between $d_1(t)$ and $d_2(t)$ are relatively small. The source TFD matrices with this region have the form of

$$\mathbf{D_{dd}}(t, f_1) = \begin{bmatrix} L & o \\ o & o \end{bmatrix}$$

where o denotes a negligibly smaller value. Similar results can be obtained for the autoterm region of $d_2(t)$, where the source TFD matrices

$$\mathbf{D_{dd}}(t, f_2) = \begin{bmatrix} o & o \\ o & L \end{bmatrix}.$$

Since both matrices have dominant diagonal elements with constant values, incorporating only autoterm points, either by joint block-diagonalization or by time-frequency averaging, usually provides good direction finding performance.

ii) *Crossterm regions.* In this region the crossterms $D_{d_1d_2}$ and $D_{d_2d_1}$ are dominant. These crossterms are conjugate to each other, and the source TFD matrices

at this region have the following form

$$\mathbf{D_{dd}}(t, f_c) = \begin{bmatrix} o & L\exp(j0.2\pi t) \\ L\exp(-j0.2\pi t) & o \end{bmatrix}.$$

which is anti-diagonal. Note that unlike a correlation matrix at coherent signal case, which is singular, the above source TFD matrix is still full rank because of the absence of dominant diagonal elements (although the matrix is not necessary positive definite). Accordingly, the noise subspace can be properly estimated, even when only the crossterm points are selected.

However, since the crossterms change with time t, taking both positive and negative values. Summing them at different (t, f) points yields small smoothed values. Therefore, the time-frequency averaging may lead very degraded performance in some cases. On the other hand, performing joint block-diagonalization instead of time-frequency averaging avoids such risk.

Fig. 4 and Fig. 5 show the estimated spatial spectra of the t-f MUSIC by using joint block-diagonalization and time-frequency averaging, respectively. From top to bottom, each figure shows the results by choosing i) autoterm regions $f(t) = f_1(t)$ and $f(t) = f_2(t)$, ii) crossterm region $f(t) = [f_1(t) + f_2(t)]/2$, iii) autoterm and crossterm regions $f(t) = f_1(t)$, $f(t) = f_2(t)$, and $f(t) = [f_1(t) + f_2(t)]/2$, and iv) autoterm region of the first signal, $f(t) = f_1(t)$.

In this case, both the joint block-diagonalization and time-frequency averaging resolve the signals in the second and third cases, where the crossterm points are included. However, the performance is degraded when using the time-frequency averaging methods. Table 1 shows the DOA variance of signal $d_1(t)$ obtained from 100 independent Monte-Carlo runs. It is evident that the joint block-diagonalization outperforms the time-frequency averaging, particularly when the crossterm region is involved. The fourth case in which only one of the two signals is selected has the best performance for both methods of joint block-diagonalization and time-frequency averaging. An interesting observation is that, in the second case, where only the crossterm region is used, the joint block-diagonalization yields second best performance, whereas the time-frequency averaging shows its worst performance.

TABLE 1
Variances of DOA estimates

	case i)	case ii)	case iii)	case iv)
Joint block-diagonalization	0.160	0.129	0.238	0.092
Time-frequency averaging	0.236	0.556	0.359	0.167

It is noted that the crossterm becomes less oscillatory as the time-frequency signatures of the two source signals become closer. When the signals are coherent, the two signals will share the same time-frequency signatures. The crossterms reside on top of the autoterms, and they will no longer oscillate along the crossterm signature. In such case, the source TFD matrices are singular at each points, and the t-f MUSIC cannot realize high-resolution DOA estimation. In this case, pre-processing methods like spatial averaging methods [12, 13] shall be used. An

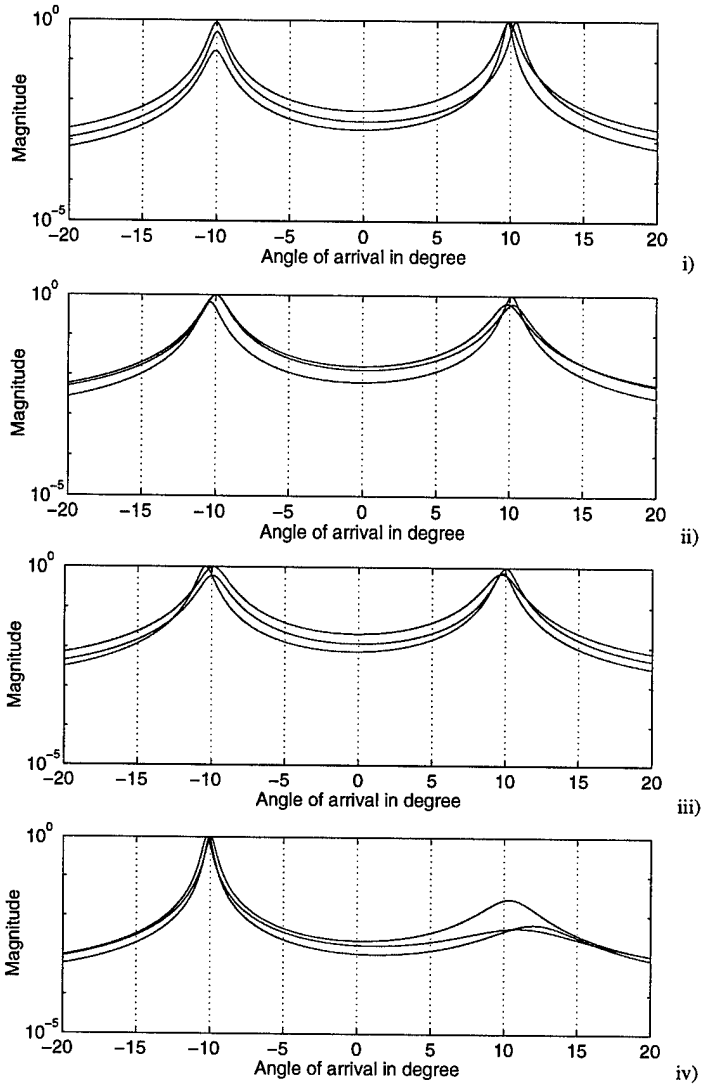

Fig. 4 Spatial spectra estimates by using joint block-diagonalization. From top:
i) autoterm regions $f(t) = f_1(t)$ and $f(t) = f_2(t)$,
ii) crossterm region $f(t) = [f_1(t) + f_2(t)]/2$,
iii) autoterm and crossterm regions specified in i) and ii), and
iv) autoterm region of the first signal, $f(t) = f_1(t)$.

alternative way is to use the time-frequency maximum likelihood (t-f ML) method [8].

5. CONCLUSIONS

The performance of time-frequency MUSIC (t-f MUSIC) has been discussed when multiple time-frequency points are incorporated and crossterm regions are involved. The analysis and simulation results have shown that the crossterm regions can be

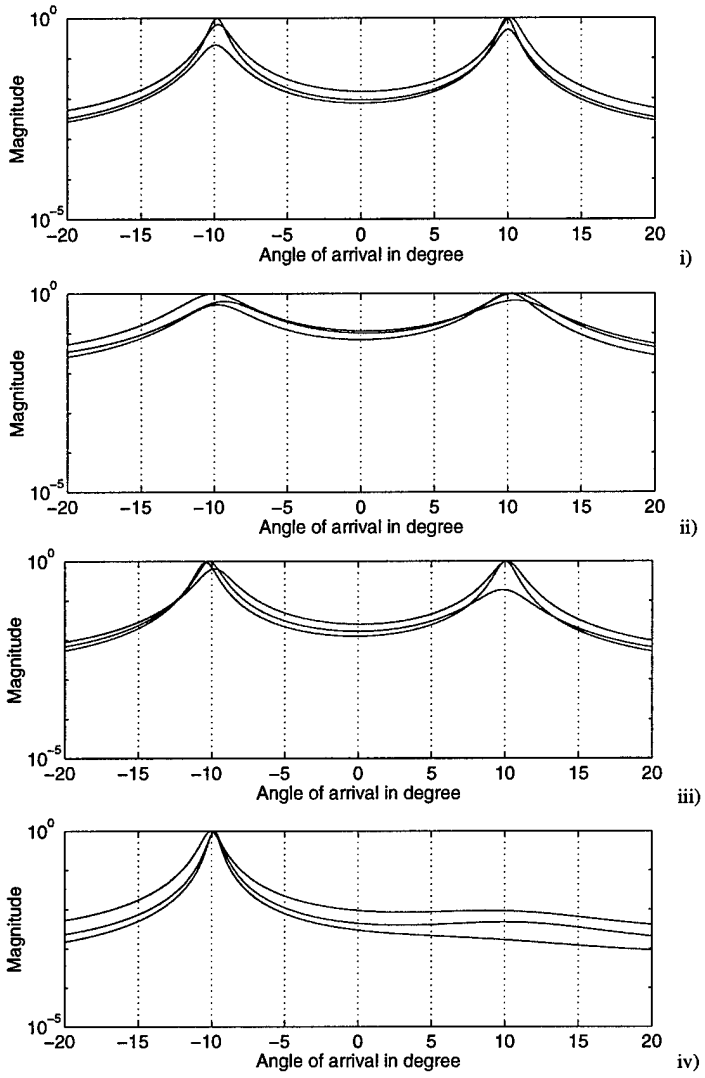

Fig. 5 Spatial spectra estimates by using time-frequency averaging. From top:
i) autoterm regions $f(t) = f_1(t)$ and $f(t) = f_2(t)$,
ii) crossterm region $f(t) = [f_1(t) + f_2(t)]/2$,
iii) autoterm and crossterm regions specified in i) and ii), and
iv) autoterm region of the first signal, $f(t) = f_1(t)$.

incorporated in direction finding. However, when the time-frequency averaging methods are used, the use of crossterms may degrade the performance.

REFERENCES

1. R. O. Schmidt, "Multiple emitter location and signal parameter estimation," *IEEE Trans. Antennas Propagat.*, vol. 34, no. 3, pp. 276–280, March 1986.

2. M. Wax and T. Kailath, "Detection of signals by information theoretic criteria," *IEEE Trans. Acoust., Speech, Signal Proc.*, vol. 33, no. 2, pp. 387–392, April 1985.

3. A. Belouchrani and M. Amin, "Blind source separation based on time-frequency signal representation," *IEEE Trans. Signal Processing*, vol. 46, no. 11, pp. 2888–2898, Nov. 1998.

4. ——, "Time-frequency MUSIC," *IEEE Signal Processing Letters*, vol. 6, no. 5, pp. 109–110, May 1999.

5. L. Cohen, *Time-Frequency Analysis*, Englewood Cliffs, NJ: Prentice Hall, 1995.

6. J. F. Cardoso and A. Souloumiac, "Blind beamforming for non-Gaussian signals," *IEE Proc. F*, vol. 140, no. 6, pp. 362–370, Dec. 1993.

7. K. Sekihara, S. Nagarajan, D. Poeppel, and Y. Miyashita, "Time-frequency MEG-MUSIC algorithm," *IEEE Trans. Medical Imaging*, vol. 18, no. 1, pp.92–97, Jan. 1999.

8. Y. Zhang, W. Mu, and M. G. Amin, "Maximum likelihood methods for array processing based on time-frequency analysis," in *Proc. SPIE: Advanced Signal Processing Algorithms, Archtectures, and Implementations IX*, vol. 3807, Denver, CO, July 1999.

9. ——, "Subspace analysis of spatial time-frequency distribution matrices," submitted to *IEEE Trans. Signal Processing*, July 1999.

10. H. Lee and M. Wengrovitz, "Resolution threshold of beamspace MUSIC for two closely spaced emitters," *IEEE Trans. Acoust., Speech, Signal Proc.*, vol. 38, pp. 1545–1559, Sept. 1990.

11. M. G. Amin, A. Belouchrani, and Y. Zhang, "The spatial ambiguity function and its applications," submitted to *IEEE Signal Processing Letters*, Sept. 1999.

12. T. J. Shan and T. kailath, "On spatial smoothing for DOA estimation of coherent sources," *IEEE Trans. Acoust., Speech, Signal Proc.*, vol. 33, no. 4, pp. 806–811, June 1985.

13. Y. Zhang and M. G. Amin, "Spatial averaging of time-frequency distributions," in *Proc. IEEE Int. Conf. Acoust., Speech, Signal Proc.*, Phoenix, AZ, vol. III, pp. 1337–1340, March 1999.

14. A. Belouchrani, M. G. Amin, and K. Abed-Meraim, "Direction finding in correlated noise fields based on joint block-diagonalization of spatio-temporal correlation matrices," *IEEE Signal Processing Letters*, vol. 4, no. 9, pp. 266–269, Sept, 1997.

15. J. Jeong and W. J. Williams, "Kernel design for reduced interference distributions," *IEEE Trans. Signal Processing*, vol. 42, no. 2, pp. 402–412, Feb. 1992.

Time-frequency maximum likelihood methods for direction finding

Yimin Zhang, Weifeng Mu, and Moeness G. Amin*

Department of Electrical and Computer Engineering,

Villanova University, Villanova, PA 19085

Abstract

This paper proposes a novel time-frequency maximum likelihood (t-f ML) method for direction-of-arrival (DOA) estimation for non-stationary signals impinging on a multi-sensor array receiver, and compares this method with conventional maximum likelihood DOA estimation techniques. Time-frequency distributions localize the signal power in the time-frequency domain, and as such enhance the effective SNR, leading to improved DOA estimation. The localization of signals with different time-frequency signatures permits the division of the time-frequency domain into smaller regions, each contains fewer signals than those incident on the array. The reduction of the number of signals within different time-frequency regions not only reduces the required number of sensors, but also decreases the computational load in multi-dimensional optimizations. Compared to the recently proposed time-frequency MUSIC (t-f MUSIC), the proposed t-f ML method can be applied in coherent environments, without the need to perform any type of preprocessing that is subject to both array geometry and array aperture.

Keywords

Time-frequency distribution, direction finding, maximum likelihood, spatial time-frequency distribution, array processing.

* Corresponding author:
Prof. Moeness G. Amin
Department of Electrical and Computer Engineering, Villanova University, Villanova, PA 19085, USA.
E-mail: moeness@ece.vill.edu; Phone: (610) 519 - 7305; Fax: (610) 519 - 4436.

1. INTRODUCTION

The localization of spatial sources by passive sensor array is one of the important problems in radar, sonar, radio-astronomy, and seismology. So far, numerous methods have been proposed for direction finding, most of which are based on the estimates of the data covariance matrix. Among these methods, the maximum likelihood (ML) technique was one of the first to be devised and investigated [1]. It has a superior performance compared to other methods, particularly when the input signal-to-noise ratio (SNR) is low, the number of data samples is small, or the sources are highly correlated [2]. Therefore, despite its complexity, the ML technique remains of practical interests.

The evaluation of quadratic time-frequency distributions of the data snapshots across the array yields what is known as spatial time-frequency distributions (STFDs) [3], [4]. STFD techniques are most appropriate to handle sources of nonstationary waveforms. STFDs spread the noise power while localizing the energy of the impinging signals in the time-frequency domain. This property leads to increasing the robustness of eigenstructure signal and noise subspace estimates with respect to the channel and receiver noise, and hence improves spatial resolution performance.

In this paper, we propose the time-frequency maximum likelihood (t-f ML) method for direction finding and provide the analysis that explains its performance. It is shown that the superior performance of the t-f ML method relative to other methods is attributed to the following three fundamental reasons: 1) Time-frequency distributions localize the signal power in the time-frequency domain, and as such enhance the effective SNR and improve the DOA estimation. 2) The localization of signals with different time-frequency signatures permits the division of the time-frequency domain into smaller regions, each contains fewer signals than those incident on the array. The reduction of the number of signals within different time-frequency regions relaxes the condition on the size of the array aperture as well as simplifies the multidimensional optimization estimation procedure. 3) Compared with the previously proposed time-frequency MUSIC (t-f MUSIC), the t-f ML method can be applied when the signal arrivals are highly correlated, whereas the t-f MUSIC algorithm cannot do so without some sort of preprocessing, such as spatial smoothing.

This paper is organized as follows. In Section 2, the signal model is established, and a brief review of the spatial time-frequency distributions is given. In Section 3, we discuss the SNR enhancement based on time-frequency distributions and its effect on the signal and noise subspaces estimates using STFD matrices. The subspace estimates obtained from the STFD matrices are more robust to SNR and angular separation compared to those obtained from data covariance matrices. Section 4 presents the t-f ML and shows its performance in time-varying environments.

2. BACKGROUND

2.1. Signal Model

In narrowband array processing, when n signals arrive at an m-element array, the linear data model

$$\mathbf{x}(t) = \mathbf{y}(t) + \mathbf{n}(t) = \mathbf{A}(\mathbf{\Theta})\mathbf{d}(t) + \mathbf{n}(t) \tag{1}$$

is commonly assumed, where the $m \times n$ spatial matrix $\mathbf{A}(\mathbf{\Theta}) = [\mathbf{a}(\theta_1)...\mathbf{a}(\theta_n)]$ represents the mixing matrix or the steering matrix, and $\mathbf{a}(\theta_i)$ are the steering vectors. Due to the mixture of the signals at each sensor, the elements of the $m \times 1$ data vector $\mathbf{x}(t)$ are multicomponent signals, whereas each source signal $d_i(t)$ of the $n \times 1$ signal vector $\mathbf{d}(t)$ is often a monocomponent signal. $\mathbf{n}(t)$ is an additive noise vector whose elements are modeled as stationary, spatially and temporally white, zero-mean complex random processes, independent of the source signals. That is,

$$E[\mathbf{n}(t+\tau)\mathbf{n}^H(t)] = \sigma\delta(\tau)\mathbf{I} \quad \text{and} \quad E[\mathbf{n}(t+\tau)\mathbf{n}^T(t)] = \mathbf{0} \quad \text{for any } \tau \tag{2}$$

where $\delta(\tau)$ is the Kronecker delta function, $\mathbf{I}$ denotes the identity matrix, σ is the noise power at each sensor, superscript ^{H} and ^{T} respectively denote conjugate transpose and transpose, and $E(\cdot)$ is the statistical expectation operator.

In equation (1), it is assumed that the number of sensors is greater than the number of sources, i.e., $m > n$, and the number of snapshots is greater than the number of array sensors, i.e., $N > m$. We also assume that matrix $\mathbf{A}$ is full column rank, which implies that the steering vectors corresponding to n different angles of arrival are linearly independent.

Under the above assumptions, the correlation matrix is given by

$$\mathbf{R_{xx}} = E[\mathbf{x}(t)\mathbf{x}^H(t)] = \mathbf{A}(\Theta)\mathbf{R_{dd}}\mathbf{A}^H(\Theta) + \sigma\mathbf{I}, \tag{3}$$

where $\mathbf{R_{dd}} = E[\mathbf{d}(t)\mathbf{d}^H(t)]$ is the signal correlation matrix. For notational convenience, we drop the argument Θ and simply use $\mathbf{A}$ instead of $\mathbf{A}(\Theta)$. If $\hat{\Theta}$ is an estimate of Θ, then we also use $\hat{\mathbf{A}}$ instead of $\mathbf{A}(\hat{\Theta})$.

Let $\lambda_1 > \lambda_2 > \cdots > \lambda_n > \lambda_{n+1} = \lambda_{n+2} = \cdots = \lambda_m = \sigma$ denote the eigenvalues of $\mathbf{R_{xx}}$. The unit-norm eigenvectors associated with $\lambda_1, ..., \lambda_n$ constitute the columns of matrix $\mathbf{S} = [\mathbf{s}_1, ..., \mathbf{s}_n]$, and those corresponding to $\lambda_{n+1}, ..., \lambda_m$ make up matrix $\mathbf{G} = [\mathbf{g}_1, ..., \mathbf{g}_{m-n}]$. Since the columns of $\mathbf{A}$ and $\mathbf{S}$ span the same subspace, then $\mathbf{A}^H\mathbf{G} = \mathbf{0}$.

In practice, $\mathbf{R_{xx}}$ is unknown, and therefore should be estimated from the available data samples (snapshots) $\mathbf{x}(i)$, $i = 1, 2, ..., N$. The estimated correlation matrix is given by

$$\hat{\mathbf{R}}_{\mathbf{xx}} = \frac{1}{N}\sum_{i=1}^{N}\mathbf{x}(i)\mathbf{x}^H(i). \tag{4}$$

Let $\{\hat{\mathbf{s}}_1, ..., \hat{\mathbf{s}}_n, \hat{\mathbf{g}}_1, ..., \hat{\mathbf{g}}_{m-n}\}$ denote the unit-norm eigenvectors of $\hat{\mathbf{R}}_{\mathbf{xx}}$, arranged in the descending order of the associated eigenvalues, and let $\hat{\mathbf{S}}$ and $\hat{\mathbf{G}}$ denote the matrices made of the set of vectors $\{\hat{\mathbf{s}}_i\}$ and $\{\hat{\mathbf{g}}_i\}$, respectively. The statistical properties of the eigenvectors of the sample covariance matrix $\hat{\mathbf{R}}_{\mathbf{xx}}$ for signals modeled as independent processes with additive white noise is given in [6].

In this paper, we focus on frequency-modulated (FM) signals, modeled as

$$\mathbf{d}(t) = [d_1(t), ..., d_n(t)]^T = [D_1 e^{j\psi_1(t)}, ..., D_n e^{j\psi_n(t)}]^T, \tag{5}$$

where D_i and $\psi_i(t)$ are the fixed amplitude and time-varying phase of the ith source signal. For each sampling time t, $d_i(t)$ has an instantaneous frequency (IF) $f_i(t) = \frac{1}{2\pi}\frac{d\psi_i(t)}{dt}$.

FM signals are often encountered in applications such as radar and sonar. The consideration of FM signals in this paper in motivated by the fact that these signals are uniquely characterized by their IFs and, therefore, they have clear time-frequency signatures that are utilized by the STFD approach. Also, FM signals have constant amplitudes and, subsequently, yield time-independent covariance matrices. This property makes them amenable to conventional array processing based on second-order statistics.

2.2. Spatial Time-Frequency Distributions

The STFDs based on Cohen's class of time-frequency distribution were introduced in [3] and its applications to direction finding has been discussed in [4]. However, the performance of direction finding based on STFD has not been made clear yet. In this paper, we focus on one key member of Cohen's class, namely the pseudo Wigner-Ville distribution (PWVD) and its respective spatial distribution. Only the time-frequency points in the autoterm regions of PWVD are considered for STFD matrix construction. In these regions, it is assumed that the crossterms are negligible. This assumption serves to simplify the analysis and does not present any condition on performance. It is noted that the crossterms in STFD matrices play similar role to the cross-correlation between source signals [5], and therefore they do not always impede the direction finding process.

The discrete form of pseudo Wigner-Ville distribution of a signal $x(t)$, using a rectangular window of length L, is given by

$$D_{xx}(t,f) = \sum_{\tau=-\frac{L-1}{2}}^{\frac{L-1}{2}} x(t+\tau)x^*(t-\tau)e^{-j4\pi f\tau}, \tag{6}$$

where * denotes complex conjugation. The spatial pseudo Wigner-Ville distribution (SPWVD) matrix is obtained by replacing $x(t)$ by the data snapshot vector $\mathbf{x}(t)$,

$$\mathbf{D_{xx}}(t,f) = \sum_{\tau=-\frac{L-1}{2}}^{\frac{L-1}{2}} \mathbf{x}(t+\tau)\mathbf{x}^H(t-\tau)e^{-j4\pi f\tau}. \tag{7}$$

Substitute (1) into (7), we obtain

$$\mathbf{D_{xx}}(t,f) = \mathbf{D_{yy}}(t,f) + \mathbf{D_{yn}}(t,f) + \mathbf{D_{ny}}(t,f) + \mathbf{D_{nn}}(t,f) \tag{8}$$

Under the assumption of uncorrelated signal and noise components and the zero-mean noise property, the expectation of the crossterm TFD matrices between the signal and noise vectors is zero, i.e., $E\left[\mathbf{D_{yn}}(t,f)\right] = E\left[\mathbf{D_{ny}}(t,f)\right] = \mathbf{0}$, and it follows

$$E\left[\mathbf{D_{xx}}(t,f)\right] = \mathbf{D_{yy}}(t,f) + E\left[\mathbf{D_{nn}}(t,f)\right] = \mathbf{A}\mathbf{D_{dd}}(t,f)\mathbf{A}^H + E\left[\mathbf{D_{nn}}(t,f)\right]. \tag{9}$$

It is noted that the relationship (9) holds true for every (t,f) point. Therefore, multiple time-frequency points can be used to reduce the effect of noise and ensure the full column rank property of the STFD matrix. In this paper, the STFD matrices over multiple time-frequency points are averaged, as is discussed in next section.

3. SUBSPACE ANALYSIS FOR STFD MATRICES

The purpose of this section is to show that the signal and noise subspaces based on time-frequency distributions for nonstationary signals are more robust than those obtained from conventional array processing.

3.1. SNR Enhancement

The ith diagonal element of TFD matrix $\mathbf{D_{dd}}(t,f)$ is given by

$$D_{d_i d_i}(t,f) = \sum_{\tau=-\frac{L-1}{2}}^{\frac{L-1}{2}} D_i^2 e^{j[\psi_i(t+\tau)-\psi_i(t-\tau)]-j4\pi f\tau}. \tag{10}$$

Assume that the third-order derivative of the phase is negligible over the window length L, then along the true time-frequency points of ith signal, $f_i = \frac{1}{2\pi}\frac{d\psi_i(t)}{dt}$, and $\psi_i(t+\tau) - \psi_i(t-\tau) - 4\pi f_i\tau \simeq 0$. Accordingly,

$$D_{d_i d_i}(t,f_i) = \sum_{\tau=-\frac{L-1}{2}}^{\frac{L-1}{2}} D_i^2 = LD_i^2. \tag{11}$$

Similarly, the noise STFD matrix $\mathbf{D_{nn}}(t,f)$ is

$$\mathbf{D_{nn}}(t,f) = \sum_{\tau=-\frac{L-1}{2}}^{\frac{L-1}{2}} \mathbf{n}(t+\tau)\mathbf{n}^H(t-\tau)e^{-j4\pi f\tau}. \tag{12}$$

Under the spatial white and temporal white assumptions, the statistical expectation of $\mathbf{D_{nn}}(t,f)$ is given by

$$E\left[\mathbf{D_{nn}}(t,f)\right] = \sum_{\tau=-\frac{L-1}{2}}^{\frac{L-1}{2}} E\left[\mathbf{n}(t+\tau)\mathbf{n}^H(t-\tau)\right] e^{-j4\pi f\tau} = \sigma\mathbf{I}. \tag{13}$$

Therefore, when we select the time-frequency points along the time-frequency signature or the IF of the ith FM signal, the SNR in model (9) is LD_i^2/σ, which has an improved factor L over the one associated with model (3).

The pseudo Wigner-Ville distribution of each FM source has a constant value over the observation period, providing that we leave out the rising and falling power distributions at both ends of the data record. For convenience of analysis, we select those $N-L+1$ time-frequency points of constant distribution value for each source signal. Therefore, the

averaged STFD over the time-frequency signatures of n_o signals, i.e., a total of $n_o(N-L+1)$ time-frequency points, is given by

$$\hat{\mathbf{D}} = \frac{1}{n_o(N-L+1)} \sum_{q=1}^{n_o} \sum_{i=1}^{N-L+1} \mathbf{D}_{\mathbf{xx}}(t_i, f_{q,i}), \tag{14}$$

where $f_{q,i}$ is the instantaneous frequency of the qth signal at the ith time sample. The expectation of the averaged STFD matrix is

$$\begin{aligned} \mathbf{D} &= E\left[\hat{\mathbf{D}}\right] = \frac{1}{n_o(N-L+1)} \sum_{q=1}^{n_o} \sum_{i=1}^{N-L+1} E\left[\mathbf{D}_{\mathbf{xx}}(t_i, f_{q,i})\right] \\ &= \frac{1}{n_o} \sum_{q=1}^{n_o} \left[LD_q^2 \mathbf{a}(\theta_q)\mathbf{a}^H(\theta_q) + \sigma\mathbf{I}\right] = \frac{L}{n_o}\mathbf{A}^o\mathbf{R}_{\mathbf{dd}}^o(\mathbf{A}^o)^H + \sigma\mathbf{I}, \end{aligned} \tag{15}$$

where $\mathbf{R}_{\mathbf{dd}}^o$ and $\mathbf{A}^o$, respectively, represent the signal correlation matrix and the mixing matrix constructed by only considering n_o signals out of the total number of signal arrivals n.

3.2. Signal and Noise Subspaces Based on STFDs

The statistical properties of the eigenstructures using the STFD matrix are provided in this subsection.

Lemma 1: Let $\lambda_1^o > \lambda_2^o > \cdots > \lambda_{n_o}^o > \lambda_{n_o+1}^o = \lambda_{n_o+2}^o = \cdots = \lambda_m^o = \sigma$ denote the eigenvalues of $\mathbf{R}_{\mathbf{xx}}^o$, which is defined from a data record of a mixture of the n_o selected FM signals. Denote the unit-norm eigenvectors associated with $\lambda_1^o, ..., \lambda_{n_o}^o$ by the columns of $\mathbf{S}^o = [\mathbf{s}_1^o, ..., \mathbf{s}_{n_o}^o]$, and those corresponding to $\lambda_{n_o+1}^o, ..., \lambda_m^o$ by the columns of $\mathbf{G}^o = [\mathbf{g}_1^o, ..., \mathbf{g}_{m-n_o}^o]$. We also denote $\lambda_1^{tf} > \lambda_2^{tf} > \cdots > \lambda_{n_o}^{tf} > \lambda_{n_o+1}^{tf} = \lambda_{n_o+2}^{tf} = \cdots = \lambda_m^{tf} = \sigma^{tf}$ as the eigenvalues of $\mathbf{D}$ defined in (15). The unit-norm eigenvectors associated with $\lambda_1^{tf}, ..., \lambda_{n_o}^{tf}$ are represented by the columns of $\mathbf{S}^{tf} = [\mathbf{s}_1^{tf}, ..., \mathbf{s}_{n_o}^{tf}]$, and those corresponding to $\lambda_{n_o+1}^{tf}, ..., \lambda_m^{tf}$ are represented by the columns of $\mathbf{G}^{tf} = [\mathbf{g}_1^{tf}, ..., \mathbf{g}_{m-n_o}^{tf}]$. Accordingly,

a) The signal and noise subspaces of $\mathbf{S}^{tf}$ and $\mathbf{G}^{tf}$ are the same as $\mathbf{S}^o$ and $\mathbf{G}^o$, respectively.

b) The eigenvalues have the following relationship:

$$\lambda_i^{tf} = \begin{cases} \frac{L}{n_o}(\lambda_i^o - \sigma) + \sigma = \frac{L}{n_o}\lambda_i^o + \left(1 - \frac{L}{n_o}\right)\sigma & i \le n_o \\ \sigma^{tf} = \sigma & n_o < i \le m. \end{cases} \tag{16}$$

Both parts of the above equations are direct results of (15). From Lemma 1 it is clear that the largest n_o eigenvalues are amplified using STFD analysis.

Lemma 2: If the third-order derivative of the phase of the FM signals is negligible over the time-period $[t-L+1, t+L-1]$, then $\hat{\mathbf{D}}-\mathbf{D}$ is a zero-mean, random matrix whose elements are asymptotically jointly Gaussian. The proof is given in Appendix A.

Lemma 3: If the third-order derivative of the phase of the FM signals is negligible over the time-period $[t-L+1, t+L-1]$, then the orthogonal projections of $\left\{\hat{\mathbf{g}}_i^{tf}\right\}$ onto the column space of $\mathbf{S}^{tf}$ are asymptotically (for $N \gg L$) jointly Gaussian distributed with zero means and covariance matrices given by

$$E\left(\mathbf{S}^{tf}\left(\mathbf{S}^{tf}\right)^H \hat{\mathbf{g}}_i^{tf}\right)\left(\mathbf{S}^{tf}\left(\mathbf{S}^{tf}\right)^H \hat{\mathbf{g}}_j^{tf}\right)^H = \frac{1}{(N-L+1)}\mathbf{U}^{tf}\delta_{i,j}, \tag{17}$$

$$E\left(\mathbf{S}^{tf}\left(\mathbf{S}^{tf}\right)^H \hat{\mathbf{g}}_i^{tf}\right)\left(\mathbf{S}^{tf}\left(\mathbf{S}^{tf}\right)^H \hat{\mathbf{g}}_j^{tf}\right)^T = \mathbf{0} \text{ for all } i,\ j, \tag{18}$$

where

$$\mathbf{U}^{tf} = \frac{\sigma L}{n_o}\left[\sum_{k=1}^{n_o}\frac{\lambda_k^{tf}}{(\sigma-\lambda_k^{tf})^2}\mathbf{s}_k^{tf}\left(\mathbf{s}_k^{tf}\right)^H\right] = \sigma\left[\sum_{k=1}^{n_o}\frac{(\lambda_k^o-\sigma)+\frac{n_o}{L}\sigma}{(\sigma-\lambda_k^o)^2}\mathbf{s}_k^o\left(\mathbf{s}_k^o\right)^H\right]. \tag{19}$$

The proof is given in [10]. For comparison, we quote the results from reference [6], which were provided using the data covariance matrix,

$$E\left(\mathbf{S}\mathbf{S}^H\hat{\mathbf{g}}_i\right)\left(\mathbf{S}\mathbf{S}^H\hat{\mathbf{g}}_j\right)^H = \frac{\sigma}{N}\left[\sum_{k=1}^{n}\frac{\lambda_k}{(\sigma-\lambda_k)^2}\mathbf{s}_k\mathbf{s}_k^H\right]\delta_{i,j} \tag{20}$$

$$E\left(\mathbf{S}\mathbf{S}^H\hat{\mathbf{g}}_i\right)\left(\mathbf{S}\mathbf{S}^H\hat{\mathbf{g}}_j\right)^T = \mathbf{0} \text{ for all } i,\ j. \tag{21}$$

where $\mathbf{S}, \mathbf{s}_k, \hat{\mathbf{g}}_k, \lambda_k$ are analogous to $\mathbf{S}^o, \mathbf{s}_k^o, \hat{\mathbf{g}}_k^o, \lambda_k^o$, respectively, except they are defined for all n signals instead of only n_o signals.

Comparing (17) and (19) with (20), two important observations are in order. First, if the signals are both localizable and separable in the time-frequency domain, then the reduction of the number of signals from n to n_o reduces the estimation error, specifically when the signals are closely spaced. The second observation relates to SNR enhancements. The above equations show that error reductions using STFDs are more pronounced for the cases of low SNR and/or closely spaced signals. It is clear from (17) and (19) that, when $\lambda_k^o \gg \sigma$ for all $k = 1, 2, ..., n_o$, the results are almost independent of L (suppose $N \gg L$ so

that $N-L+1 \simeq N$), and therefore there would be no obvious improvement in using the STFD over conventional array processing. On the other hand, when some eigenvalues are close to σ ($\lambda_k^o \simeq \sigma$, for some $k = 1, 2, ..., n_o$), which is the case of weak or closely spaced signals, the result of (17) is reduced by a factor of up to $G = \frac{L}{n_o}$. This factor represents the gain achieved using STFD processing.

4. THE TIME-FREQUENCY MAXIMUM LIKELIHOOD METHODS

In this section we analyze the performance of the maximum likelihood methods based on time-frequency distributions (t-f ML). For conventional ML methods, the joint density function of the sampled data vectors $\mathbf{x}(1), \mathbf{x}(2), ..., \mathbf{x}(N)$, is given by [2]

$$f(\mathbf{x}(1), \ldots, \mathbf{x}(N)) = \prod_{i=1}^{N} \frac{1}{\pi^m \det[\sigma \mathbf{I}]} \exp\left(-\frac{1}{\sigma}\left[\mathbf{x}(i) - \mathbf{A}\mathbf{d}(i)\right]^H \left[\mathbf{x}(i) - \mathbf{A}\mathbf{d}(i)\right]\right), \tag{22}$$

where $\det[\cdot]$ denotes the determinant. It follows from (22) that the log-likelihood function of the observations $\mathbf{x}(1), \mathbf{x}(2), \ldots, \mathbf{x}(N)$, is given by

$$L = -mN\ln\sigma - \frac{1}{\sigma}\sum_{i=1}^{N}\left[\mathbf{x}(i) - \mathbf{A}\mathbf{d}(i)\right]^H \left[\mathbf{x}(i) - \mathbf{A}\mathbf{d}(i)\right]. \tag{23}$$

To carry out this minimization, we fix $\mathbf{A}$ and minimize (23) with respect to $\mathbf{d}$. This yields the well-known solution

$$\hat{\mathbf{d}}(i) = \left[\mathbf{A}^H\mathbf{A}\right]^{-1}\mathbf{A}^H\mathbf{x}(i). \tag{24}$$

We can obtain the concentrated likelihood function as [2], [8]

$$F_{ML}(\mathbf{\Theta}) = tr\left\{\left[\mathbf{I} - \hat{\mathbf{A}}(\hat{\mathbf{A}}^H\hat{\mathbf{A}})^{-1}\hat{\mathbf{A}}^H\right]\hat{\mathbf{R}}_{\mathbf{xx}}\right\}, \tag{25}$$

where $tr(\mathbf{A})$ denotes the trace of $\mathbf{A}$. The ML estimate of $\mathbf{\Theta}$ is obtained as the minimizer of (25). Let ω_i and $\hat{\omega}_i$, respectively, denote the spatial frequency and its ML estimate associated with θ_i, then the estimation error $(\hat{\omega}_i - \omega_i)$ are asymptotically (for large N) jointly Gaussian distributed with zero means and the covariance matrix [9]

$$E\left[(\hat{\omega}_i - \omega_i)^2\right] = \frac{1}{2N}\left[\mathrm{Re}(\mathbf{H} \odot \mathbf{R}_{\mathbf{dd}}^T)\right]^{-1} \mathrm{Re}\left[\mathbf{H} \odot (\mathbf{R}_{\mathbf{dd}}\mathbf{A}^H\mathbf{U}\mathbf{A}\mathbf{R}_{\mathbf{dd}})^T\right]\left[\mathrm{Re}(\mathbf{H} \odot \mathbf{R}_{\mathbf{dd}}^T)\right]^{-1}, \tag{26}$$

where $\odot$ denotes Hadamard product. Moreover,

$$\mathbf{U}=\sum_{k=1}^{n}\frac{\lambda_k\sigma}{(\sigma-\lambda_k)^2}\mathbf{s}_k\mathbf{s}_k^H,\quad \mathbf{H}=\mathbf{C}^H\left[\mathbf{I}-\mathbf{A}(\mathbf{A}^H\mathbf{A})^{-1}\mathbf{A}^H\right]\mathbf{C},\quad \text{and}\quad \mathbf{C}=\frac{d\mathbf{A}}{d\omega}. \tag{27}$$

Next we consider the t-f ML method. As we discussed in the previous section, we select $n_o \leq n$ signals in the time-frequency domain. The concentrated likelihood function defined from the STFD matrix is similar to (25) and is obtained by replacing $\hat{\mathbf{R}}_{\mathbf{xx}}$ by $\hat{\mathbf{D}}$ (Appendix B),

$$F_{ML}^{tf}(\boldsymbol{\Theta})=tr\left[\mathbf{I}-\hat{\mathbf{A}}^o\left((\hat{\mathbf{A}}^o)^H\hat{\mathbf{A}}^o\right)^{-1}(\hat{\mathbf{A}}^o)^H\right]\hat{\mathbf{D}}. \tag{28}$$

Therefore, the estimation error $(\hat{\omega}_i^{tf}-\omega_i^{tf})$ associated with the t-f ML method are asymptotically (for $N >> L$) jointly Gaussian distributed with zero means and the covariance matrix

$$\begin{aligned}
&E\left[\left(\hat{\omega}_i^{tf}-\omega_i^{tf}\right)^2\right]\\
&=\frac{\sigma}{2(N-L+1)}\left[\mathrm{Re}(\mathbf{H}^o\odot\mathbf{D}_{\mathbf{dd}}^T)\right]^{-1}\\
&\quad\mathrm{Re}\left[\mathbf{H}^o\odot\left(\mathbf{D}_{\mathbf{dd}}(\mathbf{A}^o)^H\mathbf{U}^{tf}\mathbf{A}^o\mathbf{D}_{\mathbf{dd}}\right)^T\right]\left[\mathrm{Re}(\mathbf{H}^o\odot\mathbf{D}_{\mathbf{dd}}^T)\right]^{-1}\\
&=\frac{\sigma}{2(N-L+1)}\left[\mathrm{Re}\left(\mathbf{H}^o\odot(\mathbf{R}_{\mathbf{dd}}^o)^T\right)\right]^{-1}\\
&\quad\mathrm{Re}\left[\mathbf{H}^o\odot\left(\mathbf{R}_{\mathbf{dd}}^o(\mathbf{A}^o)^H\mathbf{U}^{tf}\mathbf{A}^o\mathbf{R}_{\mathbf{dd}}^o\right)^T\right]\left[\mathrm{Re}\left((\mathbf{H}^o\odot\mathbf{R}_{\mathbf{dd}}^o)^T\right)\right]^{-1},
\end{aligned} \tag{29}$$

where $\mathbf{U}^{tf}$ is defined in (19), and

$$\mathbf{H}^o=(\mathbf{C}^o)^H\left[\mathbf{I}-\mathbf{A}^o\left((\mathbf{A}^o)^H\mathbf{A}^o\right)^{-1}(\mathbf{A}^o)^H\right]\mathbf{C}^o,\quad \text{and}\quad \mathbf{C}^o=\frac{d\mathbf{A}^o}{d\omega}. \tag{30}$$

In the case of $n_o = n$, then $\mathbf{H}^o = \mathbf{H}$, and $\mathbf{C}^o = \mathbf{C}$.

The signal localization in the time-frequency domain enables us to select fewer signal arrivals. This fact is not only important in improving the estimation performance, particularly when the signals are closely spaced, but also reduces the dimension of optimization problem solved by the maximum likelihood algorithm, and subsequently reduces the computational requirement.

To demonstrate the advantages of t-f ML over the conventional ML and the time-frequency MUSIC (t-f MUSIC), consider a uniform linear array of 8 sensors separated by half a wavelength. Two FM signals arrive from $(\theta_1, \theta_2) = (-10°, 10°)$ with the instantaneous frequencies $f_1(t) = 0.2 + 0.1t/N + 0.2\sin(2\pi t/N)$ and $f_2(t) = 0.2 + 0.1t/N + 0.2\sin(2\pi t/N + \pi/2), t = 1, ..., N$. The SNR of both signals is -20 dB, and the number

of snapshots used in the simulation is $N = 1024$. We used L=129 for t-f ML. Figure 1 shows the PWVD of the mixed noise-free signals at the reference sensor. Figure 2 shows (θ_1, θ_2) that yield the minimum values of the likelihood function of the t-f ML and the ML methods for 20 independent trials. It is evident that the t-f ML provides much improved DOA estimation over the conventional ML.

In the next example, we compare the t-f ML and the t-f MUSIC for coherent sources. The two coherent FM signals have common instantaneous frequencies $f_{1,2}(t) = 0.2 + 0.1t/N + 0.2\sin(2\pi t/N), t = 1, ..., N$, with $\frac{\pi}{2}$ phase difference. The signals arrive at $(\theta_1, \theta_2) = (-2°, 2°)$. The SNR of both signals is 5 dB and the number of snapshots is 1024. Again, we used L=129 for both t-f ML and t-f MUSIC. Figure 3 shows the PWVD of the mixed noise-free signals, and Figure 4 shows the contour plots of the likelihood function of the t-f ML and the estimated spectra of t-f MUSIC for three independent trials. It is clear that the t-f ML can separate the two signals whereas the t-f MUSIC cannot.

5. CONCLUSIONS

The time-frequency maximum likelihood (t-f ML) method has been proposed for direction finding, which is based on the spatial time-frequency distribution (STFD) matrices. By taking frequency-modulated (FM) signals as example, we show that the STFD matrices provide more robust eigen-decomposition than covanrice matrices. The analysis and simulation results showed that the t-f ML improves over the conventional maximum likelihood technique for low SNR, and outperforms the t-f MUSIC in coherent signal environments.

APPENDIX A

Proof of Lemma 2

From (1), (14), and (15),

$$\begin{aligned}
\hat{\mathbf{D}} - \mathbf{D} &= \frac{1}{n_o(N-L+1)} \sum_{q=1}^{n_o} \sum_{i=1}^{N-L+1} \sum_{\tau=-\frac{L-1}{2}}^{\frac{L-1}{2}} \mathbf{y}(t_i+\tau)\mathbf{n}^H(t_i-\tau)e^{-j4\pi f_{q,i}\tau} \\
&+ \frac{1}{n_o(N-L+1)} \sum_{q=1}^{n_o} \sum_{i=1}^{N-L+1} \sum_{\tau=-\frac{L-1}{2}}^{\frac{L-1}{2}} \mathbf{n}(t_i+\tau)\mathbf{y}^H(t_i-\tau)e^{-j4\pi f_{q,i}\tau} \qquad \text{(A.1)} \\
&+ \frac{1}{n_o(N-L+1)} \sum_{q=1}^{n_o} \sum_{i=1}^{N-L+1} \sum_{\tau=-\frac{L-1}{2}}^{\frac{L-1}{2}} \mathbf{n}(t_i+\tau)\mathbf{n}^H(t_i-\tau)e^{-j4\pi f_{q,i}\tau} - \sigma\mathbf{I}.
\end{aligned}$$

We first consider the first term in (A.1). Denoting $t_i' = t_i - \tau$, and noting the fact that, when the third-order derivative of the phase is negligible over $[t-L+1, t+L-1]$ for any signal and any t, $d_q(t_i'+2\tau)e^{-j4\pi f_{q,i}\tau} \simeq d_q(t_i')$ at the time-frequency point $(t_i, f_{q,i})$, then

$$\begin{aligned}
&\sum_{q=1}^{n_o}\sum_{i=1}^{N-L+1}\sum_{\tau=-\frac{L-1}{2}}^{\frac{L-1}{2}} \mathbf{y}(t_i+\tau)\mathbf{n}^H(t_i-\tau)e^{-j4\pi f_{q,i}\tau} \\
&= \sum_{q=1}^{n_o}\sum_{t_i'=1}^{N-L+1}\sum_{\tau=-\frac{L-1}{2}}^{\frac{L-1}{2}} \mathbf{y}(t_i'+2\tau)\mathbf{n}^H(t_i')e^{-j4\pi f_{q,i}\tau} \qquad \text{(A.2)} \\
&\simeq \sum_{q=1}^{n_o}\sum_{t_i'=1}^{N-L+1} L d_q(t_i')\mathbf{a}(\theta_q)\mathbf{n}^H(t_i') = \sum_{t_i'=1}^{N-L+1} L\mathbf{y}(t_i')\mathbf{n}^H(t_i')
\end{aligned}$$

Therefore, the elements of the first term in equation (A.1) are clearly asymptotically jointly Gaussian from the multivariate Central Limit Theorem [7]. Similar result can be obtained for the second term of (A.1). The elements of the third term in (A.1) are also jointly Gaussian from the fact that the covariance between the (p,r)th element of $\mathbf{n}(t+\tau)\mathbf{n}^H(t-\tau)$ at time t_i and t_k is given by

$$\begin{aligned}
&E\left\{\left[\sum_{\tau_1=-\frac{L-1}{2}}^{\frac{L-1}{2}} n_p(t_i+\tau_1)n_r^*(t_i-\tau_1) - E\left(\sum_{\tau_1=-\frac{L-1}{2}}^{\frac{L-1}{2}} n_p(t_i+\tau_1)n_r^*(t_i-\tau_1)\right)\right]e^{-j4\pi f_{q,i}\tau_1}\right. \\
&\left.\left[\sum_{\tau_2=-\frac{L-1}{2}}^{\frac{L-1}{2}} n_p^*(t_k+\tau_2)n_r(t_k-\tau_2) - E\left(\sum_{\tau_2=-\frac{L-1}{2}}^{\frac{L-1}{2}} n_p^*(t_k+\tau_2)n_r(t_k-\tau_2)\right)\right]e^{-j4\pi f_{q,k}\tau_2}\right\} \\
&= \sum_{\tau_1=-\frac{L-1}{2}}^{\frac{L-1}{2}}\sum_{\tau_2=-\frac{L-1}{2}}^{\frac{L-1}{2}} E[n_p(t_i+\tau_1)n_r^*(t_i-\tau_1)]E[n_p^*(t_k+\tau_2)n_r(t_k-\tau_2)]e^{-j4\pi\left(f_{q,i}\tau_1 - f_{q,k}\tau_2\right)} \\
&+ \sum_{\tau_1=-\frac{L-1}{2}}^{\frac{L-1}{2}}\sum_{\tau_2=-\frac{L-1}{2}}^{\frac{L-1}{2}} E[n_p(t_i+\tau_1)n_p^*(t_k+\tau_2)]E[n_r^*(t_i-\tau_1)n_r(t_k-\tau_2)]e^{-j4\pi\left(f_{q,i}\tau_1 - f_{q,k}\tau_2\right)} \\
&+ \sum_{\tau_1=-\frac{L-1}{2}}^{\frac{L-1}{2}}\sum_{\tau_2=-\frac{L-1}{2}}^{\frac{L-1}{2}} E[n_p(t_i+\tau_1)n_r(t_k-\tau_2)]E[n_p^*(t_k+\tau_2)n_r^*(t_i-\tau_1)]e^{-j4\pi\left(f_{q,i}\tau_1 - f_{q,k}\tau_2\right)} \\
&- \sum_{\tau_1=-\frac{L-1}{2}}^{\frac{L-1}{2}}\sum_{\tau_2=-\frac{L-1}{2}}^{\frac{L-1}{2}} \sigma^2\delta_{p,r}e^{-j4\pi\left(f_{q,i}\tau_1 - f_{q,k}\tau_2\right)} \\
&= L\sigma^2\delta_{i,k}.
\end{aligned} \qquad \text{(A.3)}$$

Since the linear combination of joint-Gaussian processes is jointly Gaussian, then $\hat{\mathbf{D}} - \mathbf{D}$ is a random matrix whose elements are asymptotically jointly Gaussian. Also $\hat{\mathbf{D}} - \mathbf{D} \to 0$ as $N \to \infty$.

APPENDIX B

Derivation of (28)

The number of data samples available for the construction of the STFD matrix is $N - L + 1$, where the selected n_o signals are included. Denote $\hat{\mathbf{u}}_k$ as the kth column of $\hat{\mathbf{D}}$, and $\mathbf{u}_k$ the kth column of $\mathbf{D}$. From Lemma 2, we know that $\hat{\mathbf{u}}_k$ is asymptotically jointly Gaussian, and its density function is

$$f_{tf}(\hat{\mathbf{u}}_k) = \frac{1}{\pi}\det\left[\frac{1}{N-L+1}\mathbf{\Delta}_k\right]^{-\frac{1}{2}} \exp\left[-\frac{1}{2}(\hat{\mathbf{u}}_k - \mathbf{u}_k)^H(\frac{1}{N-L+1}\mathbf{\Delta}_k)^{-1}(\hat{\mathbf{u}}_k - \mathbf{u}_k)\right], \tag{B.1}$$

where $\mathbf{\Delta}_k$ stands for the asymptotic covariance matrix of $\mathbf{u}_k$

$$\mathbf{\Delta}_k \underset{=}{\triangle} \lim_{N\to\infty}(N-L+1)E\left[(\hat{\mathbf{u}}_k - \mathbf{u}_k)(\hat{\mathbf{u}}_k - \mathbf{u}_k)^H\right]. \tag{B.2}$$

From the results of Lemma 2, it is clear that $\mathbf{\Delta}_k$ is a diagonal matrix with equal diagonal elements. Denoting $\mathbf{\Delta}_k = \beta\mathbf{I}$, the log-likelihood function is given by

$$L_{tf} = -\frac{1}{2m}\frac{1}{N-L+1}\log\beta - \frac{1}{2\beta}(\hat{\mathbf{u}}_k - \mathbf{u}_k)^H(\hat{\mathbf{u}}_k - \mathbf{u}_k). \tag{B.3}$$

Maximizing L_{tf} is equivalent to minimizing

$$h_k \underset{=}{\triangle} \left[\hat{\mathbf{u}}_k - \mathbf{u}_k\right]^H\left[\hat{\mathbf{u}}_k - \mathbf{u}_k\right]. \tag{B.4}$$

For different k, we may construct the following cost function

$$\begin{aligned} h &\underset{=}{\triangle} \sum_{k=1}^{m} h_k \\ &= \sum_{k=1}^{m}\left[\hat{\mathbf{u}}_k - \mathbf{u}_k\right]^H\left[\hat{\mathbf{u}}_k - \mathbf{u}_k\right] \\ &= tr\left\{\left[\hat{\mathbf{D}} - \mathbf{D}\right]^H\left[\hat{\mathbf{D}} - \mathbf{D}\right]\right\}. \end{aligned} \tag{B.5}$$

Similar to (24), and by taking into account that we used n_o signals instead of n signals, the estimation of $\mathbf{D}$ is obtained as $\hat{\mathbf{A}}^o\left((\hat{\mathbf{A}}^o)^H\hat{\mathbf{A}}^o\right)^{-1}(\hat{\mathbf{A}}^o)^H\hat{\mathbf{D}}\hat{\mathbf{A}}^o\left((\hat{\mathbf{A}}^o)^H\hat{\mathbf{A}}^o\right)^{-1}(\hat{\mathbf{A}}^o)^H$, the minimization of equation (B.5) leads to (28).

ACKNOWLEDGMENT

This work was supported by ONR under Grant #N00014-98-1-0176.

References

[1] F. C. Schweppe, "Sensor array data processing for multiple signal estimation," *IEEE Trans. Inform. Theory*, vol. IT-14, pp. 294–305, 1968.

[2] I. Ziskind and M. Wax, "Maximum likelihood localization of multiple sources by alternating projection," *IEEE Trans. Acoust., Speech, Signal Proc.*, vol. ASSP-36, no. 10, pp. 1553–1560, Oct. 1988.

[3] A. Belouchrani and M. Amin, "Blind source separation based on time-frequency signal representation," *IEEE Trans. Signal Processing*, vol. 46, no. 11, pp. 2888–2898, Nov. 1998.

[4] A. Belouchrani and M. Amin, "Time-frequency MUSIC," *IEEE Signal Processing Letters*, vol. 6, no. 5, pp. 109–110, May 1999.

[5] Y. Zhang and M. Amin, "Spatial averaging of time-frequency distributions," in *Proc. ICASSP*, vol. III, Pheonix, AZ, pp. 1337-1340, March 1999.

[6] P. Stoica and A. Nehorai, "MUSIC, maximum lokelihood, and Cramer-Rao bound," *IEEE Trans. Acoust. Speech, Signal Processing*, vol. 37, no. 5, pp. 720–741, May 1989.

[7] T. W. Anderson, *An Introduction to Multivariate Statistical Analysis*, New York: John Wiley & Sons, 1971.

[8] P. Stoica and K. C. Sharman, "Maximum likelihood methods for direction-of-arrival estimation," *IEEE Trans. Acoust., Speech, Signal Proc.*, vol. ASSP-38, no. 7, pp. 1132–1142, July 1990.

[9] P. Stoica and A. Nehorai, "MUSIC, maximum lokelihood, and Cramer-Rao bound: futher results and comparisons," *IEEE Trans. Acoust. Speech, Signal Processing*, vol. 38, no. 12, pp. 2140–2150, Dec. 1990.

[10] Y. Zhang, W. Mu, and M. G. Amin, "Maximum likelihood methods for array processing based on time-frequency analysis," in *Proc. SPIE: Advanced Signal Processing Algorithms, Archtectures, and Implementations IX*, vol. 3807, Denver, CO, July 1999.

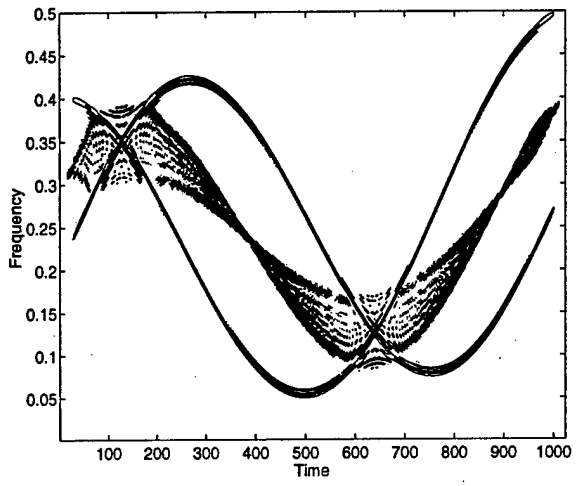

Fig. 1 Pseudo Wigner-Ville distribution of the mixture of the two FM signals.

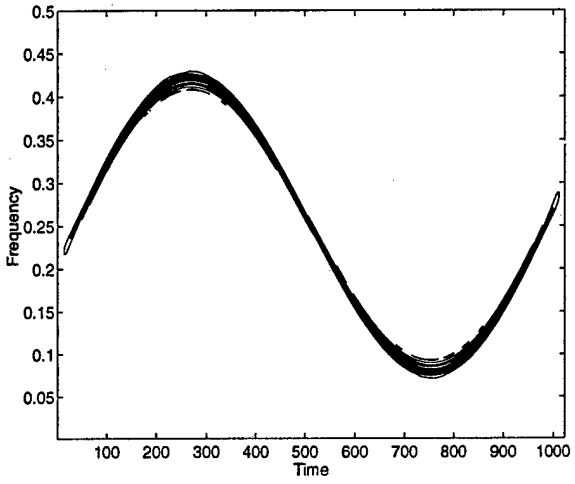

Fig. 3 Pseudo Wigner-Ville distribution of the mixture of the two coherent FM signals.

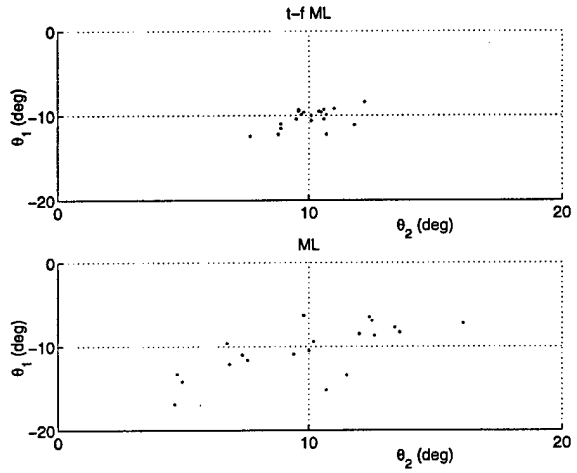

Fig. 2 (θ_1, θ_2) which minimize the t-f ML and ML likelihood functions.

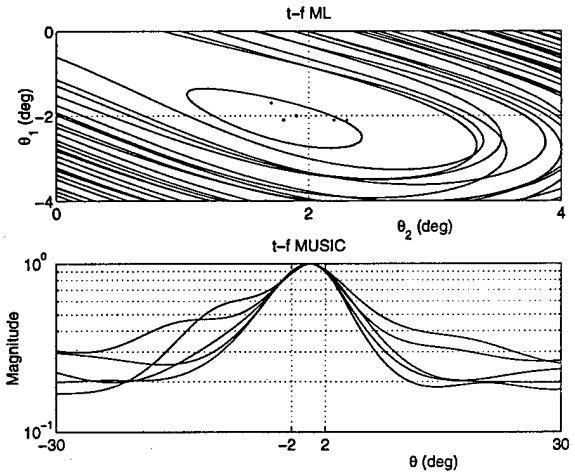

Fig. 4 Contour plots of t-f ML likelihood function and spatial spectra of t-f MUSIC.

Spatial Evolutionary Spectrum for DOA Estimation and Blind Signal Separation

A.Salim Kayhan†
Dept. of Electrical and Electronics Engineering
Hacettepe University, Beytepe
06532 Ankara
Turkey
Tel.: (+90) 312 2977090
Fax: (+90) 312 2992125
E-mail:kayhan@ee.hun.edu.tr
and
Moeness G. Amin
Dept. of Electrical and Computer Eng.
Villanova University
Villanova, PA 19085
U.S.A.
E-mail:moeness@ece.vill.edu

EDICS 2.3.3

Abstract

In this paper, we combine the concepts of the evolutionary spectrum and array processing. We present Cross-power Evolutionary Periodogram for both direction of arrival estimation and blind separation of nonstationary signals. We model nonstationary signals received by each array sensor as a sum of complex sinusoids with time-varying amplitudes. These amplitudes carry information about the direction of arrival which may also be time-varying. We first estimate the time-varying amplitudes using linear estimators obtained by minimizing the mean-squared error. Then, using the estimated time-varying amplitudes, we estimate the evolutionary cross-power distributions of the sensor data. Next, using cross-power estimates at time-frequency points of interest, we estimate the directions of arrival using one of the existing estimation methods. If the frequencies are known to be constant but the directions are time-varying, we choose the time-frequency points around the time of interest to estimate instantaneous source locations. If the sources are stationary, all time-frequency points of interest can be combined for the estimation of fixed directions. Whitening and subspace methods are used to find the mixing matrix and separate nonstationary signals received by the array. We present examples illustrating the performances of the proposed algorithms.

Permission to publish this abstract separately is granted
December 23, 1998

† Corresponding author.

1 Introduction

In many signal processing applications, such as radar, sonar, biomedical engineering and communications, direction of arrival (DOA) estimation and recovery of source signals are important problems. In general, these problems involve several signals and a multisensor array receiver. Each sensor receives a mixture of source signals. In the DOA estimation problem, the goal is the estimation of the source locations by processing the data received by the array sensors. The common presumption is that the signals are emitted from point sources placed in the farfield[6]. Further, the array manifold is assumed to be known. In the blind signal separation problem, the array parameters are generally unknown. Performance is often independent of inaccuracies in the array manifold as well as sensor displacement. A general overview and references on blind equalization can be found in recent review articles [16] and [18]. A special case is the instantaneous mixture of signals. A solution using second order statistics and applying joint diagonalization to a set of covariance matrices was presented in [1].

Recently, spatial time-frequency distributions as a generalization of bilinear have been introduced time-frequency distributions to a vector signal and used for effective direction finding and separation of nonstationary signals[3, 15, 2]. Although bilinear time-frequency distributions (TFDs) have several attractive localization properties[5], they either suffer from cross-terms or do not guarantee positivity of the spectral estimates. Alternatively, the evolutionary periodogram (EP) was proposed as an estimator of the Wold-Cramer evolutionary spectrum [8]. The EP has many desirable properties and it was shown to outperform the

spectrogram and some other bilinear distributions in estimating the spectrum of nonstationary signals. Further, the EP is computationally simple and can be efficiently implemented. In this paper, we combine the concepts of the evolutionary spectrum and array processing for problems involving nonstationary signals. We generalize the EP to form the cross-power evolutionary periodogram (CEP) for DOA estimation and blind signal separation.

The nonstationary signal received by each sensor of the array is modeled as a sum of complex sinusoids with time-varying complex amplitudes. These amplitudes carry information about the directions of arrival, which may be time-varying. We first estimate the time-varying amplitudes using linear estimators obtained via minimum mean-squared error criteria. These estimates are then used for the estimation of the time-varying cross-power distributions of the data across the array. Next, using the time-varying cross-power estimates at selected time-frequency samples, we estimate the DOAs of the signals impinging on the array using one of the existing estimation methods[6]. If the directions are time-varying, we confine the selected time-frequency points to be around the time-of interest at which the source direction is to be estimated. Evaluating at different times, we obtain the directions as a function of time. If the sources are stationary, then all time-frequency points of high power concentration can be incorporated into the estimation of the source directions. In the blind source separation problem, the proposed spatial evolutionary spectrum is used along with whitening technique and subspace methods to estimate the mixing matrix and separate the source signals. Whether it is a stationary or moving source, the use of only time-frequency points of high signal to noise ratio is bound to yield improved performance. The incorporation of multiple points along the time-frequency signature can be performed through either

averaging or joint diagonalization schemes[15],[1],[3].

The paper is organized as follows. In the next section, we briefly review the evolutionary spectrum. In Section 3, we provide the fundamental equations of spatio-temporal signal representation. In Section 4, we present the spatial evolutionary spectrum. An estimator for the cross-power evolutionary spectrum, the cross-power evolutionary periodogram, is proposed in Section 5. In Section 6, we propose estimators for the spatio-temporal evolutionary spectrum. The blind source separation using the spatial evolutionary spectrum is addressed in Section 7. Finally, in Section 8, we present examples illustrating the performances of the proposed methods.

2 Evolutionary Spectrum

A zero mean stationary random process, $v[n]$, may be represented as

$$v[n] = \int e^{j\omega n} dZ(\omega) \tag{1}$$

where $Z(\omega)$ is an incrementally orthogonal process, i.e.

$$E\{dZ(\omega)dZ^*(\omega_o)\} = \frac{1}{2\pi} S(\omega) d\omega \delta(\omega - \omega_o) \tag{2}$$

where $\delta()$ is the Kronecker delta function and $()^*$ denotes complex conjugation. Throughout the paper, the integral limits are from $-\pi$ to π. If the process is white with unit variance, then $S(\omega) = 1$.

If the unit variance process $\{v[n]\}$ passes through a time-varying channel with impulse response $h[n,m]$, then the channel output is

$$x[n] = \sum_m h[n,m]v[m]. \tag{3}$$

Spatial Evolutionary Spectrum

Substituting (1) into (3), the nonstationary process $\{x[n]\}$ may be represented as

$$x[n] = \int H(n,\omega)e^{j\omega n}dZ(\omega) \tag{4}$$

where $H(n,\omega)$ is the generalized transfer function evaluated on the unit circle,

$$H(n,\omega) = \sum_m h[n,m]e^{-j\omega(n-m)}. \tag{5}$$

Thus the nonstationary process $\{x[n]\}$ is a continuous sum of sinusoids with time-varying complex amplitudes. The instantaneous power at time n is

$$E\{\mid x[n] \mid^2\} = \frac{1}{2\pi}\int \mid H(n,\omega) \mid^2 d\omega. \tag{6}$$

Therefore, the (oscillatory) evolutionary spectrum may be defined as [9],[12]:

$$S(n,\omega) = \mid H(n,\omega) \mid^2 . \tag{7}$$

Note that $H(n,\omega)$ is slowly varying with time, so that it belongs to the class of oscillatory functions[12, 8]. The cross-power evolutionary spectrum of two processes, $\{x[n]\}$ and $\{y[n]\}$, can be obtained as[13]

$$S_{xy}(n,\omega) = H_x(n,\omega)H_y^*(n,\omega). \tag{8}$$

3 Spatio-temporal Processes

Consider a uniform linear array of L sensors. In analogy with (1), the field at the lth sensor can be expressed as [4]

$$v_l[n] = \int\int e^{j(n\omega - l\alpha)}dZ(\omega,\alpha) \tag{9}$$

where $\alpha = 2\pi\frac{\Delta}{\lambda}\sin(\theta)$, Δ is the array inter-element spacing, θ is the direction of arrival, and λ is the carrier wavelength. $Z(\omega,\alpha)$ is an incrementally orthogonal process in both the temporal frequency ω and spatial frequency α. That is,

$$E\{dZ(\omega,\alpha)dZ^*(\omega_o,\alpha_o)\} = \frac{1}{2\pi}S(\omega,\alpha)d\omega d\alpha\delta(\omega-\omega_o,\alpha-\alpha_o). \tag{10}$$

The cross-power between the data received at sensors l and m can be written as

$$\begin{aligned} E\{v_l[n]v_m^*[n]\} &= \frac{1}{2\pi}\int\int S(\omega,\alpha)e^{j(m-l)\alpha}d\omega d\alpha \\ &= \frac{1}{2\pi}\int \hat{S}(\omega,m-l)d\omega \end{aligned} \tag{11}$$

where $\hat{S}(\omega,m-l)$ represents the result of the Fourier transform with respect to α. In a single point source scenario,

$$S(\omega,\alpha) = S(\omega)\delta(\alpha-\alpha_o) \tag{12}$$

and

$$E\{v_l[n]v_m^*[n]\} = \frac{1}{2\pi}e^{j(m-l)\alpha_o}\int S(\omega)d\omega. \tag{13}$$

Note that the cross-power spectrum (11) carries information about the directions of arrival of all signals impinging on the array.

4 Spatial Evolutionary Spectrum

Assume that the propagation channel has the time-varying impulse response $h[n,m]$. Then, the sensor data takes the form

$$x_l[n] = \sum_m h[n,m]v_l[m]. \tag{14}$$

Spatial Evolutionary Spectrum

From (9) and (14)

$$\begin{aligned} x_l[n] &= \int\int H(n,\omega)e^{j(n\omega-l\alpha)}dZ(\omega,\alpha) \\ &= \int H(n,\omega)e^{jn\omega}d\hat{Z}(\omega,l) \end{aligned} \tag{15}$$

where $H(n,\omega)$ is the generalized transfer function defined in (5). Here, we assume that the phase of $H(n,\omega)$ does not change with time. $d\hat{Z}(\omega,l)$ represents the outcome of the Fourier transform with respect to the spatial frequency α.

The cross-power at time n can be written as

$$\begin{aligned} E\{x_l[n]x_m^*[n]\} &= \frac{1}{2\pi}\int\int \mid H(n,\omega) \mid^2 S(\omega,\alpha)e^{j(m-l)\alpha}d\omega d\alpha \\ &= \frac{1}{2\pi}\int \mid H(n,\omega) \mid^2 \hat{S}(\omega,m-l)d\omega \end{aligned} \tag{16}$$

where $\hat{S}(\omega,m-l)$ in this case contains the result of the Fourier transfrom with respect to α. For a single point source at $\alpha=\alpha_o$,

$$E\{v_l[n]v_m^*[n]\} = \frac{1}{2\pi}e^{j(m-l)\alpha_o}\int \mid H(n,\omega) \mid^2 S(\omega)d\omega. \tag{17}$$

Again, the evolutionary cross-power spectrum carries information about the directions of arrival. Note that if the directions are also time-varying or the channel depends on both the temporal and spatial frequencies, then we can write the following general representation

$$\begin{aligned} x_l[n] &= \int\int H(n,\omega,\alpha)e^{j(n\omega-l\alpha)}dZ(\omega,\alpha) \\ &= \int \hat{H}(n,\omega,l)e^{jn\omega}d\hat{Z}(\omega,l). \end{aligned} \tag{18}$$

The cross-power is

$$\begin{aligned} E\{x_l[n]x_m^*[n]\} &= \frac{1}{2\pi}\int\int S(n,\omega,\alpha)e^{j(m-l)\alpha}d\omega d\alpha \\ &= \frac{1}{2\pi}\int S_{l,m}(n,\omega)d\omega \end{aligned} \tag{19}$$

where $S_{l,m}(n,\omega)$ is the result of the Fourier transform and embeds both the temporal and the spatial spectra. The above equation is a general representation. It includes special common cases such as stationary source of temporal spectrum, stationary source with nonstationary temporal spectrum, moving source with stationary temporal spectrum and finally moving source with nonstationary temporal spectrum. For a single moving point source at $\alpha = \alpha_o[n]$, the cross-power is

$$E\{v_l[n]v_m^*[n]\} = \frac{1}{2\pi}e^{j(m-l)\alpha_o[n]}\int S(n,\omega)d\omega. \tag{20}$$

5 Estimation of Cross-Power Spectrum

Consider the signals $\{x_l[n]\}$, $1 \leq l \leq L$, $0 \leq n \leq N-1$, where L is the number of sensors and N is the number of the data snapshots over the observation interval,

$$x_l[n] = \int \hat{H}(n,\omega,l)e^{jn\omega}d\hat{Z}(\omega,l). \tag{21}$$

Now, consider the data at the lth sensor and frequency ω_o,

$$x_{l,\omega_o}[n] = \hat{H}(n,\omega,l)d\hat{Z}(\omega_o,l)e^{j\omega_o n},\ 1 \leq l \leq L \tag{22}$$

which is a complex sinusoid modulated by a time-varying complex amplitude. The cross-power at time n and frequency ω_o between the data at sensors l and m is

$$E\{x_{l,\omega_o}[n]x_{m,\omega_o}^*[n]\} = \hat{H}(n,\omega_o,l)\hat{H}^*(n,\omega_o,m)\frac{d\omega_o}{2\pi} = S_{l,m}(n,\omega_o)\frac{d\omega_o}{2\pi}. \tag{23}$$

5.1 Model at a Frequency ω_o

In this section, we follow the approach of [8]. For a frequency of interest ω_o, $x_l[n]$, $1 \leq l \leq L$, can be modeled as

$$\begin{aligned} x_l[n] &= x_{l,\omega_o}[n] + y_{l,\omega_o}[n] \\ &= A_l(n,\omega_o)e^{j\omega_o n} + y_{l,\omega_o}[n] \end{aligned} \tag{24}$$

where $A_l(n,\omega_o)$ is the time-varying complex amplitude and $y_{l,\omega_o}[n]$ is a zero-mean term which includes the components at frequencies different from ω_o. From (23), we have

$$E\{A_l(n,\omega_o)A_m^*(n,\omega_o)\} = S_{l,m}(n,\omega_o)\frac{d\omega_o}{2\pi}. \tag{25}$$

Hence, if we estimate the complex amplitudes, $A_l(n,\omega)$, $1 \leq l \leq L$, we can, then, estimate the cross-power evolutionary spectrum which, in turn, may be used for the estimation of the directions of arrival.

Consider the sensor data $x_l[n]$, and assume that $\{A_l(n,\omega_o)\}$ varies slowly with time so that they can be represented as an expansion of orthonormal functions $\{\beta_i[n]\}$, i.e.

$$A_l(n,\omega_o) = \sum_{i=0}^{M-1} \beta_i^*[n]a_i(\omega_o) = \underline{b}[n]^H\underline{a}(\omega_o) \tag{26}$$

where

$$\underline{a}(\omega_o) = [a_o(\omega_o), a_1(\omega_o), \ldots, a_{M-1}(\omega_o)]^T \tag{27}$$

is a vector of expansion coefficients and

$$\underline{b}[n] = [\beta_o[n], \beta_1[n], \cdots, \beta_{M-1}[n]]^T. \tag{28}$$

The notations $()^T$ and $()^H$ stand for the transpose and the Hermitian transpose, respectively.

We can express $x_l[n]$ over the observation interval in the following vector form:

$$\underline{\mathrm{x}}_l = \underline{\mathrm{F}}(\omega_o)\underline{\mathrm{a}}_l(\omega_o) + \underline{\mathrm{y}}_l(\omega_o) \tag{29}$$

where $\underline{\mathrm{F}}(\omega_o)$ is an $N \times M$ matrix with entries

$$\underline{\mathrm{F}}_{n+1,i+1} = \beta_i^*[n]e^{j\omega_o n}, 0 \leq n \leq N-1, 0 \leq i \leq M-1 \tag{30}$$

and

$$\begin{aligned} \underline{\mathrm{x}}_l &= [x_l[0], x_l[1], \cdots, x_l[N-1]]^T \\ \underline{\mathrm{y}}_l(\omega_o) &= [y_{l,\omega_o}[0], y_{l,\omega_o}[1], \cdots, y_{l,\omega_o}[N-1]]^T. \end{aligned} \tag{31}$$

In the following, we will drop the dependence on the constant frequency ω_o.

5.2 Estimation of $A_l(n, \omega_o)$

There are two approaches one could follow to estimate $\{A_l(n, \omega_o)\}$. These time-varying complex amplitudes could be either estimated for each sensor separately using only the data available from that particular sensor or they may be estimated together using the data available from all sensors. Here, we assume that signals at all sensors have similar characteristics. We can write the data snapshots in a matrix form as:

$$\underline{\mathrm{X}} = \underline{\mathrm{F}}\underline{\mathrm{A}} + \underline{\mathrm{Y}} \tag{32}$$

where

$$\begin{aligned} \underline{\mathrm{X}} &= [\underline{\mathrm{x}}_o, \underline{\mathrm{x}}_1, \cdots, \underline{\mathrm{x}}_{L-1}] \\ \underline{\mathrm{Y}} &= [\underline{\mathrm{y}}_o, \underline{\mathrm{y}}_1, \cdots, \underline{\mathrm{y}}_{L-1}] \\ \underline{\mathrm{A}} &= [\underline{\mathrm{a}}_o, \underline{\mathrm{a}}_1, \cdots, \underline{\mathrm{a}}_{L-1}]. \end{aligned} \tag{33}$$

Spatial Evolutionary Spectrum

Note that in the above matrix notation, the snapshots are row vectors and the sensor dependency is across the matrix columns. We use the same minimum mean-squared error estimator for all sensor data. Consider the vector of amplitudes at time n

$$\underline{a}[n] = \underline{b}[n]^H \underline{A} \tag{34}$$

and the following linear estimator

$$\hat{\underline{a}}[n] = \underline{w}[n]^H \underline{X} \tag{35}$$

where

$$\underline{w}[n] \;=\; [w_o[n], w_1[n], \cdots, w_{N-1}[n]]^T. \tag{36}$$

$\underline{w}[n]$ is the vector of time-varying weights. Substituting (32) into (35), we obtain

$$\hat{\underline{a}}[n] = \underline{w}[n]^H \underline{F} \underline{A} + \underline{w}[n]^H \underline{Y}. \tag{37}$$

If the estimator is unbiased then it should produce the correct time-varying amplitudes from the first term. Therefore, we provide the following constraint for an unbiased estimator

$$\underline{w}[n]^H \underline{F} \underline{A} = \underline{b}[n]^H \underline{A} \tag{38}$$

which is satisfied by the following condition

$$\underline{w}[n]^H \underline{F} = \underline{b}[n]^H. \tag{39}$$

To obtain the estimator weights, we minimize the following total mean-squared error (MSE) over all sensors subject to the above constraint

$$\text{MSE} \;=\; \frac{1}{2} E\{(\underline{a}[n] - \hat{\underline{a}}[n])(\underline{a}[n] - \hat{\underline{a}}[n])^H\}$$

$$= \frac{1}{2}\underline{w}[n]^H E\{\underline{Y}\underline{Y}^H\}\underline{w}[n]$$
$$= \frac{1}{2}\underline{w}[n]^H \underline{R}_{YY}\underline{w}[n] \quad (40)$$

where $\underline{R}_{YY} = E\{\underline{Y}\underline{Y}^H\}$. Since $\underline{Y}$ is a function of the frequency ω_o and is not known *a priori*, we make the assumption that $\underline{R}_{YY} = \underline{I}$. This allows the estimator to work in the same way at every frequency [8]. In this case,

$$\text{MSE} = \frac{1}{2}\underline{w}[n]^H\underline{w}[n]. \quad (41)$$

Incorporating the constraint (39), we seek to minimize the following cost function

$$c[n] = \frac{1}{2}\underline{w}[n]^H\underline{w}[n] - (\underline{w}[n]^H\underline{F} - \underline{b}[n]^H)\lambda \quad (42)$$

where λ is an $M \times 1$ vector of Lagrange multipliers. By setting the derivatives with respect to the unknown parameters to zero, we get the optimum weights as [8]

$$\underline{w}_{opt}[n] = \underline{F}\underline{b}[n] \quad (43)$$

and the mean-squared error as

$$\text{MSE} = \underline{b}[n]^H\underline{b}[n]. \quad (44)$$

The mean-squared error is a function of only the expansion functions. Therefore, it is time-dependent and frequency independent. Moreover, for specific orthonormal functions, such as the complex exponentials, the MSE is also constant over time. The estimates of the time-varying amplitudes are obtained by substituting (43) into (35),

$$\hat{\underline{a}}[n] = \underline{b}[n]^H\underline{F}\underline{X}. \quad (45)$$

5.3 Cross-power evolutionary spectrum estimation

Since $\{\hat{A}_l(n,\omega_o)\}$ provide the estimates of the time varying amplitudes at frequency ω_o, then by varying ω_o over all frequencies, we obtain the amplitudes over all frequencies in $-\pi \leq \omega \leq \pi$. The cross-power evolutionary spectral estimator can be obtained from (25) as

$$\begin{aligned}\hat{\underline{\mathrm{S}}}_{xx}(n,\omega) &= E\{\hat{\underline{\mathrm{a}}}[n]^H\hat{\underline{\mathrm{a}}}[n]\} \\ &= E\{\underline{\mathrm{X}}^H\underline{\mathrm{F}}^H\underline{\mathrm{b}}[n]\underline{\mathrm{b}}[n]^H\underline{\mathrm{F}}\underline{\mathrm{X}}\} \\ &= (\underline{\mathrm{b}}[n]^H\underline{\mathrm{F}}) \otimes_l \hat{\underline{\mathrm{R}}} \otimes_r (\underline{\mathrm{F}}^H\underline{\mathrm{b}}[n]) \qquad (46)\end{aligned}$$

where $\otimes$ indicates the block Kronecker product, with subscripts r and l denoting right and left operations, respectively. In the above equation, $\hat{\underline{\mathrm{R}}}$ is an $(LN) \times (LN)$ matrix, with $N \times N$ block element at location (l,m) is $\hat{\underline{\mathrm{R}}}(l,m) = \underline{\mathrm{R}}_{x_l x_m} = E\{\underline{\mathrm{x}}_l\underline{\mathrm{x}}_m^H\}$. We can write the cross-spectrum between two sensors l and m as:

$$\hat{S}_{x_l x_m}(n,\omega) = (\underline{\mathrm{b}}[n]^H\underline{\mathrm{F}}^H)\underline{\mathrm{R}}_{x_l,x_m}(\underline{\mathrm{F}}^H\underline{\mathrm{b}}[n]). \qquad (47)$$

If we drop the expectation operator in the estimation, we will obtain the cross-power evolutionary periodogram (CEP); an extension of the evolutionary periodogram (EP),

$$\hat{\underline{\mathrm{S}}}_{xx}(n,\omega) = (\underline{\mathrm{b}}[n]^H\underline{\mathrm{F}}) \otimes_l \overline{\underline{\mathrm{R}}} \otimes_r (\underline{\mathrm{F}}^H\underline{\mathrm{b}}[n]) \qquad (48)$$

where $\overline{\underline{\mathrm{R}}}(l,m) = \underline{\mathrm{x}}_l\underline{\mathrm{x}}_m^H$. Since the EP is a fast estimator and it has good performance[8], the ECP will also be a fast estimator with similar performance.

Note that although data alignment is important in multichannel spectral estimation[11, 7], it is this difference that we try to exploit for the DOA estimation.

6 Spatio-Temporal Evolutionary Spectrum Estimation

Once we have the cross-power at time n and frequency ω, we can apply one of the existing spectral estimation methods to estimate the spatio-temporal evolutionary spectrum. The peak locations in the spatio-temporal evolutionary spectrum represent the direction of arrival (DOA). Below, we present three estimators using the conventional method, a high resolution method, and a superresolution method.

The Conventional method: In this method, the cross-power matrix is directly involved. The spatial evolutionary spectrum can be written as :

$$\hat{\underline{S}}_{xx}(n,\omega,\alpha) = \underline{e}^H \hat{\underline{S}}_{xx}(n,\omega)\underline{e} \tag{49}$$

where

$$\underline{e} = [1, e^{j\alpha}, \cdots, e^{j(L-1)\alpha}]^T. \tag{50}$$

Minimum-variance distortionless response (MVDR): In this method, the inverse of the cross-power matrix is involved. Other nonlinear functions are also possible [10]. We can write the spatial evolutionary spectrum as :

$$\hat{\underline{S}}_{xx}(n,\omega,\alpha) = [\underline{e}^H \hat{\underline{S}}_{xx}^{-k}(n,\omega)\underline{e}]^{-\frac{1}{k}}. \tag{51}$$

Note that for $k = 1$, the above equation reduces to the minimum variance spectral estimator[4].

Multiple Signal Classification (MUSIC)[14]: This is an eigenstructure subspace method that uses the orthogonality between the signal space and the noise space. The cross-power

matrix can be decomposed as

$$\hat{\underline{\underline{S}}}_{xx}(n,\omega) = \underline{\underline{U}}\Lambda\underline{\underline{U}}^H \tag{52}$$

where the eigenvalues and corresponding eigenvectors are

$$\begin{aligned} \Lambda &= \text{diag}(\lambda_1,\ldots,\lambda_K,\lambda_{K+1},\ldots,\lambda_L), \lambda_1 \leq \cdots \leq \lambda_L, \\ \underline{\underline{U}} &= [\underline{u}_1,\cdots,\underline{u}_K,\underline{u}_{K+1},\cdots,\underline{u}_L]. \end{aligned} \tag{53}$$

For high signal to noise ratios (SNRs), the eigenvalues will be grouped into two sets, one corresponds to the signal components ($\{\lambda_i\}$, $i = 1,\ldots,K$) and the other, closer to zero, corresponds to the noise components ($\{\lambda_i\}$, $i = K+1,\ldots,L$). Using the property that the respective signal and noise eigenvectors are orthogonal, the directions of arrival can be obtained from the peaks of the spatio-temporal evolutionary spectrum:

$$\hat{\underline{\underline{S}}}_{xx}(n,\omega,\alpha) = \frac{1}{\sum_{i=K+1}^{L} \mid \underline{e}^H \underline{u}_i \mid^2}. \tag{54}$$

Other spectral estimation methods may also be used for the estimation of spatial-spectrum [6].

7 Blind Signal Separation

Consider the case in which the signal received at each sensor is equal to a weighted sum of K signals and additive zero-mean thermal noise with variance σ^2. The noise is assumed to be both spatially and temporally white and uncorrelated with the signals. The narrowband data model is given by

$$\underline{x}[n] = \underline{\underline{C}}\underline{s}[n] + \underline{w}[n] \tag{55}$$

where $\underline{\mathrm{C}}$ is an $L \times K$ instantaneous mixing matrix. Substituting (55) into (46), we can show that (see appendix)

$$\hat{\underline{\mathrm{S}}}_{xx}(n,\omega) = \underline{\mathrm{C}}\hat{\underline{\mathrm{S}}}_{ss}(n,\omega)\underline{\mathrm{C}}^H + \sigma^2\underline{\mathrm{b}}[n]^H\underline{\mathrm{b}}[n]\underline{\mathrm{I}}. \tag{56}$$

Note that $\hat{\underline{\mathrm{S}}}_{xx}(n,\omega)$ is an $L \times L$ matrix, whereas $\hat{\underline{\mathrm{S}}}_{ss}(n,\omega)$ is of size $K \times K$. If the signals $\{s_k[n]\}$ are uncorrelated, hence the cross-power matrix is diagonal, $\hat{\underline{\mathrm{S}}}_{ss}(n,\omega) = \Lambda$, then we obtain

$$\hat{\underline{\mathrm{S}}}_{xx}(n,\omega) = \underline{\mathrm{C}}\Lambda\underline{\mathrm{C}}^H + \sigma^2\underline{\mathrm{b}}[n]^H\underline{\mathrm{b}}[n]\underline{\mathrm{I}}. \tag{57}$$

The first term on the right hand side is of rank K and the second term is of rank L. The eigendecomposition of $\hat{S}_{xx}(n,\omega)$ provides the K signal eigenvalues $(p_1[n] + \sigma^2\underline{\mathrm{b}}^H[n]\underline{\mathrm{b}}[n], \cdots,$ $p_K[n]+\sigma^2\underline{\mathrm{b}}^H[n]\underline{\mathrm{b}}[n])$, where p_k are proportional to the powers of signals $s_k[n]$ and the $(L-K)$ noise eigenvalues $(\sigma^2\underline{\mathrm{b}}^H[n]\underline{\mathrm{b}}[n], \cdots, \sigma^2\underline{\mathrm{b}}^H[n]\underline{\mathrm{b}}[n])$, and the corresponding eigenvectors. We proceed to whiten the signal part of (56) through a whitening matrix $\underline{\mathrm{W}}$ [17]. The linear equation (55) becomes

$$\begin{aligned} \underline{\mathrm{z}}[n] &= \underline{\mathrm{W}}\underline{\mathrm{x}}[n] \\ &= \underline{\mathrm{W}}\underline{\mathrm{C}}\underline{\mathrm{s}}[n] + \underline{\mathrm{W}}\underline{\mathrm{w}}[n] \\ &= \underline{\mathrm{U}}\underline{\mathrm{s}}[n] + \underline{\mathrm{W}}\underline{\mathrm{w}}[n] \end{aligned} \tag{58}$$

where $\underline{\mathrm{U}}$ is a unitary matrix. In the absence of noise, the cross-power distribution matrix using the transformed mixture (58) is

$$\hat{\underline{\mathrm{S}}}_{zz}(n,\omega) = \underline{\mathrm{W}}C\hat{\underline{\mathrm{S}}}_{ss}(n,\omega)\underline{\mathrm{C}}^H\underline{\mathrm{W}}^H = \underline{\mathrm{U}}\hat{\underline{\mathrm{S}}}_{ss}(n,\omega)\underline{\mathrm{U}}^H. \tag{59}$$

Spatial Evolutionary Spectrum

The unitary matrix $\underline{\underline{U}}$ can be obtained by joint diagonalizing a set of cross-power distribution matrices evaluated at different time-frequency points [1],[3]. Once $\underline{\underline{U}}$ is found, the mixing matrix and the source signals can be estimated as

$$\begin{aligned} \underline{\underline{C}} &= \underline{\underline{W}}^{\#}\underline{\underline{U}} \\ \underline{s}[n] &= \underline{\underline{U}}^{H}\underline{\underline{W}}\underline{x}[n] \end{aligned} \tag{60}$$

where $\underline{\underline{W}}^{\#}$ is the pseudo inverse of the whitening matrix.

8 Experimental Results

In this section, we present simulation examples to illustrate the performance of the proposed spatial evolutionary spectrum approach for direction finding and blind source separation.

Before presenting the examples, we point out an issue regarding the implementation. Since the cross-power matrices are estimated at a number of selected time-frequency points, it is possible that we only cover one of the sources. Although we employ samples pertaining to the of signal time-frequency signatures, the noise may well effect the performances of the proposed methods. In order to increase overall robustness of the proposed methods and include all signal arrivals, we can follow two approaches. The first approach is the averaging of all the matrices so that all signal components are included in the final cross-power matrix, and also the SNR is increased further[15]. In the second approach, the cross-power matrices are diagonalized jointly[1].

In the first example, we consider two complex frequency shift keying (FSK) signals with frequencies (0.125,0.25) for the first signal and (0.25,0.375) for the second signal. The fre-

quency 0.25 is used by the signals alternately. The length of the observation period is $N = 256$. The signals arrive at a six-sensor array with $\alpha_1 = 10$ and $\alpha_2 = -10$ degrees. Figure 1 shows the spatial spectrum at SNR = -10dB for the CEP-MUSIC and the MUSIC. In this example, we use ordered Hadamard functions with $M = 4$. Eight cross-power distribution matrices are averaged. Figure 1 shows the result of 200 realizations. We observe that the CEP-MUSIC is able to depict two source locations well but the MUSIC has only one peak.

In the second example, we use the same FSK signals of the previous example except with $N = 128$ for the purpose of signal separation. The signals are shown in Figure 2. We mix the signals with the following matrix

$$\underline{C} = \begin{bmatrix} 1.0 & 0.5 \\ 0.6 & 1.0 \\ 0.4 & 0.8 \end{bmatrix}. \tag{61}$$

Figure 3 shows the EP and the bilinear TFD with Choi-Williams kernel of the mixed signal at sensor 1. We apply three different blind source separation methods, namely, the CEP-blind source separation (CEP-BLIS) method described in the previous section, the spatial bilinear TFD based blind source separation method (TFS-BLIS)[3], and the SOBI (second order blind identification) method of [1]. Figure 4 shows the error between Signal 1 and the separated Signal 1 using all three methods when there is no noise. Notice that the scale of the error signal using the CEP-BLIS is different. Figure 5 shows the mean rejection level defined as $I_{perf} = \sum_{l \neq m} E\{|\,(\hat{\underline{C}}^{\#}\underline{C})_{k,l}\,|^2\}$ [1] at different SNRs. We use joint diagonalization with eight matrices in all three methods. The figure shows the result of 200 realizations. We observe that, for this example, the performance of the CEP-BLIS continues to improve as SNR

increases whereas the performances of the SOBI and the TFS-BLIS methods insignificantly change after a threshold around 25dB.

In the final example, we consider a single source of a complex sinusoid at normalized frequency $f = 0.25$, with $N = 128$ snapshots. The distance between the source and multiple antenna array remains constant, but the source displacement is such that α changes linearly from -20 to 20 degrees. We use a two-sensor array and apply the CEP-MUSIC by averaging five matrices around the time of interest n, i.e., we obtain the cross-power matrix by averaging matrices for time-frequency points $(n-5, 0.25), (n-3, 0.25), (n, 0.25), (n+3, 0.25), (n+5, 0.25)$. We use nine complex exponentials as expansion functions. Figure 6 shows the estimates at times $n = 10, 50$ and 100. We observe that the estimator can follow the source quite well.

9 Conclusions

In this paper we combined evolutionary spectrum with spatio-temporal processing for estimation of DOA and blind signal separation. We modeled the nonstationary signals received at the different sensors as sum of complex sinusoids with time-varying complex amplitudes. The estimates of these amplitudes are used for the estimation of cross-power evolutionary spectrum, specifically, the cross-power evolutionary periodogram. Then, the cross-power evolutionary periodogram matrices at time and frequency samples of interest are combined and used in the MUSIC algorithm to obtain the spatial evolutionary spectrum. We also used the cross-power evolutionary periodogram matrices for blind signal separation. We presented examples illustrating that the proposed methods outperform some existing meth-

ods, namely, the standard MUSIC algorithm for DOA estimation, the SOBI, and the bilinear time-frequency distribution based algorithms for blind signal separation.

Appendix

Consider $\underline{x}[n] = \underline{\underline{C}}\underline{s}[n] + \underline{w}[n]$. Now we rewrite $\underline{a}[n]$ as a column vector

$$\begin{aligned} \underline{a}[n] &= \underline{\underline{C}}\left((\underline{b}[n]^H\underline{\underline{F}}) \otimes_l [\underline{s}_1^H, \cdots, \underline{s}_K^H]^H\right) + (\underline{b}[n]^H\underline{\underline{F}}) \otimes_l [\underline{w}_1^H, \cdots, \underline{w}_L^H]^H \\ \underline{a}^H[n] &= [\underline{w}_1^H, \cdots, \underline{w}_L^H] \otimes_r (\underline{\underline{F}}^H\underline{b}[n]) + \left([\underline{s}_1^H, \cdots, \underline{s}_K^H] \otimes_r (\underline{\underline{F}}^H\underline{b}[n])\right)\underline{\underline{C}}^H. \end{aligned} \tag{62}$$

Then, we can write the cross-power as

$$\begin{aligned} \hat{\underline{\underline{S}}}_{xx}(n,\omega) &= E\{\underline{a}[n]\underline{a}^H[n]\} \\ &= \underline{\underline{C}}\left[(\underline{b}[n]^H\underline{\underline{F}}^H) \otimes_l \hat{\underline{\underline{R}}}_{ss} \otimes_r (\underline{\underline{F}}^H\underline{b}[n])\right]\underline{\underline{C}}^H + \sigma^2\underline{b}[n]^H\underline{b}[n]\underline{\underline{I}} \\ &= \underline{\underline{C}}\hat{\underline{\underline{S}}}_{ss}(n,\omega)\underline{\underline{C}}^H + \sigma^2\underline{b}[n]^H\underline{b}[n]\underline{\underline{I}} \end{aligned} \tag{63}$$

where we used the property that $\underline{\underline{F}}\underline{\underline{F}}^H = \underline{\underline{I}}$.

Acknowledgement

This work was supported in part by ONR, grant no. N00014-98-1-0176, and in part by Hacettepe University, 98-530.

References

[1] A. Belouchrani, K. Abed-Meraim, J-F. Cardoso, and E. Moulines. A blind source separation technique using second-order statistics. *IEEE Trans. Signal Proc.*, 45(2):434–444, 1997.

[2] A. Belouchrani and M. Amin. Time-frequency MUSIC: An array signal processing method based on signal representation. *IEEE Signal Processing Letters.* To appear.

[3] A. Belouchrani and M. Amin. Blind source separation based on time-frequency signal representation. *IEEE Trans. Signal Proc.*, 46(11), November 1998.

[4] J. Capon. High-resolution frequency-wavenumber spectrum analysis. *Proc. IEEE*, 57(8):1408–1419, August 1969.

[5] L. Cohen. *Time-Frequency Analysis.* Prentice-Hall, 1995.

[6] D.H. Johnson and D.E. Dudgeon. *Array Signal processing: Concepts and Techniques.* Prentice-Hall, 1993.

[7] S.M. Kay. *Modern Spectral Estimation:Theory and Application.* Prentice-Hall, Englewood Cliffs, N.J., 1988.

[8] A.S. Kayhan, A. El-Jaroudi, and L.F. Chaparro. Evolutionary periodogram for nonstationary signals. *IEEE Trans. Signal Proc.*, 42(6):1527–1536, June 1994.

[9] G. Melard and A. Herteler de Schutter. Contributions to evolutionary spectral theory. *J.of Time Series Analysis*, 10(1):41–63, 1989.

[10] V.F. Pisarenko. On the estimation of spectra by means of nonlinear functions of the covariance matrix. *Geophys.J.R.Astron.Soc.*, 28:511–531, 1972.

[11] M.B. Priestley. *Spectral Analysis and Time Series.* Academic Press Inc., 1981.

[12] M.B. Priestley. *Non-linear and Non-stationary Time Series Analysis.* Academic Press Inc., London, 1988.

[13] M.B. Priestley and H. Tong. On the analysis of bivariate non-stationary processes. *J.R.Statist.Soc.B*, 35(2):153–166, 1973.

[14] R.Schmidt. Multiple emitter location and signal parameter estimation. *IEEE Trans. on Antennas and Propagation*, 34(1):276–280, 1986.

[15] K. Sekihara, S. Nagarajan, D. Poeppel, and Y. Miyashita. Time-frequency MEG-MUSIC algorithm. *IEEE Medical imaging.* Submitted.

[16] L. Tong and S. Perreau. Multichannel blind identification: From subspace to maximum likelihood methods. *Proceedings of IEEE*, 86(10):1951–1968, 1998.

[17] L. Tong, R w. Liu, V.C. Soon, and Y-F. Huang. Indeterminacy and identifiability of blind identification. *IEEE Trans. on Circuits and Systems*, 38(5):499–509, 1991.

[18] A-J. Van Der Veen. Algebraic methods for deterministic blind beamforming. *Proceedings of IEEE*, 86(10):1987–2008, 1998.

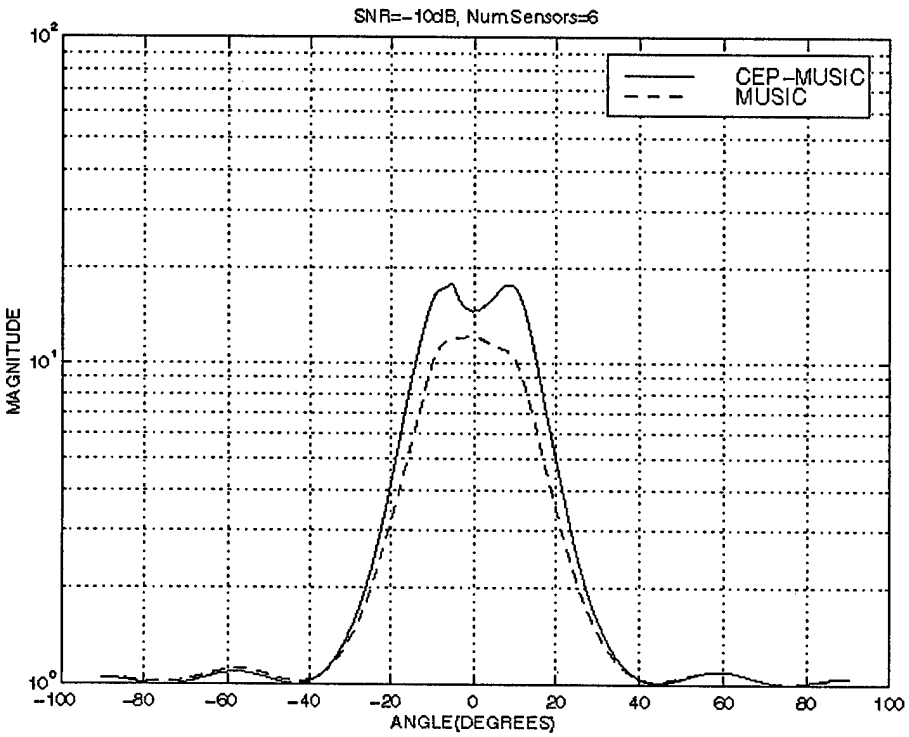

Figure 1: Spatial spectrum for two FSK signals at $\alpha_1 = -10$ and $\alpha_2 = 10$ degrees.

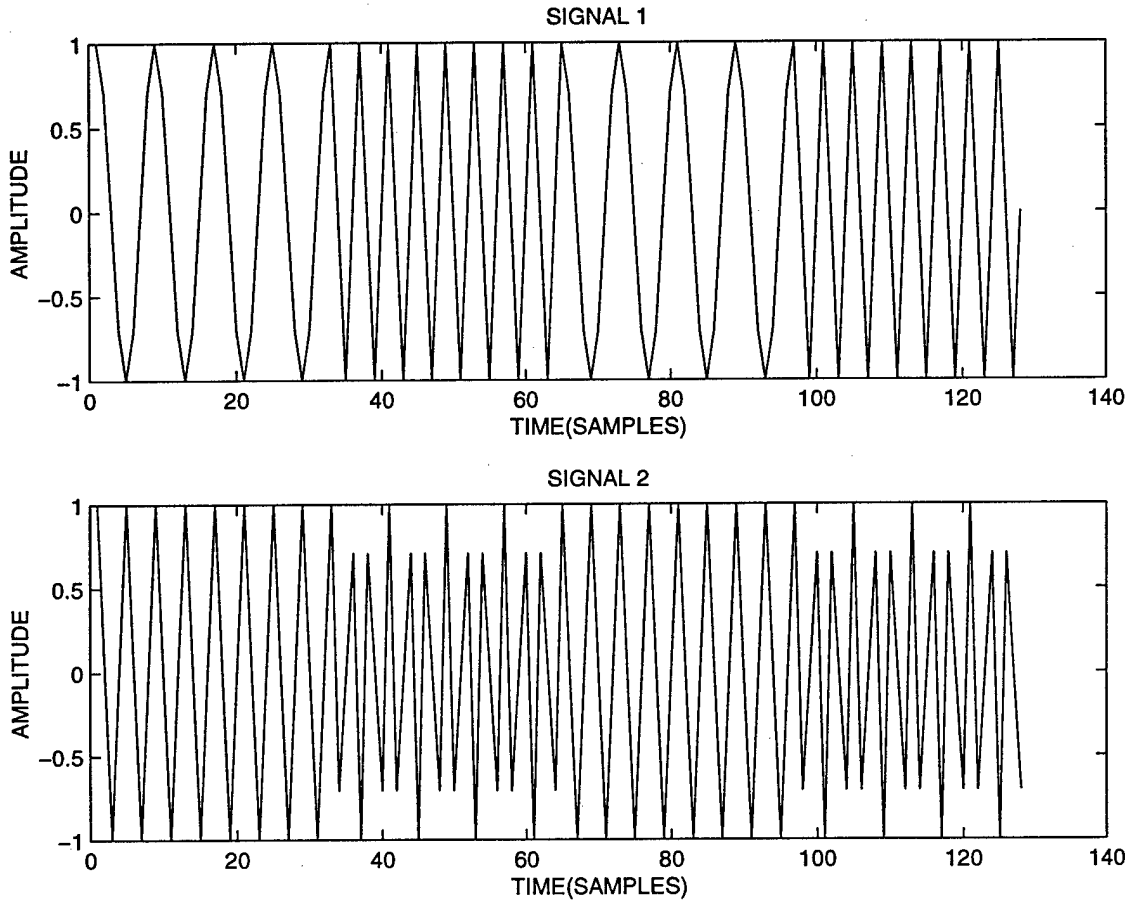

Figure 2: The FSK signals used for the blind source separation.

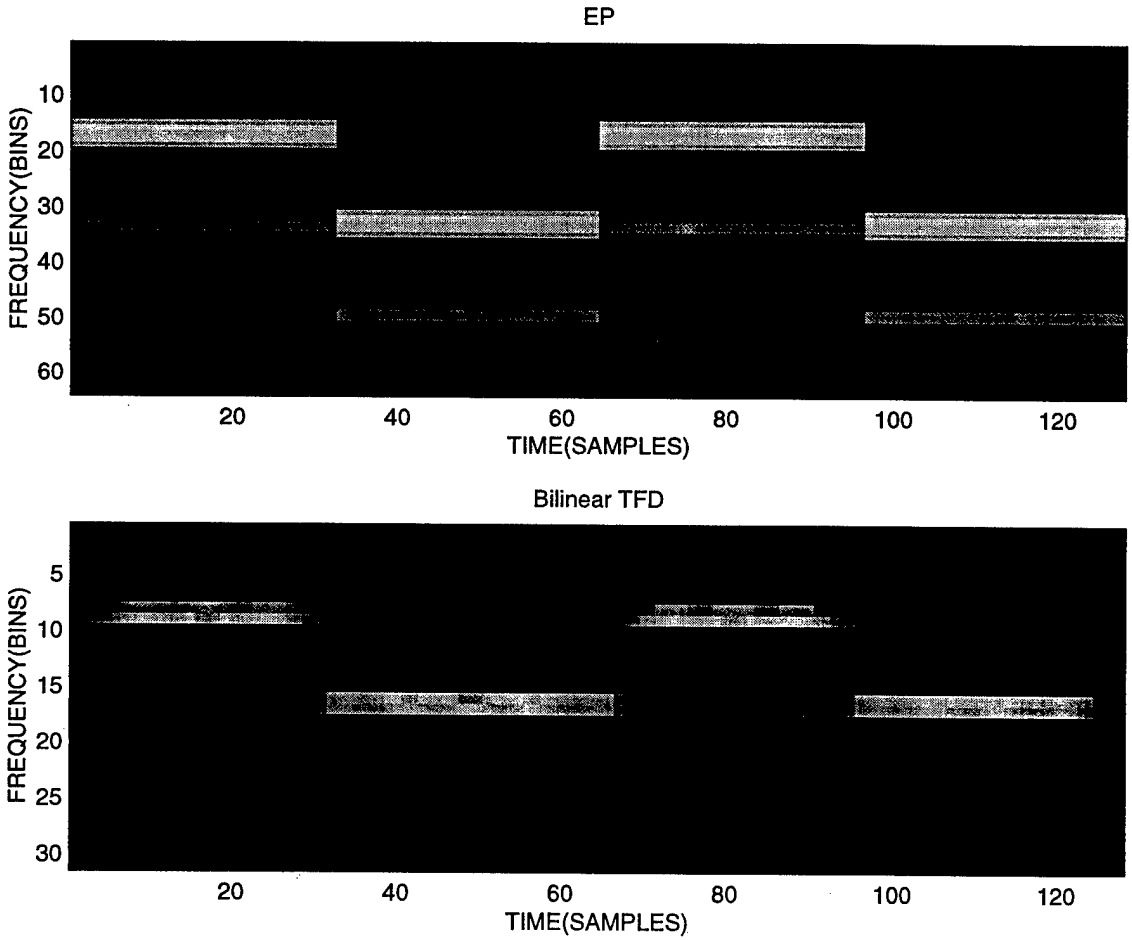

Figure 3: The EP and the bilinear TFD of the mixed signal at Sensor 1.

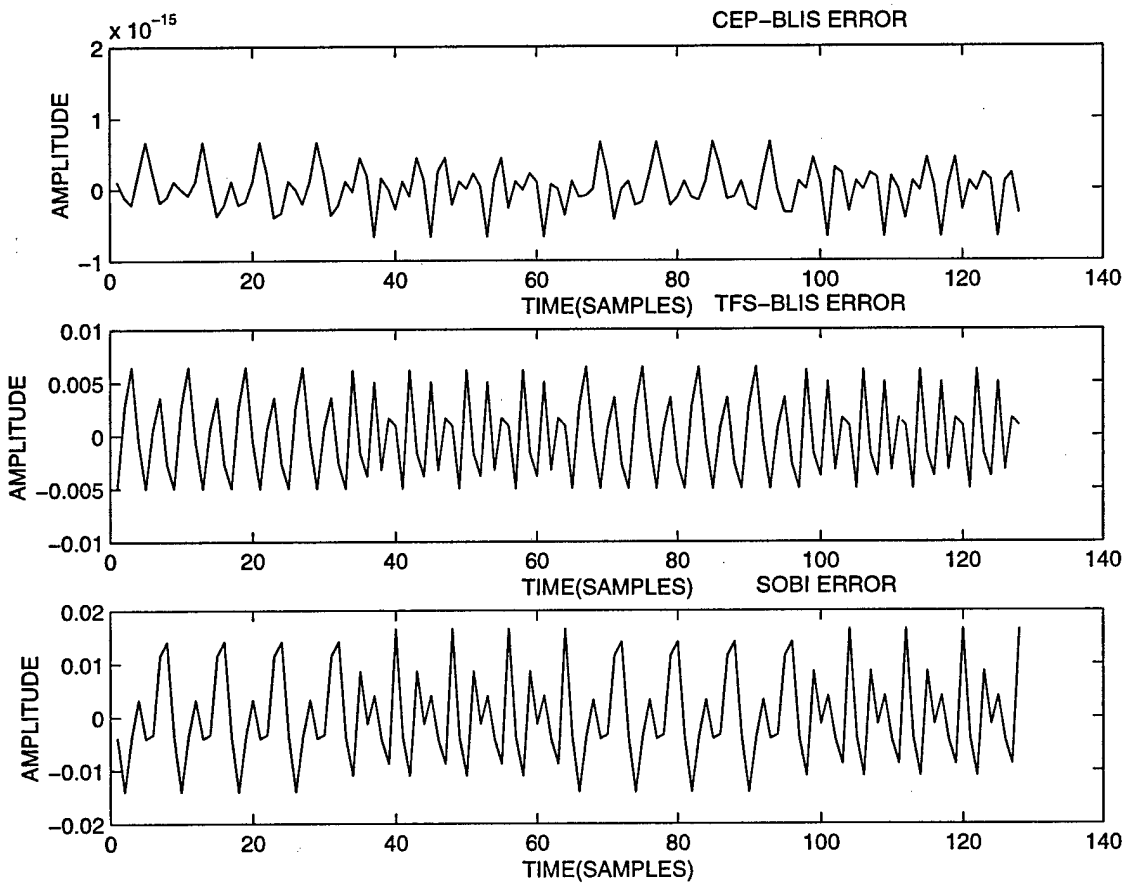

Figure 4: The errors between Signal 1 and the separated Signal 1 using (a) the CEP-BLIS, (b) the TFS-BLIS and (c) the SOBI.

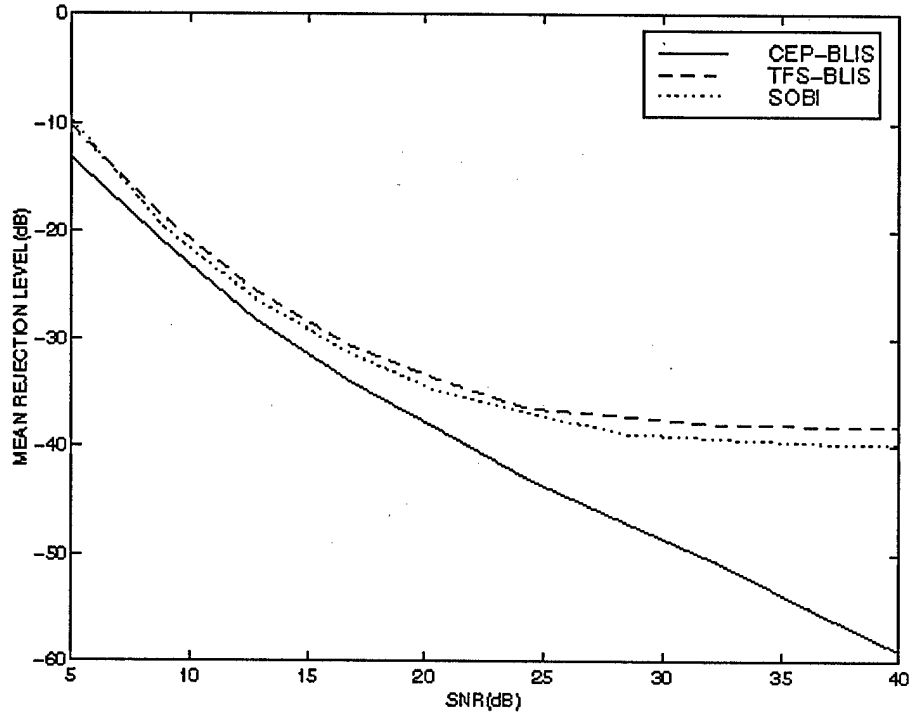

Figure 5: Mean rejection levels for the FSK signals.

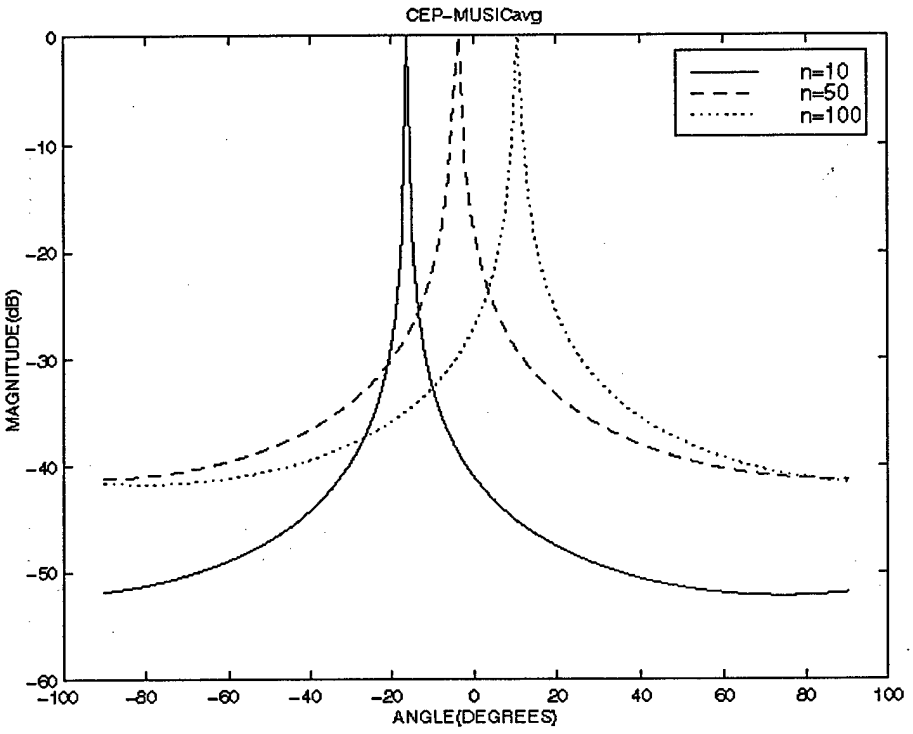

Figure 6: Spatial spectrum for a moving source with α varying linearly from -20 to 20 degrees.

SPATIAL AVERAGING OF TIME-FREQUENCY DISTRIBUTIONS

Yimin Zhang and *Moeness G. Amin*

Department of Electrical and Computer Engineering
Villanova University
Villanova, PA 19085, USA

ABSTRACT

This paper presents a novel approach based on time-frequency distributions (TFDs) for separating signals received by a multiple antenna array. This approach provides a significant improvement in performance over the recently introduced spatial time-frequency distributions, specifically for signals with close time-frequency signatures. In this approach, spatial averaging of the time-frequency distributions of the sensor data is performed to eliminate the interactions of the sources signals in the time-frequency domain, and as such restore the realness property and the diagonal structure of the source TFDs, which are necessary for source separation. It is shown that the proposed approach yields improved performance over both cases of no spatial averaging and averaging using time-frequency smoothing kernels.

1. INTRODUCTION

In this paper, we introduce a new technique for source separation based on time-frequency distribution methods. The sources have different time-frequency signatures and instantaneously mixed at the array sensors. The number of sensors is assumed to be equal to or greater than twice the number of sources. The time-frequency distributions (TFDs) of the data across the array are computed and used to construct spatial time-frequency distribution matrices (STFDs). By forcing the hermition Toeplitz structure of the STFDs and perform spatial symmetric averaging over two parts of the array, we achieve significant improvement of source separation over the case where no spatial averaging is performed.

Recently, time-frequency distributions have been applied to direction finding and blind source separation problems in array processing. The spatial time-frequency distributions are introduced in [1] and represented by a spatial matrix whose elements are the time-frequency distributions of the data across the multi-sensor array. The successful application of STFDs to separating sources with identical spectra, but different time-frequency signatures, is shown in [2]. In this application, STFD matrices computed at different t-f points are incorporated into a joint-diagnalization technique based on generalized Jacobi transform to estimate the mixing, or array manifold, matrix. This matrix is then used to estimate the sources' signals up to a multiplicative complex scalar and the order of the sources. The general theory of solving blind source seperation problems using spatial arbitrary joint variable distributions, including those of time and frequency, is given in [3]. In [4], the two arbitrary variables are chosen as the time-lag and frequency-lag, and the source separation was performed using spatial ambiguity functions. The use of STFDs as an eigenstructure-based approach for direction finding is given in [5], where the Time-Frequency MUSIC technique is proposed to estimate the signal and noise subspaces.

The importance of joint-diagonalization (JD) in the STFD context is that the diagonal structure, the distinct eigenvalues, and the full rank properties of the signal TFD matrix, necessary for source separation, can be easily violated when operating with a single t-f point. The cross time-frequency distributions of the source signals yield non-zero complex values at the off-diagonal elements, rendering the estimation of the mixing matrix difficult, or even impossible. Also, the noise contribution to all matrix elements at low SNR cannot be ignored. As the interactions of the source signals vary over the time-frequency plane, the incorporation of several STFD matrices at different t-f points into JD enhances diagonalization and leads to a successful separation of signal arrivals. It is noted that the primary motivation of using smoothing kernels and resorting to other variables than time and frequency, specifically the ambiguity-domain variables, is to allow the selection of joint-variable points where the interactions of the source signals are insignificant.

The fundamental role of the proposed technique of symmetric spatial averaging of STFDs is the effective elimination of the signals' intermodulations. It effectively restores the diagonal structure and realness property of the signal TFD matrix. Symmetric spatial averaging is a simple, well-known technique in conventional array processing [6]. It uses additional array sensors to reduce cross-correlation in coherent and correlated signal environments, and thereby permits proper angle-of-arrival estimations and source separations. It is shown that adopting this technique in the underlying TFD-based source separation JD problem gives robustness to t-f point selections and leads to improved performance over other TFD-based techniques, specifically for sources whose time-frequency signatures are not very distinct.

2. SPATIAL TIME-FREQUENCY DISTRIBUTIONS

The data vector for N-element array is given by

$$\mathbf{x}(t) = \mathbf{y}(t)+\mathbf{n}(t) = \mathbf{A}\mathbf{s}(t)+\mathbf{n}(t). \quad (1)$$

In vector forms, $\mathbf{x}(t)=[x_0(t), \ldots, x_{N-1}(t)]^T$ is a noisy instantaneous linear mixture of the source signals $\mathbf{s}(t)=[s_1(t), \ldots, s_n(t)]^T$ and $\mathbf{n}(t)$ is the additive noise. The mixing matrix $\mathbf{A}$ is the transfer function between the sources and the array sensors.

This work is supported by ONR under Grant #N00014-98-1-0176.

The discrete-time form of Cohen's class of TFD for signal $x(t)$ is given by [7]

$$D_{xx}(t,f)=\sum_{l=-\infty}^{\infty}\sum_{m=-\infty}^{\infty}\phi(m,l)x(t+m+l)x^{*}(t+m-l)e^{-j4\pi fl} \quad (2)$$

where t and f represent the time index and the frequency index, respectively. The kernel $\phi(m, l)$ characterizes the TFD and is a function of both the time and lag variables. The cross-TFD of two signals $x_i(t)$ and $x_j(t)$ is defined by

$$D_{x_ix_j}(t,f)=\sum_{l=-\infty}^{\infty}\sum_{m=-\infty}^{\infty}\phi(m,l)x_i(t+m+l)x_j^{*}(t+m-l)e^{-j4\pi fl} \quad (3)$$

The spatial time-frequency distribution (STFD) incorporates both equations (2) and (3), and is defined in [2] by,

$$\mathbf{D}_{xx}(t,f)=\sum_{l=-\infty}^{\infty}\sum_{m=-\infty}^{\infty}\Phi(m,l)\otimes\mathbf{x}(t+m+l)\mathbf{x}^{H}(t+m-l)e^{-j4\pi fl} \quad (4)$$

where $\left[\mathbf{D}_{xx}(t,f)\right]_{i,j}=D_{x_ix_j}(t,f)$, for $i, j=0, \ldots, N-1$, $\otimes$ denotes the Hadamard product, and $\left[\Phi(m,l)\right]_{i,j}=\phi_{i,j}(m,l)$ is the time-frequency kernel associated with the pair of the sensor data $x_i(t)$ and $x_j(t)$. Under the linear data model of Eq. (1) and assuming noise-free environment, the STFD matrix takes the following simple structure

$$\mathbf{D}_{xx}(t,f)=\mathbf{A}\mathbf{D}_{ss}(t,f)\mathbf{A}^{H} \quad (5)$$

where $\mathbf{D}_{ss}(t,f)$ is the signal TFD matrix whose entries are the auto- and cross-TFDs of the sources. Eq. (5) is similar to that commonly used in conventional blind source separation and direction-of-arrival (DOA) estimation problems [8,9], relating the signal correlation matrix to the data spatial correlation matrix. If $\mathbf{D}_{ss}(t,f)$ is a full-rank matrix, the two subspaces spanned by the principle eigenvectors of $\mathbf{D}_{xx}(t,f)$ and the columns of $\mathbf{A}$ become identical. In this case, directional finding techniques based on eigenstructures can be applied. If $\mathbf{D}_{ss}(t,f)$ is diagonal, i.e., the signal cross-TFDs at the time-frequency point (t,f) are zeros, the mixture matrix and the signal waveform can be recovered using blind source separation methods [1,2]. In these methods, in order to avoid potential problems associated with using a single STFD, STFDs at different (t,f) points are incorporated into a joint-diagonalization scheme. Although JD of the STFDs is effective in most cases, signals with close time-frequency signatures are still difficult to separate. As shown below, spatial averaging can be used to facilitate signal separation.

3. SPATIAL AVERAGING TIME-FREQUENCY DISTRIBUTIONS

Symmetric spatial averaging method was proposed by Pillai [6] to restore the full-rank property of the signal covariance matrix in the presence of coherent signals. In this section, we extend the spatial averaging method to TFD analysis, and propose the signal separation method by joint diagonalization (JD) based on spatial averaging TFDs.

Without loss of generality, we consider $M=2$, i.e., only two sources, $s_1(t)$ and $s_2(t)$. The result can be easily extended to multiple sources. By ignoring the effect of noise, the received signal at i-th array sensor is represented as

$$x_i(t)=x_i^{(1)}(t)+x_i^{(2)}(t)=s_1(t)e^{-jd_i\omega_1}+s_2(t)e^{-jd_i\omega_2} \quad (6)$$

where $\omega_k=2\pi\sin\phi_k/\lambda$ $(k=1,2)$ is the spatial radian frequency, λ is the RF wavelength, and d_i is the distance between 0-th and i-th array sensors. We assume the array is equi-spaced linear array. The cross-TFD of $x_i(t)$ and $x_j(t)$ is

$$\begin{aligned}&D_{x_ix_j}(t,f)\\&=D_{x_i^{(1)}x_j^{(1)}}(t,f)+D_{x_i^{(2)}x_j^{(1)}}(t,f)+D_{x_i^{(2)}x_j^{(2)}}(t,f)+D_{x_i^{(1)}x_j^{(2)}}(t,f)\\&=\left[D_{s_1s_1}(t,f)+D_{s_2s_1}(t,f)e^{-jd_i(\omega_2-\omega_1)}\right]e^{-j(d_i-d_j)\omega_1}\\&\quad+\left[D_{s_2s_2}(t,f)+D_{s_1s_2}(t,f)e^{jd_i(\omega_2-\omega_1)}\right]e^{-j(d_i-d_j)\omega_2}\end{aligned} \quad (7)$$

Since the cross-terms (second term in each bracket in (7)) are generally complex, it is clear that the TFD matrix $\mathbf{D}_{xx}(t,f)$ will not provide proper phase information for recovering the DOA of the arrived signals when cross-terms are present. However, such phase information can be restored by using spatial averaging methods. The spatial averaging of TFD allows the signal separation even when the TFDs of multiple signals have very similar shapes and are highly overlapping.

Let the number of array sensors be $2N$-1with the array center is the zeroth sensor, as shown in Fig.1. The TFD of $x_0(t)$ and $x_i(t)$, $i=0, 1, 2, \ldots, N-1$, is

$$\begin{aligned}&D_{x_0x_i}(t,f)\\&=\left[D_{s_1s_1}(t,f)+D_{s_2s_1}(t,f)\right]e^{jd_i\omega_1}+\left[D_{s_2s_2}(t,f)+D_{s_1s_2}(t,f)\right]e^{jd_i\omega_2}\end{aligned} \quad (8)$$

where we note $d_0=0$. Similarly, the TFD of $x_0(t)$ and $x_{-i}(t)$ is

$$\begin{aligned}&D_{x_0x_{-i}}(t,f)\\&=\left[D_{s_1s_1}(t,f)+D_{s_2s_1}(t,f)\right]e^{-jd_i\omega_1}+\left[D_{s_2s_2}(t,f)+D_{s_1s_2}(t,f)\right]e^{-jd_i\omega_2}\end{aligned} \quad (9)$$

The spatial averaging of (8) and (9) is given by

$$\tilde{D}_{xx}^{(i)}(t,f)=\left\{D_{x_0x_i}(t,f)+D_{x_0x_{-i}}^{*}(t,f)\right\}/2=b_1e^{jd_i\omega_1}+b_2e^{jd_i\omega_2} \quad (10)$$

where

$$b_1=D_{s_1s_1}(t,f)+\mathrm{Re}\left(D_{s_2s_1}(t,f)\right)$$

$$b_2=D_{s_2s_2}(t,f)+\mathrm{Re}\left(D_{s_1s_2}(t,f)\right)$$

Since the terms in the brackets are all real, the TFD in (10) correctly represents the phase information caused by the propagation delay between array sensors, even when the cross-terms are complex. The matrix formed from the TFDs (10)

$$\tilde{\mathbf{D}}_{xx}(t,f)=\begin{bmatrix}\tilde{D}_{xx}^{(0)}(t,f) & \tilde{D}_{xx}^{(1)}(t,f) & \cdots & \tilde{D}_{xx}^{(N-1)}(t,f)\\ \tilde{D}_{xx}^{(1)*}(t,f) & \tilde{D}_{xx}^{(0)}(t,f) & \cdots & \tilde{D}_{xx}^{(N-2)}(t,f)\\ \vdots & \vdots & \ddots & \vdots\\ \tilde{D}_{xx}^{(N-1)*}(t,f) & \tilde{D}_{xx}^{(N-2)*}(t,f) & \cdots & \tilde{D}_{xx}^{(0)}(t,f)\end{bmatrix} \quad (11)$$

is hermitian and Toeplitz. It is referred to as the spatial averaging TFD (SATFD) matrix. In the noise-free environment, the SATFD matrix can be expressed as

$$\tilde{\mathbf{D}}_{xx}(t,f) = \mathbf{A}\tilde{\mathbf{D}}_{ss}\mathbf{A}^{H} \tag{12}$$

where

$$\tilde{\mathbf{D}}_{ss}(t,f) = \mathrm{diag}[b_1 \quad b_2] \tag{13}$$

are the equivalent TFD of the signal vectors. Note that $\tilde{\mathbf{D}}_{ss}(t,f)$ no longer expresses the actual TFD. Clearly, (12) has the same format as (5), and $\tilde{\mathbf{D}}_{ss}(t,f)$ here is diagonal even when the cross-terms of the TFD of the signals are present. Therefore, the spatial averaging method will ensure the validity of the TFD-based signal separation in the presence of cross-TFD.

4. SIMULATION RESULTS

Equi-spaced 5-element linear array is used for simulation with the interelement spacing 0.5λ. When spatial averaging method is used, two sub-arrays are formed, each with 3 elements. Two sources of chirp signals

$$s_1(t) = e^{-j\mu\frac{t^2}{2}}, \quad s_2(t) = e^{-j\mu\frac{t^2}{2}-j\omega t} \tag{14}$$

are used, where μ and ω are chosen to be 0.008π and 0.02π, respectively. The DOAs of the two signals are assumed 30° and 60° from the broadside direction. No noise is considered here.

Fig.2(a) shows the Wigner-Ville distribution of each source signal, and Fig.2(b) shows the respective distributions after signal separation. It is clear that the array fails to separate $s_1(t)$ and $s_2(t)$.

In the TFD-based signal separation method, applied in Fig. 2, three points (t,f) are used for joint diagonalization at t = 32, 64, and 96. The frequency f is chosen so that the TFD at the first array sensor is the largest for a given t.

To show the effect of using a smoothing kernel, similar simulation is performed with the Choi-Williams kernel [10] with σ = 0.1. The result is shown in Fig.3. A rectangular window with 31 samples in both time and frequency scale is used. Since the two signals are closely spaced in the t-f domain, the cross-terms reduction furnished by the Choi-Williams kernel is limited, and again the array fails to separate the two signals.

Fig.4 shows the separated signals under the same conditions when the proposed spatial averaging method is applied. The signals are perfectly separated, except for their order.

5. CONCLUSIONS

Symmetric averaging of spatial time-frequency distributions has been introduced. The averaging improves the performance of source separation using joint-diagonalization techniques. It amounts to forming a spatial hermition Toeplitze matrix using the time-frequency distributions of the data across one half of the array. This matrix is then added to the spatial matrix corresponding to the other half of the array. The effect of this averaging is to remove interaction between the source signals in the time-frequency domain. Joint digonalization (JD) using a generalization of Jacobi transform is then applied to estimate the mixing matrix. By reducing the interaction of the source signals, the JD algorithm yields improved performance over the case when no averaging is performed. The paper presented an example of separating two chirps signals whose time-frequency signatures are slightly different. The proposed approach has successfully separated the two signatures, while other non-averaging methods fail.

6. REFERENCES

[1] A. Belouchrani and M. Amin, "Source separation based on the diagonalization of a combined set of spatial time-frequency distribution matrices," in *Proc. IEEE ICASSP'97*, Germany, April 1997.

[2] A. Belouchrani and M. Amin, "Blind source separation based on time-frequency signal representation," *IEEE Trans. Signal Processing*, Nov. 1998.

[3] A. Belouchrani and M. Amin, "Blind source separation using joint signal representations," in *Proc. SPIE Conf. on Advanced Algorithms and Architectures for Signal Processing*, San Diego, CA, Aug. 1997.

[4] M. Amin and A. Belouchrani, " Blind source separation using the spatial ambiguity functions," in *Proc. IEEE Int. Symp. on Time-Frequency and Time-Scale Analysis*, Pittsburgh, Pennsylvania, Oct. 1998.

[5] M. Amin and A. Belouchrani "Time-frequency MUSIC: an array signal processing method based on time-frequency signal representation," in *Proc. SPIE Conf. on Radar Processing, Technology and Applications*, San Diego, CA, July 1997.

[6] S. U. Pillai, *Array Signal Processing*, Springer-Verlog, 1989.

[7] L. Cohen, *Time-frequency Analysis*, Prentice Hall, 1995.

[8] L. Tong, Y. Inouye, and R-W. Liu, "Waveform-preserving blind estimation of multiple independent sources," *IEEE Trans. Signal Processing*, vol,41, no.7, pp.2461-2470, July 1993.

[9] A. Belouchrani, K. A. Meraim, H.-F. Cardoso, and E. Muylines, "A blind source separation techniques using second order statistics," *IEEE Trans. Signal Processing*, vol.45, no.2, pp.434-444, Feb. 1997.

[10] H. I. Choi and W. J. Williams, "Improved time-frequency representation of multicomponent signals using exponential kernels," *IEEE Trans. Acoust., Speech, Signal Processing*, vol. 37, no.6, pp.862-871, June 1989.

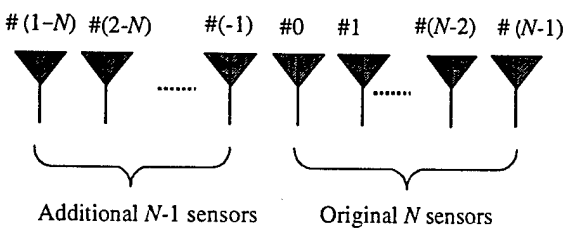

Fig.1 Array configuration for spatial averaging

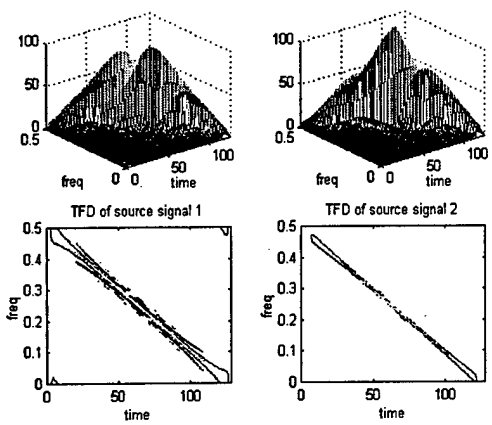

(a) TFD of the sources

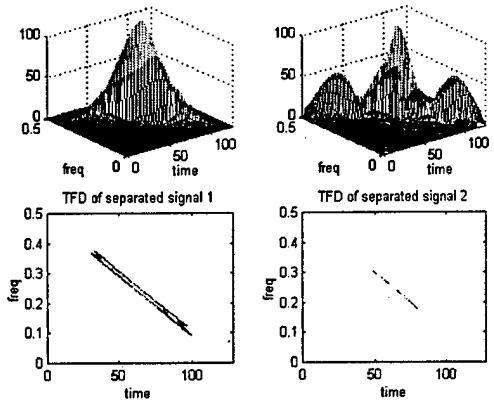

(b) TFD of the separated signals

Fig.2 TFD of the sources and the separated signals using Wigner-Ville distribution

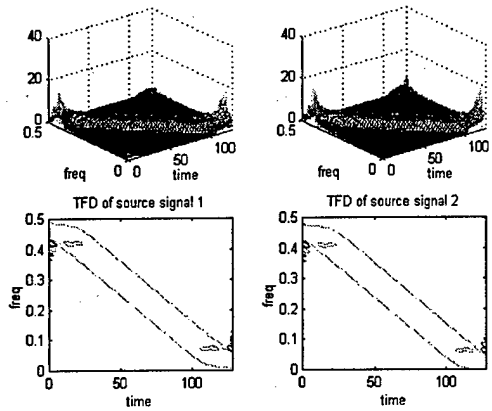

(a) TFD of the sources

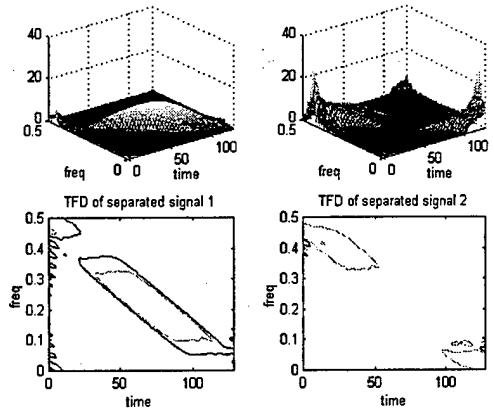

(b) TFD of the separated signals

Fig.3 TFD of the sources and the separated signals using Choi-Williams distribution

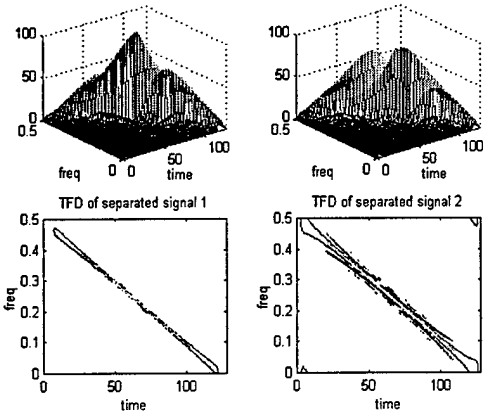

(a) Wigner-Ville distribution

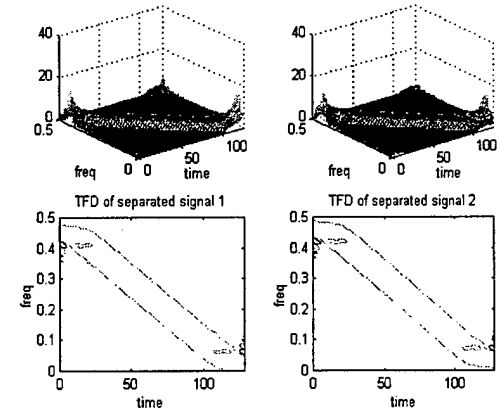

(b) Choi-Williams distribution

Fig.4 Separated signals with spatial averaging

Maximum likelihood methods for array processing based on time-frequency distributions

Yimin Zhang, Weifeng Mu, and Moeness G. Amin*
Department of Electrical and Computer Engineering,
Villanova University, Villanova, PA 19085

ABSTRACT

This paper proposes a novel time-frequency maximum likelihood (t-f ML) method for direction-of-arrival (DOA) estimation for non-stationary signals, and compares this method with conventional maximum likelihood DOA estimation techniques. Time-frequency distributions localize the signal power in the time-frequency domain, and as such enhance the effective SNR, leading to improved DOA estimation. The localization of signals with different t-f signatures permits the division of the time-frequency domain into smaller regions, each contains fewer signals than those incident on the array. The reduction of the number of signals within different time-frequency regions not only reduces the required number of sensors, but also decreases the computational load in multi-dimensional optimizations. Compared to the recently proposed time-frequency MUSIC (t-f MUSIC), the proposed t-f ML method can be applied in coherent environments, without the need to perform any type of preprocessing that is subject to both array geometry and array aperture.

Keywords: Time-frequency, DOA estimation, maximum likelihood, spatial time-frequency distribution, array processing.

1. INTRODUCTION

The localization of spatial sources by passive sensor array is one of the important problems in radar, sonar, radio-astronomy, and seismology. So far, numerous methods have been proposed for direction finding, most of which are based on the estimates of the data covariance matrix. Among these methods, the maximum likelihood (ML) technique was one of the first to be devised and investigated [1]. The ML method has a superior performance compared to other methods, particularly when the input signal-to-noise ratio (SNR) is low, the number of data samples is small, or the sources are highly correlated [2]. Therefore, despite its complexity, ML remains of practical interests.

The evaluation of quadratic time-frequency distributions of the data snapshots across the array yields what is known as spatial time-frequency distributions (STFDs) [3, 4]. STFD techniques are most appropriate to handle sources of nonstationary waveforms that are highly localized in the time-frequency domain. Spatial time-frequency distributions spread the noise power while localizing the energy of the impinging signals in the time-frequency domain. This property leads to increasing the robustness of eigenstructure signal and noise subspace estimates with respect to channel and receiver noise, and hence improves spatial resolution and signal separation performance.

Although the approach of applying the spatial time-frequency distributions to the direction-of-arrival (DOA) estimation has been introduced in [4], the performance of direction finding methods based on STFDs has not been made clear yet. In this paper, we propose the time-frequency maximum likelihood (t-f ML) method for direction finding and provide the analysis that explains its performance. It is shown that the superior performance of the t-f ML method relative to other methods is attributed to: 1) Time-frequency distributions localize the signal power in the time-frequency domain, and as such enhance the effective SNR and improve the DOA estimation. 2) The localization of signals with different time-frequency signatures permits the division of the time-frequency domain into smaller regions, each contains fewer signals than those incident on the array. The reduction of the number of signals within different time-frequency regions relaxes the condition on the array aperture and also simplifies multidimensional optimization estimation procedure. 3) Compared with the previously proposed time-frequency MUSIC (t-f MUSIC), the t-f ML method can be applied when the signal arrivals are coherent, whereas the t-f MUSIC cannot do so without some sort of preprocessing, such as spatial smoothing.

This paper is organized as follows. In Section 2, the signal model is established, and a brief review of the spatial time-frequency distributions is given. In Section 3, we discuss the SNR enhancement based on time-frequency distributions and its effect on the signal and noise subspaces estimates using STFD matrices. The results from

* Correspondence: E-mail: moeness@ece.vill.edu; Phone: (610) 519 - 7305; Fax: (610) 519 - 4436.

STFD matrices show more robustness to SNR and angular separation compared to the results obtained from data covariance matrices. Section 4 presents the t-f ML and discuss its performance.

2. BACKGROUND

2.1. Signal Model

In narrowband array processing, when n signals arrive at an m-element array, the linear data model

$$\mathbf{x}(t) = \mathbf{y}(t) + \mathbf{n}(t) = \mathbf{A}(\Theta)\mathbf{d}(t) + \mathbf{n}(t) \tag{1}$$

is commonly assumed, where the $m \times n$ spatial matrix $\mathbf{A}(\Theta) = [\mathbf{a}(\theta_1)...\mathbf{a}(\theta_n)]$ represents the mixing matrix or the steering matrix, and $\mathbf{a}(\theta_i)$ are the the steering vectors. Due to the mixture of the signals at each sensor, the elements of the $m \times 1$ data vector $\mathbf{x}(t)$ are multicomponent signals, whereas each source signal $d_i(t)$ of the $n \times 1$ signal vector $\mathbf{d}(t)$ is often a monocomponent signal. $\mathbf{n}(t)$ is an additive noise vector whose elements are modeled as stationary, spatially and temporally white, zero-mean complex random processes, independent of the source signals. That is,

$$E[\mathbf{n}(t+\tau)\mathbf{n}^H(t)] = \sigma\delta(\tau)\mathbf{I} \text{ and } E[\mathbf{n}(t+\tau)\mathbf{n}^T(t)] = \mathbf{0} \text{ for any } \tau \tag{2}$$

where $\delta(\tau)$ is the Kronecker delta function, $\mathbf{I}$ denotes the identity matrix, σ is the noise power at each sensor, superscript ^{H} and ^{T} respectively denote conjugate transpose and transpose, and $E(\cdot)$ is the statistical expectation operator.

In equation (1), it is assumed that the number of sensors is larger than the number of sources, i.e., $m > n$. Further, matrix $\mathbf{A}$ is full column rank, which implies that the steering vectors corresponding to n different angles of arrival are linearly independent. We further assume that the correlation matrix

$$\mathbf{R_{xx}} = E[\mathbf{x}(t)\mathbf{x}^H(t)] \tag{3}$$

is nonsingular, and the observation period consists of N snapshots with $N > m$.

Under the above assumptions, the correlation matrix is given by

$$\mathbf{R_{xx}} = E[\mathbf{x}(t)\mathbf{x}^H(t)] = \mathbf{A}(\Theta)\mathbf{R_{dd}}\mathbf{A}^H(\Theta) + \sigma\mathbf{I}, \tag{4}$$

where $\mathbf{R_{dd}} = E[\mathbf{d}(t)\mathbf{d}^H(t)]$ is the signal correlation matrix. For notational convenience, we drop the argument Θ in equation (1) and simply use $\mathbf{A}$ instead of $\mathbf{A}(\Theta)$. If $\hat{\Theta}$ is an estimate of Θ, then we also use $\hat{\mathbf{A}}$ instead of $\mathbf{A}(\hat{\Theta})$.

Let $\lambda_1 > \lambda_2 > \cdots > \lambda_n > \lambda_{n+1} = \lambda_{n+2} = \cdots = \lambda_m = \sigma$ denote the eigenvalues of $\mathbf{R_{xx}}$. It is assumed that λ_i, $i = 1, \cdots, n$, are distinct. The unit-norm eigenvectors associated with $\lambda_1, ..., \lambda_n$ constitute the columns of matrix $\mathbf{S} = [\mathbf{s}_1, ..., \mathbf{s}_n]$, and those corresponding to $\lambda_{n+1}, ..., \lambda_m$ make up matrix $\mathbf{G} = [\mathbf{g}_1, ..., \mathbf{g}_{m-n}]$. Since the columns of $\mathbf{A}$ and $\mathbf{S}$ span the same subspace, then $\mathbf{A}^H\mathbf{G} = \mathbf{0}$.

In practice, $\mathbf{R_{xx}}$ is unknown, and therefore should be estimated from the available data samples (snapshots) $\mathbf{x}(i)$, $i = 1, 2, ..., N$. The estimated correlation matrix is given by

$$\hat{\mathbf{R}}_{\mathbf{xx}} = \frac{1}{N}\sum_{i=1}^{N}\mathbf{x}(i)\mathbf{x}^H(i). \tag{5}$$

Let $\{\hat{\mathbf{s}}_1, ..., \hat{\mathbf{s}}_n, \hat{\mathbf{g}}_1, ..., \hat{\mathbf{g}}_{m-n}\}$ denote the unit-norm eigenvectors of $\hat{\mathbf{R}}_{\mathbf{xx}}$, arranged in the descending order of the associated eigenvalues, and let $\hat{\mathbf{S}}$ and $\hat{\mathbf{G}}$ denote the matrices made of the set of vectors $\{\hat{\mathbf{s}}_i\}$ and $\{\hat{\mathbf{g}}_i\}$, respectively. The statistical properties of the eigenvectors of the sample covariance matrix $\hat{\mathbf{R}}_{\mathbf{xx}}$ for signals modeled as independent processes with additive white noise is given in [6].

In this paper, we focus on frequency-modulated (FM) signals, modeled as

$$\mathbf{d}(t) = [d_1(t), ..., d_n(t)]^T = [D_1 e^{j\psi_1(t)}, ..., D_n e^{j\psi_n(t)}]^T, \tag{6}$$

where D_i and $\psi_i(t)$ are the amplitude and phase of ith source signal. For each sampling time t, $d_i(t)$ has an instantaneous frequency $f_i(t) = \frac{1}{2\pi}\frac{d\psi_i(t)}{dt}$.

FM signals are often encountered in applications such as radar and sonar. The consideration of FM signals in this paper in motivated by the fact that these signals are uniquely characterized by their instantaneous frequencies, and therefore, they have clear time-frequency signatures that are utilized by the STFD approach. Also, FM signals have constant amplitudes and, subsequently, yield time-independent covariance matrices. This property makes them amenable to conventional array processing based on second-order statistics.

2.2. Spatial Time-Frequency Distributions

The spatial time-frequency distributions (STFDs) based on Cohen's class of time-frequency distribution were introduced in [3] and its applications to direction finding has been discussed in [4]. In this paper, we focus one key member of Cohen's class, namely the pseudo Wigner-Ville distribution (PWVD) and its respective spatial distribution. Only the time-frequency points in the autoterm regions of PWVD are considered for STFD matrix construction. In these regions, it is assumed that the crossterms are negligible. This assumption serves to simplify the analysis and does not form a necessary condition on performance. It is noted that the crossterms in STFD matrices play similar role to the cross-correlation between source signals [5], and therefore they do not always impede the direction finding process.

The discrete form of pseudo Wigner-Ville distribution of a signal $x(t)$, using a rectangular window of length L, is given by

$$D_{xx}(t,f) = \sum_{\tau=-\frac{L-1}{2}}^{\frac{L-1}{2}} x(t+\tau)x^*(t-\tau)e^{-j4\pi f\tau}, \tag{7}$$

where * denotes complex conjugation. The spatial pseudo Wigner-Ville distribution (SPWVD) matrix is obtained by replacing $x(t)$ by the data snapshot vector $\mathbf{x}(t)$,

$$\mathbf{D_{xx}}(t,f) = \sum_{\tau=-\frac{L-1}{2}}^{\frac{L-1}{2}} \mathbf{x}(t+\tau)\mathbf{x}^H(t-\tau)e^{-j4\pi f\tau}. \tag{8}$$

Substitute (1) into (8), we obtain

$$\begin{aligned} \mathbf{D_{xx}}(t,f) &= \mathbf{D_{yy}}(t,f) + \mathbf{D_{yn}}(t,f) + \mathbf{D_{ny}}(t,f) + \mathbf{D_{nn}}(t,f) \\ &= \mathbf{D_{yy}}(t,f) + 2\mathrm{Re}\left[\mathbf{D_{yn}}(t,f)\right] + \mathbf{D_{nn}}(t,f). \end{aligned} \tag{9}$$

We note that $\mathbf{D_{xx}}(t,f)$, $\mathbf{D_{yy}}(t,f)$, $\mathbf{D_{yn}}(t,f)$, $\mathbf{D_{ny}}(t,f)$, and $\mathbf{D_{nn}}(t,f)$ are matrices of dimension $m \times m$, whereas the source TFD matrix $\mathbf{D_{dd}}(t,f)$ is of dimension $n \times n$. Under the uncorrelated signal and noise assumption and the zero-mean noise property, the expectation of the crossterm TFD matrices between the signal and noise vectors is zero, i.e., $E\left[\mathbf{D_{yn}}(t,f)\right] = E\left[\mathbf{D_{ny}}(t,f)\right] = \mathbf{0}$, and it follows

$$E\left[\mathbf{D_{xx}}(t,f)\right] = \mathbf{D_{yy}}(t,f) + E\left[\mathbf{D_{nn}}(t,f)\right] = \mathbf{A}\mathbf{D_{dd}}(t,f)\mathbf{A}^H + E\left[\mathbf{D_{nn}}(t,f)\right]. \tag{10}$$

For narrowband array signal processing applications, the mixing matrix $\mathbf{A}$ holds the spatial information and maps the auto- and cross-TFDs of the source signals into auto- and cross-TFDs of the data.

Equation (10) is similar to that which has been commonly used in DOA estimation and blind source separation problems, relating the signal correlation matrix to the data spatial correlation matrix. In the above formulation, however, the correlation matrices are replaced by the spatial time-frequency distribution matrices. This implies that key problems in various applications of array processing, specifically those dealing with nonstationary signal environments, can be approached using bilinear transformations.

It is noted that the relationship (10) holds true for every (t,f) points. In order to reduce the effect of noise and ensure the full column rank property of the STFD matrix, we consider multiple time-frequency points. This allows more information of the source signal t-f signatures to be included into their respective subspace formulation, and is similar to incorporating several snapshots in conventional array processing to perform direction finding and source separation. Joint-diagonalization [7] and time-frequency averaging are the two main approaches that have been used for this purpose [3, 4, 8]. In this paper, however, we only consider averaging over multiple time-frequency points.

3. SUBSPACE ANALYSIS FOR STFD MATRICES

The purpose of this section is to show that the signal and noise subspaces based on time-frequency distributions for nonstationary signals are more robust than those obtained from conventional array processing.

3.1. SNR Enhancement

The time-frequency distribution (TFD) maps one-dimensional signals in the time domain into two-dimensional signals in the time-frequency domain. The TFD property of concentrating the input signal around its intantaneous frequency (IF), while spreading the noise over the entire time-frequency domain increases the effective SNR and proves valuable in the underlying problem.

The ith diagonal element of TFD matrix $\mathbf{D_{dd}}(t,f)$ is given by

$$D_{d_i d_i}(t,f) = \sum_{\tau=-\frac{L-1}{2}}^{\frac{L-1}{2}} D_i^2 e^{j[\psi_i(t+\tau)-\psi_i(t-\tau)]-j4\pi f\tau}. \tag{11}$$

Assume that the third-order derivative of the phase is negligible over the window length L, then along the true time-frequency points of ith signal, $f_i = \frac{1}{2\pi}\frac{d\psi_i(t)}{dt}$, and $\psi_i(t+\tau) - \psi_i(t-\tau) - 4\pi f_i\tau \simeq 0$. Accordingly,

$$D_{d_i d_i}(t,f) = \sum_{\tau=-\frac{L-1}{2}}^{\frac{L-1}{2}} D_i^2 = LD_i^2. \tag{12}$$

Similarly, the noise STFD matrix $\mathbf{D_{nn}}(t,f)$ is

$$\mathbf{D_{nn}}(t,f) = \sum_{\tau=-\frac{L-1}{2}}^{\frac{L-1}{2}} \mathbf{n}(t+\tau)\mathbf{n}^H(t-\tau)e^{-j4\pi f\tau}. \tag{13}$$

Under the spatial white and temporal white assumptions, the statistical expectation of $\mathbf{D_{nn}}(t,f)$ is given by

$$E\left[\mathbf{D_{nn}}(t,f)\right] = \sum_{\tau=-\frac{L-1}{2}}^{\frac{L-1}{2}} E\left[\mathbf{n}(t+\tau)\mathbf{n}^H(t-\tau)\right] e^{-j4\pi f\tau} = \sigma\mathbf{I}. \tag{14}$$

Therefore, when we select the time-frequency points along the time-frequency signature or the IF of an FM signal, the SNR in model (10) is LD_i^2/σ, which has an improved factor L over the one associated with model (4).

The pseudo Wigner-Ville distribution of each FM source has a constant value over the observation period, providing that we leave out the rising and falling power distributions at both ends of the data record. For convenience of analysis, we select those $N-L+1$ time-frequency points of constant distribution value for each source signal. Therefore, the averaged STFD over the time-frequency signatures of n_o signals, i.e., a total of $n_o(N-L+1)$ time-frequency points, is given by

$$\hat{\mathbf{D}} = \frac{1}{n_o(N-L+1)} \sum_{q=1}^{n_o} \sum_{i=1}^{N-L+1} \mathbf{D_{xx}}(t_i, f_{q,i}), \tag{15}$$

where $f_{q,i}$ is the instantaneous frequency of the qth signal at the ith time sample. The expectation of the averaged STFD matrix is

$$\begin{aligned} \mathbf{D} &= E\left[\hat{\mathbf{D}}\right] = \frac{1}{n_o(N-L+1)} \sum_{q=1}^{n_o} \sum_{i=1}^{N-L+1} E\left[\mathbf{D_{xx}}(t_i, f_{q,i})\right] \\ &= \frac{1}{n_o} \sum_{p=1}^{n_o} \left[LD_p^2 \mathbf{a}(\theta_p)\mathbf{a}^H(\theta_p) + \sigma\mathbf{I}\right] = \frac{L}{n_o}\mathbf{A}^o\mathbf{R}_{\mathbf{dd}}^o(\mathbf{A}^o)^H + \sigma\mathbf{I}, \end{aligned} \tag{16}$$

where $\mathbf{R}_{\mathbf{dd}}^o$ and $\mathbf{A}^o$, respectively, represent the signal correlation matrix and the mixing matrix constructed by only considering n_o signals out of the total number of signal arrivals n.

It is clear from (16) that, when n_o signals are selected, the SNR improvement becomes $G = L/n_o$ (we assume $L > n_o$ throughout this paper). Therefore, from the SNR perspective, it is better to select (t,f) points that

belong to individual signals, and to separately evaluate the respective STFD matrices. Accordingly, STFD-based direction finding is, in essence, a discriminatory technique in the sense that it does not require simultaneous localization and extraction of all unknown signals received by the array. With STFDs, direction finding can be performed using STFDs of a subclass of the impinging signals with specific time-frequency signatures. In this respect, the proposed direction finding technique acts as a spatial filter, removing all other signals from consideration and, subsequently, saves any downstream processing that is required to separate interference and signals of interest. It is also important to note that with the ability to construct the STFD matrix from one or few signal arrivals, the well known $m > n$ condition on source localization using arrays can be relaxed, i.e., we can perform direction finding or source separation with the number of array sensors smaller than the number of impinging signals [9]. From the angular resolution perspective, closely spaced sources with different time-frequency signatures can be resolved by constructing two separate STFDs, each corresponds to one source, and then proceed with subspace decomposition for each STFD matrix, followed by a appropriate source localization method (ML, for example). The drawback of performing several direction finding using different STFD matrices is clearly the need for repeated computations of eigendecompositions and source localizations.

3.2. Signal and Noise Subspaces Based on STFDs

The statistical properties of the eigenstructures using the STFD matrix are provided in this subsection.

Lemma 1: Let $\lambda_1^o > \lambda_2^o > \cdots > \lambda_{n_o}^o > \lambda_{n_o+1}^o = \lambda_{n_o+2}^o = \cdots = \lambda_m^o = \sigma$ denote the eigenvalues of $\mathbf{R}_{\mathbf{xx}}^o$, which is defined from a data record of a mixture of the n_o selected FM signals. Denote the unit-norm eigenvectors associated with $\lambda_1^o, ..., \lambda_{n_o}^o$ by the columns of $\mathbf{S}^o = [\mathbf{s}_1^o, ..., \mathbf{s}_{n_o}^o]$, and those corresponding to $\lambda_{n_o+1}^o, ..., \lambda_m^o$ by the columns of $\mathbf{G}^o = [\mathbf{g}_1^o, ..., \mathbf{g}_{m-n_o}^o]$. We also denote $\lambda_1^{tf} > \lambda_2^{tf} > \cdots > \lambda_{n_o}^{tf} > \lambda_{n_o+1}^{tf} = \lambda_{n_o+2}^{tf} = \cdots = \lambda_m^{tf} = \sigma^{tf}$ as the eigenvalues of $\mathbf{D}$ defined in (16). The unit-norm eigenvectors associated with $\lambda_1^{tf}, ..., \lambda_{n_o}^{tf}$ are represented by the columns of $\mathbf{S}^{tf} = [\mathbf{s}_1^{tf}, ..., \mathbf{s}_{n_o}^{tf}]$, and those corresponding to $\lambda_{n_o+1}^{tf}, ..., \lambda_m^{tf}$ are represented by the columns of $\mathbf{G}^{tf} = [\mathbf{g}_1^{tf}, ..., \mathbf{g}_{m-n_o}^{tf}]$. Accordingly,

a) The signal and noise subspaces of $\mathbf{S}^{tf}$ and $\mathbf{G}^{tf}$ are the same as $\mathbf{S}^o$ and $\mathbf{G}^o$, respectively.

b) The eigenvalues have the following relationship:

$$\lambda_i^{tf} = \begin{cases} \frac{L}{n_o}(\lambda_i^o - \sigma) + \sigma = \frac{L}{n_o}\lambda_i^o + \left(1 - \frac{L}{n_o}\right)\sigma & i \le n_o \\ \sigma^{tf} = \sigma & n_o < i \le m. \end{cases} \tag{17}$$

Both parts of the above equations are direct results of (16).

A very important conclusion from Lemma 1 is that, the largest n_o eigenvalues are amplified using STFD analysis. The amplification of the largest n_o eigenvalues improves detection of the number of impinging signals on the array, as it widens the separation between dominant and noise-level eigenvalues. This property allows us to determine the appropriate number of signals when SNR is low, or the signals are closely spaced.

Next we consider the signal and noise subspace estimates from a finite number of data samples. The STFD matrix is constructed from the true (t, f) points along the n_o FM signals. We have the following Lemmas.

Lemma 2: If the third-order derivative of the phase of the FM signals is negligible over the time-period $[t - L + 1, t + L - 1]$, then $\hat{\mathbf{D}} - \mathbf{D}$ is a zero-mean, random matrix whose elements are asymptotically jointly Gaussian.

Proof: From (1), (15), and (16), we have

$$\begin{aligned} \hat{\mathbf{D}} - \mathbf{D} &= \frac{1}{n_o(N-L+1)} \sum_{q=1}^{n_o} \sum_{i=1}^{N-L+1} \sum_{\tau=-\frac{L-1}{2}}^{\frac{L-1}{2}} \mathbf{y}(t_i+\tau)\mathbf{n}^H(t_i-\tau)e^{-j4\pi f_{q,i}\tau} \\ &+ \frac{1}{n_o(N-L+1)} \sum_{q=1}^{n_o} \sum_{i=1}^{N-L+1} \sum_{\tau=-\frac{L-1}{2}}^{\frac{L-1}{2}} \mathbf{n}(t_i+\tau)\mathbf{y}^H(t_i-\tau)e^{-j4\pi f_{q,i}\tau} \\ &+ \frac{1}{n_o(N-L+1)} \sum_{q=1}^{n_o} \sum_{i=1}^{N-L+1} \sum_{\tau=-\frac{L-1}{2}}^{\frac{L-1}{2}} \mathbf{n}(t_i+\tau)\mathbf{n}^H(t_i-\tau)e^{-j4\pi f_{q,i}\tau} - \sigma\mathbf{I}. \end{aligned} \tag{18}$$

We first consider the first term in (18). Denoting $t_i' = t_i - \tau$, and noting the fact that, when the third-order derivative of the phase is negligible over $[t-L+1, t+L-1]$ for any signal and any t, $d_q(t_i'+2\tau)e^{-j4\pi f_{q,i}\tau} \simeq d_q(t_i')$ at the time-frequency point $(t_i, f_{q,i})$, then

$$\begin{aligned}
&\sum_{q=1}^{n_o}\sum_{i=1}^{N-L+1}\sum_{\tau=-\frac{L-1}{2}}^{\frac{L-1}{2}} \mathbf{y}(t_i+\tau)\mathbf{n}^H(t_i-\tau)e^{-j4\pi f_{q,i}\tau} \\
&= \sum_{q=1}^{n_o}\sum_{t_i'=1}^{N-L+1}\sum_{\tau=-\frac{L-1}{2}}^{\frac{L-1}{2}} \mathbf{y}(t_i'+2\tau)\mathbf{n}^H(t_i')e^{-j4\pi f_{q,i}\tau} \\
&\simeq \sum_{q=1}^{n_o}\sum_{t_i'=1}^{N-L+1} L d_q(t_i')\mathbf{a}(\theta_q)\mathbf{n}^H(t_i') = \sum_{t_i'=1}^{N-L+1} L\mathbf{y}(t_i')\mathbf{n}^H(t_i')
\end{aligned} \tag{19}$$

Therefore, the elements of the first term in equation (18) are clearly asymptotically jointly Gaussian from the multivariate Central Limit Theorem [10]. Similar result can be obtained for the second term of (18). The elements of the third term in (18) are also jointly Gaussian from the fact that the covariance between the (p,r)th element of $\mathbf{n}(t+\tau)\mathbf{n}^H(t-\tau)$ at time t_i and t_k is given by

$$\begin{aligned}
&E\left\{\left[\sum_{\tau_1=-\frac{L-1}{2}}^{\frac{L-1}{2}} n_p(t_i+\tau_1)n_r^*(t_i-\tau_1) - E\left(\sum_{\tau_1=-\frac{L-1}{2}}^{\frac{L-1}{2}} n_p(t_i+\tau_1)n_r^*(t_i-\tau_1)\right)\right]e^{-j4\pi f_{q,i}\tau_1}\right. \\
&\left.\left[\sum_{\tau_2=-\frac{L-1}{2}}^{\frac{L-1}{2}} n_p^*(t_k+\tau_2)n_r(t_k-\tau_2) - E\left(\sum_{\tau_2=-\frac{L-1}{2}}^{\frac{L-1}{2}} n_p^*(t_k+\tau_2)n_r(t_k-\tau_2)\right)\right]e^{-j4\pi f_{q,k}\tau_2}\right\} \\
&= \sum_{\tau_1=-\frac{L-1}{2}}^{\frac{L-1}{2}}\sum_{\tau_2=-\frac{L-1}{2}}^{\frac{L-1}{2}} E[n_p(t_i+\tau_1)n_r^*(t_i-\tau_1)]E[n_p^*(t_k+\tau_2)n_r(t_k-\tau_2)]e^{-j4\pi(f_{q,i}\tau_1 - f_{q,k}\tau_2)} \\
&+ \sum_{\tau_1=-\frac{L-1}{2}}^{\frac{L-1}{2}}\sum_{\tau_2=-\frac{L-1}{2}}^{\frac{L-1}{2}} E[n_p(t_i+\tau_1)n_p^*(t_k+\tau_2)]E[n_r^*(t_i-\tau_1)n_r(t_k-\tau_2)]e^{-j4\pi(f_{q,i}\tau_1 - f_{q,k}\tau_2)} \\
&+ \sum_{\tau_1=-\frac{L-1}{2}}^{\frac{L-1}{2}}\sum_{\tau_2=-\frac{L-1}{2}}^{\frac{L-1}{2}} E[n_p(t_i+\tau_1)n_r(t_k-\tau_2)]E[n_p^*(t_k+\tau_2)n_r^*(t_i-\tau_1)]e^{-j4\pi(f_{q,i}\tau_1 - f_{q,k}\tau_2)} \\
&- \sum_{\tau_1=-\frac{L-1}{2}}^{\frac{L-1}{2}}\sum_{\tau_2=-\frac{L-1}{2}}^{\frac{L-1}{2}} \sigma^2\delta_{p,r}e^{-j4\pi(f_{q,i}\tau_1 - f_{q,k}\tau_2)} \\
&= \sigma^2\delta_{i,k}.
\end{aligned} \tag{20}$$

Since the linear combination of joint-Gaussian processes is jointly Gaussian, then $\hat{\mathbf{D}} - \mathbf{D}$ is a random matrix whose elements are asymptotically jointly Gaussian. It is clear that $\hat{\mathbf{D}} - \mathbf{D} \to 0$ as $N \to \infty$.

Lemma 3: If the third-order derivative of the phase of the FM signals is negligible over the time-period $[t-L+1, t+L-1]$, then the orthogonal projections of $\left\{\hat{\mathbf{g}}_i^{tf}\right\}$ onto the column space of $\mathbf{S}^{tf}$ are asymptotically (for $N \gg L$) jointly Gaussian distributed with zero means and covariance matrices given by

$$\begin{aligned}
&E\left(\mathbf{S}^{tf}\left(\mathbf{S}^{tf}\right)^H\hat{\mathbf{g}}_i^{tf}\right)\left(\mathbf{S}^{tf}\left(\mathbf{S}^{tf}\right)^H\hat{\mathbf{g}}_j^{tf}\right)^H \\
&= \frac{\sigma L}{n_o(N-L+1)}\left[\sum_{k=1}^{n_o}\frac{\lambda_k^{tf}}{(\sigma-\lambda_k^{tf})^2}\mathbf{s}_k^{tf}\left(\mathbf{s}_k^{tf}\right)^H\right]\delta_{i,j} \triangleq \frac{1}{(N-L+1)}\mathbf{U}^{tf}\delta_{i,j},
\end{aligned} \tag{21}$$

$$E\left(\mathbf{S}^{tf}\left(\mathbf{S}^{tf}\right)^{H}\hat{\mathbf{g}}_i^{tf}\right)\left(\mathbf{S}^{tf}\left(\mathbf{S}^{tf}\right)^{H}\hat{\mathbf{g}}_j^{tf}\right)^{T}=\mathbf{0}\ \text{ for all } i,\ j. \tag{22}$$

The proof is given in Appendix A.

To clearly demonstrate the performance gain in using STFDs, we substitute (17) into (21),

$$E\left(\mathbf{S}^{tf}\left(\mathbf{S}^{tf}\right)^{H}\hat{\mathbf{g}}_i^{tf}\right)\left(\mathbf{S}^{tf}\left(\mathbf{S}^{tf}\right)^{H}\hat{\mathbf{g}}_j^{tf}\right)^{H}=\frac{\sigma}{N-L+1}\left[\sum_{k=1}^{n_o}\frac{(\lambda_k^o-\sigma)+\frac{n_o}{L}\sigma}{(\sigma-\lambda_k^o)^2}\mathbf{s}_k^o\left(\mathbf{s}_k^o\right)^H\right]\delta_{i,j}. \tag{23}$$

For comparison, we quote the results from reference [6], which were provided using the data covariance matrix,

$$E\left(\mathbf{S}\mathbf{S}^H\hat{\mathbf{g}}_i\right)\left(\mathbf{S}\mathbf{S}^H\hat{\mathbf{g}}_j\right)^H=\frac{\sigma}{N}\left[\sum_{k=1}^{n}\frac{\lambda_k}{(\sigma-\lambda_k)^2}\mathbf{s}_k\mathbf{s}_k^H\right]\delta_{i,j} \tag{24}$$

$$E\left(\mathbf{S}\mathbf{S}^H\hat{\mathbf{g}}_i\right)\left(\mathbf{S}\mathbf{S}^H\hat{\mathbf{g}}_j\right)^T=\mathbf{0}\ \text{ for all } i,\ j. \tag{25}$$

where $\mathbf{S},\mathbf{s}_k,\hat{\mathbf{g}}_k,\lambda_k$ are analogous to $\mathbf{S}^o,\mathbf{s}_k^o,\hat{\mathbf{g}}_k^o,\lambda_k^o$, respectively, except they are defined for all n signals instead of only n_o signals.

Comparing (23) with (24), two important observations are in order. First, if the signals are both localizable and separable in the time-frequency domain, then the reduction of the number of signals from n to n_o greatly reduces the estimation error, specifically when the signals are closely spaced. The examples, given in the following section, show the advantages of using t-f ML with partially selected signals. The second observation relates to SNR enhancements. The above equations show that error reductions using STFDs are more pronounced for the cases of low SNR and/or closely spaced signals. It is clear from (23) that, when $\lambda_k^o \gg \sigma$ for all $k=1,2,...,n_o$, the results are almost independent of L (suppose $N \gg L$ so that $N-L+1 \simeq N$), and therefore there would be no obvious improvement in using the STFD over conventional array processing. On the other hand, when some eigenvalues are close to σ ($\lambda_k^o \simeq \sigma$, for some $k=1,2,...,n_o$), which is the case of weak or closely spaced signals, the result of (23) is reduced by a factor of up to $G=\frac{L}{n_o}$. This factor represents the gain achieved from using STFD processing.

4. THE TIME-FREQUENCY MAXIMUM LIKELIHOOD METHODS

In this section we analyze the performance of the maximum likelihood methods based on time-frequency distributions (t-f ML). For conventional ML methods, the joint density function of the sampled data $\mathbf{x}(1),\mathbf{x}(2),...,\mathbf{x}(N)$, is given by [2]

$$f(\mathbf{x}(1),\ldots,\mathbf{x}(N))=\prod_{i=1}^{N}\frac{1}{\pi^m\det[\sigma\mathbf{I}]}\exp\left(-\frac{1}{\sigma}\left[\mathbf{x}(i)-\mathbf{A}\mathbf{d}(i)\right]^H\left[\mathbf{x}(i)-\mathbf{A}\mathbf{d}(i)\right]\right), \tag{26}$$

where det[·] denotes the determinant. It follows from (26) that the log-likelihood function of the observations $\mathbf{x}(1),\mathbf{x}(2),\ldots,\mathbf{x}(N)$, is given by

$$L=-mN\ln\sigma-\frac{1}{\sigma}\sum_{i=1}^{N}\left[\mathbf{x}(i)-\mathbf{A}\mathbf{d}(i)\right]^H\left[\mathbf{x}(i)-\mathbf{A}\mathbf{d}(i)\right]. \tag{27}$$

To carry out this minimization, we fix $\mathbf{A}$ and minimize (27) with respect to $\mathbf{d}$. This yields the well-known solution

$$\mathbf{d}(i)=\left[\mathbf{A}^H\mathbf{A}\right]^{-1}\mathbf{A}^H\mathbf{x}(i). \tag{28}$$

We can obtain the concentrated likelihood function as [2, 11]

$$F_{ML}(\theta)=tr\left\{\left[\mathbf{I}-\hat{\mathbf{A}}(\hat{\mathbf{A}}^H\hat{\mathbf{A}})^{-1}\hat{\mathbf{A}}^H\right]\hat{\mathbf{R}}_{\mathbf{xx}}\right\}, \tag{29}$$

where $tr\mathbf{A}$ denotes the trace of $\mathbf{A}$. The ML estimate of θ is obtained as the minimizer of (29), and the estimation error $(\hat{\omega}_i-\omega_i)$ associated with the ML method are asymptotically (for large N) jointly Gaussian distributed with zero means and the following covariance matrix [12]

$$E\left(\hat{\omega}_i-\omega_i\right)^2=\frac{1}{2N}\left[\mathrm{Re}(\mathbf{H}\odot\mathbf{R}_{\mathbf{dd}}^T)\right]^{-1}\mathrm{Re}\left[\mathbf{H}\odot(\mathbf{R}_{\mathbf{dd}}\mathbf{A}^H\mathbf{U}\mathbf{A}\mathbf{R}_{\mathbf{dd}})^T\right]\left[\mathrm{Re}(\mathbf{H}\odot\mathbf{R}_{\mathbf{dd}}^T)\right]^{-1}, \tag{30}$$

where $\odot$ denotes Hadamard product. Moreover,

$$\mathbf{U}=\sum_{k=1}^{n}\frac{\lambda_k\sigma}{(\sigma-\lambda_k)^2}\mathbf{s}_k\mathbf{s}_k^H,\quad \mathbf{H}=\mathbf{C}^H\left[\mathbf{I}-\mathbf{A}(\mathbf{A}^H\mathbf{A})^{-1}\mathbf{A}^H\right]\mathbf{C},\quad\text{and}\quad \mathbf{C}=\frac{d\mathbf{A}}{d\omega}. \tag{31}$$

Next we consider the t-f ML method. As we discussed in the previous section, for t-f ML we select $n_o\le n$ signals in the time-frequency domain. The concentrated likelihood function defined from the STFD matrix is similar to (29) and is obtained by replacing $\hat{\mathbf{R}}_{\mathbf{xx}}$ by $\hat{\mathbf{D}}$ (Appendix B),

$$F_{ML}^{tf}(\phi)=tr\left[\mathbf{I}-\hat{\mathbf{A}}^o\left((\hat{\mathbf{A}}^o)^H\hat{\mathbf{A}}^o\right)^{-1}(\hat{\mathbf{A}}^o)^H\right]\hat{\mathbf{D}}, \tag{32}$$

Therefore, the estimation error $(\hat{\omega}_i^{tf}-\omega_i^{tf})$ associated with the t-f ML method are asymptotically (for $N>>L$) jointly Gaussian distributed with zero means and the following matrix

$$\begin{aligned}&E\left(\hat{\omega}_i^{tf}-\omega_i^{tf}\right)^2\\&=\frac{\sigma}{2(N-L+1)}\left[\mathrm{Re}(\mathbf{H}^o\odot\mathbf{D}_{\mathbf{dd}}^T)\right]^{-1}\mathrm{Re}\left[\mathbf{H}^o\odot(\mathbf{D}_{\mathbf{dd}}\mathbf{A}^H\mathbf{U}^{tf}\mathbf{A}\mathbf{D}_{\mathbf{dd}})^T\right]\left[\mathrm{Re}(\mathbf{H}^o\odot\mathbf{D}_{\mathbf{dd}}^T)\right]^{-1}\\&=\frac{\sigma}{2(N-L+1)}\left[\mathrm{Re}\left(\mathbf{H}^o\odot(\mathbf{R}_{\mathbf{dd}}^o)^T\right)\right]^{-1}\mathrm{Re}\left[\mathbf{H}^o\odot(\mathbf{R}_{\mathbf{dd}}^o\mathbf{A}^H\mathbf{U}^{tf}\mathbf{A}\mathbf{R}_{\mathbf{dd}}^o)^T\right]\left[\mathrm{Re}\left((\mathbf{H}^o\odot\mathbf{R}_{\mathbf{dd}}^o)^T\right)\right]^{-1},\end{aligned} \tag{33}$$

where $\mathbf{U}^{tf}$ is defined in (21), and

$$\mathbf{H}^o=(\mathbf{C}^o)^H\left[\mathbf{I}-\mathbf{A}^o\left((\mathbf{A}^o)^H\mathbf{A}^o\right)^{-1}(\mathbf{A}^o)^H\right]\mathbf{C}^o,\quad\text{and}\quad \mathbf{C}^o=\frac{d\mathbf{A}^o}{d\omega}. \tag{34}$$

In the case of $n_o=n$, then $\mathbf{H}^o=\mathbf{H}$, and $\mathbf{C}^o=\mathbf{C}$.

The signal localization in the time-frequency domain enables us to select fewer signal arrivals. This fact is not only important in improving the estimation performance, particularly when the signals are closely spaced, it also reduces the dimension of optimization required by the maximum likelihood algorithm, as such the computations can be greatly reduced.

To demonstrate the advantages of t-f ML over conventional ML and time-frequency MUSIC (t-f MUSIC), consider a uniform linear array of 8 sensors separated by half a wavelength. Two chirp signals arrive from $(\theta_1,\theta_2)=(-10°,10°)$, where the start and end frequencies of the signal from θ_1 are 0 and π, whereas the start and end frequencies of the signal from θ_2 are π and 0, respectively. The SNR of both signals is -20 dB. Fig. 1 shows the contour plots of the likelihood function of the t-f ML and ML for three independent trials, where the dots show the positions of minimum of cost function. L=129 is used for t-f ML. It is evident that the t-f ML resolvs DOAs, whereas the ML fails.

Fig. 2 compares the t-f ML and t-f MUSIC for coherent signal arrivals. Two coherent chirp signals have their common start and end frequencies $f_s=0$ and $f_e=0.5$ and a $\frac{\pi}{2}$ phase difference. The signals arrive at $(\theta_1,\theta_2)=(-2°,2°)$. The SNR of both signals is 5dB. L=129 is used for t-f ML and t-f MUSIC. It is clear that the t-f ML can separate the two signals where as the t-f MUSIC cannot.

5. CONCLUSIONS

The subspace analysis of spatial time-frequency distribution (STFD) matrices has been presented. We have shown that for signals that are localizable in the time-frequency domain, such as frequency modulated (FM) signals, the signal-to-noise ratio (SNR) can be enhanced by utilizing time-frequency distributions, and subsequently improve the robustness of the signal and noise subspaces. Such improvement is particularly evident when some of the largest signal eigenvalues are close to the noise power. In this situation, the conventional array processing methods may encounter difficulty in establishing the proper signal and noise subspace.

The subspace analysis of STFD matrices has motivated the introduction of t-f ML methods for direction finding. The analysis and simulation results showed that the t-f ML improves over conventional maximum likelihood techniques for low SNR, and outperforms the t-f MUSIC in coherent signal environments.

APPENDIX A

For complex Gaussian random variable x_1, x_2, x_3, x_4 with non-zero means,

$$E[x_1x_2x_3x_4] = E[x_1x_2]E[x_3x_4] + E[x_1x_3]E[x_2x_4] + E[x_1x_4]E[x_2x_3] - 2E[x_1]E[x_2]E[x_3]E[x_4]. \tag{A.1}$$

and for zero-mean circular complex Gaussian noise vector and deterministic source signal vector,

$$E[\mathbf{x}(t_r)] = \mathbf{y}(t_r),$$

$$E\left[\mathbf{x}(t_r)\mathbf{x}^H(t_q)\right] = \mathbf{y}(t_r)\mathbf{y}^H(t_q) + \sigma\mathbf{I}\delta_{r,q},$$

$$E\left[\mathbf{x}(t_r)\mathbf{x}^T(t_q)\right] = \mathbf{y}(t_r)\mathbf{y}^T(t_q),$$

For an array mixture of FM signals, we select points from n_o signals at the time-frequency domain, where the pseudo Wigner-Ville distribution matrix is defined in (8). We define $\hat{\mathbf{D}}$ in terms of a random perturbation to $\mathbf{D}$ with a perturbation factor p, $0 < p \ll 1$. Thus,

$$\hat{\mathbf{D}} = \mathbf{D} + (\hat{\mathbf{D}} - \mathbf{D}) = \mathbf{D} + p\mathbf{B} \tag{A.2}$$

From Lemma 2, $\mathbf{B}$ is a Hermitian, zero-mean random matrix with elements that are asymptotically jointly Gaussian. Using (A.2) and (8), we have

$$\begin{aligned}
&E\left[\mathbf{v}_1^H\mathbf{B}\mathbf{v}_2\mathbf{v}_3^H\mathbf{B}\mathbf{v}_4\right] \\
&= \frac{1}{p^2}E\left[\mathbf{v}_1^H\left(\hat{\mathbf{D}}-\mathbf{D}\right)\mathbf{v}_2\mathbf{v}_3^H\left(\hat{\mathbf{D}}-\mathbf{D}\right)\mathbf{v}_4\right] \\
&= \frac{1}{(n_op(N-L+1))^2}E\left[\left(\sum_{q=1}^{n_o}\sum_{i=1}^{N-L+1}\mathbf{v}_1^H\mathbf{D}_{\mathbf{xx}}(t_i,f_{q,i})\mathbf{v}_2\right)\left(\sum_{q=1}^{n_o}\sum_{i=1}^{N-L+1}\mathbf{v}_3^H\mathbf{D}_{\mathbf{xx}}(t_i,f_{q,i})\mathbf{v}_4\right)\right] \\
&\quad -\frac{1}{p^2}\mathbf{v}_1^H\mathbf{D}\mathbf{v}_2\mathbf{v}_3^H\mathbf{D}\mathbf{v}_4 \\
&= \frac{1}{(n_op(N-L+1))^2}\sum_{q_1=1}^{n_o}\sum_{q_2=1}^{n_o}\sum_{i_1=1}^{N-L+1}\sum_{i_2=1}^{N-L+1}\sum_{\tau_1=-\frac{L-1}{2}}^{\frac{L-1}{2}}\sum_{\tau_2=-L/2+1}^{L/2}e^{-j4\pi\left[f_{q_1,i_1}\tau_1+f_{q_2,i_2}\tau_2\right]}\times \\
&\quad \Big\{E\left[\mathbf{v}_1^H\mathbf{x}(t_{i_1}+\tau_1)\mathbf{x}^H(t_{i_1}-\tau_1)\mathbf{v}_2\right]E\left[\mathbf{v}_3^H\mathbf{x}(t_{i_2}+\tau_2)\mathbf{x}^H(t_{i_2}-\tau_2)\mathbf{v}_4\right] \\
&\quad +E\left[\mathbf{v}_1^H\mathbf{x}(t_{i_1}+\tau_1)\mathbf{v}_3^H\mathbf{x}(t_{i_2}+\tau_2)\right]E\left[\mathbf{x}^H(t_{i_1}-\tau_1)\mathbf{v}_2\mathbf{x}^H(t_{i_2}-\tau_2)\mathbf{v}_4\right] \\
&\quad +E\left[\mathbf{v}_1^H\mathbf{x}(t_{i_1}+\tau_1)\mathbf{x}^H(t_{i_2}-\tau_2)\mathbf{v}_4\right]E\left[\mathbf{v}_3^H\mathbf{x}(t_{i_2}+\tau_2)\mathbf{x}^H(t_{i_1}-\tau_1)\mathbf{v}_2\right] \\
&\quad -2E\left[\mathbf{v}_1^H\mathbf{x}(t_{i_1}+\tau_1)\right]E\left[\mathbf{x}^H(t_{i_1}-\tau_1)\mathbf{v}_2\right]E\left[\mathbf{v}_3^H\mathbf{x}(t_{i_2}+\tau_2)\right]E\left[\mathbf{x}^H(t_{i_2}-\tau_2)\mathbf{v}_4\right]\Big\} \\
&\quad -\frac{1}{p^2}\mathbf{v}_1^H\mathbf{D}\mathbf{v}_2\mathbf{v}_3^H\mathbf{D}\mathbf{v}_4 \\
&= \frac{1}{(n_op(N-L+1))^2}\sum_{q_1=1}^{n_o}\sum_{q_2=1}^{n_o}\sum_{i_1=1}^{N-L+1}\sum_{i_2=1}^{N-L+1}\sum_{\tau_1=-\frac{L-1}{2}}^{\frac{L-1}{2}}\sum_{\tau_2=-\frac{L-1}{2}}^{\frac{L-1}{2}}e^{-j4\pi\left[f_{q_1,i_1}\tau_1+f_{q_2,i_2}\tau_2\right]}\times \\
&\quad \Big[\mathbf{v}_1^H\mathbf{y}(t_{i_1}+\tau_1)\mathbf{y}^H(t_{i_2}-\tau_2)\mathbf{v}_4\sigma\delta_{\mathbf{v}_2,\mathbf{v}_2}\delta_{t_{i1}-\tau_1,t_{i2}+\tau_2} \\
&\quad +\sigma\delta_{\mathbf{v}_1,\mathbf{v}_4}\delta_{t_{i_1}+\tau_1,t_{i_2}-\tau_2}\mathbf{v}_3^H\mathbf{y}(t_{i_2}+\tau_2)\mathbf{y}^H(t_{i_1}-\tau_1)\mathbf{v}_2+\sigma^2\delta_{\mathbf{v}_1,\mathbf{v}_4}\delta_{\mathbf{v}_2,\mathbf{v}_3}\delta t_{i_1},t_{i_2}\delta\tau_1,\tau_2\Big]
\end{aligned} \tag{A.3}$$

Under the assumption of no crossterms, q_1 should be equivalent to q_2 to have non-zero values, and in this case $q_1 = q_2 = q$. Note that within the time-frequency region of qth signal, $\mathbf{y}(t) = \mathbf{y}_q(t) \triangleq \mathbf{A}\mathbf{d}_q(t)$. When the third-order derivative of the phase is negligible over $[t-L+1, t+L-1]$ for any signal and any t, we have

$$
\begin{aligned}
& E\left[\mathbf{v}_1^H \mathbf{B} \mathbf{v}_2 \mathbf{v}_3^H \mathbf{B} \mathbf{v}_4\right] \\
& \simeq \frac{1}{(Np(N-L+1))^2} \sum_{q=1}^{n_o} \sum_{i_1=1}^{N-L+1} \sum_{i_2=1}^{N-L+1} \sum_{\tau=-\frac{L-1}{2}}^{\frac{L-1}{2}} \sum_{\tau_2=-L/2+1}^{L/2} \times \\
& \quad \left[\mathbf{v}_1^H \mathbf{y}(t_{i_1}+\tau_1)\mathbf{y}^H(t_{i_1}+\tau_1)\mathbf{v}_4 \sigma \delta_{\mathbf{v}_2,\mathbf{v}_2} \delta_{t_{i1}-\tau_1,t_{i2}+\tau_2}\right. \\
& \quad \left. + \sigma \delta_{\mathbf{v}_1,\mathbf{v}_4} \delta_{t_{i_1}+\tau_1,t_{i_1}-\tau_1} \mathbf{v}_3^H \mathbf{y}(t_{i_2}+\tau_2)\mathbf{y}^H(t_{i_1}-\tau_1)\mathbf{v}_2\right] \\
& \quad + \frac{\sigma^2 L}{n_o(N-L+1)p^2} \delta_{\mathbf{v}_1,\mathbf{v}_4} \delta_{\mathbf{v}_2,\mathbf{v}_3} \\
& \simeq \frac{\sigma L}{n_o(N-L+1)p^2} \left[\frac{L}{n_o}(\lambda_{\mathbf{v}_1}-\sigma) + (\lambda_{\mathbf{v}_2}-\sigma) + \sigma\right] \delta_{\mathbf{v}_1,\mathbf{v}_4} \delta_{\mathbf{v}_2,\mathbf{v}_3} \\
& = \frac{\sigma L}{n_o(N-L+1)p^2} \left[(\lambda_{\mathbf{v}_1}^{tf} + \lambda_{\mathbf{v}_2}^{tf} - \sigma)\right] \delta_{\mathbf{v}_1,\mathbf{v}_4} \delta_{\mathbf{v}_2,\mathbf{v}_3}
\end{aligned} \tag{A.4}
$$

Denote $\mathbf{\Gamma} = \left(\mathbf{S}^{tf}\right)^H \hat{\mathbf{D}} \mathbf{G}^{tf}$, and γ_i the $i$the column of $\mathbf{\Gamma}$. Use the results of (A.3) – (A.4) and the fact that $\left(\mathbf{S}^{tf}\right)^H \mathbf{D} \mathbf{G}^{tf} = \mathbf{0}$, we have

$$
E\left[\gamma_i \gamma_j^H\right]_{t,q} = E\left[\left(\left(\mathbf{s}_t^{tf}\right)^H \hat{\mathbf{D}} \mathbf{g}_i^{tf}\right)\left(\left(\mathbf{g}_j^{tf}\right)^H \hat{\mathbf{D}} \mathbf{s}_q^{tf}\right)\right] = \frac{\sigma L}{n_o(N-L+1)} \lambda_t^{tf} \delta_{t,q} \delta_{i,j}. \tag{A.5}
$$

Subsequently

$$
E\left[\gamma_i \gamma_j^H\right] = E\left[\left(\left(\mathbf{S}^{tf}\right)^H \hat{\mathbf{D}} \mathbf{g}_i^{tf}\right)\left(\left(\mathbf{g}_j^{tf}\right)^H \hat{\mathbf{D}} \mathbf{S}^{tf}\right)\right] = \frac{\sigma L}{n_o(N-L+1)} \mathbf{\Lambda}^{tf} \delta_{i,j}. \tag{A.6}
$$

where $\mathbf{\Lambda}^{tf} = diag\left[\lambda_1^{tf}, ..., \lambda_{n_o}^{tf}\right]$. Similarly,

$$
E\left[\gamma_i \gamma_j^T\right]_{t,q} = E\left[\left(\left(\mathbf{s}_t^{tf}\right)^H \hat{\mathbf{D}} \mathbf{g}_i^{tf}\right)\left(\left(\mathbf{s}_q^{tf}\right)^H \hat{\mathbf{D}} \mathbf{g}_j^{tf}\right)\right] = 0, \tag{A.7}
$$

and subsequently

$$
E\left[\gamma_i \gamma_j^T\right] = \mathbf{0}. \tag{A.8}
$$

Since $\mathbf{S}^{tf}\left(\mathbf{S}^{tf}\right)^H \hat{\mathbf{g}}_i^{tf}$ has the same limiting distribution as that of $-\mathbf{S}^{tf}(\mathbf{\Gamma} - \sigma\mathbf{I})^{-1}\gamma_i$ [6], then it follows that

$$
\begin{aligned}
& E\left(\mathbf{S}^{tf}\left(\mathbf{S}^{tf}\right)^H \hat{\mathbf{g}}_i^{tf}\right)\left(\mathbf{S}^{tf}\left(\mathbf{S}^{tf}\right)^H \hat{\mathbf{g}}_j^{tf}\right)^H \\
& = \frac{\sigma L}{n_o(N-L+1)} \left[\mathbf{S}(\mathbf{\Lambda}^{tf} - \sigma\mathbf{I})^{-1} \mathbf{\Lambda}^{tf} (\mathbf{\Lambda}^{tf} - \sigma\mathbf{I})^{-1} \mathbf{S}^H\right] \delta_{i,j} \\
& = \frac{\sigma L}{n_o(N-L+1)} \left[\sum_{k=1}^{n_o} \frac{\lambda_k^{tf}}{(\sigma - \lambda_k^{tf})^2} \mathbf{s}_k^{tf}\left(\mathbf{s}_k^{tf}\right)^H\right] \delta_{i,j}
\end{aligned} \tag{A.9}
$$

and

$$
E\left(\mathbf{S}^{tf}\left(\mathbf{S}^{tf}\right)^H \hat{\mathbf{g}}_i^{tf}\right)\left(\mathbf{S}^{tf}\left(\mathbf{S}^{tf}\right)^H \hat{\mathbf{g}}_j^{tf}\right)^T = \mathbf{0} \text{ for all } i,\ j. \tag{A.10}
$$

APPENDIX B

The number of data samples available for the construction of the STFD matrix is $N-L+1$, where the selected n_o signals are included. Denote $\hat{\mathbf{u}}_k$ as the kth column of $\hat{\mathbf{D}}$, and $\mathbf{u}_k$ the kth column of $\mathbf{D}$. From Lemma 2, we know that $\hat{\mathbf{u}}_k$ is asymptotically jointly Gaussian, and its density function is

$$
f_{tf}(\hat{\mathbf{u}}_k) = \frac{1}{\pi} \det\left[\frac{1}{N-L+1}\mathbf{\Delta}_k\right]^{-\frac{1}{2}} \exp\left[-\frac{1}{2}(\hat{\mathbf{u}}_k - \mathbf{u}_k)^H \left(\frac{1}{N-L+1}\mathbf{\Delta}_k\right)^{-1} (\hat{\mathbf{u}}_k - \mathbf{u}_k)\right], \tag{B.1}
$$

where $\mathbf{\Delta}_k$ stands for the asymptotic covariance matrix of $\mathbf{u}_k$

$$\mathbf{\Delta}_k \underset{=}{\Delta} \lim_{N\to\infty} (N-L+1)E\left[(\hat{\mathbf{u}}_k - \mathbf{u}_k)(\hat{\mathbf{u}}_k - \mathbf{u}_k)^H\right]. \tag{B.2}$$

From the results of Lemma 2, it is clear that $\mathbf{\Delta}_k$ is a diagonal matrix with equal elements. Denoting $\mathbf{\Delta} = \beta\mathbf{I}$, the log-likelihood function is given by

$$L_{tf} = -\frac{1}{2m}\frac{1}{N-L+1}\log\beta - \frac{1}{2\beta}(\hat{\mathbf{u}}_k - \mathbf{u}_k)^H(\hat{\mathbf{u}}_k - \mathbf{u}_k), \tag{B.3}$$

Maximizing L_{tf} is equivalent to minimizing

$$h_k \underset{=}{\Delta} \left[\hat{\mathbf{u}}_k - \mathbf{u}_k\right]^H \left[\hat{\mathbf{u}}_k - \mathbf{u}_k\right]. \tag{B.5}$$

For different k, we may construct the following cost function

$$\begin{aligned} h &\underset{=}{\Delta} \sum_{k=1}^{m} h_k \\ &= \sum_{k=1}^{m} \left[\hat{\mathbf{u}}_k - \mathbf{u}_k\right]^H \left[\hat{\mathbf{u}}_k - \mathbf{u}_k\right] \\ &= tr\left\{\left[\hat{\mathbf{D}} - \mathbf{D}\right]^H \left[\hat{\mathbf{D}} - \mathbf{D}\right]\right\}. \end{aligned} \tag{B.5}$$

Similar to (28), and by taking into account that we used n_o signals instead of n signals, the estimation of $\mathbf{D}$ is obtained as $\hat{\mathbf{A}}^o\left((\hat{\mathbf{A}}^o)^H\hat{\mathbf{A}}^o\right)^{-1}(\hat{\mathbf{A}}^o)^H\hat{\mathbf{D}}\hat{\mathbf{A}}^o\left((\hat{\mathbf{A}}^o)^H\hat{\mathbf{A}}^o\right)^{-1}(\hat{\mathbf{A}}^o)^H$, the minimization of equation (B.4) leads to (32).

ACKNOWLEDGMENT

This work was supported by ONR under Grant #N00014-98-1-0176.

REFERENCES

1. F. C. Schweppe, "Sensor array data processing for multiple signal estimation," *IEEE Trans. Inform. Theory*, vol. IT-14, pp. 294–305, 1968.
2. I. Ziskind and M. Wax, "Maximum likelihood localization of multiple sources by alternating projection," *IEEE Trans. Acoust., Speech, Signal Proc.*, vol. ASSP-36, no. 10, pp. 1553–1560, Oct. 1988.
3. A. Belouchrani and M. Amin, "Blind source separation based on time-frequency signal representation," *IEEE Trans. Signal Processing*, vol. 46, no. 11, pp. 2888–2898, Nov. 1998.
4. A. Belouchrani and M. Amin, "Time-frequency MUSIC," *IEEE Signal Processing Letters*, vol. 6, no. 5, pp. 109–110, May 1999.
5. Y. Zhang and M. Amin, "Spatial averaging of time-frequency distributions," in *Proc. ICASSP*, vol. III, pp. 1337-1340, March 1999.
6. P. Stoica and A. Nehorai, "MUSIC, maximum lokelihood, and Cramer-Rao bound," *IEEE Trans. Acoust. Speech, Signal Processing*, vol. 37, no. 5, pp. 720–741, May 1989.
7. G. H. Golub and C. F. Van Loan, *Matrix Computations*, 3rd edition. Baltimore, Maryland: Johns Hopkins University Press, 1996.
8. K. Sekihara, S. Nagarajan, D. Poeppel, and Y. Miyashita, "Time-frequency MEG-MUSIC algorithm," *IEEE Trans. Medical Imaging*, vol. 18, no. 1, pp.92-97, Jan. 1999.
9. M. G. Amin, "Spatial time-frequency distributions for direction finding and blind source separation," (invited paper) in *Proc. SPIE: Wavelet Applications IV*, vol.3723, pp.62-70, April 1999.
10. T. W. Anderson, *An Introduction to Multivariate Statistical Analysis*, New York: John Wiley & Sons, 1971.
11. P. Stoica and K. C. Sharman, "Maximum likelihood methods for direction-of-arrival estimation," *IEEE Trans. Acoust., Speech, Signal Proc.*, vol. ASSP-38, no. 7, pp. 1132–1142, July 1990.
12. P. Stoica and A. Nehorai, "MUSIC, maximum lokelihood, and Cramer-Rao bound: futher results and comparisons," *IEEE Trans. Acoust. Speech, Signal Processing*, vol. 38, no. 12, pp. 2140–2150, Dec. 1990.

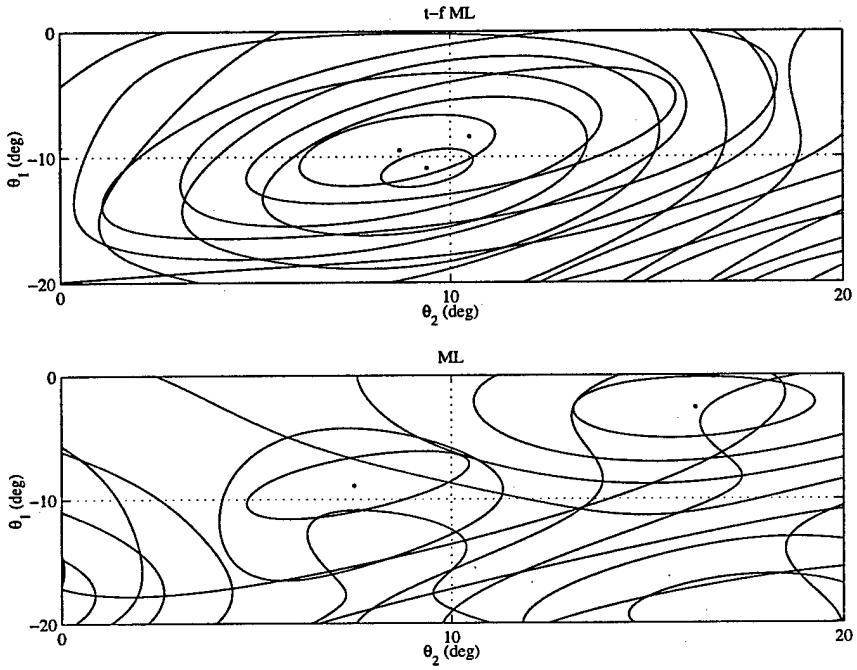

Fig. 1 Contour plots of t-f ML and ML likelihoof functions.

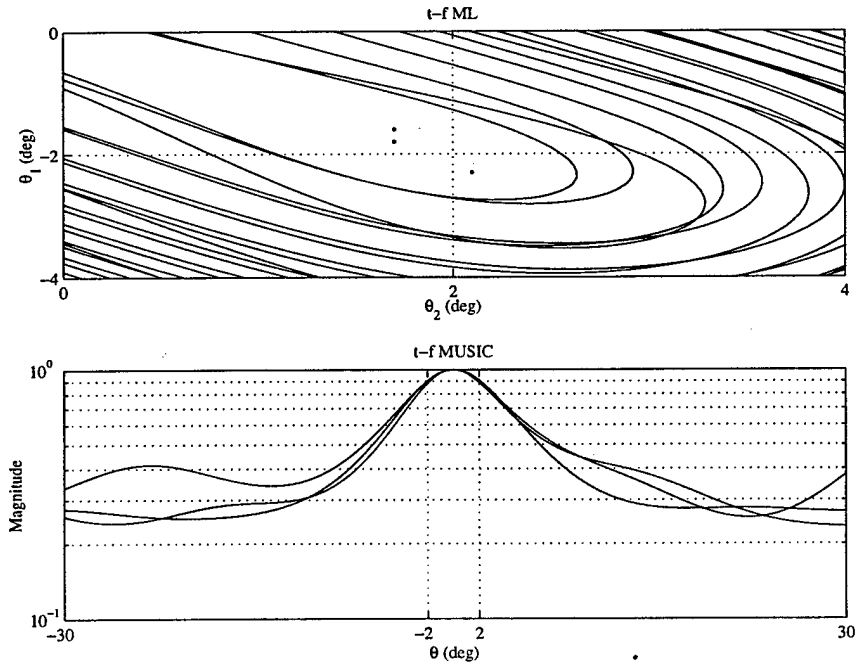

Fig. 2 Contour plots of t-f ML likelihood function and spatial spectra of t-f MUSIC.

Spatial evolutionary spectrum for DOA estimation and blind signal separation

A.Salim Kayhan*[a] and Moeness G. Amin[b]

[a]Dept. of Electrical and Electronics Engineering, Hacettepe University, 06532 Ankara, Turkey
[b]Dept. of Electrical and Computer Engineering, Villanova University, PA 19085, U.S.A.

ABSTRACT

In this paper, we combine the concepts of the evolutionary spectrum and array processing. We present Cross-power Evolutionary Periodogram for direction of arrival estimation and blind separation of nonstationary signals. We model nonstationary signals received by each sensor in the array as a sum of complex sinusoids with time-varying amplitudes. These amplitudes carry information about the direction of arrival which may also be time-varying. We first estimate the time-varying amplitudes, then use them for the estimation of evolutionary cross-power distributions of the sensor data. Next, using cross-power estimates at time and frequency samples of interest, we estimate the directions of arrival using one of the existing estimation methods. If the directions are time-varying, we choose time-frequency points around the time of interest for estimation of directions. Evaluating at different times, we obtain the directions as a function of time. If the sources are stationary, then we can use all time-frequency points of interest for the estimation of fixed directions. We also use whitening and subspace methods to find the mixing matrix and separate the signals received by the array. We present examples illustrating the performances of the proposed algorithms.

Keywords: Array processing, evolutionary spectrum, direction of arrival, blind source separation

1. INTRODUCTION

In many signal processing applications, such as radar, sonar, biomedical engineering and communications, direction of arrival (DOA) estimation and recovery of source signals are important problems. In general, these problems involve several signals and a multisensor array receiver. Each sensor receives a mixture of source signals. In the DOA estimation problem, the goal is the estimation of the source locations by processing the data received by the array sensors. The common presumption is that the signals are emitted from point sources placed in the farfield.[1] Further, the array manifold is assumed to be known. In the blind signal separation problem, the array parameters are generally unknown. Performance is often independent of inaccuracies in the array manifold as well as sensor displacement. Thus, the problem is separation of signals using received signals with the help of structural a priori information. A special case is the instantaneous mixture of signals. A solution using second order statistics and applying joint diagonalization to a set of covariance matrices was presented.[4] Recently, spatial time-frequency distributions have been introduced for direction finding and separation of nonstationary signals.[5–7]

In this paper, we combine the concepts of the evolutionary spectrum and array processing for problems involving nonstationary signals. We generalize the evolutionary periodogram (EP), an estimator of the evolutionary spectrum,[9] to form the cross-power evolutionary periodogram (CEP) for DOA estimation and blind signal separation. The CEP has the same desirable peoperties as the EP.

The nonstationary signal received by each sensor of the array is modeled as a sum of complex sinusoids with time-varying complex amplitudes. These amplitudes carry information about the directions of arrival, which may be time-varying. We first estimate the time-varying amplitudes using linear estimators obtained via minimum mean-squared error criteria. These estimates are then used for the estimation of the time-varying cross-power distributions of the data across the array. Next, using the time-varying cross-power estimates at selected time-frequency samples, we estimate the DOAs of the signals impinging on the array using one of the existing estimation methods.[1] If the directions are time-varying, we confine the selected time-frequency points to be around the time-of interest at which the source direction is to be estimated. Evaluating at different times, we obtain the directions as a function

*Correspondence: Email: kayhan@ee.hun.edu.tr

of time. If the sources are stationary, then all time-frequency points of high power concentration can be used for the estimation of source directions. In the blind source separation problem, the proposed spatial evolutionary spectrum is used along with whitening and subspace methods to estimate the mixing matrix and separate the source signals. Whether it is a stationary or moving source, the use of only time-frequency points with high signal to noise ratio yields improved performance. The incorporation of the desirable time-frequency points can be performed through either averaging or joint diagonalization schemes,[6] ,[4,5]

2. EVOLUTINARY SPECTRUM

A zero mean stationary random process, $v[n]$, may be represented as

$$v[n] = \int e^{j\omega n} dZ(\omega) \tag{1}$$

where $Z(\omega)$ is an incrementally orthogonal process, i.e.

$$E\{dZ(\omega)dZ^*(\omega_o)\} = \frac{1}{2\pi} S(\omega) d\omega \delta(\omega - \omega_o) \tag{2}$$

where $\delta()$ is the Kronecker delta function and $()^*$ denotes complex conjugation. Throughout the paper, the integral limits are from $-\pi$ to π. If the process is white with unit variance, then $S(\omega) = 1$.

If the unit variance white process $\{v[n]\}$ passes through a time-varying channel with impulse response $h[n,m]$, then the channel output is

$$x[n] = \sum_m h[n,m]v[m]. \tag{3}$$

Substituting (1) into (3), the nonstationary process $\{x[n]\}$ may be represented as

$$x[n] = \int H(n,\omega) e^{j\omega n} dZ(\omega) \tag{4}$$

where $H(n,\omega)$ is the generalized transfer function evaluated on the unit circle,

$$H(n,\omega) = \sum_m h[n,m] e^{-j\omega(n-m)}. \tag{5}$$

Thus the nonstationary process $\{x[n]\}$ is a continuous sum of sinusoids with time-varying complex amplitudes. The power at time n is:

$$E\{|\, x[n]\,|^2\} = \frac{1}{2\pi} \int |\, H(n,\omega)\,|^2 \, d\omega. \tag{6}$$

Therefore, the (oscillatory) evolutionary spectrum may be defined as,[10,11]:

$$S(n,\omega) = |\, H(n,\omega)\,|^2 \,. \tag{7}$$

Note that $H(n,\omega)$ is slowly varying with time, so that it belongs to the class of oscillatory functions.[11,9] The cross-power evolutionary spectrum of two processes, $\{x[n]\}$ and $\{y[n]\}$, can be obtained as[12]

$$S_{xy}(n,\omega) = H_x(n,\omega) H_y^*(n,\omega). \tag{8}$$

3. SPATIO-TEMPORAL PROCESSES

Consider a uniform linear array of L sensors. In analogy with (1), the field at the lth sensor can be expressed as[13]

$$v_l[n] = \int\int e^{j(n\omega - l\alpha)} dZ(\omega,\alpha) \tag{9}$$

where $\alpha = 2\pi \frac{\Delta}{\lambda} \sin(\theta)$, Δ is the array inter-element spacing, θ is the direction of arrival, and λ is the carrier wavelength. $Z(\omega,\alpha)$ is an incrementally orthogonal process in both the temporal frequency ω and spatial frequency α. That is,

$$E\{dZ(\omega,\alpha)dZ^*(\omega_o,\alpha_o)\} = \frac{1}{2\pi} S(\omega,\alpha) d\omega d\alpha \delta(\omega - \omega_o, \alpha - \alpha_o). \tag{10}$$

The cross-power between the data received at sensors l and m can be written as

$$\begin{aligned} E\{v_l[n]v_m^*[n]\} &= \frac{1}{2\pi}\int\int S(\omega,\alpha)e^{j(m-l)\alpha}d\omega d\alpha \\ &= \frac{1}{2\pi}\int \hat{S}(\omega,m-l)d\omega \end{aligned} \tag{11}$$

where $\hat{S}(\omega,m-l)$ represents the result of the Fourier transform with respect to α. In a single point source scenario ,

$$S(\omega,\alpha) = S(\omega)\delta(\alpha-\alpha_o) \tag{12}$$

and

$$E\{v_l[n]v_m^*[n]\} = \frac{1}{2\pi}e^{j(m-l)\alpha_o}\int S(\omega)d\omega. \tag{13}$$

Note that the cross-power spectrum (11) carries information about the directions of arrival of all signals impinging on the array.

4. SPATIAL EVOLUTIONARY SPECTRUM

Assume that the propagation channel has the time-varying impulse response $h[n,m]$. Then the sensor data takes the form

$$x_l[n] = \sum_m h[n,m]v_l[m]. \tag{14}$$

Then, from (9) and (14)

$$\begin{aligned} x_l[n] &= \int\int H(n,\omega)e^{j(n\omega-l\alpha)}dZ(\omega,\alpha) \\ &= \int H(n,\omega)e^{jn\omega}d\hat{Z}(\omega,l) \end{aligned} \tag{15}$$

where $H(n,\omega)$ is the generalized transfer function defined in (5). Here, we assume that the phase of $H(n,\omega)$ does not change with time. $d\hat{Z}(\omega,l)$ represents outcome of the Fourier transform with respect to the spatial frequency α.

The cross-power at time n can be written as

$$\begin{aligned} E\{x_l[n]x_m^*[n]\} &= \frac{1}{2\pi}\int\int \mid H(n,\omega)\mid^2 S(\omega,\alpha)e^{j(m-l)\alpha}d\omega d\alpha \\ &= \frac{1}{2\pi}\int \mid H(n,\omega)\mid^2 \hat{S}(\omega,m-l)d\omega \end{aligned} \tag{16}$$

where $\hat{S}(\omega,m-l)$ contains the result of the Fourier transfrom with respect to α. For a single point source at $\alpha=\alpha_o$,

$$E\{v_l[n]v_m^*[n]\} = \frac{1}{2\pi}e^{j(m-l)\alpha_o}\int \mid H(n,\omega)\mid^2 S(\omega)d\omega. \tag{17}$$

Again, the evolutionary cross-power spectrum carries information about the directions of arrival. Note that if the directions are also time-varying or the channel depends on both the temporal and spatial frequencies, then we can write the following general representation

$$\begin{aligned} x_l[n] &= \int\int H(n,\omega,\alpha)e^{j(n\omega-l\alpha)}dZ(\omega,\alpha) \\ &= \int \hat{H}(n,\omega,l)e^{jn\omega}d\hat{Z}(\omega,l). \end{aligned} \tag{18}$$

The cross-power is

$$\begin{aligned} E\{x_l[n]x_m^*[n]\} &= \frac{1}{2\pi}\int\int S(n,\omega,\alpha)e^{j(m-l)\alpha}d\omega d\alpha \\ &= \frac{1}{2\pi}\int S_{l,m}(n,\omega)d\omega \end{aligned} \tag{19}$$

where $S_{l,m}(n,\omega)$ is the result of the Fourier transform and it contains information about both the temporal and the spatial spectrum. The above equation is a general representation. It includes special cases such as stationary source and temporal spectrum, stationary source and nonstationary temporal spectrum, moving source with stationary temporal spectrum and finally moving source with nonstationary temporal spectrum. For a single moving point source at $\alpha = \alpha_o[n]$, the cross-power is

$$E\{v_l[n]v_m^*[n]\} = \frac{1}{2\pi}e^{j(m-l)\alpha_o[n]}\int S(n,\omega)d\omega. \tag{20}$$

5. ESTIMATION OF CROSS-POWER SPECTRUM

Consider the signals $\{x_l[n]\}$, $1 \le l \le L$, $0 \le n \le N-1$, where L is the number of sensors and N is the number of the data snapshots over the observation interval,

$$x_l[n] = \int \hat{H}(n,\omega,l)e^{jn\omega}d\hat{Z}(\omega,l). \tag{21}$$

Now, consider the data at the lth sensor and frequency ω_o,

$$x_{l,\omega_o}[n] = \hat{H}(n,\omega,l)d\hat{Z}(\omega_o,l)e^{j\omega_o n},\ 1 \le l \le L \tag{22}$$

which is a complex sinusoid modulated by a time-varying complex amplitude. The cross-power at time n and frequency ω_o between the data at sensors l and m is

$$E\{x_{l,\omega_o}[n]x_{m,\omega_o}^*[n]\} = \hat{H}(n,\omega_o,l)\hat{H}^*(n,\omega_o,m)\frac{d\omega_o}{2\pi} = S_{l,m}(n,\omega_o)\frac{d\omega_o}{2\pi}. \tag{23}$$

5.1. Model at a Frequency ω_o

In this section, we follow the approach of.[9] For a frequency of interest ω_o, $x_l[n]$, $1 \le l \le L$, can be modeled as

$$\begin{aligned} x_l[n] &= x_{l,\omega_o}[n] + y_{l,\omega_o}[n] \\ &= A_l(n,\omega_o)e^{j\omega_o n} + y_{l,\omega_o}[n] \end{aligned} \tag{24}$$

where $A_l(n,\omega_o)$ is the time-varying complex amplitude and $y_{l,\omega_o}[n]$ is a zero-mean term which includes the components at frequencies different from ω_o. From (23), we have

$$E\{A_l(n,\omega_o)A_m^*(n,\omega_o)\} = S_{l,m}(n,\omega_o)\frac{d\omega_o}{2\pi}. \tag{25}$$

Hence, if we estimate the complex amplitudes, $A_l(n,\omega)$, $1 \le l \le L$, we can, then, estimate the cross-power evolutionary spectrum which can, in turn, be used for the estimation of the directions of arrival.

Consider the sensor data $x_l[n]$, assume that $\{A_l(n,\omega_o)\}$ varies slowly with time so that they can be represented as an expansion of orthonormal functions $\{\beta_i[n]\}$, i.e.

$$A_l(n,\omega_o) = \sum_{i=0}^{M-1}\beta_i^*[n]a_i(\omega_o) = \underline{b}[n]^H\underline{a}(\omega_o) \tag{26}$$

where

$$\underline{a}(\omega_o) = [a_o(\omega_o), a_1(\omega_o), \ldots, a_{M-1}(\omega_o)]^T \tag{27}$$

is a vector of expansion coefficients and

$$\underline{b}[n] = [\beta_o[n], \beta_1[n], \cdots, \beta_{M-1}[n]]^T. \tag{28}$$

The notations $()^T$ and $()^H$ stand for the transpose and the Hermitian transpose, respectively.

We can express $x_l[n]$ over the observation interval in the following vector form:

$$\underline{x}_l = \underline{F}(\omega_o)\underline{a}_l(\omega_o) + \underline{y}_l(\omega_o) \tag{29}$$

where $\underline{\underline{F}}(\omega_o)$ is an $N \times M$ matrix with entries

$$\underline{\underline{F}}_{n+1,i+1} = \beta_i^*[n]e^{j\omega_o n}, 0 \leq n \leq N-1, 0 \leq i \leq M-1 \tag{30}$$

and

$$\begin{aligned} \underline{x}_l &= [x_l[0], x_l[1], \cdots, x_l[N-1]]^T \\ \underline{y}_l(\omega_o) &= [y_{l,\omega_o}[0], y_{l,\omega_o}[1], \cdots, y_{l,\omega_o}[N-1]]^T. \end{aligned} \tag{31}$$

In the following, we will drop the dependence on the constant frequency ω_o.

5.2. Estimation of $A_l(n, \omega_o)$

There are two approaches one could follow to estimate $\{A_l(n, \omega_o)\}$. These time-varying complex amplitudes could be either estimated for each sensor separately using only the data available from that particular sensor or they may be estimated together using the data available from all sensors. Here, we assume that signals at all sensors have similar characteristics. We can write the data at all sensors in a matrix form as:

$$\underline{\underline{X}} = \underline{\underline{F}}\underline{\underline{A}} + \underline{\underline{Y}} \tag{32}$$

where

$$\begin{aligned} \underline{\underline{X}} &= [\underline{x}_o, \underline{x}_1, \cdots, \underline{x}_{L-1}] \\ \underline{\underline{Y}} &= [\underline{y}_o, \underline{y}_1, \cdots, \underline{y}_{L-1}] \\ \underline{\underline{A}} &= [\underline{a}_o, \underline{a}_1, \cdots, \underline{a}_{L-1}]. \end{aligned} \tag{33}$$

Note that in the above matrix notation, the snapshots are row vectors and the sensor dependency is across the matrix columns. We use the same minimum mean-squared error estimator for all sensor data. Consider the vector of amplitudes at time n

$$\underline{a}[n] = \underline{b}[n]^H \underline{\underline{A}} \tag{34}$$

and the following linear estimator

$$\hat{\underline{a}}[n] = \underline{w}[n]^H \underline{\underline{X}} \tag{35}$$

where

$$\underline{w}[n] = [w_o[n], w_1[n], \cdots, w_{N-1}[n]]^T. \tag{36}$$

$\underline{w}[n]$ is the vector of time-varying weights. Substituting (32) into (35), we get

$$\hat{\underline{a}}[n] = \underline{w}[n]^H \underline{\underline{F}}\underline{\underline{A}} + \underline{w}[n]^H \underline{\underline{Y}}. \tag{37}$$

If the estimator is unbiased then it should produce the correct time-varying amplitude from the first term. Therefore, we get the following constraint for an unbiased estimator

$$\underline{w}[n]^H \underline{\underline{F}}\underline{\underline{A}} = \underline{b}[n]^H \underline{\underline{A}} \tag{38}$$

which is satisfied by the following condition

$$\underline{w}[n]^H \underline{\underline{F}} = \underline{b}[n]^H. \tag{39}$$

To obtain the estimator weights, we minimize the following total mean-squared error (MSE) over all sensors subject to the above constraint

$$\begin{aligned} \text{MSE} &= \frac{1}{2} E\{(\underline{a}[n] - \hat{\underline{a}}[n])(\underline{a}[n] - \hat{\underline{a}}[n])^H\} \\ &= \frac{1}{2} \underline{w}[n]^H E\{\underline{\underline{Y}}\underline{\underline{Y}}^H\} \underline{w}[n] \\ &= \frac{1}{2} \underline{w}[n]^H \underline{\underline{R}}_{YY} \underline{w}[n] \end{aligned} \tag{40}$$

where $\underline{\underline{R}}_{YY} = E\{\underline{Y}\underline{Y}^H\}$. Since $\underline{Y}$ is a function of the frequency ω_o and is not known *a priori*, we make the assumption that $\underline{\underline{R}}_{YY} = \underline{\underline{I}}$. This way the estimator works the same way at every frequency.[9] In this case,

$$\text{MSE} = \frac{1}{2}\underline{w}[n]^H\underline{w}[n]. \tag{41}$$

Incorporating the constraint (39), we seek to minimize the following cost function

$$c[n] = \frac{1}{2}\underline{w}[n]^H\underline{w}[n] - (\underline{w}[n]^H\underline{\underline{F}} - \underline{b}[n]^H)\lambda \tag{42}$$

where λ is an $M \times 1$ vector of Lagrange multipliers. By setting the derivatives with respect to the unknown parameters to zero, we get the optimum weights as[9]

$$\underline{w}_{opt}[n] = \underline{\underline{F}}\underline{b}[n] \tag{43}$$

and the mean-squared error as

$$\text{MSE} = \underline{b}[n]^H\underline{b}[n]. \tag{44}$$

The mean-squared error is a function of only the expansion functions. Therefore, it is time-dependent and frequency independent. However, for specific orthonormal functions, such as the complex exponentials, the MSE is also constant over time. The estimates of the time-varying amplitudes are obtained by substituting (43) into (35),

$$\hat{\underline{a}}[n] = \underline{b}[n]^H\underline{\underline{F}}\underline{X}. \tag{45}$$

5.3. Cross-power Evolutionary Spectrum Estimation

Since $\{\hat{A}_l(n,\omega_o)\}$ provide estimates of the time varying amplitudes at frequency ω_o, by varying ω_o over all frequencies, we obtain the amplitudes over all frequencies in $-\pi \leq \omega \leq \pi$. Then, the cross-power evolutionary spectral estimator can be obtained from (25) as

$$\begin{aligned}\hat{\underline{\underline{S}}}_{xx}(n,\omega) &= E\{\hat{\underline{a}}[n]^H\hat{\underline{a}}[n]\} \\ &= E\{\underline{X}^H\underline{\underline{F}}^H\underline{b}[n]\underline{b}[n]^H\underline{\underline{F}}\underline{X}\} \\ &= (\underline{b}[n]^H\underline{\underline{F}}) \otimes_l \hat{\underline{\underline{R}}} \otimes_r (\underline{\underline{F}}^H\underline{b}[n])\end{aligned} \tag{46}$$

where $\otimes$ indicates the block Kronecker product, with subscripts r and l denoting right and left operations, respectively. In the above equation, $\hat{\underline{\underline{R}}}$ is an $(LN) \times (LN)$ matrix, with $N \times N$ block element at location (l,m) is $\hat{\underline{\underline{R}}}(l,m) = \underline{\underline{R}}_{x_l x_m} = E\{\underline{x}_l\underline{x}_m^H\}$. We can write the cross-spectrum between two sensors l and m as:

$$\hat{S}_{x_l x_m}(n,\omega) = (\underline{b}[n]^H\underline{\underline{F}}^H)\underline{\underline{R}}_{x_l,x_m}(\underline{\underline{F}}^H\underline{b}[n]). \tag{47}$$

If we drop the expectation operator in the estimation, we will get the cross-power evolutionary periodogram (CEP), extension of the evolutionary periodogram (EP),

$$\hat{\underline{\underline{S}}}_{xx}(n,\omega) = (\underline{b}[n]^H\underline{\underline{F}}) \otimes_l \overline{\underline{\underline{R}}} \otimes_r (\underline{\underline{F}}^H\underline{b}[n]) \tag{48}$$

where $\overline{\underline{\underline{R}}}(l,m) = \underline{x}_l\underline{x}_m^H$. Since the EP is a fast estimator and it has good performance,[9] the ECP will also be a fast estimator with similar performance.

Note that although data alignment is important in multichannel spectral estimation,[14,15] it is this difference that we try to exploit for the DOA estimation.

6. SPATIO-TEMPORAL EVOLUTIONARY SPECTRUM ESTIMATION

Once we have the cross-power at time n and frequency ω, we can apply one of the existing spectral estimation methods[1] to estimate the spatio-temporal evolutionary spectrum. The peaks of the spatio-temporal evolutionary spectrum show the direction of arrival (DOA). One of these methods is the multiple signal classification(MUSIC).[17]

This is an eigenstructure subspace method that uses the orthogonality between the signal space and the noise space. The cross-power matrix can be decomposed as

$$\hat{\underline{\underline{S}}}_{xx}(n,\omega) = \underline{\underline{U}}\Lambda\underline{\underline{U}}^H \tag{49}$$

where the eigenvalues and corresponding eigenvectors are

$$\begin{aligned} \Lambda &= \text{diag}(\lambda_1,\ldots,\lambda_K,\lambda_{K+1},\ldots,\lambda_L), \lambda_1 \leq \cdots \leq \lambda_L, \\ \underline{\underline{U}} &= [\underline{u}_1,\cdots,\underline{u}_K,\underline{u}_{K+1},\cdots,\underline{u}_L]. \end{aligned} \tag{50}$$

For high signal to noise ratios (SNRs), the eigenvalues will be grouped into two sets, one corresponds to the signal components ($\{\lambda_i\}$, $i = 1,\ldots,K$) and the other, closer to zero, corresponds to the noise components ($\{\lambda_i\}$, $i = K+1,\ldots,L$). Using the property that the respective signal and noise eigenvectors are orthogonal, the directions of arrival can be obtained from the peaks of the spatio-temporal evolutionary spectrum:

$$\hat{\underline{\underline{S}}}_{xx}(n,\omega,\alpha) = \frac{1}{\sum_{i=K+1}^{L} \mid \underline{e}^H \underline{u}_i \mid^2}. \tag{51}$$

7. BLIND SIGNAL SEPARATION

Consider the case in which the signal received at each sensor is equal to a weighted sum of K signals and additive zero-mean thermal noise with variance σ^2. The noise is assumed to be both spatially and temporally white and uncorrelated with the signals. The narrowband data model is given by

$$\underline{x}[n] = \underline{\underline{C}}\underline{s}[n] + \underline{w}[n] \tag{52}$$

where $\underline{\underline{C}}$ is an $L \times K$ instantaneous mixing matrix. Substituting (52) into (46), we can show that (see appendix)

$$\hat{\underline{\underline{S}}}_{xx}(n,\omega) = \underline{\underline{C}}\hat{\underline{\underline{S}}}_{ss}(n,\omega)\underline{\underline{C}}^H + \sigma^2\underline{b}[n]^H\underline{b}[n]\underline{\underline{I}}. \tag{53}$$

Note that $\hat{\underline{\underline{S}}}_{xx}(n,\omega)$ is an $L \times L$ matrix, whereas $\hat{\underline{\underline{S}}}_{ss}(n,\omega)$ is of size $K \times K$. If the signals $\{s_k[n]\}$ are uncorrelated, hence the cross-power matrix is diagonal, $\hat{\underline{\underline{S}}}_{ss}(n,\omega) = \Lambda$, then we obtain

$$\hat{\underline{\underline{S}}}_{xx}(n,\omega) = \underline{\underline{C}}\Lambda\underline{\underline{C}}^H + \sigma^2\underline{b}[n]^H\underline{b}[n]\underline{\underline{I}}. \tag{54}$$

The first term on the right hand side is of rank K and the second term is of rank L. The eigendecomposition of $\hat{S}_{xx}(n,\omega)$ provides the K signal eigenvalues $(p_1[n]+\sigma^2\underline{b}^H[n]\underline{b}[n],\cdots,p_K[n]+\sigma^2\underline{b}^H[n]\underline{b}[n])$, where p_k are proportional to the powers of signals $s_k[n]$ and the $(L-K)$ noise eigenvalues $(\sigma^2\underline{b}^H[n]\underline{b}[n],\cdots,\sigma^2\underline{b}^H[n]\underline{b}[n])$, and the corresponding eigenvectors. We proceed to whiten the signal part of (53) through a whitening matrix $\underline{\underline{W}}$.[18] The linear equation (52) becomes

$$\begin{aligned} \underline{z}[n] &= \underline{\underline{W}}\underline{x}[n] \\ &= \underline{\underline{W}}\underline{\underline{C}}\underline{s}[n] + \underline{\underline{W}}\underline{w}[n] \\ &= \underline{\underline{U}}\underline{s}[n] + \underline{\underline{W}}\underline{w}[n] \end{aligned} \tag{55}$$

where $\underline{\underline{U}}$ is a unitary matrix. In the absence of noise, the cross-power distribution matrix using the transformed mixture (55) is

$$\hat{\underline{\underline{S}}}_{zz}(n,\omega) = \underline{\underline{W}}\underline{\underline{C}}\hat{\underline{\underline{S}}}_{ss}(n,\omega)\underline{\underline{C}}^H\underline{\underline{W}}^H = \underline{\underline{U}}\hat{\underline{\underline{S}}}_{ss}(n,\omega)\underline{\underline{U}}^H. \tag{56}$$

The unitary matrix $\underline{\underline{U}}$ can be obtained by joint diagonalizing a set of cross-power distribution matrices evaluated at different time-frequency points,[4,5] Once $\underline{\underline{U}}$ is found, the mixing matrix and the source signals can be estimated as

$$\begin{aligned} \underline{\underline{C}} &= \underline{\underline{W}}^{\#}\underline{\underline{U}} \\ \underline{s}[n] &= \underline{\underline{U}}^H\underline{\underline{W}}\underline{x}[n] \end{aligned} \tag{57}$$

where $\underline{\underline{W}}^{\#}$ is the pseudo inverse of the whitening matrix.

8. EXPERIMENTAL RESULTS

In this section, we present simulation examples to illustrate the performance of the proposed spatial evolutionary spectrum approach for direction finding and blind source separation.

Before presenting the examples, we point out an issue regarding the implementation. Since the cross-power matrices are estimated for a number of selected time-frequency points, some of them may contain information about only one of the sources. We try to take samples from the regions of signal time-frequency signatures. However, the noise in these regions effects the performances of the proposed methods. In order to increase overall robustness of the proposed methods, we can follow two approaches. The first approach is the averaging of all the matrices so that all signal components are included in the final cross-power matrix, and also the SNR is increased further.[6] In the second approach, the cross-power matrices are diagonalized jointly.[4]

In the first example, we consider two complex frequency shift keying (FSK) signals with frequencies (0.125,0.25) for the first signal and (0.25,0.375) for the second signal. The frequency 0.25 is used by the signals alternately. The length of the observation period is $N = 256$. The signals arrive at a six-sensor array with $\alpha_1 = 10$ and $\alpha_2 = -10$ degrees. Figure 1 shows the spatial spectrum at SNR = -10dB for the CEP-MUSIC and the MUSIC. In this example, we use ordered Hadamard functions with $M = 4$. Eight cross-power distribution matrices are averaged. Figure 1 shows the result of 200 realizations. We observe that the CEP-MUSIC is able to indicate two source locations well but the MUSIC has only one peak.

In the second example, we use the same FSK signals of the previous example except with $N = 128$ for the purpose of signal separation. The signals are shown in Figure 2. We mix the signals with the following matrix

$$\underline{C} = \begin{bmatrix} 1.0 & 0.5 \\ 0.6 & 1.0 \\ 0.4 & 0.8 \end{bmatrix}. \tag{58}$$

We apply three different blind source separation methods, namely, the CEP-blind source separation (CEP-BLIS) method described in the previous section, the spatial TFD (with Choi-Williams kernel) based blind source separation method (TFS-BLIS),[5] and the SOBI (second order blind identification) method of.[4] Figure 3 shows the mean rejection level defined as $I_{perf} = \sum_{l \neq m} E\{|\,(\hat{\underline{C}}^{\#}\underline{C})_{k,l}\,|^2\}^4$ at different SNRs. We use joint diagonalization with eight matrices in all three methods. The figure shows the result of 200 realizations. We observe that, for this example, the performance of the CEP-BLIS continues to improve as SNR increases whereas the performances of the SOBI and the TFS-BLIS methods insignificantly change after a threshold around 25dB.

In the final example, we consider a single source of a complex sinusoid at normalized frequency $f = 0.25$, with $N = 128$ snapshots. The distance between the source and multiple antenna array remains constant, but the source displacement is such that α changes linearly from -20 to 20 degrees. We use a two-sensor array and apply the CEP-MUSIC by averaging five matrices around the time of interest n. We use nine complex exponentials as expansion functions. Figure 4 shows the estimates under no noise case at times $n = 10, 50$ and 100. We observe that the estimator can follow the source quite well.

9. CONCLUSION

In this paper we combined evolutionary spectrum with spatio-temporal processing for estimation of DOA and blind signal separation. We modeled the nonstationary signals received at sensors as sum of complex sinusoids with time-varying complex amplitudes. The estimates of these amplitudes are used for the estimation of cross-power evolutionary spectrum, specifically, the cross-power evolutionary periodogram. Then, the cross-power evolutionary periodogram matrices at time and frequency samples of interest are combined and used in the MUSIC algorithm to obtain the spatial evolutionary spectrum. We also used the cross-power evolutionary periodogram matrices for blind signal separation. We presented examples illustrating that the proposed methods outperform some existing methods, i.e., the MUSIC for DOA estimation and the SOBI and the bilinear time-frequency distribution based algorithms for blind signal separation.

APPENDIX

Consider $\underline{x}[n] = \underline{C}\underline{s}[n] + \underline{w}[n]$. Now we rewrite $\underline{a}[n]$ as a column vector

$$\begin{aligned} \underline{a}[n] &= \underline{C}\left((\underline{b}[n]^H\underline{F}) \otimes_l [\underline{s}_1^H, \cdots, \underline{s}_K^H]^H\right) + (\underline{b}[n]^H\underline{F}) \otimes_l [\underline{w}_1^H, \cdots, \underline{w}_L^H]^H \\ \underline{a}^H[n] &= [\underline{w}_1^H, \cdots, \underline{w}_L^H] \otimes_r (\underline{F}^H\underline{b}[n]) + \left([\underline{s}_1^H, \cdots, \underline{s}_K^H] \otimes_r (\underline{F}^H\underline{b}[n])\right)\underline{C}^H. \end{aligned} \quad (59)$$

Then, we can write the cross-power as

$$\begin{aligned} \hat{\underline{S}}_{xx}(n,\omega) &= E\{\underline{a}[n]\underline{a}^H[n]\} \\ &= \underline{C}\left[(\underline{b}[n]^H\underline{F}^H) \otimes_l \hat{\underline{R}}_{ss} \otimes_r (\underline{F}^H\underline{b}[n])\right]\underline{C}^H + \sigma^2\underline{b}[n]^H\underline{b}[n]\underline{I} \\ &= \underline{C}\hat{\underline{S}}_{ss}(n,\omega)\underline{C}^H + \sigma^2\underline{b}[n]^H\underline{b}[n]\underline{I} \end{aligned} \quad (60)$$

where we used the property that $\underline{F}\underline{F}^H = \underline{I}$.

ACKNOWLEDGMENTS

This work was supported in part by ONR, grant no. N00014-98-1-0176, and in part by Hacettepe University, 98-530.

REFERENCES

1. D.H. Johnson and D.E. Dudgeon. *Array Signal processing: Concepts and Techniques.* Prentice-Hall, 1993.
2. L. Tong and S. Perreau. Multichannel blind identification: From subspace to maximum likelihood methods. *Proceedings of IEEE*, 86(10):1951–1968, 1998.
3. A-J. Van Der Veen. Algebraic methods for deterministic blind beamforming. *Proceedings of IEEE*, 86(10):1987–2008, 1998.
4. A. Belouchrani, K. Abed-Meraim, J-F. Cardoso, and E. Moulines. A blind source separation technique using second-order statistics. *IEEE Trans. Signal Proc.*, 45(2):434–444, 1997.
5. A. Belouchrani and M. Amin. Blind source separation based on time-frequency signal representation. *IEEE Trans. Signal Proc.*, 46(11), November 1998.
6. K. Sekihara, S. Nagarajan, D. Poeppel, and Y. Miyashita. Time-frequency MEG-MUSIC algorithm. *IEEE Medical imaging.* Submitted.
7. A. Belouchrani and M. Amin. Time-frequency MUSIC: An array signal processing method based on signal representation. *IEEE Signal Processing Letters.* To appear.
8. D.H. Johnson and D.E. Dudgeon. *Time-Frequency Analysis.* Prentice-Hall, 1995.
9. A.S. Kayhan, A. El-Jaroudi, and L.F. Chaparro. Evolutionary periodogram for nonstationary signals. *IEEE Trans. Signal Proc.*, 42(6):1527–1536, June 1994.
10. G. Melard and A. Herteler de Schutter. Contributions to evolutionary spectral theory. *J.of Time Series Analysis*, 10(1):41–63, 1989.
11. M.B. Priestley. *Non-linear and Non-stationary Time Series Analysis.* Academic Press Inc., London, 1988.
12. M.B. Priestley and H. Tong. On the analysis of bivariate non-stationary processes. *J.R.Statist.Soc.B*, 35(2):153–166, 1973.
13. J. Capon. High-resolution frequency-wavenumber spectrum analysis. *Proc. IEEE*, 57(8):1408–1419, August 1969.
14. M.B. Priestley. *Spectral Analysis and Time Series.* Academic Press Inc., 1981.
15. S.M. Kay. *Modern Spectral Estimation:Theory and Application.* Prentice-Hall, Englewood Cliffs, N.J., 1988.
16. V.F. Pisarenko. On the estimation of spectra by means of nonlinear functions of the covariance matrix. *Geophys.J.R.Astron.Soc.*, 28:511–531, 1972.
17. R.Schmidt. Multiple emitter location and signal parameter estimation. *IEEE Trans. on Antennas and Propagation*, 34(1):276–280, 1986.
18. L. Tong, R w. Liu, V.C. Soon, and Y-F. Huang. Indeterminacy and identifiability of blind identification. *IEEE Trans. on Circuits and Systems*, 38(5):499–509, 1991.

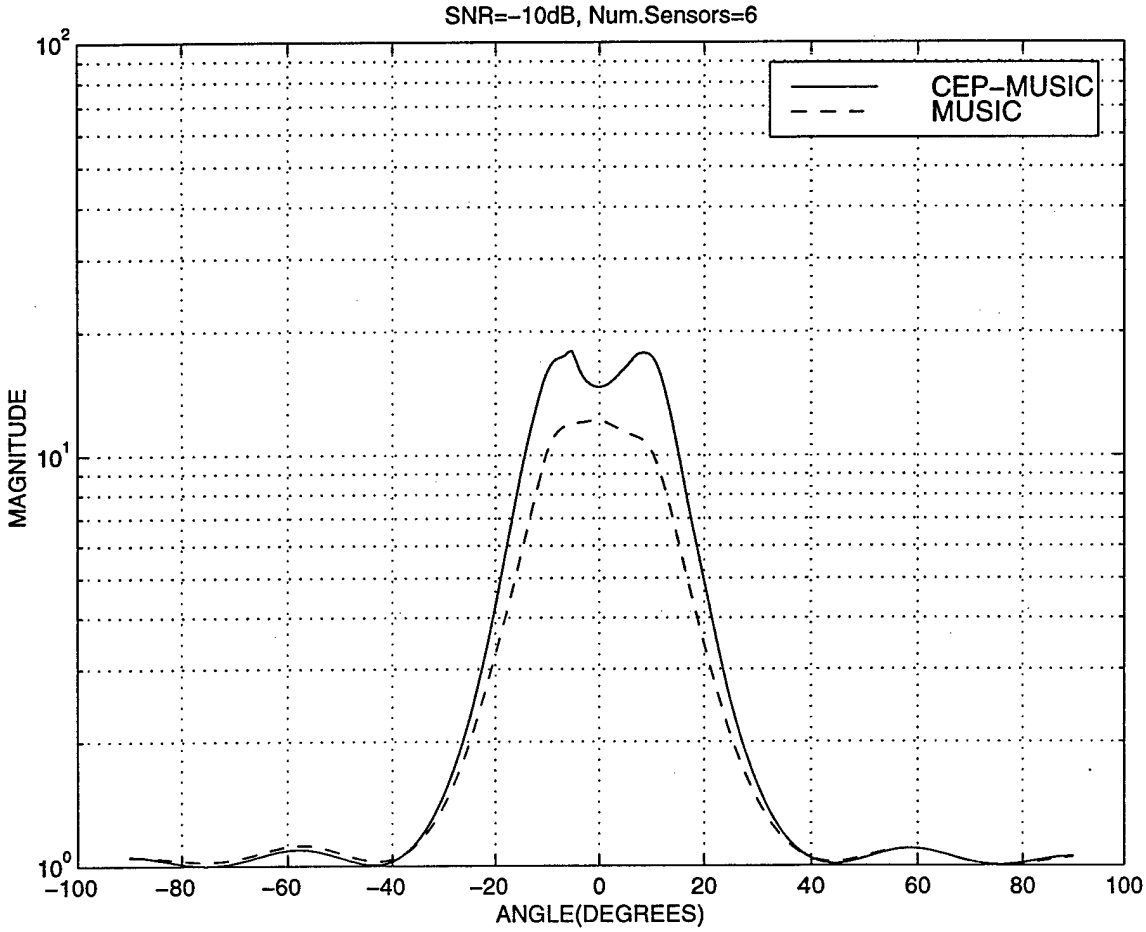

Figure 1. Spatial spectrum for two FSK signals at $\alpha_1 = -10$ and $\alpha_2 = 10$ degrees.

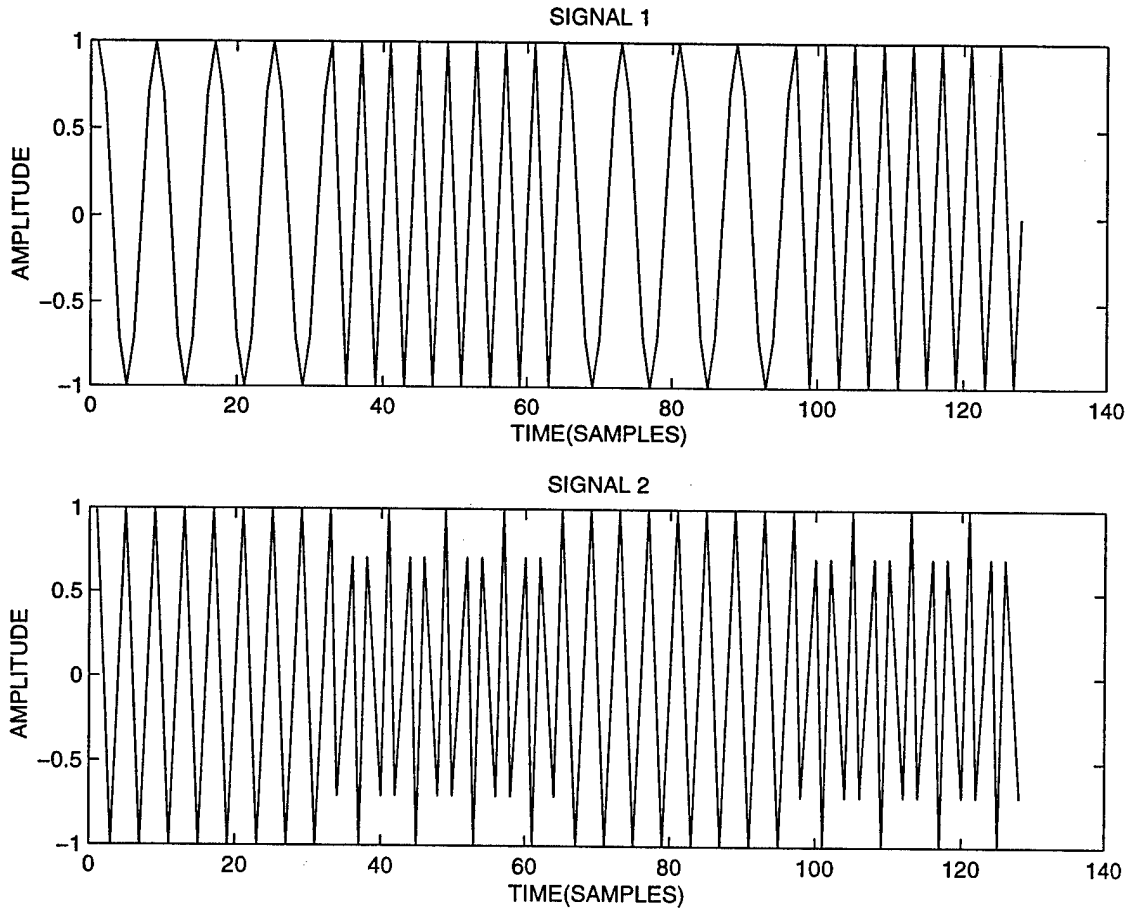

Figure 2. The FSK signals used for the blind source separation.

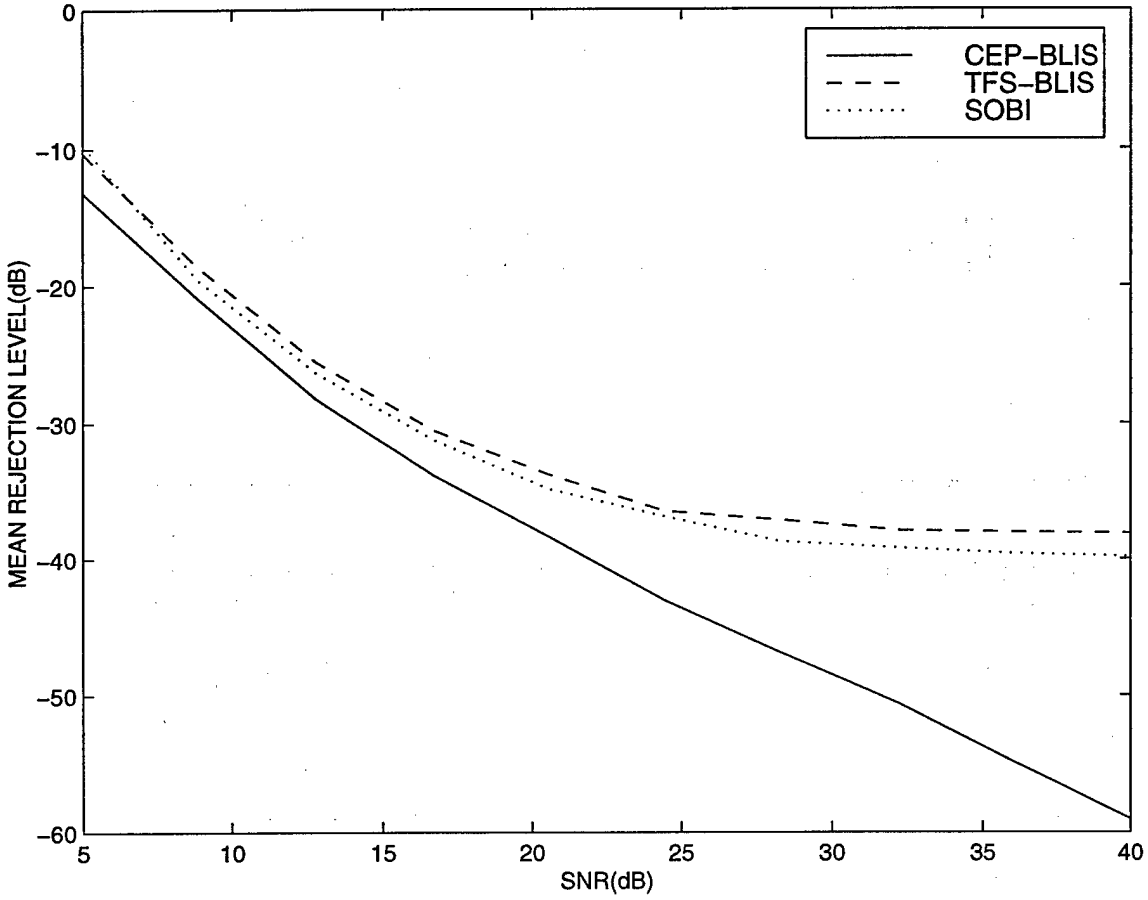

Figure 3. Mean rejection levels for the FSK signals.

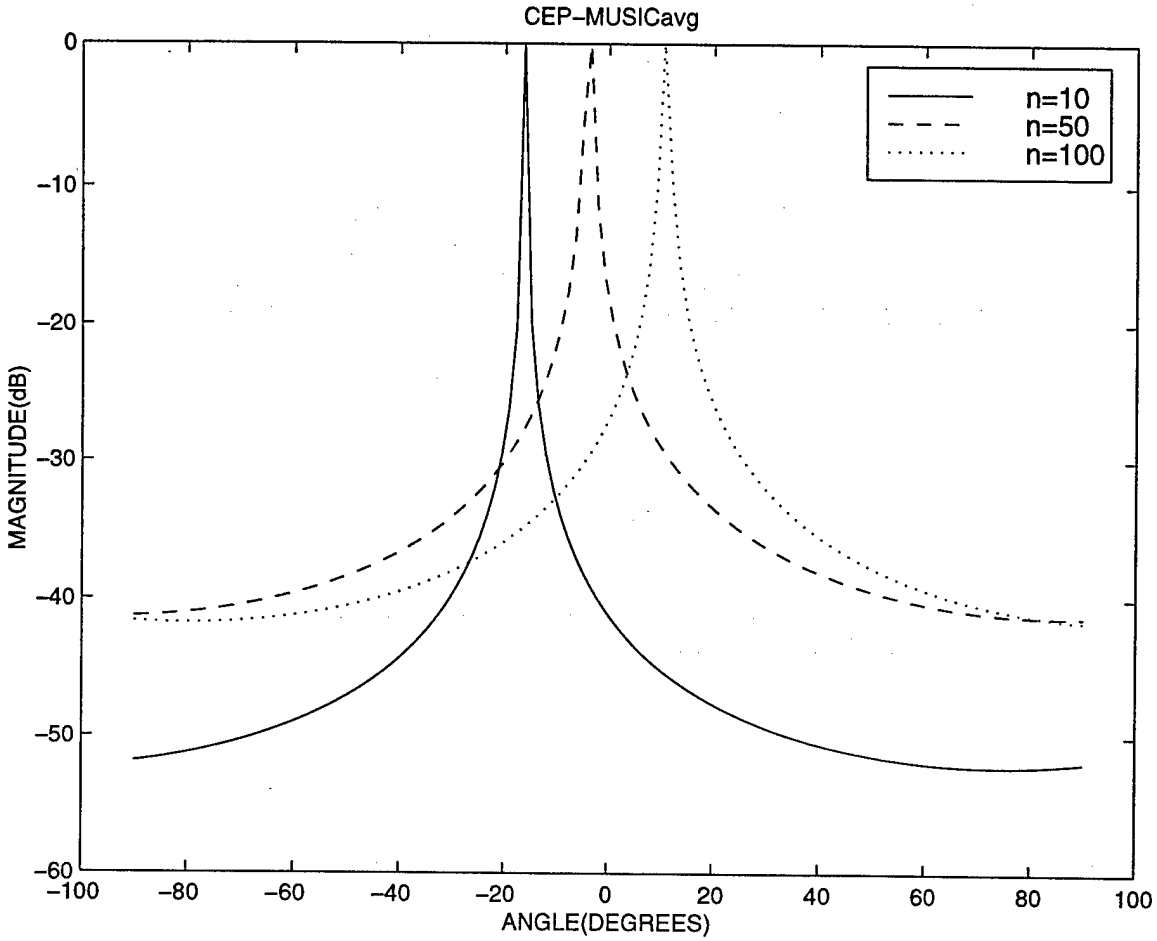

Figure 4. Spatial spectrum for a moving source with α varying linearly from -20 to 20 degrees.

Direction Finding Based on Spatial Time-Frequency Distribution Matrices

Moeness G. Amin

Department of Electrical and Computer Engineering,
Villanova University, Villanova, PA 19085
Phone: (610)519-7305 Fax: (610)519-4436
E-mail: moeness@ece.vill.edu

Spatial time-frequency distributions (STFDs) have been recently shown to be a powerful tool for solving direction finding and blind source separation problems for multi-sensor array receivers. These spatial distributions are the natural means to deal with source signals that are localizable in the time-frequency domain. This paper examines the eigenstructure of the spatial time-frequency distribution matrices. It is shown that improved estimates of the signal and noise subspaces are achieved by constructing the subspaces from the time-frequency signatures of the signal arrivals rather than from the data covariance matrices. This improvement is more evident in low signal-to-noise ratio (SNR) environment and in the cases of closely spaced sources. The paper considers the MUSIC technique to demonstrate the advantages of STFDs and uses it as grounds for comparison between time-frequency and conventional subspace estimates.

Key Words: time-frequency analysis; subspace analysis; time-frequency MUSIC; spatial time-frequency distributions; array signal processing

1. INTRODUCTION

Although the applications of the spatial time-frequency distributions to blind source separation and DOA problems using multiple antenna arrays in nonstationary environments have been introduced in [1,2], yet so far there has not been sufficient analysis that explains their offerings and justifies their performance. The aim of this paper is to examine the eigenstructure of the spatial time-frequency distribution matrices and provide statistical analysis of their respective signal and noise subspaces. The paper shows that the subspaces obtained from the STFDs are robust to both noise and angular separation of the waveforms incident on the array. This robustness is primarily due to spreading the noise power while localizing the source energy in the time-frequency domain. By forming the STFD matrices from

This work was supported by ONR under Grant #N00014-98-1-0176.

the points residing on the source time-frequency signatures, we in essence, increase the input signal to noise ratio, and hence improve subspace estimates.

This paper is organized as follows. Section 2 presents the signal model and gives a brief review of the definition and basic properties of the spatial time-frequency distributions. In Section 3, we consider nonstationary environment characterized by frequency-modulated (FM) source signals, and show the potential improvement in direction-of-arrival (DOA) estimation using STFDs. Section 4 examines the performance of the direction finding MUSIC technique based on the covariance and STFD noise subspace estimates.

2. BACKGROUND

2.1. Signal Model

In narrowband array processing, when n signals arrive at an m-element array, the linear data model

$$\mathbf{x}(t) = \mathbf{y}(t) + \mathbf{n}(t) = \mathbf{A}(\Theta)\mathbf{d}(t) + \mathbf{n}(t) \tag{1}$$

is commonly assumed, where the $m \times n$ spatial matrix $\mathbf{A}(\Theta) = [\mathbf{a}(\theta_1)...\mathbf{a}(\theta_n)]$ represents the mixing matrix or the steering matrix, and $\mathbf{a}(\theta_i)$ are the steering vectors. Due to the mixture of the signals at each sensor, the elements of the $m \times 1$ data vector $\mathbf{x}(t)$ are multicomponent signals, whereas each source signals $d_i(t)$ of the $n \times 1$ signal vector $\mathbf{d}(t)$ are often a monocomponent signal. $\mathbf{n}(t)$ is an additive noise vector whose elements are modeled as stationary, spatially and temporally white, zero-mean complex random processes, independent of the source signals. That is,

$$E[\mathbf{n}(t+\tau)\mathbf{n}^H(t)] = \sigma\delta(\tau)\mathbf{I} \quad \text{and} \quad E[\mathbf{n}(t+\tau)\mathbf{n}^T(t)] = \mathbf{0} \quad \text{for any } \tau \tag{2}$$

where $\delta(\tau)$ is the Kronecker delta function, $\mathbf{I}$ denotes the identity matrix, σ is the noise power at each sensor, superscript ^{H} and ^{T} respectively denote conjugate transpose and transpose, and $E(\cdot)$ is the statistical expectation operator.

In equation (1), it is assumed that the number of sensors is larger than the number of sources, i.e., $m > n$. Further, matrix $\mathbf{A}$ is full column rank, which implies that the steering vectors corresponding to n different angles of arrival are linearly independent. We further assume that the correlation matrix

$$\mathbf{R}_{\mathbf{xx}} = E[\mathbf{x}(t)\mathbf{x}^H(t)] \tag{3}$$

is nonsingular, and the observation period consists of N snapshots with $N > m$.

Under the above assumptions, the correlation matrix is given by

$$\mathbf{R}_{\mathbf{xx}} = E[\mathbf{x}(t)\mathbf{x}^H(t)] = \mathbf{A}(\Theta)\mathbf{R}_{\mathbf{dd}}\mathbf{A}^H(\Theta) + \sigma\mathbf{I}, \tag{4}$$

where $\mathbf{R}_{\mathbf{dd}} = E[\mathbf{d}(t)\mathbf{d}^H(t)]$ is the signal correlation matrix. For notational convenience, we drop the argument Θ in equation (1) and simply use $\mathbf{A}$ instead of $\mathbf{A}(\Theta)$.

2.2. Spatial Time-Frequency Distributions

The spatial time-frequency distributions (STFDs) based on Cohen's class of time-frequency distribution were introduced in [1] and its applications to direction find-

ing and blind source separation have been discussed in [2] and [1], respectively. In this paper, we focus one key member of Cohen's class, namely the pseudo Wigner-Ville distribution (PWVD) and its respective spatial distribution. Only the time-frequency (t-f) points in the autoterm regions of PWVD are considered for STFD matrix construction. In these regions, it is assumed that the crossterms are negligible. The discrete form of pseudo Wigner-Ville distribution of a signal $x(t)$, using a rectangular window of odd length L, is given by

$$D_{xx}(t,f) = \sum_{\tau=-\frac{L-1}{2}}^{\frac{L-1}{2}} x(t+\tau)x^*(t-\tau)e^{-j4\pi f\tau}, \tag{5}$$

where * denotes complex conjugation. The spatial pseudo Wigner-Ville distribution (SPWVD) matrix is obtained by replacing $x(t)$ by the data snapshot vector $\mathbf{x}(t)$,

$$\mathbf{D_{xx}}(t,f) = \sum_{\tau=-\frac{L-1}{2}}^{\frac{L-1}{2}} \mathbf{x}(t+\tau)\mathbf{x}^H(t-\tau)e^{-j4\pi f\tau}. \tag{6}$$

Substitute (1) into (6), we obtain

$$\mathbf{D_{xx}}(t,f) = \mathbf{D_{yy}}(t,f) + 2\mathrm{Re}\left[\mathbf{D_{yn}}(t,f)\right] + \mathbf{D_{nn}}(t,f). \tag{7}$$

We note that $\mathbf{D_{xx}}(t,f)$, $\mathbf{D_{yy}}(t,f)$, $\mathbf{D_{yn}}(t,f)$, $\mathbf{D_{ny}}(t,f)$, and $\mathbf{D_{nn}}(t,f)$ are matrices of dimension $m \times m$, whereas the source TFD matrix $\mathbf{D_{dd}}(t,f)$ is of dimension $n \times n$. Under the uncorrelated signal and noise assumption and the zero-mean noise property, the expectation of the crossterm TFD matrices between the signal and noise vectors is zero, i.e., $E\left[\mathbf{D_{yn}}(t,f)\right] = E\left[\mathbf{D_{ny}}(t,f)\right] = \mathbf{0}$, and it follows

$$E\left[\mathbf{D_{xx}}(t,f)\right] = \mathbf{D_{yy}}(t,f) + E\left[\mathbf{D_{nn}}(t,f)\right] = \mathbf{A}\mathbf{D_{dd}}(t,f)\mathbf{A}^H + E\left[\mathbf{D_{nn}}(t,f)\right]. \tag{8}$$

For narrowband array signal processing applications, the mixing matrix $\mathbf{A}$ holds the spatial information and maps the auto- and cross-TFDs of the source signals into auto- and cross-TFDs of the data.

It is noted that relationship (8) holds true for every (t,f) points. In order to reduce the effect of noise and ensure the full column rank property of the STFD matrix, we consider multiple time-frequency points. This allows more information of the source signal t-f signatures to be included into their respective subspace formulation. Joint-diagonalization [3] and time-frequency averaging are the two main approaches that have been used for this purpose [1, 2, 4]. In this paper, we only consider averaging over multiple time-frequency points.

3. SUBSPACE ANALYSIS FOR FM SIGNALS

In this paper, we focus on frequency modulation (FM) signals, modeled as

$$\mathbf{d}(t) = [d_1(t), ..., d_n(t)]^T = [D_1 e^{j\psi_1(t)}, ..., D_n e^{j\psi_n(t)}]^T, \tag{9}$$

where D_i and $\psi_i(t)$ are the amplitude and phase of ith source signal. For each sampling time t, $d_i(t)$ has an instantaneous frequency $f_i(t) = \frac{1}{2\pi}\frac{d\psi_i(t)}{dt}$. To simplify the analysis, we assume that the FM signals are mutually uncorrelated over the observation period. That is,

$$\frac{1}{N}\sum_{k=1}^{N} d_i(k)d_j^*(k) = 0 \qquad \text{for } i \neq j,\ i,j = 1,...,n. \tag{10}$$

In this case, the signal correlation matrix in (4) is

$$\mathbf{R_{dd}} = diag\left[D_i^2,\ i = 1,2,...,n\right]$$

where $diag[\cdot]$ is the diagonal matrix formed with the elements of its vector valued arguments. The ith diagonal element of TFD matrix $\mathbf{D_{dd}}(t,f)$ in (8) is given by

$$D_{d_i d_i}(t,f) = \sum_{\tau=-\frac{L-1}{2}}^{\frac{L-1}{2}} D_i^2 e^{j[\psi_i(t+\tau)-\psi_i(t-\tau)]-j4\pi f\tau}. \tag{11}$$

Assuming that the third-order derivative of the phase is negligible over the window length L, then $f_i = \frac{1}{2\pi}\frac{d\psi_i(t)}{dt}$, and $\psi_i(t+\tau) - \psi_i(t-\tau) - 4\pi f_i\tau = 0$. Accordingly,

$$D_{d_i d_i}(t,f) = \sum_{\tau=-\frac{L-1}{2}}^{\frac{L-1}{2}} D_i^2 = LD_i^2. \tag{12}$$

Similarly, the noise STFD matrix $\mathbf{D_{nn}}(t,f)$ is

$$\mathbf{D_{nn}}(t,f) = \sum_{\tau=-\frac{L-1}{2}}^{\frac{L-1}{2}} \mathbf{n}(t+\tau)\mathbf{n}^H(t-\tau)e^{-j4\pi f\tau}. \tag{13}$$

Under the assumption of temporally and spatially white noise, the statistical expectation of $\mathbf{D_{nn}}(t,f)$ is given by

$$E\left[\mathbf{D_{nn}}(t,f)\right] = \sum_{\tau=-\frac{L-1}{2}}^{\frac{L-1}{2}} E\left[\mathbf{n}(t+\tau)\mathbf{n}^H(t-\tau)\right] e^{-j4\pi f\tau} = \sigma\mathbf{I}. \tag{14}$$

Therefore, when we select the time-frequency points along the t-f signature or the IF of an FM signal, the SNR in model (8) is LD_i^2/σ, which has an improved factor L over the one associated with model (4).

The pseudo Wigner-Ville distribution of each FM source has a constant value over the observation period, providing that we leave out the rising and falling power distributions at both ends of the data record. For convenience of analysis, we select those $N - L + 1$ t-f points of constant distribution value for each source signal. Therefore, the averaged STFD over the time-frequency signatures of n_o signals, i.e., $n_o(N - L + 1)$ t-f points, is given by

$$\hat{\mathbf{D}} = \frac{1}{n_o(N-L+1)}\sum_{q=1}^{n_o}\sum_{i=1}^{N-L+1} \mathbf{D_{xx}}(t_i, f_{q,i}), \tag{15}$$

where $f_{q,i}$ is the instantaneous frequency of the qth signal at the ith time sample. The expectation of the averaged STFD matrix is

$$\mathbf{D} = E\left[\hat{\mathbf{D}}\right] = \frac{1}{n_o}\sum_{p=1}^{n_o}\left[LD_p^2\mathbf{a}(\theta_p)\mathbf{a}^H(\theta_p) + \sigma\mathbf{I}\right] = \frac{L}{n_o}\mathbf{A}^o\mathbf{R}_{\mathbf{dd}}^o(\mathbf{A}^o)^H + \sigma\mathbf{I}, \quad (16)$$

where $\mathbf{R}_{\mathbf{dd}}^o$ and $\mathbf{A}^o$, respectively, represent the signal correlation matrix and the mixing matrix constructed by only considering n_o signals out of the total number of signal arrivals n.

It is clear from (16) that, when n_o signals are selected, the SNR improvement becomes $G = L/n_o$ (we assume $L > n_o$ throughout this paper). Therefore, from the SNR perspective, it is better to select (t, f) points that belong to individual signals, and to separately evaluate the respective STFD matrices. Accordingly, STFD-based direction finding is, in essence, a discriminatory technique in the sense that it does not require simultaneous localization and extraction of all unknown signals received by the array. With STFDs, direction finding can be performed using STFDs of a subclass of the impinging signals with specific time-frequency signatures. In this respect, the proposed direction finding technique acts as a spatial filter, removing all other signals from consideration and, subsequently, saves any downstream processing that is required to separate interference and signals of interest. It is also important to note that with the ability to construct the STFD matrix from one or few signal arrivals, the well known $m > n$ condition on source localization using arrays can be relaxed, i.e., we can perform direction finding or source separation with the number of array sensors smaller than the number of impinging signals [5]. From the angular resolution perspective, closed spaced sources with different t-f signatures can be resolved by constructing two separate STFDs, each corresponds to one source, and then proceed with subspace decomposition for each STFD matrix separately, followed by a appropriate source localization method (MUSIC, for example). The drawback of performing several direction finding using different STFD matrices is clearly the need for repeated computations of eigendecompositions and source localizations.

4. SIMULATIONS

The t-f MUSIC is introduced in [2], where the angles of arrival are estimated by locating the highest peaks of the spectrum provided by using the noise subspace of the STFD matrix, rather the covariance matrix, which is the case in conventional MUSIC.

The following example compares the performance of conventional and t-f MUSIC. Consider a uniform linear array of 8 sensors separated by half a wavelength. Two chirp signals emitted from two sources positioned at angle θ_1 and θ_2. The start and end frequencies of the chirp signal of the source at θ_1 are $\omega_{s1} = 0$ and $\omega_{e1} = \pi$, while the corresponding two frequencies for the signal of the other source at θ_2 are $\omega_{s2} = \pi$ and $\omega_{e2} = 0$, respectively. The noise used in this simulation is zero-mean, Gaussian distributed, and temporally white. The noise power, σ, is adjusted to give the desired $SNR = -10log(\sigma)$.

Fig. 1 displays the variance of the estimated DOA $\hat{\theta}_1$ versus SNR fro the case $(\theta_1, \theta_2) = (-10°, 10°)$. The curves in this figure show the theoretical and experimental results of the conventional MUSIC and t-f MUSIC (for L=33 and 129). The CRB is also shown in Fig. 1. Both impinging signals are selected when performing t-f MUSIC ($n_o = n = 2$). We assume that the number of signals is correctly estimated for each case. Simulation results are averaged over 100 independent trials of Monte Carlo experiments. The advantages of t-f MUSIC in low SNR cases are evident from this figure.

5. CONCLUSIONS

The advantages of STFD-based direction finding over traditional direction finding methods using data covariance matrices were demonstrated using the MUSIC algorithm. The t-f MUSIC technique outperforms the conventional MUSIC technique in the two situations of low SNR and closely spaced sources. Detailed performance analysis of DOA-based STFD is given in reference [6].

REFERENCES

1. A. Belouchrani and M. Amin, "Blind source separation based on time-frequency signal representation," *IEEE Trans. Signal Processing*, vol. 46, no. 11, pp. 2888-2898, Nov. 1998.
2. A. Belouchrani and M. Amin, "Time-frequency MUSIC," *IEEE Signal Processing Letters*, vol. 6, no. 5, pp. 109-110, May 1999.
3. G. H. Golub and C. F. Van Loan, *Matrix Computations*, 3rd edition. Baltimore, Maryland: Johns Hopkins University Press, 1996.
4. K. Sekihara, S. Nagarajan, D. Poeppel, and Y. Miyashita, "Time-frequency MEG-MUSIC algorithm," *IEEE Trans. Medical Imaging*, vol. 18, no. 1, pp.92-97, Jan. 1999.
5. M. G. Amin, "Spatial time-frequency distributions for direction finding and blind source separation," in *Proc. SPIE: Wavelet Applications IV*, vol.3723, pp.62-70, April 1999.
6. Y. Zhang, W. Mu, and M. G. Amin, "Subspace analysis of spatial time-frequency distribution matrices," submitted to *IEEE Trans. Signal Processing*, June 1999.

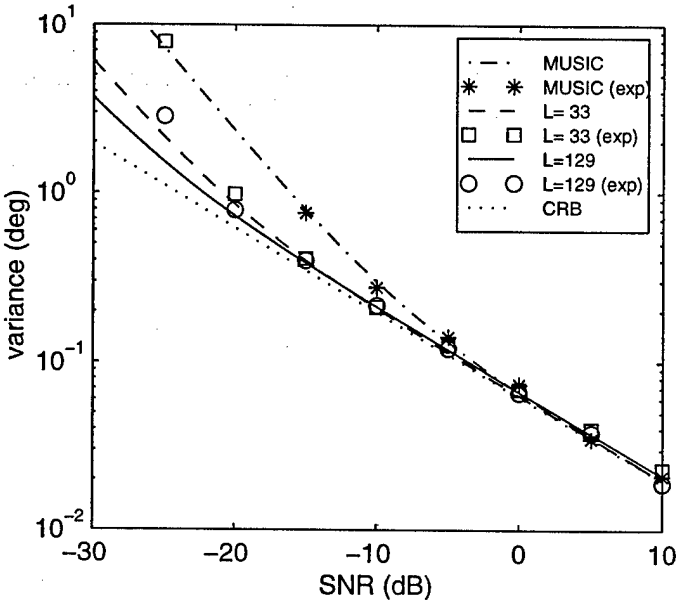

FIG. 1. Variance of DOA estimation vs. SNR.

Spatial Bilinear Distributions for Direction Finding and Blind Source Separations

Moeness G. Amin
Department of Electrical and Computer Engineering,
Villanova University,
Villanova, PA 19085, USA

Summary: This paper discusses the application of the new concept of spatial time-frequency distribution (STFD), and more generally the spatial arbitrary joint-variable distribution (SJVD), to key array signal processing problems including blind source separations and high resolution direction finding of narrowband and broadband sources with stationary and nonstationary temporal characteristics. The STFD can be formulated based on the widely used class of time-frequency distributions, namely Cohen's class, or it can be devised by incorporating other classes of quadratic distributions, such as the Hyperbolic class and the Affine class. The paper delineates the fundamental offerings of STFDs, presents three examples of array signal processing using the localization properties of time-frequency distributions of the impinging signals, and shows how spatial averaging can be combined with time-frequency averaging for improved performance.

I. INTRODUCTION

In many signal processing applications, the multidimensional signal is directly utilized to estimate some signal parameters, such as the number of sources and their directions of arrival. Subspace-based methods use a geometrical relation involving the exact moments of the data. The desired signal parameters are extracted by solving this relation in some approximate sense, and using sample moments instead of the exact ones. The commonly applied eigenstructure subspace methods assume stationary signals. Although, when the frequency content of the measured data is time-varying, these methods can still be used, yet their performance can be significantly improved by proper use of the information on the data time-frequency characteristics. In general, conventional blind source separation and direction finding techniques based on second and higher order statistics are not well structured to exploit the non-overlapping properties of the signal arrivals in the time-frequency domain. These properties can, for example, be employed to achieve spatial nulling and removal of undesired sources without resorting to beamspace processing and decreasing the available number of degrees of freedom.

The evaluation of quadratic time frequency distributions of the data snapshots across the array yields spatial time-frequency distributions, which permit the application of eigenstructure subspace techniques to solving a large class of channel estimation and equalization, blind source separation, and high resolution direction of arrival estimation problems. Spatial time-frequency distribution techniques are most appropriate to handle sources of nonstationary waveforms that are highly localized in the time-frequency domain. In the area of blind source separation, the spatial time-frequency distributions allow the separation of Gaussian sources with identical spectral shape, but with different time-frequency localization properties, i.e., different signatures in the time-frequency domain. For signal separation and direction of arrival estimation problems, spreading the noise power while localizing the source energy in the time-frequency domain amounts to increasing the robustness of eigenstructure signal and noise subspace estimation methods with respect to channel and receiver noise, and hence improves resolution and signal separation performance.

In this paper, we consider the applications of time-frequency distributions to the two important areas of direction finding and blind source separation using multiple antenna arrays. While time-frequency distributions have been sought out and successfully used in the areas of speech, biomedicine, automotive industry, and machine monitoring, their applications to sensor and spatial signal processing have not been properly investigated. The time-frequency distribution in all its bilinear and higher order forms represents a powerful tool for superresolution angle of arrival estimation and recovery of the signals which have been mixed across the array, specifically those of nonstationary temporal characteristics. The proper utilization of the time-frequency signatures and the power localization properties of the desired and jammer signals over time and frequency, or any appropriate joint-variables, increases the effective signal to noise ratio and casts time-frequency distributions as an important and essential part of array processing. For different jamming environments and a large class of signals, time-frequency based direction finding and blind source separation methods offer performance that is beyond the capabilities of traditional techniques based on second or higher order statistics.

2. SPATIAL CONSIDERATION OF TFDS

Time-frequency distributions have been shown to be a powerful tool in nonstationary signal analysis [1,2,3]. So far, most of the work on this subject has focused on temporal signal processing without much attention given to the spatial variable. The spatial dimension, properly incorporated into time-frequency signal representations, allows an effective angle-of-arrival estimation and separation of nonstationary signals impinging on the antenna array.

To present the spatial time-frequency distribution, we first recall that Cohen's class of time-frequency distribution (TFD) of a signal $x(t)$ is given by [1]

$$D_{xx}(t,f) = \int_{-\infty}^{\infty}\int_{-\infty}^{\infty} \phi(t-u,\tau)x(u+\tau/2)x^*(u-\tau/2)e^{-j2\pi f\tau}\,du\,d\tau \quad (1)$$

where t and f define the time index and the frequency index, respectively. The kernel $\phi(t,\tau)$ is a function of the time and lag variables. The cross-TFD of two signals $x_1(t)$ and $x_2(t)$ is defined by

$$D_{x_1x_2}(t,f) = \int_{-\infty}^{\infty}\int_{-\infty}^{\infty} \phi(t-u,\tau)x_1(u+\tau/2)x_2^*(u-\tau/2)e^{-j2\pi f\tau}\,du\,d\tau \quad (2)$$

Expressions (1) and (2) are now used to define the following data spatial time-frequency distribution (STFD),

$$\mathbf{D}_{xx}(t,f) = \int_{-\infty}^{\infty}\int_{-\infty}^{\infty} \phi(t-u,\tau)\mathbf{x}(u+\tau/2)\mathbf{x}^H(u-\tau/2)e^{-j2\pi f\tau}\,du\,d\tau \quad (3)$$

where $[\mathbf{D}_{xx}(t,f)]_{ij} = D_{x_ix_j}(t,f)$, for $i,j = 1,2,....,n$, and the superscript "H" denotes the complex conjugate transpose of a matrix or a vector.

In several applications such as semiconductor manufacturing process, narrowband array processing, and image reconstruction, the following linear data model is assumed,

$$\mathbf{x}(t) = \mathbf{A}\mathbf{s}(t) + \mathbf{n}(t) \quad (4)$$

where the m x n spatial matrix **A** may be a mixing matrix or a steering matrix, depending on the application under consideration. The elements of the m x 1 vector **x**(t), which represents the measured or sensor data, are multicomponent signals, while the elements of the n x 1 vector **s**(t) are often monocomponent signals. **n**(t) is an additive noise, which is zero mean, white and Gaussian distributed process.

Due to the linear data model, the STFD takes the following structure

$$\mathbf{D}_{xx}(t,f) = \mathbf{A}\mathbf{D}_{ss}(t,f)\mathbf{A}^H \quad (5)$$

where $\mathbf{D}_{ss}(t,f)$ is the source TFD matrix of s(t), and the noise is neglected as a first step. We note that $\mathbf{D}_{xx}(t,f)$ is a matrix of dimension m x m, whereas $\mathbf{D}_{ss}(t,f)$ is of dimension n x n. For narrowband array signal processing applications, **A** holds the spatial information and maps the auto- and cross-TFDs of the source signals into auto- and cross-TFDs of the data.

Expression (5) is similar to that which has been commonly used in blind source separation and direction of arrival (DOA) estimation problems, relating the signal correlation matrix to the data spatial correlation matrix [4,5,6]. Here, these correlation matrices are replaced by the source and spatial time-frequency distribution matrices. This means that we can solve these problems in various applications using a new formulation which is more tuned to nonstationary signal environments.

The two subspaces spanned by the principle eigenvectors of $\mathbf{D}_{xx}(t,f)$ and the columns of **A** are identical. Since the off-diagonal elements are cross-terms of $\mathbf{D}_{ss}(t,f)$, then this matrix is diagonal for all (t-f) points which correspond only to the signal autoterms. In practice, to simplify the selection of such points of true high power localization, we apply the smoothing kernel $\phi(t,\tau)$ that may significantly decrease the contribution of the cross-terms in the t-f plane.

The new concept of the spatial time frequency distribution discussed above opens a new area of research in the field of nonstationary signal processing and allows time-frequency and bilinear distributions to play an important role in sensor signal processing.

3. FUNDAMENTAL OFFERINGS OF STFDS

There are five key advantages of array processing using time-frequency distributions which have not yet been properly presented and fully utilized. In order to clearly explain these advantages, we use the diagram in Fig.1. Two sources A and B are incident on a multisensor array. Source A occupies the time-frequency region R_a, whereas source B occupies the time-frequency region R_b. The time-frequency signatures of the two sources overlap, but each source still has a time-frequency region that is not intruded over by the other source. We will assume that the background noise is white.

1) Equation (5) can be easily derived for any arbitrary joint-variables. Time and frequency are indeed the two most commonly used and physically understood parameters. However, by replacing the spatial time-frequency distributions by spatial arbitrary joint-variable distributions, one can relate the sensor joint-variable distributions to the sources joint-variable distributions through the same mixing matrix **A**. As shown below, there are situations where it is preferable to consider other domains such as the ambiguity domain, where the locations of the signals and their cross-terms are guided by properties and mechanisms different than those associated with the time-frequency domain.

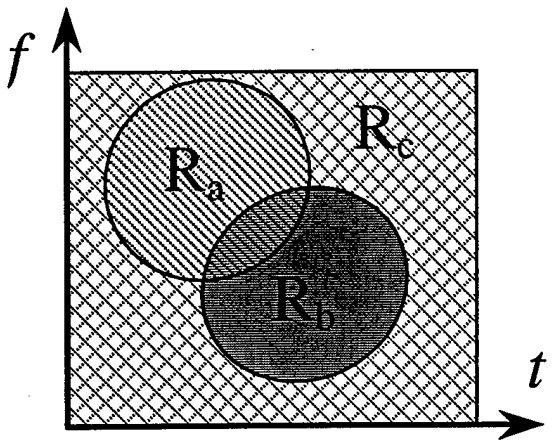

Fig.1 Signals with different time-frequency signatures

2) Equation (5) is valid for all time-frequency points. The main question is whether one time-frequency point suffices for adequate direction finding and source separation, and how sensitive the performance is to a random choice of a t-f point? Further, if several t-f points are used, then how to choose and combine these points for improved performance, and whether the method of combining should differ depending on the task in hand? Direction finding techniques require $\mathbf{D}_{ss}(t,f)$ to be full rank, preferably diagonal. Some blind source separation techniques demand the diagonal structure of the same matrix without degenerate eigenvalues. These properties along with high SNR requirements may be difficult to achieve using a single time-frequency point. We have identified two different methods to integrate several t-f points into equation (5). One method is based on a simple averaging performed over parts or the entire time-frequency regions of the signals of interest. The second method incorporates desirable time-frequency points into joint diagonalization or joint block diagonalization schemes. To illustrate both methods, we use in Section 4 the former scheme for direction finding whereas the second scheme is employed in Section 5 for blind source separation. Both methods aim to fully utilize the points of maximum power concentration and avoid the time-frequency region of significant noise contamination.

3) The time-frequency distribution of the white noise is distributed all over the time-frequency domain, whereas the TFDs of the source and jammer waveforms are likely to be confined to much smaller regions. Referring to Fig.1, the noise is spread over both R_a and R_b as well as the complement region R_c. If the time-frequency points (t,f) used in either the averaging or joint diagonalization approaches belong the noise only region R_c, then no information of the incident waveforms is used and, as such, no reasonable source localization and signal separation outcomes can be obtained. Accordingly the performance is expected to be worse than conventional approaches. On the other hand, if all points (t,f) in Fig.1 are used, and the employed TFD satisfies the marginal constraints such as the Wigner distribution, then it is easily shown that only the average power is considered. As a result, the problem simplifies to the second order covariance based matrix approach, traditionally used in high resolution angle of arrival estimation. This is an important property, as it casts the conventional techniques as special cases of the proposed framework based on time-frequency analysis. Finally, if we confine the (t,f) points to R_a and R_b, then only the noise part in these regions is included. The result of leaving out the points (t,f) which are not part of the time-frequency signatures of the signal arrivals is enhancing the input SNR to the source localization and signal separation techniques.

4) By only selecting (t,f) points which belong to the t-f signature of one source, then this source will be the only one considered by equation (5). This is, in essence, equivalent to implicitly performing spatial filtering to remove other sources from consideration. It is important to note that such removal does not come at the expense of reduction of the number of degrees of freedom, as it is the case in beamspace processing, but the problem remains a sensor space processing with the original number of degrees of freedom remains intact. This represents a key contribution of TFDs to the direction finding and angle estimation area. An antenna array can be used to localize a number of sources equal or even greater than its number of sensors. The fundamental condition is that there must be time-frequency regions over which the respective time-frequency signatures of the sources do not overlap. In principle, the lower limit on the size of such regions is a single time-frequency point. Referring to Fig.1 and considering the case of two sensors, if all t-f points incorporated in direction finding belong to region R_a and not R_b, then the signal subspace defined by equation (5) is one-dimensional. In effect, by excluding source B, a one-dimensional noise subspace is established. This allows us to proceed with noise-subspace based high resolution techniques for localization of source A. Within the proposed framework, one can localize one source at a time or a set of selected sources, depending on the array size, overlapping and distinct time-frequency regions, and the dimension of the noise subspace necessary to achieve the required resolution performance. The same concepts and advantages of t-f point selection discussed above for direction finding can be applied to blind source separations.

5) The a priori knowledge of some temporal characteristics or the nature of time-varying frequency contents of the sources may permit direct selection of the t-f regions used in equation (5). In general, if we choose a joint-variable domain, where a class of signals collapses to a specific known joint-variable region, then one can perform direction finding and source separation for only this specific class. For instance, it is known that in the ambiguity domain all fixed frequency sinusoidal signals map to the vertical axis, no matter what their amplitudes, frequencies, and phases are. By only incorporating the points on the vertical axis, which

represents the time-lag variable, we have, in fact, focussed on separating and localizing narrowband components in the presence of broadband signals or jammers.

4. THE JOINT-VARIABLE MUSIC (JV MUSIC)

The joint-variable MUSIC is a new array signal processing method which is based on joint-variable signal representations. This method computes the spatial joint-variable distributions to solve the problem of the direction of arrival (DOA) estimation. In this approach, we average the spatial joint-variable matrices over several joint-variable points for the purpose of noise and crossterm reduction.

Let the spatial joint-variable distribution define all spatial distributions for which the respective source and sensor bilinear distributions are related by matrix **A**, as in equation (5). By performing the singular value decomposition (SVD) [7] of the spatial joint-variable matrix $\mathbf{D}_{xx}(\alpha,\beta)$, we obtain

$$\mathbf{D}_{xx}(\alpha,\beta)=[\mathbf{E}_s\ \mathbf{E}_n]\mathbf{D}[\mathbf{E}_s\ \mathbf{E}_n]^H \qquad (6)$$

where $\mathbf{D}$ is a diagonal matrix. $\mathbf{E}_s$ and $\mathbf{E}_n$, which respectively span the signal subspace and the noise subspace, are fixed and independent of the joint-variable point (α,β). The columns of $\mathbf{E}_s$ span the signal subspace, which is also spanned by the columns of matrix **A**. A simple way to estimate $\mathbf{E}_s$ and $\mathbf{E}_n$ is to perform the SVD on a single matrix $\mathbf{D}_{xx}(\alpha,\beta)$. But one time-frequency point may carry insufficient SNR or be highly contaminated by crossterms. To avoid this problem, we propose to perform averaging over several (α,β) points, exploiting the joint structure of the spatial matrices. If averaging is performed over the joint-variable region $\Omega, (\alpha_i,\beta_i)\in\Omega$, then the SVD applied to the averaged spatial joint-variable matrix leads to

$$\overline{\mathbf{D}}_{xx}(\alpha,\beta)=\sum_{i\in\Omega}\mathbf{D}_{xx}(\alpha_i,\beta_i)=[\overline{\mathbf{E}}_s\ \overline{\mathbf{E}}_n]\overline{\mathbf{D}}[\overline{\mathbf{E}}_s\ \overline{\mathbf{E}}_n]^H \qquad (7)$$

In the presence of noise, the MUSIC algorithm is applied to the perturbed noise subspace matrix $\hat{\overline{\mathbf{E}}}_n$. The joint-variable MUSIC (JV-MUSIC) algorithm estimates the DOAs by finding the N largest peaks of the localization function

$$f(\theta)=\left|\hat{\overline{\mathbf{E}}}_n^H\mathbf{a}(\theta)\right|^{-2}. \qquad (8)$$

where $\mathbf{a}(\theta)$ is the steering vector. The value of N is determined by the number of sources captured in the region Ω. If the joint-variable distribution satisfies the marginal constraints, then averaging over the entire domain will lead to the total power, yielding the conventional MUSIC. In the following, we present two simple cases of the joint-variable MUSIC, namely, the *Time-Frequency MUSIC* and the *Ambiguity-Domain MUSIC.*

4.1. Time-Frequency MUSIC (TF MUSIC)

The purpose of this example is to show that the TF MUSIC based on joint diagonalization gives good angle estimation performance for various time-frequency kernels. The performance of the classical MUSIC [4] is compared to that of the proposed TF-MUSIC using: i) the Wigner kernel ii) the Choi-Williams kernel [1], and iii) the Born-Jordan kernel [1]. Consider a uniform linear array of 4 sensors separated by half a wavelength and receiving signals from 2 sources. The source signal arriving at θ_1 = 10 degrees and θ_2 = -10 degrees, respectively, are of unit variance. The signal is composed of a chirp signal whose start and end frequencies are $\omega_1 = 0.17\pi$ and $\omega_2 = 0.67\pi$, respectively. The noise used in this simulation is zero-mean, Gaussian distributed, and temporally white. The noise power or σ^2 is adjusted to give the desired $SNR=10\log_{10}(\sigma^{-2})$. Fifty STFD matrices corresponding to (t,f) autoterm points are averaged. The variance of the estimated DOAs is computed over 100 independent trials. Figure 2 displays the variance of the estimated DOA $\hat{\theta}_1$ versus SNR for 500 samples. The solid line presents the classical MUSIC algorithm. The dashed line, the dash-dot line and the dotted line correspond to the TF-MUSIC using Choi-Williams kernel, Born-Jordan kernel and Wigner kernel, respectively. According to this plot, the convetional MUSIC and TF-MUSIC based on the above three kernels give similar results. The offerings and advantages of the TF MUSIC in direction finding for different classes of nonstationary signals require extensive analysis and simulations, which are not presented in this paper.

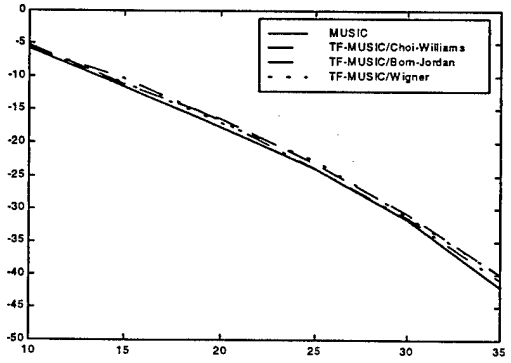

Fig.2 Variance of $\hat{\theta}_1$ vs. SNR

4.2. Ambiguity-Domain MUSIC (AD MUSIC)

Consider the scenario of a four-element equi-spaced linear array, where one chirp signal and two sinusoidal signals are received. All three signals have the same

power of 20 dB, whereas the noise power is assumed to be 0 dB. The angles of arrival of the chirp signal and the sinusoidal signals are 15, 10, and 0 degrees, respectively. The joint-variables are now the frequency-lag and the time-lag $(\alpha,\beta)=(\theta,\tau)$. While the ambiguity function of the chirp signal sweeps the ambiguity domain with contribution at the origin, the exact autoterm ambiguity function $A(\theta,\tau)$ of the narrowband arrivals $s_1(t)$ and $s_2(t)$ is zero for non-zero frequency-lags and may have non-zero values only along the vertical axis θ=0. This function is given by

$$A(\theta,\tau)=C(s_1(\tau)+s_2(\tau))\delta(\theta) \qquad (9)$$

where C is a constant which depends on the signal power, and $\delta(\theta)$ is the Kronecker delta function. In this simulation example, we selected 14 points on the time-lag axis, excluding the origin, and as such emphasizing the narrowband components. The data record has 128 samples and the ambiguity function is computed by taking 128-by-128 FFT of the Wigner distribution. Figure 3 shows the ambiguity-domain where the two vertical lines represent the crossterms between the sinusoidal components. Fig. 4 shows two MUSIC spectra, one corresponds to the conventional method and the other corresponds to the ambiguity-domain (AD) MUSIC. There are two dominant eigenvalues for the case of the AD MUSIC, since we have not deliberately considered the chirp signal through our careful selection of the ambiguity-domain points. It is clear that the AD MUSIC resolves the two sinusoidal signals, while the conventional MUSIC could not separate the three signals. Next, in order to show that non-careful point selections may prove unwise as well as to illustrate the ineffectiveness of working with joint-variable regions with no signal power, we average over the region Ω indicated in the Fig. 3, where the incoming signals have very weak presence. The result is shown in Fig. 5. It is evident from this figure that because of the lack of information in this region, the AD MUSIC fails to localize any of the three signals.

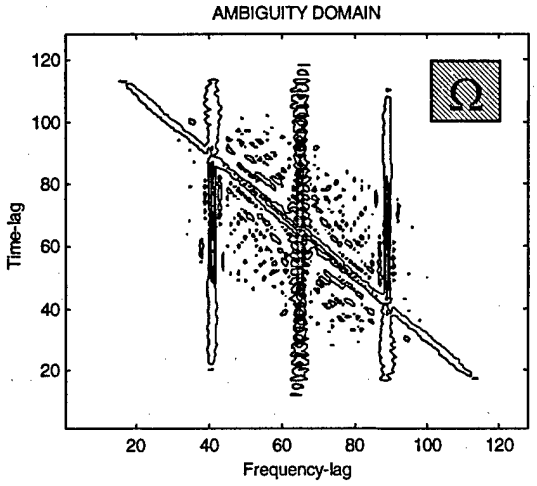

Fig.3 Ambiguity domain of one chirp and two sinusoidal signals (Ω: A region used to estimate the AD MUSIC spectrum in Fig. 5)

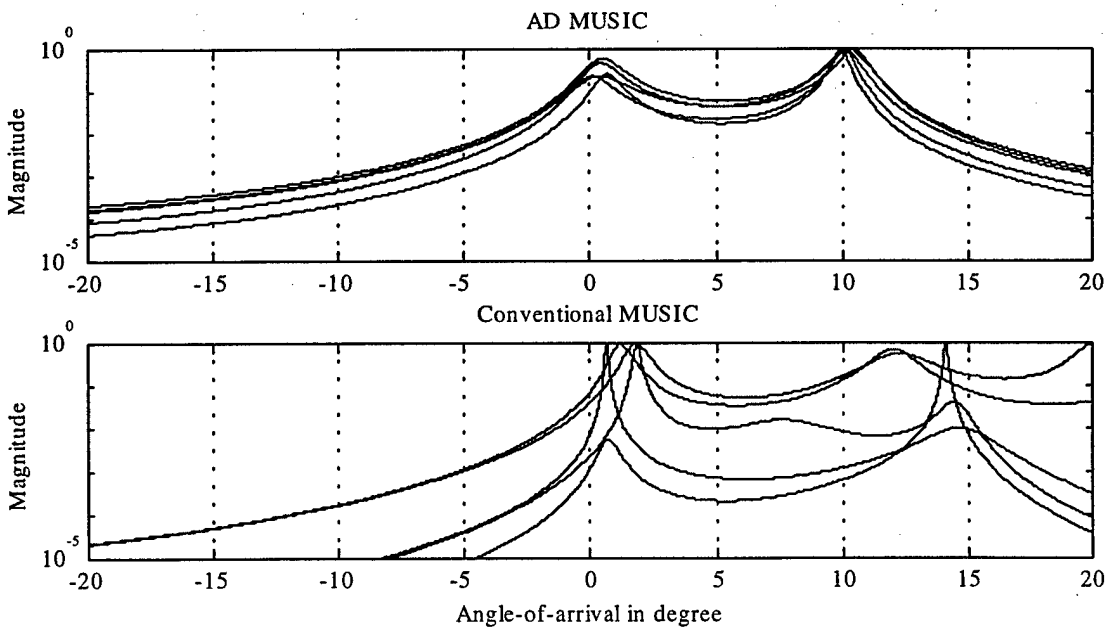

Fig.4 AD MUSIC and conventional MUSIC spectra

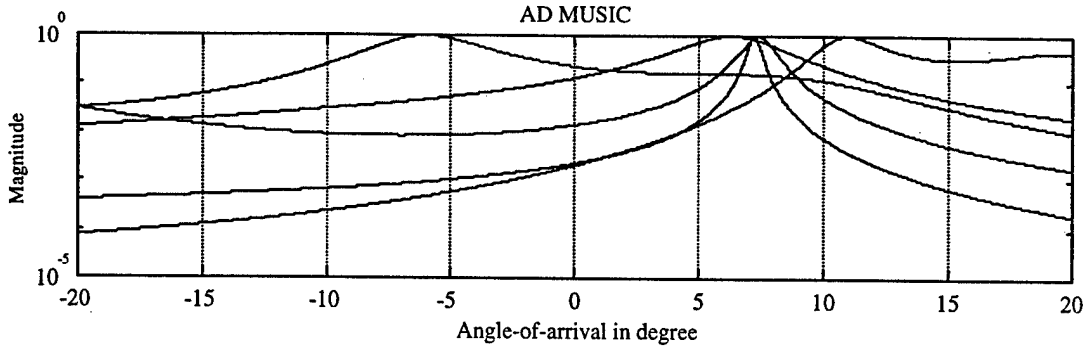

Fig.5 AD MUSIC spectrum

5. THE JOINT-VARIABLE BLIND SOURCE SEPARATION

Let $\mathbf{W}$ denote n x m matrix such that $(\mathbf{WA})(\mathbf{WA})^H = \mathbf{UU}^H = \mathbf{I}$, i.e., $\mathbf{WA}$ is an n x n unitary matrix (This matrix is referred to as a whitening matrix, since it whitens the signal part of the observations). Pre- and post-multiplying the spatial joint-variable distribution matrices $\mathbf{D}_{xx}(\alpha,\beta)$ by $\mathbf{W}$, we obtain the whitened spatial matrix

$$\tilde{\mathbf{D}}_{xx}(\alpha,\beta) = \mathbf{W}\mathbf{D}_{xx}(\alpha,\beta)\mathbf{W}^H \qquad (10)$$

From equations (5) and (10), we may express $\tilde{\mathbf{D}}_{xx}(\alpha,\beta)$ as

$$\tilde{\mathbf{D}}_{xx}(\alpha,\beta) = \mathbf{U}\mathbf{D}_{ss}(\alpha,\beta)\mathbf{U}^H \qquad (11)$$

Since matrix $\mathbf{U}$ is unitary and $\mathbf{D}_{ss}(\alpha,\beta)$ is diagonal, expression (11) shows that any whitened data spatial JV distribution (SJVD)-matrix is diagonal in the basis of the columns of the matrix $\mathbf{U}$ (the eigenvalues of $\tilde{\mathbf{D}}_{xx}(\alpha,\beta)$ being the diagonal entries of $\mathbf{D}_{ss}(\alpha,\beta)$).

If, for the (α_i,β_i) point, the diagonal elements of $\mathbf{D}_{ss}(\alpha_i,\beta_i)$ are all distinct, the unitary matrix $\mathbf{U}$ may be 'uniquely' (i.e. up to permutation and phase shifts) retrieved by computing the eigendecomposition of $\tilde{\mathbf{D}}_{xx}(\alpha,\beta)$. However, when the α-β domain signatures of the different signals are not highly overlapping or frequently intersecting, which is likely to be the case, the selected (α_i,β_i) point often corresponds to a single signal auto-term, rendering matrix $\mathbf{D}_{ss}(\alpha_i,\beta_i)$ deficient. That is, only one diagonal element of $\mathbf{D}_{ss}(\alpha_i,\beta_i)$ is different from zero. It follows that the determination of the matrix $\mathbf{U}$ from the eigendecomposition of a single whitened data SJVD-matrix is no longer 'unique' in the sense defined above. The situation is more favorable when considering simultaneous diagonalization of a combined set $\{\tilde{\mathbf{D}}_{xx}(\alpha_i,\beta_i) \mid i = 1,.....,p\}$ of p matrices. This amounts to incorporating several (α_i,β_i) points in the source separation problem. It is noteworthy that two source signals with identical (α_i,β_i) signatures can not be separated even with the inclusion of all information in the α-β plane.

The joint diagonalization (JD) [8,9] can be explained by first noting that the problem of the diagonalization of a single n x n normal matrix $\mathbf{M}$ is equivalent to the minimization of the criterion [7]

$$\mathbf{C}(\mathbf{M},\mathbf{V}) \stackrel{def}{=} -\sum_i \mid \mathbf{v}_i^* \mathbf{M} \mathbf{v}_i \mid^2 \qquad (12)$$

over the set of unitary matrices $\mathbf{V} = [\mathbf{v}_1,...,\mathbf{v}_n]$. Hence, the joint diagonalization of a set $\{M_k \mid k = 1..k\}$ of K arbitrary n x n matrices is defined as the minimization of the following JD criterion:

$$\mathbf{C}(\mathbf{V}) \stackrel{def}{=} -\sum_k \mathbf{C}(\mathbf{M}_k,\mathbf{V}) = -\sum_{ki} \mid \mathbf{v}_i^* \mathbf{M}_k \mathbf{v}_i \mid^2 \qquad (13)$$

under the same unitary constraint. An efficient joint approximate diagonalization algorithm exists in [8] and it is a generalization of the Jacobi technique [7] for the exact diagonalization of a single normal matrix.

Equations (10) - (13) constitute the blind source separation approach based on joint-variable distributions which is summarized by the following steps:

- Determine the whitening matrix $\hat{\mathbf{W}}$ from the eigendecomposition of an estimate of the covariance matrix of the data,

- Determine the unitary matrix $\hat{\mathbf{U}}$ by minimizing the joint approximate diagonalization criterion for a specific set of whitened JVD matrices $\{\tilde{\mathbf{D}}_{xx}(\alpha_i,\beta_i) \mid i = 1,.....,p\}$,

- Obtain an estimate of the mixture matrix $\hat{\mathbf{A}}$ as $\hat{\mathbf{A}} = \hat{\mathbf{W}}^{\#}\hat{\mathbf{U}}$, where the superscript # denotes the Pseudo-inverse, and an estimate of the source signals $\hat{\mathbf{s}}(t)$ as $\hat{\mathbf{s}}(t) = \hat{\mathbf{U}}^H \mathbf{W}\mathbf{x}(t)$.

In Figure 6, we show an example of the application of the proposed spatial joint-variable distributions to the

blind source separation problem. In this case, the two variables are time and frequency [10]. A three-element equi-spaced linear array is considered. Two chirp signals arrive from far-field at -10 and 10 degrees. The number of data samples used to compute the STFD is 128. The number of t-f points employed in the joint-diagonalization is p=128, with equal number of points on each signature. In this example, the mixing matrix **A** is chosen to be

$$\mathbf{A} = \begin{bmatrix} 1 & 1 \\ 0.8549+0.5189i & 0.8549-0.5189i \\ 0.4615+0.8871i & 0.4615-0.8871i \end{bmatrix}$$

Fig.6(b) shows the time-frequency distributions of two linear mixtures of the original chirp signals depicted in Fig.6(a), corresponding to the data at the first and the second sensors. Using the spatial time frequency distributions, we are able to recover the original signals from their observed mixture, as shown in Fig.6(c).

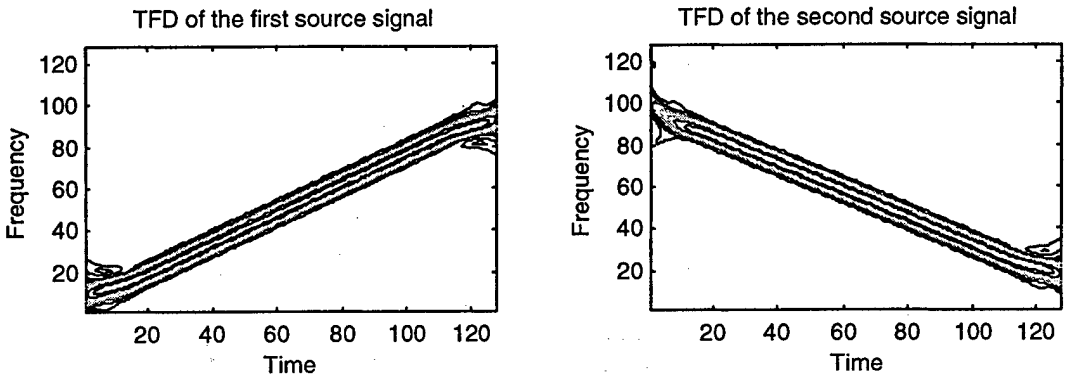

(a) TFD of the source signals

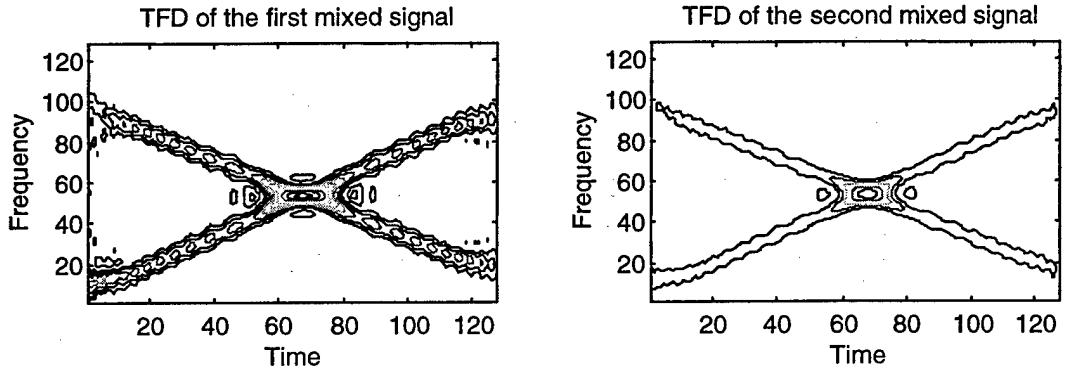

(b) TFD of the mixed signals

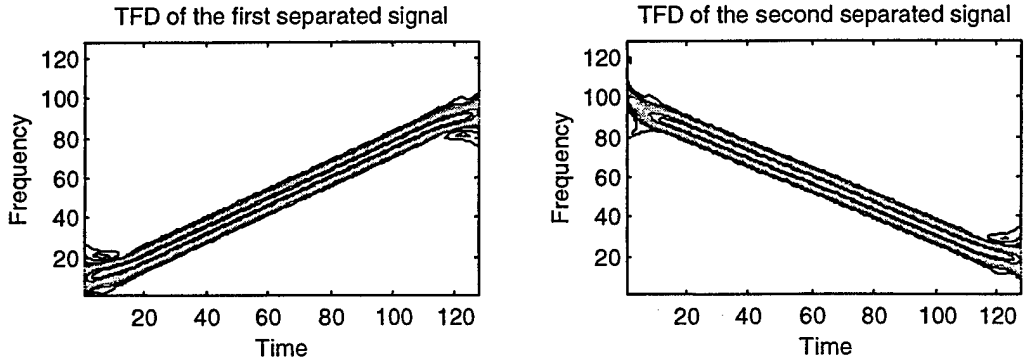

(c) TFD of the separated signals

Fig.6 Blind source separation based on spatial time-frequency distribution

6. SPATIAL AVERAGING TIME-FREQUENCY DISTRIBUTIONS

Symmetric spatial averaging method was proposed by Pillai [6] to restore the full-rank property of the signal covariance matrix in the presence of coherent signals. Unlike other spatial smoothing methods [11,12], which only restore the full rank property of the mixing matrix when the impinging signals are coherent, the symmetric spatial averaging method decorrelates the signal arrival in the sense that it imposes a diagonal structure on the signal correlation matrix. This property is essential to source separation methods, as previously discussed. Here we extend the spatial averaging method to TFD analysis, and propose the signal separation method by joint diagonalization (JD) based on spatial averaging TFDs.

The basic idea of symmetric spatial averaging is to use a symmetric subarray to obtain an averaged covariance matrix, or in the underlying problem, an averaged STFD matrix, with a diagonal structure.

To simplify the notation, we use the same model of two signal arrivals, $s_1(t)$ and $s_2(t)$. The result is generally true for n sources and N sensors as long as $n<N$. The cross-TFD of the data $x_0(t)$ and $x_i(t)$, i= 0, 1, 2, ..., N-1, is

$$D_{x_0x_i}(t,f) = \left[D_{s_1s_1}(t,f)+D_{s_2s_1}(t,f)\right]e^{jd_i\omega_1}+\left[D_{s_2s_2}(t,f)+D_{s_1s_2}(t,f)\right]e^{jd_i\omega_2} \quad (14)$$

where we used d_0=0. Denote $b_1 = D_{s_1s_1}(t,f)+D_{s_2s_1}(t,f)$ and $b_1 = D_{s_2s_2}(t,f)+D_{s_1s_2}(t,f)$. The values of b_1 and b_2 are generally complex. We add N-1 array sensors symmetrically about the reference point, as shown in Fig.7. Thus, we have the new cross-TFD of $x_0(t)$ and $x_{-i}(t)$,

$$D_{x_0x_{-i}}(t,f) = \left[D_{s_1s_1}(t,f)+D_{s_2s_1}(t,f)\right]e^{-jd_i\omega_1}+\left[D_{s_2s_2}(t,f)+D_{s_1s_2}(t,f)\right]e^{-jd_i\omega_2} \quad (15)$$

The spatial averaging of (14) and (15) is given by

$$\tilde{D}_{xx}^{(i)}(t,f) = \left\{D_{x_0x_i}(t,f)+D^*_{x_0x_{-i}}(t,f)\right\}/2 = b_1 e^{jd_i\omega_1}+b_2 e^{jd_i\omega_2} \quad (16)$$

where

$$b_1 = D_{s_1s_1}(t,f)+\mathrm{Re}\left\{D_{s_2s_1}(t,f)\right\}$$
$$b_2 = D_{s_2s_2}(t,f)+\mathrm{Re}\left\{D_{s_1s_2}(t,f)\right\}$$

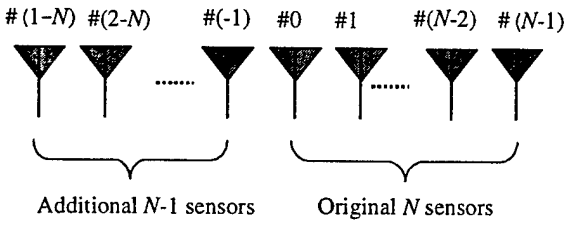

Fig.7 Array configuration for spatial averaging

The matrix

$$\tilde{\mathbf{D}}_{xx}(t,f) = \begin{bmatrix} \tilde{D}_{xx}^{(0)}(t,f) & \tilde{D}_{xx}^{(1)}(t,f) & \cdots & \tilde{D}_{xx}^{(N-1)}(t,f) \\ \tilde{D}_{xx}^{(1)*}(t,f) & \tilde{D}_{xx}^{(0)}(t,f) & \cdots & \tilde{D}_{xx}^{(N-2)}(t,f) \\ \vdots & \vdots & \ddots & \vdots \\ \tilde{D}_{xx}^{(N-1)*}(t,f) & \tilde{D}_{xx}^{(N-2)*}(t,f) & \cdots & \tilde{D}_{xx}^{(0)}(t,f) \end{bmatrix} \quad (17)$$

is Hermitian and Toeplitz. It is referred to as the spatially- averaged TFD (SATFD) matrix. In the noise-free environment, the SATFD matrix can be expressed as

$$\tilde{\mathbf{D}}_{xx}(t,f) = \mathbf{A}\tilde{\mathbf{D}}_{ss}\mathbf{A}^H \quad (18)$$

where

$$\tilde{\mathbf{D}}_{ss}(t,f) = \mathrm{diag}[b_1 \quad b_2] \quad (19)$$

is the equivalent TFD matrix of the source signals. Note that the diagonal terms in $\tilde{\mathbf{D}}_{ss}(t,f)$ are real and made up of both autoterms and crossterms. Clearly, (18) has the same format as (5), but $\tilde{\mathbf{D}}_{ss}(t,f)$ here is diagonal even with the presence of TFD crossterms. As such, symmetric spatial averaging ensures the validity of the TFD-based signal separation in the presence of cross-TFD. The procedure for source separation using spatially-averaged STFD at several (t,f) points is the same as the steps outlined in Section 5.

The effectiveness of the spatially-averaged time-frequency distribution in source separation is demonstrated by the following examples. The joint diagonalization is used for incorporating multiple time-frequency points into the proposed spatial averaging method. In all simulations, there are two sources with chirp signals

$$s_1(t) = e^{-j\mu\frac{t^2}{2}}, \quad s_2(t) = e^{-j\mu\frac{t^2}{2}-j\omega t},$$

where μ is chosen as 0.008π. Different values of ω are considered. 128 data samples are used, from which a time-frequency matrix of 128 x 128 is formed. The DOAs of the two signals $s_1(t)$ and $s_2(t)$ are set equal to 30° and 60°, respectively, from the broadside direction. Furthermore, we assume an equi-spaced 5-element linear array with the interelement spacing 0.5λ, where λ is the wavelength. Subsequently, when spatial averaging method is used, two sub-arrays are formed, each with 3 elements.

The Wigner-Ville (WV) distribution of each signal is shown in Fig.8, where δf (=$\omega/2\pi$) is set equal to 0.05. Fig.9 shows the mixed time-frequency distribution at the center array sensor. No noise is present for this case. It is clear that crossterms lie in the middle of the two chirps, and their amplitudes change periodically. Fig.10(a) shows the WV distributions of the separated signals, where joint diagonalization is used without the utilization of the proposed spatial averaging method.

Three time-frequency (t, f) points are used at t = 32, 64, and 96. The frequency f is chosen so that the TFD at the center array sensor is the largest at each value of t. Peak values of the WV distribution may either correspond to autoterm or crossterm. In this case, out of three (t, f) points, one crossterm point is selected. The obtained $\hat{\mathbf{A}}^{\#}\mathbf{A}$ matrix is

$$\hat{\mathbf{A}}^{\#}\mathbf{A} = \begin{bmatrix} 0.46 + j0.46 & 0.82 - j0.44 \\ 0.54 - j0.46 & 0.17 + j0.44 \end{bmatrix}$$

and the computed global rejection level I_{perf} is –1.8 dB. This level is defined as

$$I_{perf} = \sum_{q \neq p} I_{pq} \qquad (20)$$

where $I_{pq} = E\left|(\hat{\mathbf{A}}^{\#}\mathbf{A})_{pq}\right|^2$ measures the ratio of the power of the interference of qth source to the power of the pth source signal. The above result is unsatisfactory, as the matrix $\hat{\mathbf{A}}^{\#}\mathbf{A}$ is far from diagonal and the crossterms clearly appear at the separated signals.

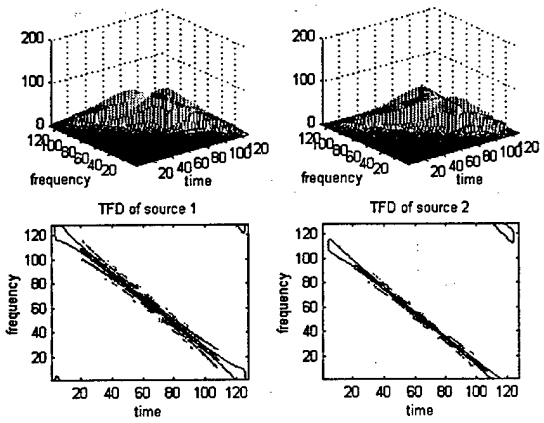

Fig.8 TFD of the source signals

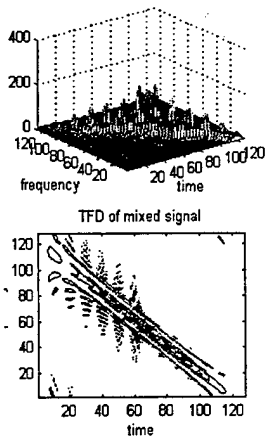

Fig.9 TFD of the mixed signal

Next, we force the selection of autoterm points along the instantaneous frequency of the two input signals. Although no crossterm point is selected, yet because of the finite data record, the crossterms leak into autoterm regions and cause different degrees of contamination. We show in Fig.10(b) the result of source separation when only the autoterm points are used. The obtained $\hat{\mathbf{A}}^{\#}\mathbf{A}$ matrix becomes

$$\hat{\mathbf{A}}^{\#}\mathbf{A} = \begin{bmatrix} 1.00 + j0.01 & 0.00 - j0.06 \\ 0.00 - j0.01 & 1.00 + j0.06 \end{bmatrix}$$

and the computed global rejection level I_{perf} is –23.9 dB. It is clear that the source separation performance is greatly improved. This implies that crossterm contribution at the selected (t, f) points were insignificant.

Fig.11(a) and Fig.11(b) show the time-frequency distributions of the separated signals under the same conditions as in Fig.10(a) and Fig.10(b), respectively, except with the utilization of the spatial averaging method. The spatial averaging entirely mitigates the

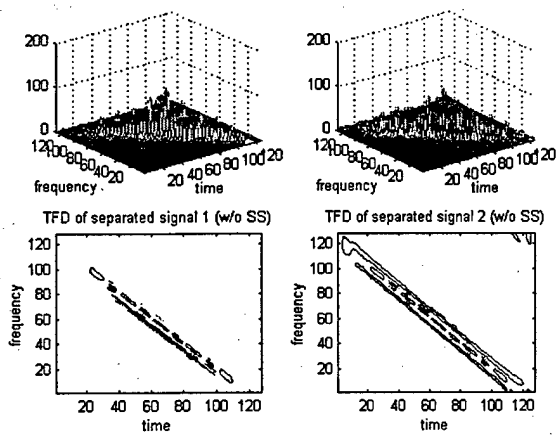

(a) TFD evaluated at peak points

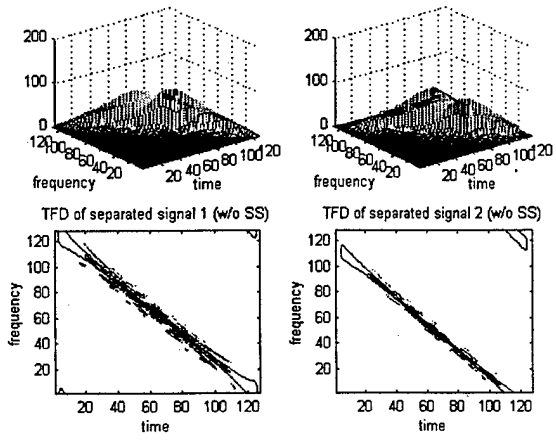

(b) TFD evaluated at autoterm points

Fig.10 TFD of the separated signals without spatial averaging

effect of crossterm.

It is clear that the time-frequency distributions of the separated signals in both cases are the same as those of the original source signals, and $\hat{\mathbf{A}}^{\#}\mathbf{A}$ are exactly identity matrices.

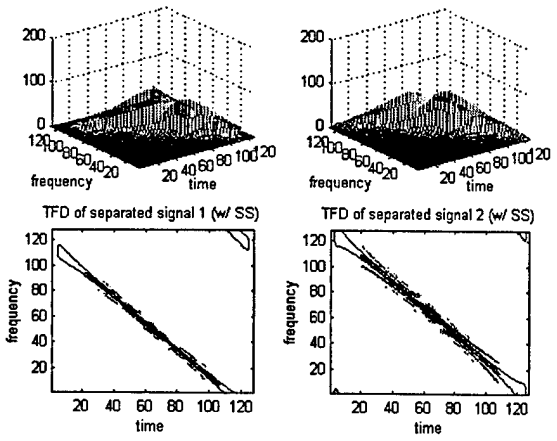

(a) TFD evaluated at peak points

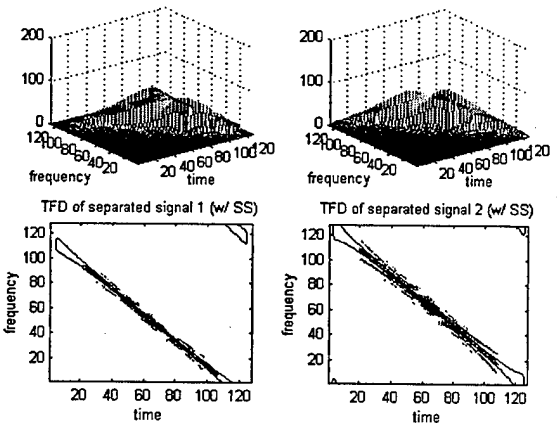

(b) TFD evaluated at peak points

Fig.11 TFD of the separated signals with spatial averaging

Fig.12 shows the global rejection level I_{perf} versus the frequency difference δf between the two chirps, where the input SNR is 20dB. When the proposed spatial averaging method is applied, the global rejection level keeps very low value, irrespective of whether some or all of the (t, f) points correspond to autoterms. On the other hand, without spatial averaging, the results show very high global rejection levels. The main reason of large variation of the I_{perf} without using the spatial averaging method is that the number as well as the influence of crossterm points selected is dependent on the frequency difference δf (when δf =0.1, no crossterm points are chosen). Note that crossterms of the WV distribution remain high even when the frequency difference is large, and therefore when selected they cause tremendous error, as evident in the figure. When only autoterm (t, f) points are used, the global rejection level decreases as δf increases. In this case, the crossterm contribution at the autoterm points becomes smaller for higher values of δf.

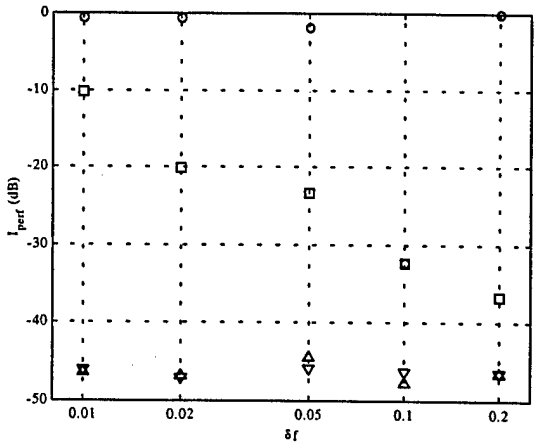

Fig.12 Global rejection level versus. frequency difference (input SNR=20 dB, o: without spatial averaging, Δ: with spatial averaging, □: without spatial averaging using autoterm points, ∇: with spatial averaging using autoterm points)

7. CONCLUSIONS

The main objectives of this paper were twofold: 1) demonstrating that high resolution subspace-based methods can be performed by involving no longer the exact moments but rather the auto- and cross- time-frequency distributions of the data received by the multisensor array; 2) developing blind source separation methods based on the difference in the time-frequency localization properties of the signal arrivals and provide a generalization to arbitrary joint variables. Also, the paper presented, in general terms, the key offerings and advantages of utilizing the power localization properties of the signals incident on an antenna array to improve array performance. There are still important issues in the above two applications of time-frequency distributions remain to be explored and resolved. Among these issues are performance dependence on noise level, smoothing kernels, spatial smoothing and subarray averaging, non-localizable source signals, correlated and coherent sources, and spatial distributed sources due to local scattering.

Symmetric spatial averaging of spatial time-frequency distributions has also been introduced. The spatial averaging of the spatial time-frequency distributions of the data across an antenna array removes cross-terms in between the impinging signals. These terms reside along the off-diagonal entries of the source time-frequency distribution matrix, and consequently impede the source separation performance, which is based on the matrix diagonal structure. Spatial averaging amounts to forming

a spatial Hermition Toeplitze matrix using the time-frequency distributions of the data across one half of the array. This matrix is then added to the spatial matrix corresponding to the other half of the array. The desired effect of this averaging is moving the interaction between the source signals in the time-frequency domain from the off-diagonal locations to the diagonal elements of the TFD matrix [13,14]. In this respect, unlike the method proposed in [10], cross-terms, due to their high potential values, are regarded as useful components that could be properly used for improved performance. Spatial averaging can be applied to all members of Cohen's class of TFDs, irrespective of the employed smoothing kernel. When using a time-frequency kernel, the problem amounts to averaging in all three dimensions of time, frequency, and space.

Two source separation schemes incorporating the spatially averaged time-frequency distributions can be applied [14]. The first scheme is the same as the one introduced in reference [10], where joint diagonalization is applied to several spatially averaged TFD matrices corresponding to multiple time-frequency points. In the second scheme, the spatially- averaged TFD matrices evaluated at different t-f points are averaged and the result is then diagonalized and used for estimating the source signals. Both schemes are based on converting the problem into unitary mixture through whitening the original mixture. The source signals are then provided from the estimated unitary matrix through Pseudo matrix inversion. With cross-terms moved to the diagonal entries of the TFD matrix, the prime task of either source separation scheme is to avoid degenerate eigenvalues which are responsible for non-uniqueness solution of the problem.

Simulations examples were presented to illustrate the effectiveness of the new approach based on joint diagonalization. The two performance measures used were the global rejection level and the values of the off-diagonal elements of the product of the mixing matrix and the Pseudo inverse of its estimate. Two sources and five sensors were considered. The source signal were chirp signals with the same sweeping frequency, but their constant frequencies were offset by different values. The Wigner-Ville distribution was considered. It was shown that the spatial averaging method significantly improves the performance measures over the non-spatially averaging method, specifically when the two signals have close time-frequency signatures. Without spatial-averaging, performance is very sensitive to whether the auto-term or cross-term points, or their mix, are incorporated in the source separation procedure. With spatial averaging, this is no longer a concern, since both terms become diagonal entries of the TFD matrix.

8. ACKNOWLEDGEMENTS

This work is supported by ONR under Grant #N00014-98-1-0176.

9. REFERENCES

[1] L. Cohen, "Time-frequency distributions - a review," *Proceedings of the IEEE*, vol. 77, no. 7, pp. 941-981, July 1989.

[2] B. Boashash, " Time-frequency signal analysis," in *Advances in Spectrum Analysis and Array Processing*, S. Haykin, editor, vol. 1 and 2, Chapter 9, pages 418-517, Prentice-Hall, Englewood Cliffs, New Jersey, 1990.

[3] S. Qian and D. Chen, *Joint Time-Frequency Analysis - Methods and Applications*, Prentice-Hall, Englewood Cliffs, New Jersey, 1996.

[4] R. O. Schmidt, "Multiple emitter location and signal parameter estimation," *IEEE Trans. Antennas and Propagation.*, vol. 34, no. 3, pp. 276-280, March 1986.

[5] D. Johnson and S. DeGraaf, "Improving the resolution of bearing in passive sonar arrays by eigenvalue analysis," *IEEE Transactions on Acoustics, Speech, and Signal Processing*, vol. 30, no. 4, pp. 638-648, Aug., 1992.

[6] S. U. Pillai, *Array Signal Processing*, Springer-Verlog, 1989.

[7] G. H. Golub and C.F. Van Loan, *Matrix Computations*, The Johns Hopkins University Press, 1989.

[8] A. Belouchrani, K. A. Meraim, H.-F. Cardoso, and E. Moulines, "A blind source separation techniques using second order statistics," *IEEE Transactions on Signal Processing*, vol. 45, no. 2, pp. 434-444, Feb. 1997.

[9] M. Wax and J. Sheinvald, "A least squares approach to joint diagonalization," *IEEE Signal Processing Letters*, vol. 41, pp. 52-52, Feb. 1997.

[10] A. Belouchrani and M. Amin, "Blind source separation based on time-frequency signal representation," *IEEE Transactions on Signal Processing*, vol. 46, no. 11, pp. 2888-2898, Nov. 1998.

[11] J. E. Evans, J. R. Johnson, D. F. Sun, "High resolution angular spectrum estimation techniques for terrain scattering analysis and angle of arrival estimation," in *Proc. 1st ASSP Workshop on Spectral Estimation*, Hamilton, Canada, Aug. 1981.

[12] T. J. Shan and T. Kailath, "On spatial smoothing for DOA estimation of coherent sources," *IEEE Trans. Acoust., Speech, Signal Processing*, vol.33, no.4, pp.806-811, 1985.

[13] Y. Zhang and M. Amin, "Spatial averaging of time-frequency distributions", in *Proc. 1999 IEEE International Conference on Acoustics, Speech, and Signal Processing*, Phoenix, Arizona, March 1999.

[14] Y. Zhang and M. Amin, "Spatial averaging of time-frequency distributions for source separations", submitted to *IEEE Trans. Signal Processing*, Feb. 1999.

A Subband MUSIC Technique for Direction Finding

Weifeng Mu, Yimin Zhang, and Moeness G. Amin
Department of Electrical and Computer Engineering
Villanova University, Villanova, PA 19085

Abstract

The problem of direction finding of waveforms incident on a multi-sensor array is of importance in many areas, including wireless communications. The MUSIC and maximum likelihood techniques have been widely and successfully applied to solve this problem. This paper examines the performance of a hybrid technique that combines the MUSIC algorithm and subband signal decompositions. It is shown that, for narrowband and polynomial phase signals, the subband decomposition increases the input signal-to-noise ratio, and thus yields improved performance over the conventional MUSIC technique. This improvement is more pronounced for high noise power levels.

I. Introduction

The problem of direction finding of waveforms incident on a multi-sensor array has drawn much attention during the past two decades [1]. Among various methods, the MUSIC [2] and maximum likelihood (ML) [3] techniques have been the front candidates to solve this problem. The eigenstructure-based approach underlying the MUSIC technique permits high resolution direction finding of multiple signals to be realized by a single spatial search instead of multi-dimensional costly optimization scheme, which is required for the ML method. Several papers have been written analyzing the performance of the MUSIC algorithm, including [4,5]. One fundamental drawback of the MUSIC technique, however, is that when the noise level is high, the signal and noise subspaces may be significantly corrupted, leading to highly biased and unstable estimates of the angles-of-arrival (AOAs) of the impinging waveforms[1].

In this paper, we propose a subband MUSIC approach to overcome the above drawback and improve the localization performance of the traditional MUSIC technique under high noise levels. Both narrowband signals and non-stationary polynomial phase signals are considered. The proposed method is a hybrid technique that combines both the MUSIC algorithm and subband signal processing. In the presence of narrowband or polynomial phase signals, the new method increases the input signal-to-noise ratio (SNR) by discarding the noise-only frequency samples computed over successive overlapping and disjoint data blocks. The effect of enhancing the SNR on performance is more pronounced for weak signals than signals with high SNR. It is shown that for high noise power conditions, the increase in SNR due to subband decompositions results in an improved MUSIC algorithm.

This work is supported by ONR Grant no. N00014-98-1-0176

II. Problem formulation

Assume n plane waves incident on an array of m sensors where $n<m$. The variance of the MUSIC AOA estimation error of the ith incident waveform, $\mathrm{var}_{MU}(\hat{\omega}_i)$, is given in [4] as

$$\mathrm{var}_{MU}(\hat{\omega}_i) = \frac{\sigma^2}{2N \cdot h(\omega_i)}\left[\sum_{k=1}^{n}\frac{\lambda_k}{(\sigma^2-\lambda_k)^2}\left|a^H(\omega_i)s_k\right|^2\right] \quad (1)$$

where N, σ^2, and $a(\omega)$ are, respectively, the total number of data samples, the noise level, and the steering vector. In equation (1), λ_k (k=1, 2, ..., n) and s_k denote the largest n eigenvalues of the data covariance matrix and the corresponding eigenvectors. $\omega_i = \pi sin(\theta_i)$ defines the ith spatial frequency of the respective AOA θ_i whose estimate is denoted as $\hat{\omega}_i$. The function $h(\omega_i)$ is given by

$$h(\omega_i) = d^H(\omega_i)GG^Hd(\omega_i) \quad (2)$$

where $d(\omega)=da(\omega)/d\omega$ is the derivative of the steering vector relative to the spatial frequency, and G is the matrix consisting of the noise-only eigenvectors g_k.

In the case of *uncorrelated signals*, equation (1) simplifies to [4]

$$\mathrm{var}_{MU}(\hat{\omega}_i) = \frac{1}{2N \cdot \mathrm{SNR}_i}\cdot\frac{1}{h(\omega_i)}\left[1+\frac{[(A^HA)^{-1}]_{ii}}{\mathrm{SNR}_i}\right] \quad (3)$$

where SNR_i represents the SNR of the ith source and A is the array steering matrix.

From (3), it is clear that low SNRs result in high error variances of the AOA estimates, and subsequently degrade the performance of the MUSIC technique.

III. Improved SNR via subband decomposition

Let

$$x(k) = s(k) + n(k) \qquad 0 \le k \le N-1 \qquad (4)$$

where $s(k)$ is the sampled version of the signal waveform and $n(k)$ is an additive white noise sequence with variance σ^2. The input SNR is typically defined in the time-domain as

$$\mathrm{SNR} = \frac{E(|s(k)|^2)}{E(|n(k)|^2)} \approx \frac{\frac{1}{N}\sum_{k=0}^{N-1}|s(k)|^2}{\sigma^2} \qquad (5)$$

If the signal is transformed into a new domain using orthogonal transforms, one can still define the signal-to-noise ratio using expression (5). In this case, k denotes the transform bin number, and $s(k)$ becomes the transformed signal[6]. It should be noted that in the case of discrete Fourier transform (DFT), the white noise power uniformly extends over all frequency bins.

Equation (5) evaluates the SNR over the entire transform domain. If the SNR is to be computed over one or specific transform bins, then the numerator in (5) should be taken over only the bins of interest, and σ^2 becomes the total noise captured in the transform bins considered in this summation. Therefore, if the signal occupies much narrower bandwidth than that of the noise, the SNR can be improved, if it is evaluated over the signal bandwidth, instead of the entire Nyquist interval. The greater difference between the signal and noise bandwidth, the more significant the SNR improvement becomes.

Consider a sinusoidal signal corrupted by white noise with SNR=0dB, where the signal length N=512 (Fig. 1-a). An N-point discrete Fourier transform (DFT) is applied to the signal, and the frequency band with the greatest power is selected. The signal power is concentrated in one transform bin, whereas the noise power is uniformly distributed over the whole spectrum (Fig. 1-b). It is straightforward to show that, at the input sinusoidal frequency, the transform domain SNR is N times the SNR defined in the time-domain through equation (5). It is noted, however, that in this case, the number of samples of interest decreases from N in the time-domain to only 1 in the transform (frequency) domain. Generally, if the signal occupies one subband out of K subbands, then by only considering the signal subband, the SNR improves by K, while the number of independent samples decreases to N/K. That implies that, the product of SNR and the number of samples remains unchanged.

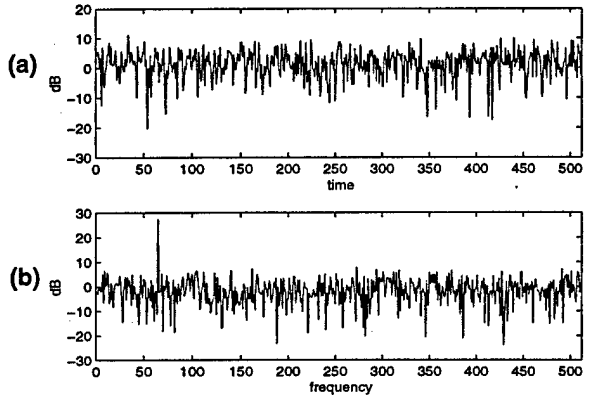

Fig. 1 Sinusoid signal corrupted by noise (SNR=0dB)
(a) Time-domain (b) Frequency-domain

IV. Subband MUSIC

Equation (3) shows that, the dependence of $\mathrm{var}_{\mathrm{MU}}(\hat{\omega}_i)$ on SNR is such that:

(1) For low SNR, i.e., the noise level is relatively high,

$$\mathrm{var}_{\mathrm{MU}}(\hat{\omega}_i) \propto \frac{1}{N \cdot \mathrm{SNR}_i^{\,2}} .$$

(2) For high SNR, $\mathrm{var}_{\mathrm{MU}}(\hat{\omega}) \propto \frac{1}{N \cdot \mathrm{SNR}_i}$.

That is, as SNR increases, the relationship between the error variance of the AOA estimate and SNR changes from square inverse proportionality to just an inverse proportionality.

The proposed subband MUSIC technique is described as follows:

(1) Divide the input signal into separate blocks, each of length K.
(2) Apply K-point FFT to each block, and select the subband with the maximum power. This results in a new sequence of length N/K. The SNR of the new sequence is K times the original one.
(3) Apply the high resolution eigenstructure-based MUSIC technique to the new sequence.

To further demonstrate how the subband MUSIC works, we consider the case of an m-sensor array with only one arrival signal, i.e., n=1. To simplify notation, the subscript i is omitted hereafter. For K-subband MUSIC, equation (3) can be written as

$$\mathrm{var}_{\mathrm{MU}}(\hat{\omega}) = \frac{1}{2N \cdot \mathrm{SNR}} \cdot \frac{1}{h(\omega)}\left[1 + \frac{1}{m \cdot K \cdot \mathrm{SNR}}\right] \qquad (6)$$

$h(\omega)$ is obtained using equation (2) with

$$a(\omega) = \left[1 \; e^{j\omega} \; \ldots \; e^{j(m-1)\omega}\right]^T \qquad (7)$$

$$d(\omega) = \frac{da(\omega)}{d\omega} = j\left[0 \; e^{j\omega} \; \ldots \; (m-1)e^{j(m-1)\omega}\right]^T \quad (8)$$

$$G = I - \frac{1}{m}a(\omega)a^H(\omega) \quad (9)$$

Substituting (7-9) into (2), and after some mathematical manipulation, we obtain

$$h(\omega) = \frac{m(m+1)(m-1)}{12} \quad (10)$$

which implies that $h(\omega)$ is a constant and does not change with the spatial frequency ω. Therefore, for fixed values of N and SNR, $\mathrm{var}_{MU}(\hat{\omega})$ is proportional to the factor $c = 1 + \frac{1}{m \cdot K \cdot \mathrm{SNR}}$. Two observations are now in order:

(1) For high SNR, $c \approx 1$, independent of K. This indicates that no improvement in performance is expected via subband processing.

(2) When SNR is sufficiently low, $c>>1$ for K=1 and $c \approx 1$ as $K \to \infty$. Therefore, the proposed subband MUSIC technique will be able to considerably reduce the value of $\mathrm{var}_{MU}(\hat{\omega})$.

From a windowing perspective, partitioning the data record of length N into separate blocks is equivalent to applying non-overlapping data windows(NOW). However, subband MUSIC technique can also be implemented using a moving window(MW), whereby the data window is shifted by only one snapshot each time. The moving window subband MUSIC method is more appropriate for non-stationary signals whose frequencies change with time.

The NOW subband MUSIC method can be modified to include more frequency bins instead of only one bin. This modification is important in time-varying environment as it provides additional information of the non-stationary signal. However, such modification is not necessary for MW technique, since it is possible to effectively track the changes of the signal frequency characteristics with time through the continuous time displacement of the data window.

V. Simulation

Three simulation examples are presented below to illustrate the effectiveness of the proposed subband MUSIC technique.

(1) Sinusoid signal

In the first example, both NOW and MW methods are used to implement subband MUSIC. Only one frequency bin is considered. In this example, we use a four-sensor array which receives a sinusoid signal of SNR=-15dB arriving at AOA=10° from the broadside. N and K are set equal to 2048 and 256, respectively. The results of AOA estimation based on the classical MUSIC and the subband MUSIC incorporating both the moving window and the non-overlapping window are shown in Fig. 2. From the plots in Fig. 2, it is evident that at low SNR, the fluctuations of AOA estimate using classical MUSIC is more severe than those from the subband MUSIC technique, whereas there is no obvious differences between the performance of the two subband MUSIC methods based on the NOW and MW approaches.

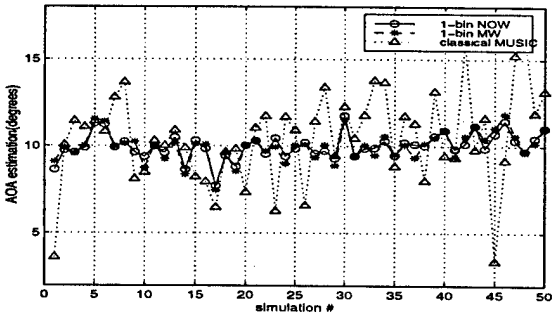

Fig. 2 Estimation of 1-bin NOW, MW subband MUSIC and classical MUSIC using a stationary signal

(2) Relationship with input SNR

The second simulation example is to examine the relationship between $\mathrm{var}_{MU}(\hat{\omega})$ and SNR that further illustrates the results in the first simulation example. In this example, we change SNR from-30dB to 10 dB and consider different values of K=1, 16, 256. All other parameters are the same as those used in the previous example. For each SNR, the angle of the peak value of the MUSIC spectrum is found and the square of the difference between this angle and the exact one is computed and averaged over 50 different trials to get an empirical value of $\mathrm{var}_{MU}(\hat{\omega})$. The results are plotted in Fig. 3, with the x-axis representing SNR in dB, and the y-axis representing $\mathrm{var}_{MU}(\hat{\omega})$. The dashed lines are the empirical values, whereas the solid lines represent the corresponding theoretical curves.

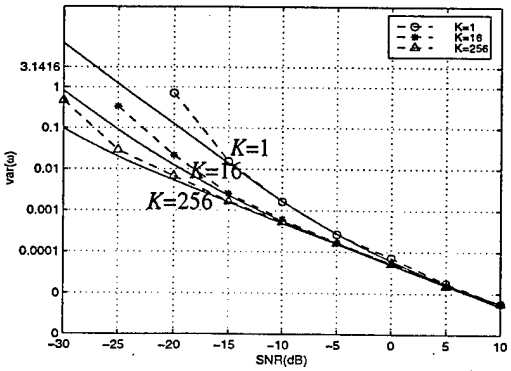

Fig. 3 Variance of estimation error vs SNR

It is clear from Fig. 3 that the improvement of the sub-

band MUSIC over the classical MUSIC becomes more pronounced at lower SNR. Also noted that the smaller SNR, the greater difference is between the theoretical and experiment curves. One fundamental reason for such discrepancy is that the high-power noise may corrupt the eigenvalues to the extent that the eigenvector corresponding to the maximum eigenvalue is no longer the closest basis to the signal vector. Another reason is that the theoretical result given by equation (1) is based on Taylor series expansion, and as $\hat{\omega} - \omega$ gets larger, $\mathrm{var}_{MU}(\hat{\omega})$ would not follow the curve, as higher expansion terms are no longer negligible. When SNR increases, the subband and the classical direction-finding methods tend to converge to the same values. So, using subband techniques in high SNR environment does not improve performance.

(3) Polynomial-phase signal

In the third simulation, a slowly varying chirp signal defined by equation (11) is used as the incident signal.

$$s(k) = e^{j2\pi\left(\frac{10^{-4}}{2}k^2 + 0.8k\right)} \qquad (11)$$

This is a *non-stationary* case. All other parameters are the same as in previous simulations. Fig. 4 shows the AOA estimates obtained using the above three MUSIC methods. In this figure, the MW subband MUSIC yields the smallest AOA estimation fluctuation. The NOW subband MUSIC and classical MUSIC follow. The difference between the MW and the NOW subband MUSIC methods lies in the fact that the former can track the frequency-changing signal, yet the NOW method partially loses the information between the adjacent non-overlapping windows.

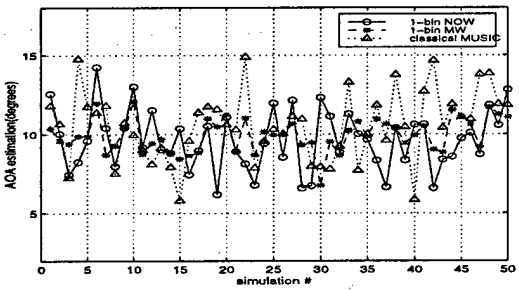

Fig. 4 Estimation of 3-bin NOW, MW subband MUSIC and classical MUSIC using non-stationary signal

Using the same data but including three dominant frequency bins in both NOW and MW subband MUSIC methods yields different set of curves, as shown in Fig. 5.

The variances calculated from Fig. 4 and Fig. 5 are listed in Table 1. Repeated simulations show that for a chirp signal, considering the signals over multiple-subbands at any given window position may improve the performance of the NOW method because it could offer more information on the desired signal. In the MW scenario, however, this improvement is limited. This means information provided by additional subbands is insignificant.

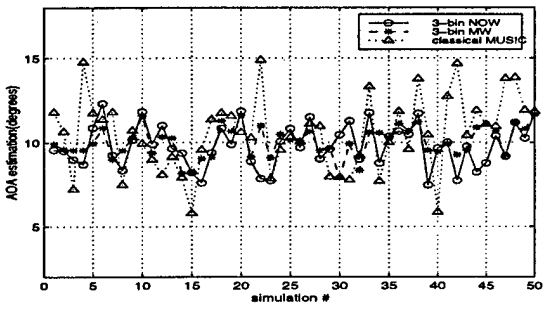

Fig. 5 Estimation of 3- bin NOW, MW subband MUSIC and classical MUSIC using non-stationary signal

Table 1: variance from Fig. 4 and Fig. 5

	NOW	MW	classical MUSIC
1-bin	0.1034	0.0575	0.1209
3-bin	0.0677	0.0497	0.1209

VI. Conclusion

We have proposed a subband-MUSIC-based direction finding technique which combines subband signal processing with the conventional MUSIC technique. Subband methods improve the SNR when the bandwidth of the signal is narrower than that of the noise. From both analysis and simulations, we have demonstrated that at low SNR, the subband MUSIC technique using both moving window (MW) and non-overlapping window (NOW) methods offers better performance than classical MUSIC. For non-stationary signals, it is shown that using moving windows yields smaller variance than using non-overlapping windows. However, the performance of NOW method could be improved by utilizing more subband components instead of only one.

References

[1] L. C. Godara, "Application of antenna arrays to mobile communications, part II: beam-forming and direction-of-arriaval considerations," *Proc. IEEE*, vol. 85, pp. 1195-1245, August 1997.

[2] R. O. Schmidt, "Multiple emitter location and signal parameter estimation," *IEEE Trans. Antennas and Propagation*, vol. 34, no. 3, pp. 276-280, March 1986.

[3] R. Kumaresan and A. K. Shaw, "High resolution bearing estimation without eigendecomposition", in *Proc. IEEE Int. Conf. Acoust. Speech, Signal Processing*, Tampa, Fl, pp. 576-579, March 1985.

[4] P. Stoica and A. Nehorai, "MUSIC, maximum likelihood, and cramer-rao bound," *IEEE Trans. Acoust., Speech, Signal Processing*, vol. 37, pp. 720-741, May 1989.

[5] M. Kaveh and A.J. Barabell, "The statistical performance of the MUSIC and the minimum-norm algorithms in resolving plane waves in noise," *IEEE Trans. Acoust., Speech, Signal Processing*, vol. ASSP-34, pp. 331-340, Apr. 1986

[6] X. Xia, "A quantitative analysis of SNR in the short-time Fourier transform domain for multicompoent signals," *IEEE Trans. Signal Processing*, vol. 46, pp. 200-203, Jan. 1998.

Beamspace Time-Frequency MUSIC with Application to Airborne Antenna Arrays

Yimin Zhang and Moeness G. Amin
Department of Electrical and Computer Engineering
Villanova University, Villanova, PA 19085

Abstract

We introduce the beamspace time-frequency (t-f) MUSIC as a hybrid scheme which combines the advantages of beamspace processing and time-frequency distributions for high resolution directional finding of signals with time-varying characteristics. The proposed beamspace t-f MUSIC performs high resolution angle-of-arrival estimation using the time-frequency signatures of the outputs of the beams, rather than the sensor data, as previously proposed. Two beamspace t-f MUSIC techniques are presented, one is based on joint block-diagonalization of multiple t-f points whereas the other is based on averaging over t-f regions prior to subspace estimation. Both techniques utilize the power distribution of the signal arrivals within different beams over both time and frequency.

1. Introduction

The evaluation of quadratic time frequency distributions of the data snap shots across the array yields, what is referred to as, the spatial time-frequency distributions (STFDs)[1]. The STFD permits the application of eigenstructure subspace techniques to solve a large class of channel estimation and equalization, blind source separation, and high resolution direction of arrival estimation problems. Spatial time-frequency distribution techniques are most appropriate to handle sources of nonstationary waveforms that are highly localized in the time-frequency domain, or any other domain of a different joint variable signal representations.

The time-frequency MUSIC was introduced in [2] to utilize the time-frequency signatures into the signal and noise subspace estimation. In this respect, the t-f MUSIC is an eigenstructure method for direction finding involving no longer the exact statistical moments but rather the auto- and cross- time-frequency distributions of the data received by the multisensor array. Several t-f points corresponding to true power concentration of the different source signals are incorporated into a joint diagonalization scheme that yields the unitary matrix whose columns are the orthonormal basis vectors for the signal and noise subspaces. The block-diagonalization technique fundamentally aims at performing one search of spectral peaks to estimate the angles of arrival of all sources. As such, the t-f points selected should include auto-terms from the signatures of all signals incident on the array. A different method for direction finding using spatial time-frequency distributions is introduced in [3]. In this method, averaging over high power concentration regions is performed and the result is used in place of the covariance matrix in the traditional MUSIC technique to obtain the noise subspace. This time-frequency averaging method may also be employed to resolve one signal at a time. This requires averaging to be performed over the t-f regions where signals do not overlap, and the method must then be used repeatedly until all signals are resolved. With increased dimension of noise subspace, performance is likely to improve at the expense of performing several projections and single peak searches in multiple spectra.

In this paper, we extend both of the above methods to beamspace processing [4, 5]. Beamspace time-frequency MUSIC can be used in different applications including an airborne array mounted on aircraft with propellers. The propeller scatters represent signals which are highly correlated with direct path signal arrivals. Such strong correlation causes degradation in performance of direction finding using sensor data. Since the propeller coordinate positions are known, beamspace processing may be used to eliminate contribution of the scatterers to subspace estimation.

2. Analysis Model

2.1 Time-frequency MUSIC

Consider an array with N sensors and P sources. The signal vector at the array sensors is given by

$$\mathbf{x}(t) = \mathbf{y}(t) + \mathbf{n}(t) = \mathbf{A}(\mathbf{\Theta}_s)\mathbf{s}(t) + \mathbf{n}(t) \quad (1)$$

where $\mathbf{s}(t)=[s_1(t), s_2(t), \ldots, s_P(t)]^T$ is the signal vector and $\mathbf{\Theta}_s = [\theta_1, \theta_2, \ldots, \theta_P]^T$ is the vector of angles-of-arrival

This work is supported by ONR Grant no. N00014-98-1-0176.

(AOAs) which are assumed unknown but constant over the observation period. $\mathbf{a}(\theta)$ represents the array steering vector at AOA θ, and $\mathbf{A}(\Theta_s)=[\mathbf{a}(\theta_1),\mathbf{a}(\theta_2),...,\mathbf{a}(\theta_P)]^T$. $\mathbf{n}(t)$ is the additive noise vector.

The discrete-time form of Cohen's class of spatial time-frequency distribution (STFD) matrix of the signal vector $\mathbf{x}(t)$ is defined as [1]

$$\mathbf{D}_{xx}(t,f)=\sum_{l=-\infty}^{\infty}\sum_{m=-\infty}^{\infty}\Phi(m,l)\otimes\mathbf{x}(t+m+l)\mathbf{x}^H(t+m-l)e^{-j4\pi fl} \quad (2)$$

where m and f represent the time index and the frequency index, respectively. $\otimes$ denotes the Hadamard product, and $[\Phi(m,l)]_{i,j}=\phi_{i,j}(m,l)$ is the time-frequency kernel associated with the pair of the sensor data $x_i(t)$ and $x_j(t)$.

Under the linear data model of eq. (1), the STFD matrix takes the following simple structure

$$\mathbf{D}_{xx}(t,f)=\mathbf{D}_{yy}(t,f)+\mathbf{D}_{yn}(t,f)+\mathbf{D}_{ny}(t,f)+\mathbf{D}_{nn}(t,f) \quad (3)$$

where

$$\mathbf{D}_{yy}(t,f)=\sum_{l=-\infty}^{\infty}\sum_{m=-\infty}^{\infty}\Phi(m,l)\otimes\mathbf{y}(t+m+l)\mathbf{y}^H(t+m-l)e^{-j4\pi fl}, \quad (4)$$

$$\mathbf{D}_{yn}(t,f)=\sum_{l=-\infty}^{\infty}\sum_{m=-\infty}^{\infty}\Phi(m,l)\otimes\mathbf{y}(t+m+l)\mathbf{n}^H(t+m-l)e^{-j4\pi fl}, \quad (5)$$

and

$$\mathbf{D}_{nn}(t,f)=\sum_{l=-\infty}^{\infty}\sum_{m=-\infty}^{\infty}\Phi(m,l)\otimes\mathbf{n}(t+m+l)\mathbf{n}^H(t+m-l)e^{-j4\pi fl}. \quad (6)$$

We note that

$$\mathbf{D}_{yy}(t,f)=\mathbf{A}(\Theta_s)\,\mathbf{D}_{ss}(t,f)\,\mathbf{A}^H(\Theta_s) \quad (7)$$

where

$$\mathbf{D}_{ss}(t,f)=\sum_{l=-\infty}^{\infty}\sum_{m=-\infty}^{\infty}\Phi(m,l)\otimes\mathbf{s}(t+m+l)\mathbf{s}^H(t+m-l)e^{-j4\pi fl} \quad (8)$$

is the signal TFD matrix whose entries are the auto- and cross-TFDs of the sources.

Two different approaches have been proposed to use the spatial time-frequency distribution over different (t,f) points. The first approach relies on joint block-diagonalization [2], while the second is based on integrating the time-frequency distribution over high power concentration regions [3]. The two approaches are summarized below.

Let $\mathbf{G}$ denote the integrated STFD matrix $\mathbf{D}(t,f)$ over the time-frequency region Ω, i.e.,

$$\mathbf{G}=\iint_{\Omega}\mathbf{D}(t,f)dtdf \quad (9)$$

where $\iint_{\Omega}$ indicates the integral over the t-f region Ω. Accordingly, we can define the following two matrices which, respectively, correspond to the sensors and the sources,

$$\mathbf{G}_{xx}=\iint_{\Omega}\mathbf{D}_{xx}(t,f)dtdf, \quad (10)$$

and

$$\mathbf{G}_{ss}=\iint_{\Omega}\mathbf{D}_{ss}(t,f)dtdf. \quad (11)$$

We denote the number of sources which fully or in part occupy energetically the region Ω as P_Ω. In this case, the dimension of $\mathbf{G}_{ss}$ is P_Ω x P_Ω. Proper selection of the t-f region Ω with high signal concentration enhances the signal-to-noise ratio (SNR), leading to improved performance. It is noted that the condition for AOA estimation using the noise subspace of the P_Ω sources is $P_\Omega<N$. Therefore, in principle, an N element array can separate more than N sources if we perform the t-f MUSIC technique over different noise subspaces, each corresponds to a region Ω containing no more than (N-1) sources. From (3),

$$\mathbf{G}_{xx}=\mathbf{G}_{yy}+\mathbf{G}_{yn}+\mathbf{G}_{ny}+\mathbf{G}_{nn}. \quad (12)$$

We assume that the noise and signal are uncorrelated in the region Ω. If this region is sufficiently large, then $\mathbf{G}_{yn}=\mathbf{0}$ and $\mathbf{G}_{ny}=\mathbf{0}$. We also assume that the noise is white and Gaussian, so that $\mathbf{G}_{nn}=\sigma^2\mathbf{I}$, where σ^2 is the average noise power within Ω, and $\mathbf{I}$ is the identity matrix. From (7) and (12), we obtain

$$\mathbf{G}_{xx}=\mathbf{G}_{yy}+\mathbf{G}_{nn}=\mathbf{A}(\Theta_s)\,\mathbf{G}_{ss}\,\mathbf{A}^H(\Theta_s)+\sigma^2\mathbf{I}. \quad (13)$$

Eq. (13) is similar to that commonly used in conventional AOA estimation problems [6], relating the signal covariance matrix to the data spatial covariance matrix. If $\mathbf{G}_{ss}(t,f)$ is a full-rank matrix, the two subspaces spanned by the principle eigenvectors of $\mathbf{G}_{xx}(t,f)$ and the columns of $\mathbf{A}(\Theta_s)$ become identical. In this case, directional finding techniques based on eigenstructures, like MUSIC, can be applied.

The eigen-decomposition of $\mathbf{G}_{xx}$ leads to

$$\mathbf{G}_{xx}=[\mathbf{U}_s\,\mathbf{U}_n]\,\Lambda\,[\mathbf{U}_s\,\mathbf{U}_n]^H, \quad (14)$$

where the columns of $\mathbf{U}_s$ are the P_Ω eigenvectors which span the signal subspace, and those of $\mathbf{U}_n$ are the N–P_Ω eigenvectors which span the noise subspace. Since the subspace spanned by $\mathbf{U}_s$ is identical to that spanned by $\mathbf{A}(\Theta_s)$, then

$$\mathbf{A}^H(\Theta_s)\,\mathbf{U}_n=\mathbf{0}. \quad (15)$$

Thus, the AOA of the signal is found by the time-frequency MUSIC, which maximizes the localization function (spatial spectrum)

$$P(\theta)=\left|\hat{\mathbf{U}}_n^H\mathbf{a}(\theta)\right|^{-2}, \quad (16)$$

where $\hat{\mathbf{U}}_n$ spans the noise subspace of the estimated $\hat{\mathbf{G}}_{xx}$ matrix.

Another time-frequency MUSIC method is based on the joint block-diagonalization of the combined set of $\mathbf{D}_{xx}(t_k,f_k)$, $(t_k,f_k)\subset\Omega$ for $k=1, 2, ..., K$. The joint block-diagonalization is achieved by the maximization under

unitary transform of the following criterion,

$$C(\mathbf{U}) = \sum_{k=1}^{K} \sum_{i,j=1}^{P_\Omega} \left| \mathbf{u}_i^H \mathbf{D}_{xx}(t_k, f_k) \mathbf{u}_j \right|^2 \quad (17)$$

over the set of unitary matrices $\mathbf{U}=[\mathbf{u}_1, \mathbf{u}_2, \ldots, \mathbf{u}_N]$. An efficient algorithm for solving (17) is presented in [1]. Once the signal and the noise subspace are estimated, (15) and (16) can be applied. The AOAs of the sources are estimated by finding the P_Ω largest peaks of the localization function given by (16).

2.2 Beamspace time-frequency MUSIC

Although time-frequency MUSIC is effective for the AOA estimation of non-stationary source signals, the performance may degrade when some of the sources are highly correlated. This problem becomes even more difficult when the coherent sources are spatially distributed. For example, the scatters from the aircraft body and the propellers are spatial distributed sources and highly correlated with the line-of-sight signal, and it is difficult to separate them in the time-frequency domain. Reducing the signal coherence by using spatial smoothing methods [6] is difficult to apply due to insufficient number of sensors.

Here we propose the beamspace time-frequency MUSIC method to overcome the difficulties encountered by decorrelation filters when dealing with the spatially distributed coherent scatters. The proposed method combines the advantages of the beamspace MUSIC [4, 5] and time-frequency MUSIC [2, 3]. The proposed beamspace time-frequency MUSIC method, in essence, removes the undesired signals by utilizing the *a priori* partial spatial information about the signals, multipaths, and interferers, as well as their respective signatures in the time-frequency domain. Spatial filtering approach makes use of the conventional bandpass filters (BPF) to filter out the unwanted scatters in spatial frequency domain. It improves the AOA estimates of direct signals by suppressing instead of decoupling their coherent counterparts.

To model the coherent environment, we add Q local scatterers, which may be spatially distributed, to the scenario discussed above. Thus, the data vector at the array sensors will be

$$\mathbf{x}(t) = \mathbf{y}(t) + \mathbf{n}(t) = \mathbf{s}(t)\mathbf{A}(\Theta_s) + \sum_{i=1}^{Q} \int_{\Theta_i} \mathbf{a}(\theta)\mathbf{s}_i(t, \theta : \psi_i) d\theta + \mathbf{n}(t) \quad (18)$$

where $s_i(t, \theta ; \psi_i)$ (i=1, 2, ..., Q) are the scatterers with the spatial bandwidth Θ_i, and ψ_i are vectors containing the parameters which determine the characteristics of the spatial distribution.

To mitigate the effect of the scattering, the proposed beamspace time-frequency MUSIC method performs spatial filtering to filter out the local scattering before AOA estimation. When it is known that the desire signal lies within a specific sector, the data can be processed in a manner that retains information from that sector, but eliminates all arrivals from other sectors via beamspace MUSIC [4,5]. It is noted that the proposed beamspace MUSIC is applicable even when the scatters have high signal coherence with the other sources [4].

Let $\mathbf{C}$ be an N x J (J<N) dimensional beamformer matrix with orthogonal columns. Matrix $\mathbf{C}$ transforms an element-space observation vector $\mathbf{a}(\theta)$ into a beamspace vector $\mathbf{b}(\theta)$. The signal vector in the beamspace is

$$\mathbf{x}_b(t) = \mathbf{C}^H \mathbf{x}(t). \quad (19)$$

From (18) and (19), the beamspace output is

$$\begin{aligned} \mathbf{x}_b(t) &= \mathbf{y}_b(t) + \mathbf{n}_b(t) \\ &= \mathbf{s}(t)\mathbf{C}^H\mathbf{A}(\Theta_s) + \sum_{i=1}^{Q} \int_{\Theta_i} \mathbf{C}^H \mathbf{a}(\theta)\mathbf{s}_i(t, \theta : \psi_i) d\theta + \mathbf{n}_b(t) \end{aligned} \quad (20)$$

The second term is the residual scatters which should be removed. $\mathbf{n}_b(t) = \mathbf{C}^H\mathbf{n}(t)$ is the noise vector at the beamspace domain. Note that the noise over the spatial stopband is filtered out so that the overall input SNR is improved.

The primary objective of a beamformer design is to make the array gain $g(\theta)$ satisfy [7]

$$g(\theta) = \frac{\mathbf{b}^H(\theta)\mathbf{b}(\theta)}{\mathbf{a}^H(\theta)\mathbf{a}(\theta)} = \frac{\mathbf{a}^H(\theta)\mathbf{C}\mathbf{C}^H\mathbf{a}(\theta)}{\mathbf{a}^H(\theta)\mathbf{a}(\theta)} = \begin{cases} 1 & \theta \in \Theta_{pass} \\ 0 & \theta \in \Theta_{stop} \end{cases} \quad (21)$$

where $\Theta_{pass} \supseteq \Theta_s$ is the spatial passband including all possible signal AOA, and $\Theta_{stop} \supseteq \Theta_1 \cup \Theta_2 \cup \ldots \cup \Theta_Q$ is the combined stopband spatial sector. When $g(\theta)$=0 is satisfied for $\theta \in \Theta_{stop}$, the spatially distributed local scattering are removed and, in turn, $\mathbf{x}_b(t)$ becomes interference-free. Therefore, when (21) holds, (20) becomes

$$\mathbf{x}_b(t) = \mathbf{y}_b(t) + \mathbf{n}_b(t) = \mathbf{s}(t)\mathbf{C}^H\mathbf{A}(\Theta_s) + \mathbf{n}_b(t) \quad (22)$$

Similar to the element-space time-frequency MUSIC, we define the STFD of the beamspace array output as

$$\mathbf{D}_{b,xx}(t, f) = \sum_{l=-\infty}^{\infty} \sum_{m=-\infty}^{\infty} \Phi(m, l) \otimes \mathbf{x}_b(t + m + l)\mathbf{x}_b^H(t + m - l) e^{-j4\pi fl}. \quad (23)$$

For the time-frequency MUSIC using averaging technique, the integrated STFD matrix is

$$\mathbf{G}_{b,xx} = \iint_{\Omega} \mathbf{D}_{b,xx}(t, f) dt df. \quad (24)$$

Clearly, we have

$$\mathbf{D}_{b,xx}(t, f) = \mathbf{C}^H \mathbf{D}_{xx}(t, f) \mathbf{C}. \quad (25)$$

and

$$\mathbf{G}_{b,xx} = \mathbf{G}_{b,yy} + \mathbf{G}_{b,nn} = \mathbf{C}^H\mathbf{A}(\Theta_s)\mathbf{G}_{ss}\mathbf{A}^H(\Theta_s)\mathbf{C} + \sigma^2\mathbf{C}^H\mathbf{C}. \quad (26)$$

The eigen-decomposition of $\mathbf{G}_{b,xx}$ leads to

$$\mathbf{G}_{b,xx} = [\mathbf{U}_{b,s}\ \mathbf{U}_{b,n}]\ \Lambda_b\ [\mathbf{U}_{b,s}\ \mathbf{U}_{b,n}]^H, \quad (27)$$

where $\mathbf{U}_{b,s}$ is made up of the P_Ω eigenvectors which span the signal subspace, and the columns of $\mathbf{U}_{b,n}$ is the $J-P_\Omega$ eigenvectors, which span the noise subspace. For beamspace time-frequency MUSIC, $J>P_\Omega$ should be satisfied to separate the sources.

Since the subspace spanned by $\mathbf{U}_{b,s}$ is identical to that spanned by $\mathbf{C}^H\mathbf{A}(\Theta_s)$, we get

$$\mathbf{A}^H(\Theta_s)\,\mathbf{C}\,\mathbf{U}_{b,n}=0. \tag{28}$$

Thus, in beamspace time-frequency MUSIC, the AOA of the signal is found by maximizing the localization function

$$P_b(\theta)=\frac{\mathbf{b}^H(\theta)\mathbf{b}(\theta)}{\left|\hat{\mathbf{U}}_{b,n}^H\mathbf{C}^H\mathbf{a}(\theta)\right|^2}, \tag{29}$$

where $\hat{\mathbf{U}}_{b,n}$ spans the noise subspace of estimated $\hat{\mathbf{G}}_{b,xx}$.

For the other time-frequency MUSIC method, the joint block-diagonalization is achieved by the minimization of the unitary transform of

$$C_b(\mathbf{U})=\sum_{k=1}^{K}\sum_{i,j=1}^{P_\Omega}\left|\mathbf{u}_{b,i}^H\mathbf{D}_{b,xx}(t_k,f_k)\mathbf{u}_{b,j}\right|^2. \tag{30}$$

Again, the AOAs are estimated by finding the P_Ω largest peaks of the localization function given by (29).

3. Computer Simulation

To confirm the effectiveness of the beamspace time-frequency MUSIC, we consider the scenario of an airborne radar system. An echo signal arrives from a target and gets scattered by the propellers. The signal from the target is generally a chirp signal. To simply the simulation, the propellers are considered as point scatterers and the scattered signals are considered to have the same waveform of that from the target. Fig. 1 shows the Choi-Williams time-frequency distribution of the chirp signal $s(t)=\exp(-j\mu t^2/2)$, where $t=[0,1]$ and $\mu=2\pi$. 256 points are used for both the time and frequency scale. For the t-f MUSIC methods, the 256 points along the chirp are chosen over the auto-term t-f region.

A 6-element equi-spaced linear array is considered where the interelement spacing is half wavelength. For beamspace array processing, the minimum bias multiple taper [8, 9] is used, and the selected beam bins are shown in Fig.2. Only the angular range $[0, \pi]$ is considered here. The spatial stopband is considered to be $\theta > 50$ degrees and $\theta < -50$ degrees. It is seen that the beamformer attenuates more than 10 dB at the direction of propellers.

Fig.3 shows the element-space results for two types of t-f MUSIC, as well as the traditional MUSIC. One target is assumed with AOA of 10 degrees. Two scattering signals, whose strength are assumed to be -10dB with respect to the direct signal from the target, are from θ=-60 degrees and θ=60 degrees. The ratio of the direct signal power and the noise power is 10 dB. It is seen that, due to the presence of the scatters, the estimation of the AOA of the target is generally bad. Meanwhile, it is noted that the t-f MUSIC based on joint block-diagonalization provides stable spatial spectrum.

Fig.4 shows the results when beamspace array is used for the same scenario. The estimation of the AOA is greatly improved after the beamspace processing. Again the results show the t-f MUSIC with joint block-diagonalization gives the best performance, while the traditional MUSIC is the worst.

4. Conclusion

The beamspace time-frequency (t-f) MUSIC was proposed as a hybrid scheme which combines the advantages of beamspace processing and time-frequency distributions for high resolution directional finding of signals with time-varying characteristics. Two t-f beamspace MUSIC techniques have been presented, one is based on joint block-diagonalization of multiple t-f points, whereas the other is based on averaging over t-f regions prior to subspace estimation. Our results show that, the beamspace processing is effective to remove coherent scatterers, and time-frequency MUSIC methods provide improved performance over traditional MUSIC.

References

[1] A. Belouchrani and M. G. Amin, "Blind source separation based on time-frequency representation," *IEEE Trans. Signal Proc*, vol.46, no.11, pp.2888-2897, Nov. 1998.

[2] M. G. Amin and A. Belouchrani, "Time-frequency MUSIC: an array signal processing method based on time-frequency signal representation," *Proc. of SPIE*, vol.3462, pp.186-194, July 1998.

[3] K. Sekihara, S. Nagarajan, D. Poeppel, and Y. Miyashita, "Estimating neural sources from each time-frequency component of magnetoencephalo-graphic data", in *Proc. IEEE SP Int. Symp. on Time-Frequency and Time-Scale Analysis*, Pittsburgh, PA, pp. 69-72, Oct. 1998.

[4] C. Zhou, F. Haber, and Q. Shi, "On spatial filtering for angle-of-arrival estimation in a scattering environment by eigendecomposition-based methods," *IEEE Trans. Antennas Propagat.*, vol.38, no.6, pp.931-934, June 1990.

[5] D. A. Linebarger, R. D. DeGroat, E. M. Dowling, P. Stoica, and G. L. Fudge, "Incorporating *a priori* information into MUSIC-algorithms and analysis," *Signal Processing*, vol. 46, pp. 85-104, 1995.

[6] R. O. Schmidt, "Multiple emitter location and signal parameter estimation," *IEEE Trans. Antennas Propagat.*, vol.34, no.3, pp.276-280, March 1986.

[7] K. M. Buckley and X.-L. Xu, "Spatial-spectrum estimation in a location sector," *IEEE Trans. Acoust. Speech Signal Proc.*, vol.38, no.11, pp.1842-1852, Nov. 1990.

[8] K. Riedel and A. Sidorenko, "Minimum bias multiple taper spectrum estimation", *IEEE Trans. Signal Proc.*, vol.43, no.1, pp.188-195, Jan. 1995.

[9] M. G. Amin and N. Bhalla, "Minimum bias spatial filter for beaspace direction-of-arrival estimation", *Journal of Franklin Institute*, March 1997.

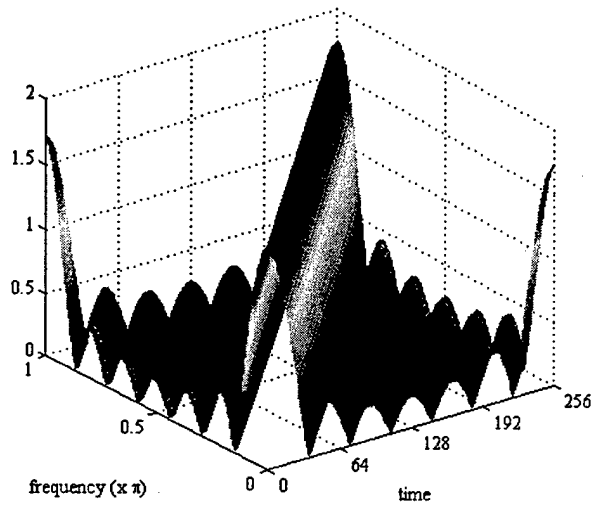

Fig.1 Time-frequency distribution of the signal

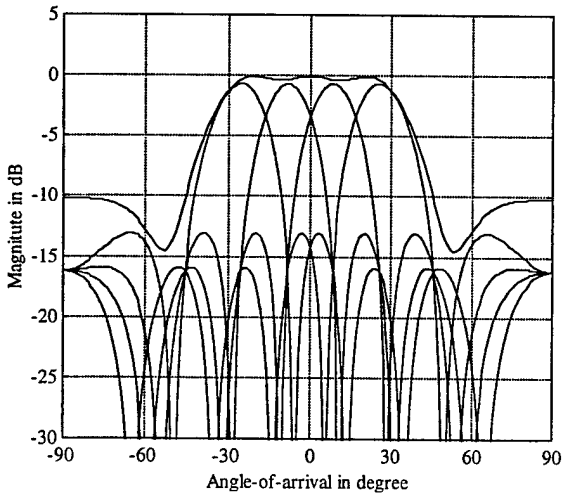

Fig.2 Beamspace bins

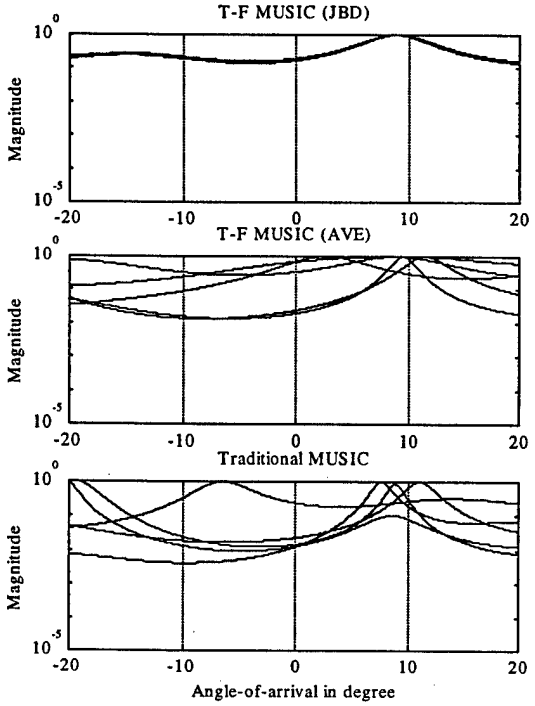

Fig.3 Element-space MUSIC spectrum

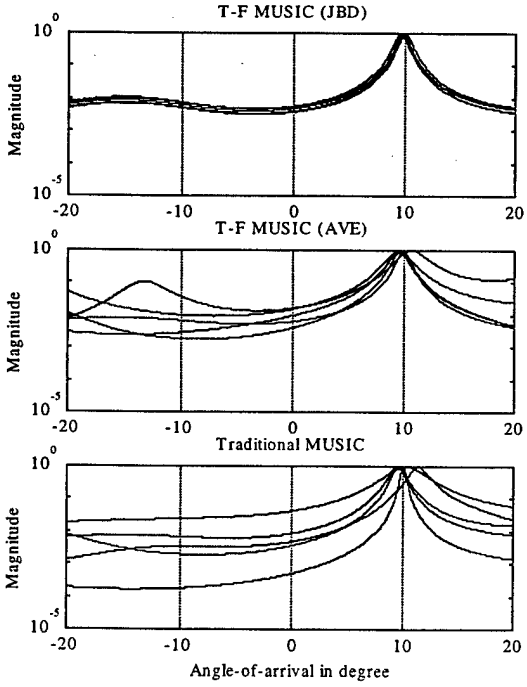

Fig.4 Beamspace MUSIC spectrum

Nonstationary Interference Excision in Spread Spectrum Communications Using Projection Filtering Methods

Moeness G. Amin and Govind R. Mandapati

Department of Electrical and Computer Engineering
Villanova University,Villanova, PA 19085

Abstract

A new nonstationary interference excision technique in direct sequence spread spectrum (DSSS) communication is introduced. This technique is based on the notion that both the additive noise and the DSSS signal cover the entire time-frequency(t-f) domain, whereas the jammer occupies a small t-f region. A projection filter is constructed using the jammer underlying t-f signature or its expected occupancy region in the t-f domain. The filter output is either directly despreaded or first subtracted from the input data and then despreaded by the PN sequence, depending on whether the filter passes or removes the jammer signal. We derive the SNR of the DSSS receiver implementing the projection filters and discuss its relation to existing excision methods based on instantaneous frequency information.

1. Introduction

One of the fundamental application of the direct sequence(DS) spread spectrum (SS) communications is that of interference mitigation. Frequently signal processing techniques are used in conjunction with the DS/SS receiver to augment the processing gain, permitting greater interference protection without an increase in the bandwidth.The recent development of the bilinear time-frequency distributions (TFD's) for improved signal power localization in the time-frequency plane has motivated several new approaches for the nonstationary interference excision in the DSSS systems. Utilization of the jammer instantaneous frequency (IF), as obtained via TFD's, to design an open loop adaptive notch filter in the time domain, has been thoroughly discussed in [1, 2]. However, this technique has three drawbacks. First, it becomes difficult to remove more than one jammer component at any time instant. Second, this method creates a significant amount of self noise (induced correlation) that in some cases reduces the performance of the spread spectrum receiver. Third, the open loop adaptive filter is only effective in removing jammer signals characterized by their instantaneous frequency, i.e., polynomial phase signals.

An alternate approach to broadband interference excision in DS/SS systems has been presented in [3]. This technique uses the TFD to depict a locally narrowband (FM, hopped, chirp, etc.,) jammer over time and frequency. Time-varying filtering is then achieved by masking the regions of high power concentration in the t-f domain, followed by a least-squares synthesis technique to recover the interference signal. The constructed jammer waveform is then subtracted from the incoming data to remove the interference component in the time domain. However, since this excision method is based on masking and approximation of Wigner distribution, the performance is potentially poor due to the effect of high nonlinear filtering as well as the quadratic nature of the Wigner distribution.

Motivated by the work on time-frequency filtering [4] to overcome the drawbacks of the least-squares synthesis method, we propose in this paper a new approach for nonstationary interference excision in DSSS communications using projection filtering techniques. The proposed excision approach is depicted in Fig.1. The projection filter may be constructed from the jammer IF information, as in the case of the polynomial phase signals, or from the t-f region which captures most or all of the jammer power. In the former, the jammer subspace is one dimensional, whereas in the latter, the dimension is defined by the instantaneous bandwidth and can be obtained using subspace construction techniques [4]. These techniques are applicable to any size and shape of the t-f region. The t-f region can be chosen such that the corresponding linear subspace gives accurate description of different jammer signals which are likely to be received. Often, a threshold must be imposed on the eigenvalues, which are defined by the t-f region R. A low threshold increases subspace dimensionality, but allows better representation of the jammer signal.

It is interesting to note that the above two approaches can be cast from a subspace projection filtering perspec-

*Supported by the ONR Grant no.N00014-98-0176

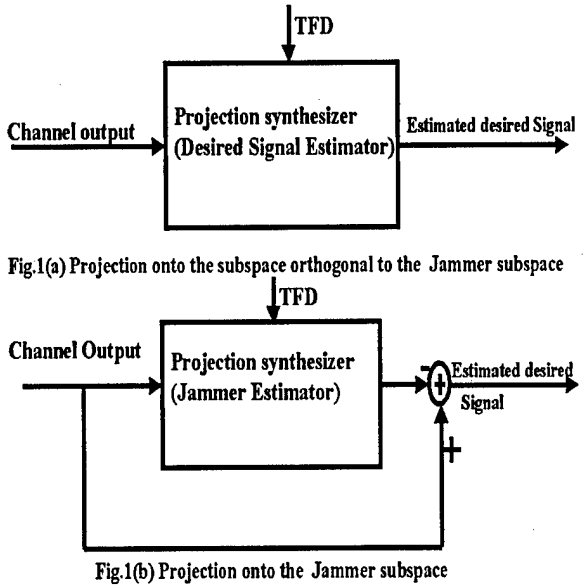

Figure 1. Projection Filtering Approach

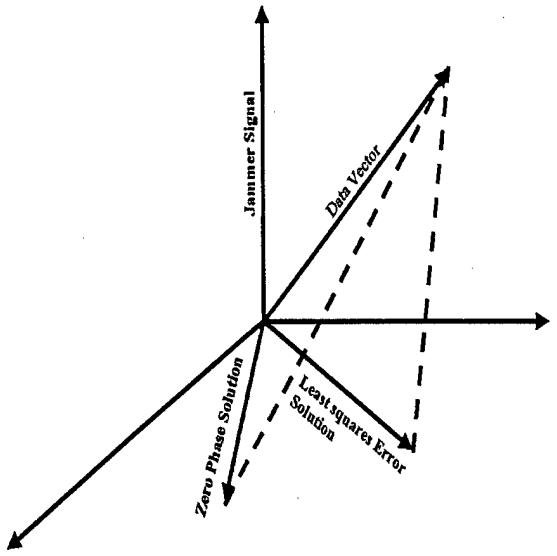

Figure 2. Vectorial Representation

tive. In the three-coefficient notch filter technique, we are in essence projecting the data, three samples at a time, onto the orthogonal subspace of the jammer. Within this two-dimensional subspace, we search for the symmetric vector corresponding to a zero-phase filter, as depicted in Fig.2. In the synthesis approach, we attempt to construct a two dimensional subspace representation of the jammer signal through synthesizing the even-indexed and odd-indexed parts of its waveform. These two parts represent independent vectors and span a two-dimensional subspace. The phase matching procedure that follows to align the synthesized waveform with the received one [5] can be viewed as the projection of the input data vector onto the two dimensional jammer subspace.

The a priori-knowledge of the constant modulus property of the jammer renders the least squares synthesis technique unnecessary. With a good IF estimator in place, the one-dimensional jammer subspace can be directly and easily constructed from from the jammer's instantaneous frequency. Removing a polynomial phase or constant modulus interference via projection filter may, therefore, be carried out using successive projections, as in the case of the time-varying notch filter approach, or through a single projection incorporating the jammer instantaneous frequency over the time-period of interest. In DSSS communications, this period is the symbol width. We note that there is a difference in computations and receiver performance between using a single projection at the end of the bit period vs. consecutive projections in smaller dimensions along the bit period. This difference increases with the spread spectrum signal bandwidth

2. Projection Filtering Approach

Let $\mathbf{x}$ denote the input data vector over one bit period.The data vector consists of the SS signal vector $\mathbf{s}$, the jammer vector $\mathbf{j}$, and the noise vector $\mathbf{n}$,

$$\mathbf{x} = \mathbf{s} + \mathbf{j} + \mathbf{n}. \tag{1}$$

All the vectors in the above equation are of length L, which is the number of chips per symbol. Let the jammer approximately occupy the q-dimensional subspace S_j^q, where $q \leq L$. Define matrix $\mathbf{U}$ whose columns are the orthonormal basis vectors that span the subspace $\bar{S}_j^q$ orthogonal to S_j^q. The $L \times L$ projection matrix $\mathbf{V}$ onto the subspace $\bar{S}_j^q$ is given by

$$\mathbf{V} = \mathbf{U}\mathbf{U}^H \tag{2}$$

The resultant vector obtained by projecting the data vector $\mathbf{x}$ onto $\bar{S}_j^q$ represents the projection filter output,

$$\begin{aligned} \mathbf{x_o} &= \mathbf{V}\mathbf{x} \\ &= \mathbf{V}[\mathbf{s} + \mathbf{j} + \mathbf{n}] = \mathbf{s_o} + \mathbf{j_o} + \mathbf{n_o} \end{aligned} \tag{3}$$

If the jammer lies in S_j^q, then $\mathbf{j_o} = \mathbf{0}$, and full interference excision is achieved. The decision variable,y, at the receiver is the inner product $< \mathbf{x}_0, \mathbf{s} >$, i.e.,

$$y = \mathbf{x}_o^H \mathbf{s} \tag{4}$$

which is the sum of three different terms y_1,y_2 and y_3, due to the SS, the jammer, and the noise components of the input data, repectively

$$y = y_1 + y_2 + y_3 \tag{5}$$

where

$$\begin{aligned} y_1 &= \mathbf{s}^H\mathbf{V}^H\mathbf{s} \\ y_2 &= \mathbf{j}^H\mathbf{V}^H\mathbf{s} \\ y_3 &= \mathbf{n}^H\mathbf{V}^H\mathbf{s} \end{aligned}$$

The receiver signal-to-noise ratio(SNR) is given by [5]

$$SNR = \frac{E[y]^2}{var(y)} \tag{6}$$

The mean of the decision variable y,

$$E[y] = E[y_1] + E[y_2] + E[y_3] \tag{7}$$

where $E[.]$ is the expectation operator and

$$\begin{aligned} E[y_1] &= E[\mathbf{s}^H\mathbf{V}^H\mathbf{s}] = E\left[\sum_i\sum_j s_j^* v_{ji}^* s_i\right] \\ &= \sum_i\sum_j v_{ji}^* E[s_j^* s_i] = \sum_i v_{ii} = trace(\mathbf{V}) \end{aligned} \tag{8}$$

The second and the third terms in equation (5) are zeros, since both the jammer and the noise are uncorrelated with the PN sequence. With full jammer excision, the second moment of y is given by

$$\begin{aligned} E[|y|^2] &= E[|y_1 + y_3|^2] \\ &= E[|y_1|^2 + |y_3|^2 + y_1 y_3^* + y_1^* y_3] \end{aligned} \tag{9}$$

The cross-correlation term

$$\begin{aligned} E[y_1 y_3^*] &= E\left[\sum_i\sum_j\sum_k\sum_l s_l^* v_{lk}^* s_k s_j^* v_{ji} n_i\right] \\ &= \sum_i\sum_j\sum_k\sum_l v_{lk}^* v_{ji} E\left[s_l^* s_k s_j^* n_i\right] = 0 \end{aligned} \tag{10}$$

Similarly

$$E[y_1^* y_3] = 0 \tag{11}$$

Consider

$$\begin{aligned} E[|y_3|^2] &= E\left[\sum_i\sum_j\sum_k\sum_l n_l^* v_{lk}^* s_k s_j^* v_{ji} n_i\right] \\ &= \sum_i\sum_j\sum_k\sum_l v_{lk}^* v_{ji} E\left[n_l^* s_k s_j^* n_i\right] \\ &= \sigma^2 trace(\mathbf{V}) \end{aligned} \tag{12}$$

where σ^2 is the noise power. The second moment of y_1 is given by

$$\begin{aligned} E[|y_1|^2] &= E\left[\sum_i\sum_j\sum_k\sum_l s_l^* v_{lk}^* s_k s_j^* v_{ji} s_i\right] \\ &= \sum_i\sum_j\sum_k\sum_l v_{lk}^* v_{ji} E\left[s_l^* s_k s_j^* s_i\right] \\ &= \sum_i\sum_j |v_{ij}|^2 + \sum_i\sum_l v_{ll}^* v_{ii} - \sum_i |v_{ii}|^2 \\ &= \|\mathbf{V}\|_2^2 + \sum_i\sum_l v_{ll}^* v_{ii} - \sum_i |v_{ii}|^2 \end{aligned} \tag{13}$$

where $\|\mathbf{V}\|_2$ is the Frobenius Norm. It is straightforward to show that $\|\mathbf{V}\|_2^2 = trace(\mathbf{V}) = (L-q)$. Accordingly,

$$\begin{aligned} var(y_1) &= (L-q) + (L-q)^2 - \sum_i |v_{ii}|^2 - (L-q)^2 \\ &= (L-q) - \sum_i |v_{ii}|^2 \end{aligned} \tag{14}$$

The second term in (14) is the sum of the squares of the diagonal elements of the projection matrix. This term is approximately equal to $(L-2)$ for $L \gg 1$. From equations (6) - (14), the receiver SNR for $L \gg 1$ can be expressed as

$$SNR_o \approx \frac{L-q}{\sigma^2} \tag{15}$$

3. Time Frequency Subspace Filtering

3.1. Polynomial Phase Jammers

For a constant modulus or a polynomial phase jammer

$$j[n] = Ae^{j\phi(n)}, n = 1, 2, \ldots, L \tag{16}$$

where A is a complex factor. The instantaneous frequency of the jammer can be obtained using several methods, including time-frequency distributions [6]. The jammer subspace is one dimensional with the basis vector,

$$\mathbf{c} = [c_j] \tag{17}$$

where $c_j = \frac{1}{\sqrt{L}} e^{j\phi(n)}$. In this case, $q = 1$, and the receiver SNR becomes

$$SNR_o \approx \frac{L-1}{\sigma^2} \tag{18}$$

It should be noted that if the preprocessing of jammer excision is disabled, then we obtain the well known formula

$$SNR_o \approx \frac{L}{\rho^2 + \sigma^2} \tag{19}$$

where ρ^2 is the average jammer power. Comparing equations (18) and (19), the projection filter allows total jammer removal at the cost of reducing the processing gain by 1. Further, the interference excision using projection filters

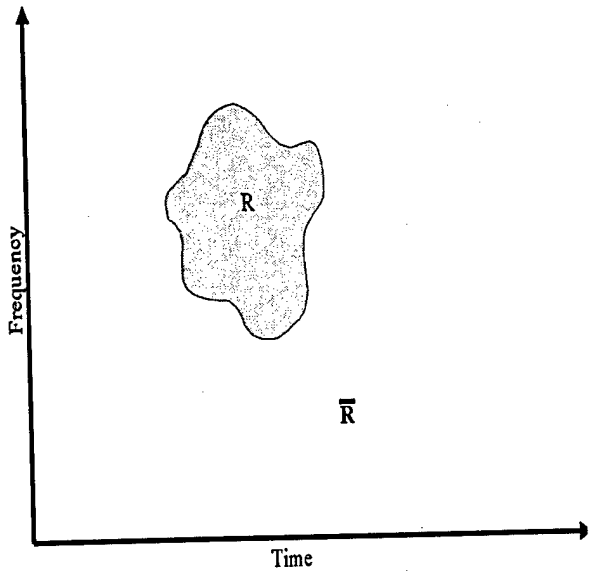

Figure 3. The region R in the TF domain

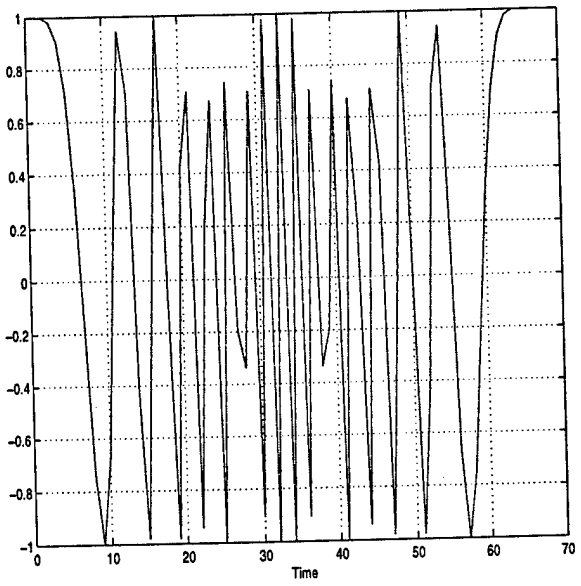

Figure 4. Jammer signal

yields a receiver SNR, that is independent of the jammer IF, as evident from (18).

It is noteworthy that the notch excision filter approach introduced in [1] yields the receiver SNR

$$SNR \approx \frac{L}{1+2\sigma^2} \tag{20}$$

which is approximately half of the processing gain offered by the proposed projection filter approach.

For a sum of q polynomial phase jammers, $j_k[n], k = 1, 2, \ldots, q$, the corresponding jammer vectors,

$$\begin{aligned} \mathbf{c}_k &= [c_{kn}] \\ &= j_k[n] = A_k e^{j\phi_k[n]}, \quad k = 1, 2, \ldots, q \end{aligned} \tag{21}$$

span the subspace S_j^q. The orthonormal basis vectors of S_j^q can be obtained by performing the SVD of the matrix

$$\mathbf{c} = [\mathbf{c}_1 | \mathbf{c}_2 \ldots | \mathbf{c}_q] \tag{22}$$

and retaining the q singular vectors corresponding to the q non-zero singular values. According to equation (15) the receiver SNR reduces linearly with q. In this case, notch excision filter approach fails to excise multiple jammers due to insufficient number of degrees of freedom, and is clearly inferior compared to the projection filtering approach.

3.2. General Classe of Jammer Signals

For any other type of jammers, the subspaces $\bar{S}_j^q$ and S_j^q can be constructed from the time-frequency region R, shown in Fig.3. The subspace S_j^q fills out the jammer t-f region R energitically, but has little or no energy outside R. The t-f filter corresponding to Fig.1(a) is the orthogonal projection operator on the t-f subspace $\bar{S}_j^q$, whereas the t-f filter corresponding to Fig.1(b) is the orthogonal projection operator on the t-f subspace S_j^q, occupying the complement region $\bar{R}$. The preference between the two filters depends on the relative dimensions of their corresponding subspaces and the shape of R. Optimum design of the t-f subspaces using the two criteria of maximum concentration (MC) and minimum localization error (MLE) are detailed in [4] . It is noted that the priori knowledge that the jammer is a polynomail signal simplifies subspace construction to that described in section 3.1.

4. Example

In this example, we show the difference in distortion to the PN sequence incurred by using the projection filter approach vs. the notch filter approach for polynomial phase jammers in spread spectrum DSSS communications. A 64-chip PN sequence is generated and added to a chirp jammer, which is shown in Fig.4.

Using the jammer IF, the projection filter is constructed and used to project both the jammer and the PN sequence onto $\bar{S}_j^q$. The jammer is totally removed. The filter output for the PN sequence is shown in Fig.5. It is clear that there is a negligible difference between the input and output of the filter. This result is expected as the PN sequence distributes its power uniformly over the basis vectors of the 64-dimensional space. The removal of the sequence contribution along one of these vectors leads to insignificant

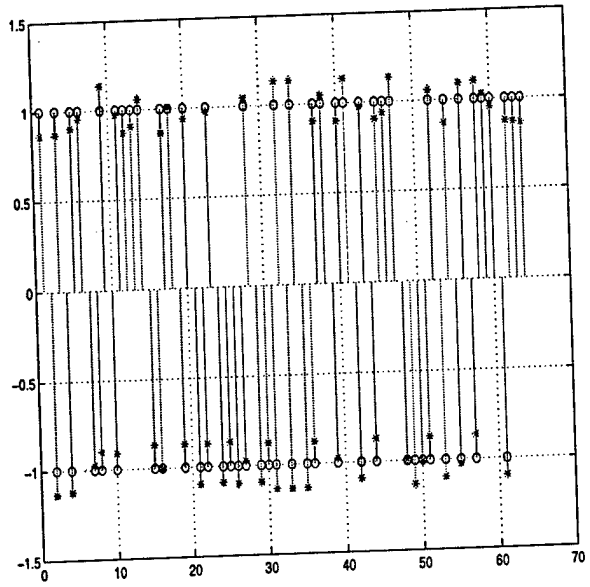

Figure 5. Input PN sequence,"o" and the constructed signal,"*" using Projection filter

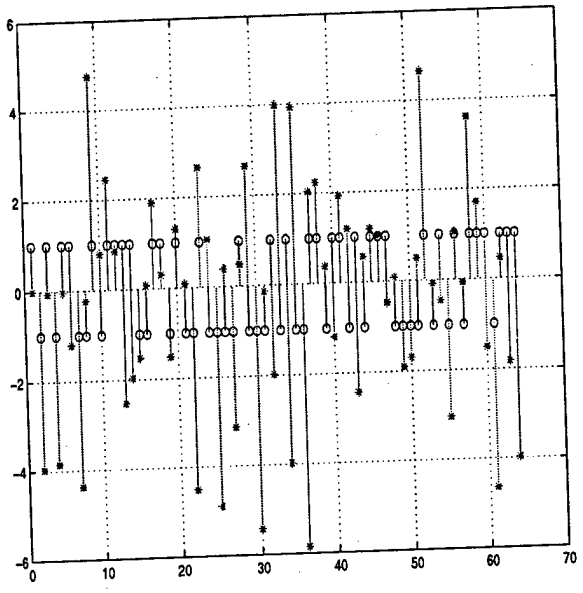

Figure 6. Input PN sequence,"o" and the constructed signal,"*" using notch filter

changes to the sequence temporal characteristics, specifically for $L \gg 1$. In Fig.6, we show the result for the three-coefficient zero-phase excision filter, where there is a clear distortion to the PN sequence caused by the filter wide notch.

5. Conclusions

We have presented a new approach for nonstationary interference excision in spread spectrum communications. This approach is based on the use of projection filers to remove the jammer, or at least a major portion of its power. We have distinguished between two classes of jammer signals; those of polynomial phase characteristics and others with both amplitude and frequency modulations. A polynomial phase jammer occupies a one-dimensional subspace, which is easily constructed using its instantaneous frequency estimate. The subspaces of other types of jammers may be constructed from their time-frequency regions using optimum design of t-f subspaces discussed in [4] . It is shown that jammer excision using projection filters only causes a reduction of the spreading gain by the dimension of the jammer subspace, which is one for the polynomial phase case. The main advantages of the proposed excision method over the notch filter approach is the ability to handle multiple jammers, jammers with arbitrary t-f charactersitics, and significant improvement of the receiver perfromance.

References

[1] M. Amin, "Interference mitigation in spread spectrum communication system using time-frequency distributions," *IEEE Transactions on Signal Processing*, 45:pp.90–102, January 1997.

[2] C. Wang and M. Amin, "Performance analysis of instantaneous frequency based interference excision techniques in spread spectrum communications," *IEEE Transactions on Signal Processing*, January 1998.

[3] S. Lach and M. Amin, "Broadband nonstationary interference excision for the spread spectrum communications using time-frequency synthesis," *ICASSP98*, May 1998.

[4] F. Hlawatsch and W. Kozek, "Time-frequency projection filters and time-frequency signal expansions," *IEEE Transactions on Signal Processing*, 42:pp.3321–3334, December 1994.

[5] J. Ketchum and J. Proakis, "Adaptive algorithms for estimating and suppressing narrowband interference in pn spread spectrum systems," *IEEE Transactions on Communications*, COM-30:pp.913–924, May 1982.

[6] B. Boashash, "Estimating and interpreting the instantaneous frequency of a signal," *IEEE Proceedings*, vol.80,No.12, December 1990.

Spatial time-frequency distributions for direction finding and blind source separation

Moeness G. Amin
Department of Electrical and Computer Engineering, Villanova University,
Villanova, PA 19085

ABSTRACT

This paper discusses the application of the new concept of spatial time-frequency distribution (STFD), and more generally the spatial arbitrary joint-variable distribution (SJVD), to key array signal processing problems including blind source separations and high resolution direction finding of narrowband and broadband sources with stationary and nonstationary temporal characteristics. The STFD can be formulated based on the widely used class of time-frequency distributions, namely Cohen's class, or it can be devised by incorporating other classes of quadratic distributions, such as the Hyperbolic class and the Affine class. The paper delineates the fundamental offerings of STFDs, presents three examples of array signal processing using the localization properties of time-frequency distributions of the impinging signals, and summarizes recent contributions in this area.

I. INTRODUCTION

In many signal processing applications, the multidimensional signal is directly utilized to estimate some signal parameters, such as the number of sources and their directions of arrival. Subspace-based methods use a geometrical relation involving the exact moments of the data. The desired signal parameters are extracted by solving this relation in some approximate sense, and using sample moments instead of the exact ones. The commonly applied eigenstructure subspace methods assume stationary signals. Although, when the frequency content of the measured data is time-varying, these methods can still be used, yet the proper use of the information on the data time-frequency characteristics can significantly improve their performance. In general, conventional blind source separation and direction finding techniques based on second and higher order statistics are not structured to exploit the non-overlapping properties of the signal arrivals in the time-frequency domain. These properties can, for example, be employed to achieve spatial nulling and removal of undesired sources without resorting to beamspace processing and decreasing the available number of degrees of freedom.

The evaluation of quadratic time frequency distributions of the data snapshots across the array yields spatial time-frequency distributions, which permit the application of eigenstructure subspace techniques to solving a large class of channel estimation and equalization, blind source separation, and high resolution direction of arrival estimation problems. Spatial time-frequency distribution techniques are most appropriate to handle sources of nonstationary waveforms that are highly localized in the time-frequency domain. In the area of blind source separation, the spatial time-frequency distributions allow the separation of Gaussian sources with identical spectral shape, but with different time-frequency localization properties, i.e., different signatures in the time-frequency domain. For signal separation and direction of arrival estimation problems, spreading the noise power while localizing the source energy in the time-frequency domain amounts to increasing the robustness of eigenstructure signal and noise subspace estimation methods with respect to channel and receiver noise, and hence improves resolution and signal separation performance.

In this paper, we consider the applications of time-frequency distributions to the two areas of direction finding and blind source separation using multiple antenna arrays. While time-frequency distributions have been sought out and successfully used in the areas of speech, biomedicine, automotive industry, and machine monitoring, their applications to sensor and spatial signal processing have not been properly investigated. The time-frequency distribution in all its bilinear and higher order forms represents a powerful tool for superresolution angle of arrival estimation and recovery of the signals which have been mixed across the array, specifically those of nonstationary temporal characteristics. The proper utilization of the time-frequency signatures and the power localization properties of the desired and jammer signals over time and frequency, or any appropriate joint-variables, increases the effective signal to noise ratio and casts time-frequency distributions as an important and essential part of array processing. For different jamming environments and a large class of signals, time-frequency based direction finding and blind source separation methods offer performance that is beyond the capabilities of traditional techniques based on second or higher order statistics.

2. SPATIAL CONSIDERATION OF TFDS

Time-frequency distributions have been shown to be a powerful tool in nonstationary signal analysis [1,2,3,4,5]. So far, most of the work on this subject has focused on temporal signal processing without much attention given to the spatial variable. The spatial dimension, properly incorporated into time-frequency signal representations, allows an effective angle estimation, separation and synthesis of nonstationary signals to be performed.

To present the spatial time-frequency distribution, we first recall that Cohen's class of time-frequency distribution (TFD) of a signal $x(t)$ is given by [1]

$$D_{xx}(t,f)=\int_{-\infty}^{\infty}\int_{-\infty}^{\infty}\phi(t-u,\tau)x(u+\tau/2)x^{*}(u-\tau/2)e^{-j2\pi f\tau}dud\tau \tag{1}$$

where t and f define the time index and the frequency index, respectively. The kernel $\phi(t,\tau)$ is a function of the time and lag variables. The cross-TFD of two signals $x_1(t)$ and $x_2(t)$ is defined by

$$D_{x_1x_2}(t,f)=\int_{-\infty}^{\infty}\int_{-\infty}^{\infty}\phi(t-u,\tau)x_1(u+\tau/2)x_2^{*}(u-\tau/2)e^{-j2\pi f\tau}dud\tau \tag{2}$$

Expressions (1) and (2) are now used to define the following data spatial time-frequency distribution (STFD),

$$\mathbf{D}_{xx}(t,f)=\int_{-\infty}^{\infty}\int_{-\infty}^{\infty}\phi(t-u,\tau)\mathbf{x}(u+\tau/2)\mathbf{x}^{H}(u-\tau/2)e^{-j2\pi f\tau}dud\tau \tag{3}$$

where $[\mathbf{D}_{xx}(t,f)]_{ij}=D_{x_ix_j}(t,f)$, for $i,j=1,2,....,n$, and the superscript "H" denotes the complex conjugate transpose of a matrix or a vector.

In several applications such as semiconductor manufacturing process, narrowband array processing, and image reconstruction, the following linear data model is assumed,

$$\mathbf{x}(t)=\mathbf{A}\mathbf{s}(t)+\mathbf{n}(t) \tag{4}$$

where the m x n spatial matrix **A** may be a mixing matrix or a steering matrix, depending on the application under consideration. The elements of the m x 1 vector **x**(t), which represents the measured or sensor data, are multicomponent signals, while the elements of the n x 1 vector **s**(t) are often monocomponent signals. **n**(t) is an additive noise, which is zero mean, white and Gaussian distributed process.

Due to the linear data model, the STFD takes the following structure

$$\mathbf{D}_{xx}(t,f)=\mathbf{A}\mathbf{D}_{ss}(t,f)\mathbf{A}^{H} \tag{5}$$

where $\mathbf{D}_{ss}(t,f)$ is the STFD of **s**(t), and the noise is neglected as a first step. We note that $\mathbf{D}_{xx}(t,f)$ is a matrix of dimension m x m, whereas $\mathbf{D}_{ss}(t,f)$ is of dimension n x n. For narrowband array signal processing applications, **A** holds the spatial information and maps the auto- and cross-TFDs of the source signals into auto- and cross-TFDs of the data.

Expression (5) is similar to that which has been commonly used in blind source separation and direction of arrival (DOA) estimation problems, relating the signal correlation matrix to the data spatial correlation matrix [6,7,8,9]. Here, these correlation matrices are replaced by spatial time-frequency distribution matrices. This means that we can solve these problems in various applications using a new formulation which is more tuned to nonstationary signal environments.

The two subspaces spanned by the principle eigenvectors of $\mathbf{D}_{xx}(t,f)$ and the columns of **A** are identical. Since the off-diagonal elements are cross-terms of $\mathbf{D}_{ss}(t,f)$, then this matrix is diagonal for all (t-f) points which correspond only to the signal autoterms. In practice, to simplify the selection of such points of true high power localization, we apply the smoothing kernel $\phi(t,\tau)$ that may significantly decrease the contribution of the cross-terms in the t-f plane.

The new concept of the spatial time frequency distribution discussed above opens a new area of research in the field of nonstationary signal processing and bring time-frequency and bilinear distributions to play an important role in sensor signal processing.

3. FUNDAMENTAL OFFERINGS OF STFDS

There are five key advantages of array processing using time-frequency distributions which have not yet been presented and fully utilized. In order to clearly explain these advantages, we use the diagram in Fig.1. Two sources A and B are incident on a multisensor array. Source A occupies the time-frequency region R_a, whereas source B occupies the time-frequency region R_b. The time-frequency signatures of the two sources overlap, but each source still has a time-frequency region that is not intruded over by the other source. We will assume that the background noise is white.

1) Equation (5) can be easily derived for any arbitrary joint-variables. Time and frequency are indeed the two most commonly used and physically understood parameters. However, by replacing the spatial time-frequency distributions by spatial arbitrary joint-variable distributions, one can relate the sensor joint-variable distributions to the sources joint-variable distributions through the same mixing matrix **A**. As shown below, there are situations where it is preferable to consider other domains such as the ambiguity domain, where the locations of the signals and their cross-terms are guided by properties and mechanisms different than those associated with the time-frequency domain.

2) Equation (5) is valid for all time-frequency points. The main question is whether one time-frequency point suffices for adequate direction finding and source separation, and how sensitive the performance is to a random choice of a t-f point? Further, if several t-f points are used, then how to choose and combine these points for improved performance, and whether the method of combining should differ depending on the task in hand? Direction finding techniques require $\mathbf{D}_{ss}(t,f)$ to be full rank, preferably diagonal. Some blind source separation techniques demand the diagonal structure of the same matrix without degenerate eigenvalues. These properties along with high SNR requirements may be difficult to achieve using a single time-frequency point. We have identified two different methods to integrate several t-f points into equation (5). One method is based on a simple averaging performed over parts or the entire time-frequency regions of the signals of interest. The second method incorporates desirable time-frequency points into joint diagonalization or joint block diagonalization schemes. To illustrate both methods, we use in Section 4 the former scheme for direction finding whereas the second scheme is employed in Section 5 for blind source separation. Both methods aim to fully utilize the points of maximum power concentration and avoid the time-frequency region of significant noise contamination.

3) The time-frequency distribution of the white noise is distributed all over the time-frequency domain, whereas the TFDs of the source and jammer waveforms are likely to be confined to much smaller regions. Referring to Fig.1, the noise is spread over both R_a and R_b as well as the complement region R_c. If the time-frequency points (t,f) used in either the averaging or joint diagonalization approaches belong the noise only region R_c, then no information of the incident waveforms is used and, as such, no reasonable source localization and signal separation outcomes can be obtained. Accordingly the performance is expected to be worse than conventional approaches. On the other hand, if all points (t,f) in Fig.1 are used, and the employed TFD satisfies the marginal constraints such as the Wigner distribution, then it is easily shown that only the average power is considered. As a result, the problem simplifies to the second order covariance based matrix approach, traditionally used in high resolution angle of arrival estimation. This is an important property, as it casts the conventional techniques as special cases of the proposed framework based on time-frequency analysis. Finally, if we confine the (t,f) points to R_a and R_b, then only the noise part in these regions is included. The result of leaving out the points (t,f) which are not part of the time-frequency signatures of the signal arrivals is enhancing the input SNR to the source localization and signal separation techniques.

4) By only selecting (t,f) points which belong to the t-f signature of one source, then this source will be the only one considered by equation (5). This is, in essence, equivalent to implicitly performing spatial filtering to remove other sources from consideration. It is important to note that such removal does not come at the expense of reduction of the number of degrees of freedom, as it is the case in beamspace processing, but the problem remains a sensor space processing with the original number of degrees of freedom remains intact. This represents a key contribution of TFDs to the direction finding and angle estimation area. An antenna array can be used to localize a number of sources equal or even greater than its number of sensors. The fundamental condition is that there must be time-frequency regions over which the respective time-frequency signatures of the sources do not overlap. In principle, the lower limit on the size of such regions is a single time-frequency point. Referring to Fig.1 and considering the case of two sensors, if all t-f points incorporated in direction finding belong to region R_a and not R_b, then the signal subspace defined by equation (5) is one-dimensional. In effect, by excluding source B, a one-dimensional noise subspace is established. This allows us to proceed with noise-subspace based high resolution techniques for localization of source A. Within the proposed framework, one can localize one source at a time or a set of selected sources, depending on the array size, overlapping and distinct time-frequency regions, and the dimension of the noise subspace necessary to achieve the required resolution performance. The same concepts and advantages of t-f point selection discussed above for direction finding can be applied to blind source separations.

5) The a priori knowledge of some temporal characteristics or the nature of time-varying frequency contents of the sources may permit direct selection of the t-f regions used in equation (5). In general, if we choose a joint-variable domain, where a class of signals collapses to a specific known joint-variable region, then one can perform direction finding and source separation for only this specific class. For instance, it is known that in the ambiguity domain all fixed frequency sinusoidal signals map to the vertical axis, no matter what their amplitudes, frequencies, and phases are. By only incorporating the points on the vertical axis, which represents the time-lag variable, we have, in fact, focussed on separating and localizing narrowband components in the presence of broadband signals or jammers.

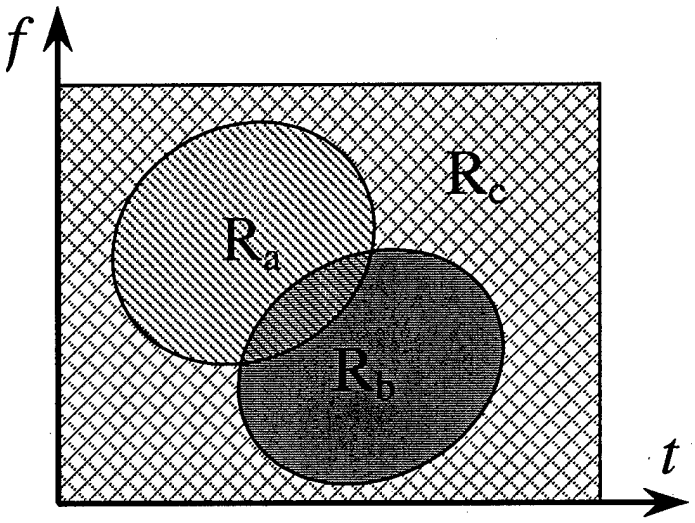

Fig.1 Signals with different time-frequency signature

4. THE JOINT-VARIABLE MUSIC (JV MUSIC)

The joint-variable MUSIC is a new array signal processing method which is based on joint-variable signal representations. This method computes the spatial joint-variable distributions to solve the problem of the direction of arrival (DOA) estimation. In this approach, we average the spatial joint-variable matrices over several joint-variable points for the purpose of noise and crossterm reduction.

Let the spatial joint-variable distribution define all spatial distributions for which the respective source and sensor bilinear distributions are related by matrix **A**, as in equation (5). By performing the singular value decomposition (SVD) [10] of the spatial joint-variable matrix $\mathbf{D}_{xx}(\alpha,\beta)$, we obtain

$$\mathbf{D}_{xx}(\alpha,\beta)=[\mathbf{E}_s\ \mathbf{E}_n]\mathbf{D}[\mathbf{E}_s\ \mathbf{E}_n]^H \tag{6}$$

where $\mathbf{D}$ is a diagonal matrix. $\mathbf{E}_s$ and $\mathbf{E}_n$, which respectively span the signal subspace and the noise subspace, are fixed and independent of the joint-variable point (α,β). The columns of $\mathbf{E}_s$ span the signal subspace, which is also spanned by the columns of matrix **A**. A simple way to estimate $\mathbf{E}_s$ and $\mathbf{E}_n$ is to perform the SVD on a single matrix $\mathbf{D}_{xx}(\alpha,\beta)$. But one time-frequency point may carry insufficient SNR or be highly contaminated by crossterms. To avoid this problem, we propose to perform averaging over several points, exploiting the joint structure of the spatial matrices. If averaging is performed over the joint-variable region $\Omega, (\alpha_i,\beta_i)\in\Omega$, then the SVD applied to the averaged spatial joint-variable matrix leads to

$$\overline{\mathbf{D}}_{xx}(\alpha,\beta)=\sum_{i\in\Omega}\mathbf{D}_{xx}(\alpha_i,\beta_i)=[\overline{\mathbf{E}}_s\ \overline{\mathbf{E}}_n]\overline{\mathbf{D}}[\overline{\mathbf{E}}_s\ \overline{\mathbf{E}}_n]^H \tag{7}$$

In the presence of noise, the MUSIC algorithm is applied to the perturbed noise subspace matrix $\hat{\overline{\mathbf{E}}}_n$. The joint-variable MUSIC (JV-MUSIC) algorithm estimates the DOAs by finding the N largest peaks of the localization function

$$f(\theta) = \left| \hat{\mathbf{E}}_n^H \mathbf{a}(\theta) \right|^{-2} . \tag{8}$$

where $\mathbf{a}(\theta)$ is the steering vector. The value of N is determined by the number of sources captured in the region Ω. If the joint-variable distribution satisfies the marginal constraints, then averaging over the entire domain will lead to the total power, yielding the conventional MUSIC. In the following, we present two simple cases of the joint-variable MUSIC, namely, the *Time-Frequency MUSIC* and the *Ambiguity-Domain MUSIC*.

4.1. Time-Frequency MUSIC (TF MUSIC)

The purpose of this example is to show that the TF MUSIC based on joint diagonalization gives good angle estimation performance for various kernels. The performance of the classical MUSIC [6] is compared to that of the proposed TF-MUSIC using: i) the Wigner kernel ii) the Choi-Williams kernel [1], and iii) the Born-Jordan kernel [1]. Consider a uniform linear array of 4 sensors separated by half a wavelength and receiving signals from 2 sources. The source signal arrives at $\theta_1 = 10$ degrees and of unit variance. The signal is composed of a chirp signal whose start and end frequencies are $\omega_1 = 0.17\pi$ and $\omega_2 = 0.67\pi$, respectively. The noise used in this simulation is zero-mean, Gaussian distributed, and temporally white. The noise power or σ^2 is adjusted to give the desired $SNR = 10\log_{10}(\sigma^{-2})$. Fifty STFD matrices corresponding to (t,f) autoterm points are averaged. The variance of the estimated DOAs is computed over 100 independent trials. Figure 2 displays the variance of the estimated DOA $\hat{\theta}_1$ versus SNR for 500 samples. The solid line presents the classical MUSIC algorithm. The dashed line, the dash-dot line and the dotted line correspond to the TF-MUSIC using Choi-Williams kernel, Born-Jordan kernel and Wigner kernel, respectively. According to this plot, the convetional MUSIC and TF-MUSIC based on the above three kernels give similar results. The offerings and advantages of the TF MUSIC in direction finding for different classes of nonstationary signals require extensive analysis and simulations, which are not presented in this paper.

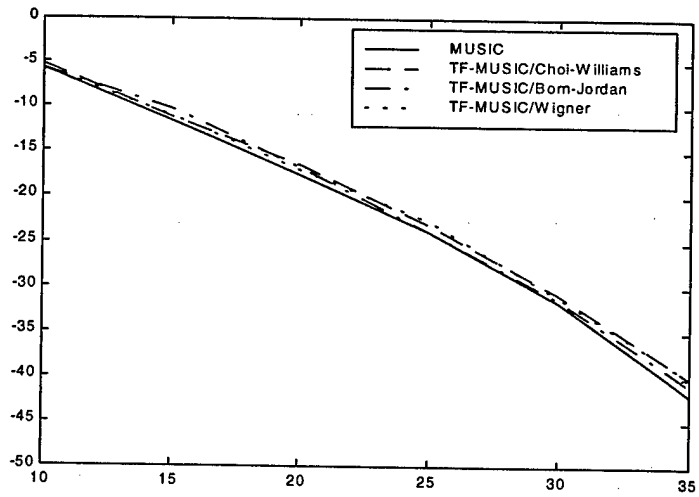

Fig.2 Variance of $\hat{\theta}_1$ vs. SNR

4.2. Ambiguity-Domain MUSIC (AD MUSIC)

Consider the scenario of a four-element equi-spaced linear array, where one chirp signal and two sinusoidal signals are received. All three signals have the same power of 20 dB, whereas the noise power is assumed to be 0 dB. The angles of arrival of the chirp signal and the sinusoidal signals are 15, 10, and 0 degrees, respectively. The joint-variables are now the frequency-lag and the time-lag $(\alpha,\beta) = (\theta,\tau)$. While the ambiguity function of the chirp signal sweeps the ambiguity domain with contribution at the origin, the autoterm ambiguity function $A(\theta,\tau)$ of the narrowband arrivals $s_1(t)$ and $s_2(t)$ is zero for non-zero frequency-lags and may have non-zero values only along the vertical axis. This function is given by

$$A(\theta,\tau) = C(s_1(\tau) + s_2(\tau))\delta(\theta) \tag{9}$$

where C is a constant which depends on the signal power, and $\delta(\theta)$ is the Kronecker delta function. In this simulation example, we selected 14 points on the time-lag axis, excluding the origin, and as such emphasizing the narrowband components. The data record has 128 samples and the ambiguity function is computed by taking 128-by-128 FFT of the Wigner distribution. Figure 3 shows the ambiguity-domain where the two vertical lines represent the crossterms between the sinusoidal components. Fig. 4 shows two MUSIC spectra, one corresponds to the conventional method and the other corresponds to the ambiguity-domain (AD) MUSIC. There are two dominant eigenvalues for the case of the AD MUSIC, since we have not deliberately considered the chirp signal through our careful selection of the ambiguity-domain points. It is clear that the AD MUSIC resolves the two sinusoidal signals, while the conventional MUSIC could not separate the three signals. Next, in order to show that non-careful point selections may prove unwise as well as to illustrate the ineffectiveness of working with joint-variable regions with no signal power, we average over the region Ω indicated in the Fig. 3, where the incoming signals have very weak presence. The result is shown in Fig. 5. It is evident from this figure that because of the lack of information in this region, the AD MUSIC fails to localize any of the three signals.

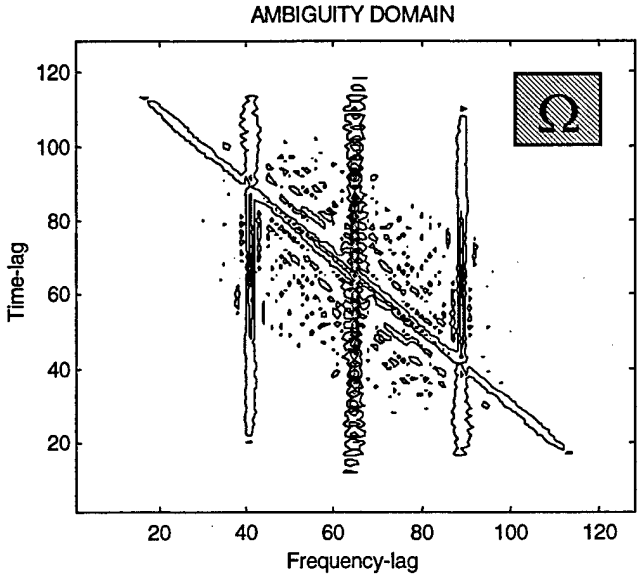

Fig.3 Ambiguity domain of one chirp and two sinusoidal signals
(Ω: A region used to estimate the AD MUSIC spectrum in Fig. 5)

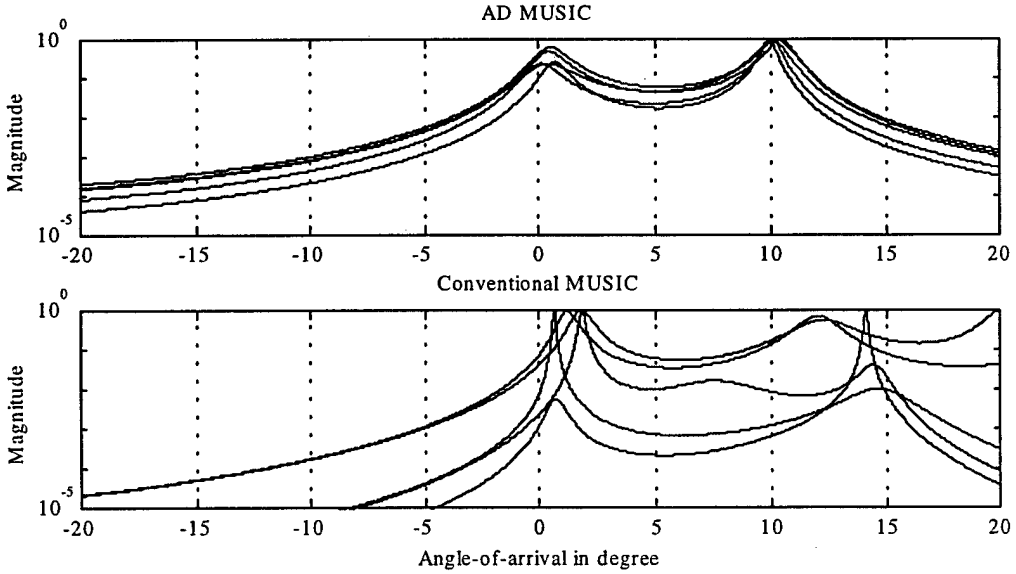

Fig.4 AD MUSIC and conventional MUSIC spectrum estimation

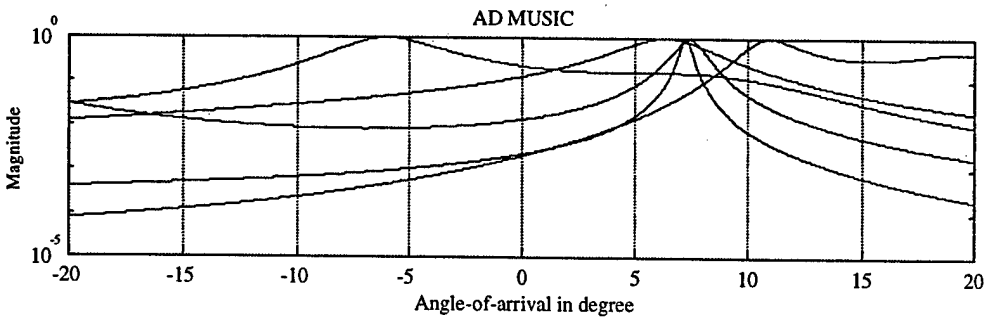

Fig.5 AD MUSIC spectrum estimation

5. THE JOINT-VARIABLE BLIND SOURCE SEPARATION

Let **W** denote n x m matrix such that $(\mathbf{WA})(\mathbf{WA})^H = \mathbf{UU}^H = \mathbf{I}$, i.e., **WA** is an n x n unitary matrix (This matrix is referred to as a whitening matrix, since it whitens the signal part of the observations). Pre- and post-multiplying the spatial joint-variable distribution matrices $\mathbf{D}_{xx}(\alpha,\beta)$ by **W**, we obtain the whitened spatial matrix

$$\tilde{\mathbf{D}}_{xx}(\alpha,\beta) = \mathbf{W}\mathbf{D}_{xx}(\alpha,\beta)\mathbf{W}^H \tag{10}$$

From equations (5) and (10), we may express $\tilde{\mathbf{D}}_{xx}(\alpha,\beta)$ as

$$\tilde{\mathbf{D}}_{xx}(\alpha,\beta) = \mathbf{U}\mathbf{D}_{ss}(\alpha,\beta)\mathbf{U}^H \tag{11}$$

Since matrix **U** is unitary and $\mathbf{D}_{ss}(\alpha,\beta)$ is diagonal, expression (11) shows that any whitened data spatial JV distribution (SJVD)-matrix is diagonal in the basis of the columns of the matrix **U** (the eigenvalues of $\tilde{\mathbf{D}}_{xx}(\alpha,\beta)$ being the diagonal entries of $\mathbf{D}_{ss}(\alpha,\beta)$).

If, for the (α_i,β_i) point, the diagonal elements of $\mathbf{D}_{ss}(\alpha_i,\beta_i)$ are all distinct, the missing unitary matrix **U** may be 'uniquely' (i.e. up to permutation and phase shifts) retrieved by computing the eigendecomposition of $\tilde{\mathbf{D}}_{xx}(\alpha,\beta)$. However, when the α-β domain signatures of the different signals are not highly overlapping or frequently intersecting, which is likely to be the case, the selected (α_i,β_i) point often corresponds to a single signal auto-term, rendering matrix $\mathbf{D}_{ss}(\alpha_i,\beta_i)$ deficient. That is, only one diagonal element of $\mathbf{D}_{ss}(\alpha_i,\beta_i)$ is different from zero. It follows that the determination of the matrix **U** from the eigendecomposition of a single whitened data SJVD-matrix is no longer 'unique' in the sense defined above. The situation is more favorable when considering simultaneous diagonalization of a combined set $\{\tilde{\mathbf{D}}_{xx}(\alpha_i,\beta_i) \mid i = 1,.....,p\}$ of p matrices. This amounts to incorporating several (α_i,β_i) points in the source separation problem. It is noteworthy that two source signals with identical (α_i,β_i) signatures can not be separated even with the inclusion of all information in the α-β plane.

The joint diagonalization (JD) [11, 12] can be explained by first noting that the problem of the diagonalization of a single n x n normal matrix **M** is equivalent to the minimization of the criterion [10]

$$\mathbf{C}(\mathbf{M},\mathbf{V}) \overset{def}{=} -\sum_i \mid \mathbf{v}_i^* \mathbf{M}\mathbf{v}_i \mid^2 \tag{12}$$

over the set of unitary matrices $\mathbf{V} = [\mathbf{v}_1,...,\mathbf{v}_n]$. Hence, the joint diagonalization of a set $\{M_k \mid k = 1..k\}$ of K arbitrary n x n matrices is defined as the minimization of the following JD criterion:

$$\mathbf{C}(\mathbf{V}) \overset{def}{=} -\sum_k \mathbf{C}(\mathbf{M}_k,\mathbf{V}) = -\sum_{ki} \mid \mathbf{v}_i^* \mathbf{M}_k \mathbf{v}_i \mid^2 \tag{13}$$

under the same unitary constraint. An efficient joint approximate diagonalization algorithm exists in [11] and it is a generalization of the Jacobi technique [10] for the exact diagonalization of a single normal matrix.

Equations (10)-(13) constitute the blind source separation approach based on joint-variable distributions which is summarized by the following steps:

- Determine the whitening matrix $\hat{\mathbf{W}}$ from the eigendecomposition of an estimate of the covariance matrix of the data,
- Determine the unitary matrix $\hat{\mathbf{U}}$ by minimizing the joint approximate diagonalization criterion for a specific set of whitened JVD matrices $\{\tilde{\mathbf{D}}_{\mathbf{xx}}(\alpha_i, \beta_i) \mid i = 1,....., p\}$,
- Obtain an estimate of the mixture matrix $\hat{\mathbf{A}}$ as $\hat{\mathbf{A}} = \hat{\mathbf{W}}^{\#}\hat{\mathbf{U}}$, where the superscript # denotes the Pseudo-inverse, and an estimate of the source signals $\hat{\mathbf{s}}(t)$ as $\hat{\mathbf{s}}(t) = \hat{\mathbf{U}}^{H}\mathbf{W}\mathbf{x}(t)$.

In Figure 6, we show an example of the application of the proposed spatial joint-variable distributions to the blind source separation problem. In this case, the two variables are time and frequency [13]. A three-element equi-spaced linear array is considered. Two chirp signals arrive from far-field at -10 and 10 degrees. The number of data samples used to compute the STFD is 128. The number of t-f points employed in the joint-diagonalization is p=128, with equal number of points on each signature. In this example, the mixing matrix **A** is chosen to be

$$\mathbf{A} = \begin{bmatrix} 1 & 1 \\ 0.8549 + 0.5189i & 0.8549 - 0.5189i \\ 0.4615 + 0.8871i & 0.4615 - 0.8871i \end{bmatrix}$$

Fig.6(b) shows the time-frequency distributions of two linear mixtures of the original chirp signals depicted in Fig.6(a), corresponding to the data at the first and the second sensors. Using the spatial time frequency distributions, we are able to recover the original signals from their observed mixture, as shown in Fig.6(c).

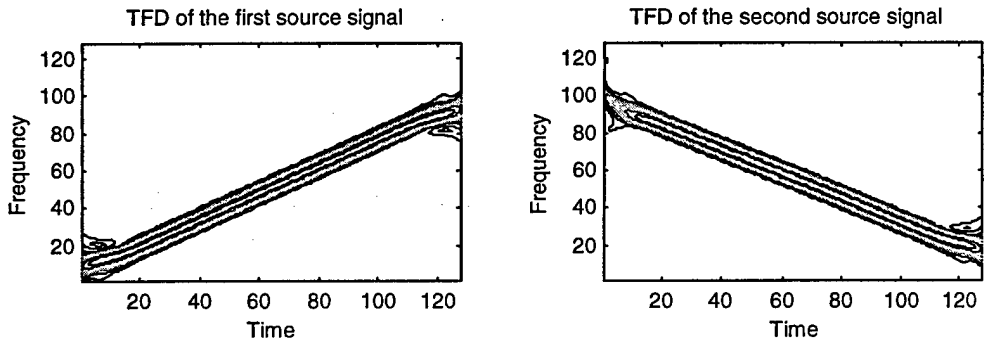

(a) TFD of the source signals

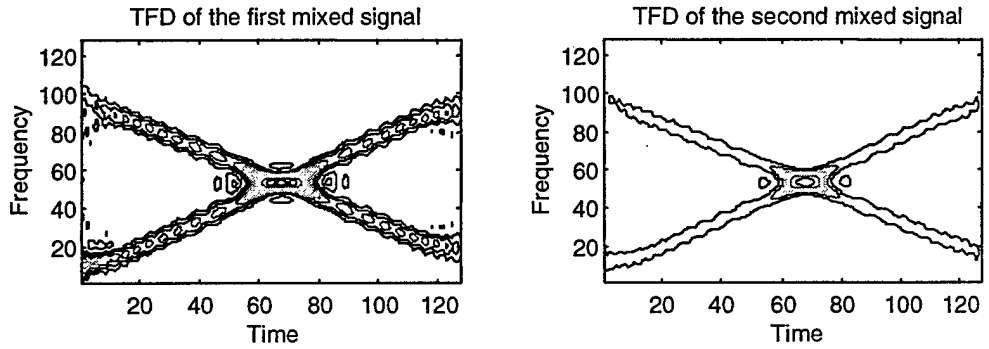

(b) TFD of the mixed signals

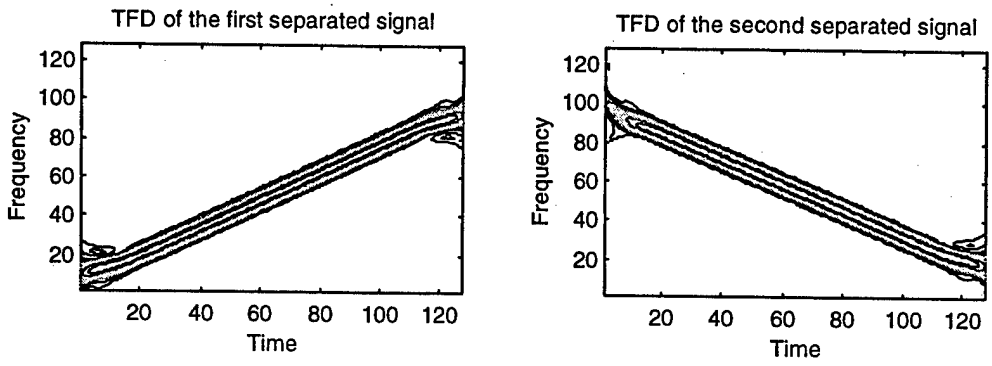

(c) TFD of the separated signals

Fig.6 Blind source separation based on spatial time-frequency distribution

6. CONCLUSIONS

The main objectives of this paper were twofold: 1) demonstrating that high resolution subspace-based methods can be performed by involving no longer the exact moments but rather the auto- and cross- time-frequency distributions of the data received by the multisensor array; 2) developing blind source separation methods based on the difference in the time-frequency localization properties of the signal arrivals and provide a generalization to arbitrary joint variables. Also, the paper presented, in general terms, the key offerings and advantages of utilizing the power localization properties of the signals incident on an antenna array to improve array performance. There are still important issues in the above two applications of time-frequency distributions remain to be explored and resolved. Among these issues are performance dependence on noise level, smoothing kernels, spatial smoothing and subarray averaging, non-localizable source signals, correlated and coherent sources, and spatial distributed sources due to local scattering.

7. ACKNOWLEDGEMENTS

This work is supported by ONR under Grant #N00014-98-1-0176.

8. REFERENCES

1. L. Cohen, "Time-frequency distributions - a review," *Proceedings of the IEEE*, vol. 77, no. 7, pp. 941-981, July 1989.
2. B. Boashash, " Time-frequency signal analysis," in *Advances in Spectrum Analysis and Array Processing*, S. Haykin, editor, vol. 1 and 2, Chapter 9, pages 418-517, Prentice-Hall, Englewood Cliffs, New Jersey, 1990.
3. F. Hlawatsch and G. Boudreaux-Bartels, "Linear and quadratic time-frequency signal representations," *IEEE Signal Processing Magazine*, vol. 9, no. 2, pp. 21-68, April 1992.
4. L. Cohen, *Time-Frequency Analysis*, Prentice Hall, Prentice-Hall, Englewood Cliffs, New Jersey, 1995.
5. S. Qian and D. Chen, *Joint Time-Frequency Analysis - Methods and Applications*, Prentice-Hall, Englewood Cliffs, New Jersey, 1996.
6. R. O. Schmidt, "Multiple emitter location and signal parameter estimation," *IEEE Trans. Antennas and Propagation.*, vol. 34, no. 3, pp. 276-280, March 1986.
7. D. Johnson and S. DeGraaf " Improving the resolution of bearing in passive sonar arrays by eigenvalue analysis," *IEEE Transactions on Acoustics, Speech, and Signal Processing*, vol. 30, no. 4, pp. 638-648, Aug., 1992.
8. S. U. Pillai, Array Signal Processing, Springer-Verlog, 1989.
9. A. Paulraj and C. Papadias, " Space-time processing for wireless communications," *IEEE Signal Processing Magazine*, pp. 49-83, Nov. 1997.
10. G. H. Golub and C.F. Van Loan, *Matrix Computations*, The Johns Hopkins University Press, 1989.
11. A. Belouchrani, K. A. Meraim, H.-F. Cardoso, and E. Moulines, "A blind source separation techniques using second order statistics," *IEEE Transactions on Signal Processing*, vol. 45, no. 2, pp. 434-444, Feb. 1997.
12. M. Wax and J. Sheinvald, "A least squares approach to joint diagonalization," *IEEE Signal Processing Letters*, vol. 41, pp. 52-52, Feb. 1997.
13. A. Belouchrani and M. Amin, "Blind source separation based on time-frequency signal representation," *IEEE Transactions on Signal Processing*, vol. 46, no. 11, pp. 2888-2898, Nov. 1998.

Adaptive blind spatial processing for frequency diversity spread spectrum communications

Miguel A. Lagunas, Ana I. Perez-Neira, Moeness G. Amin *

TSC Departamento, Modulo D5
Campus Nord UPC c/ Ran Capita s/n
08034 Barcelona- SPAIN
Department of Electrical and Computer Engineering
Villanova University, Villanova, Pa 19085,USA

ABSTRACT

Frequency Diversity Spread Spectrum (FDSS) systems have been evolved as a valuable alternative to traditional direct sequence and frequency hopping systems to combat partial band jamming. In FDSS system, the communication frequency band is partitioned into N disjoint subbands on which N replicas of the signal are simultaneously transmitted. The objective is not to erase the signal replicas hit by the jammer, but rather erase the jammer from the replicas. This work describes the use of beamforming to process the spatial diversity for optimum symbol by symbol detection. The procedure is adaptive and suitable for time varying environments. The beamformer corresponding to each frequency diversity component is updated using a gradient algorithm. This algorithm incorporates automatic gain control and is derived based on the fact that the desired signal is present in every frequency component. The optimum detector for FDSS is described and shown to be fully compatible with spatial processing techniques

Keywords: Adaptive array processing, Frequency diversity spread spectrum communications, Partial jamming.

1. INTRODUCTION

Frequency Diversity Spread Spectrum (FDSS) has been evolved as a valid alternative to strict direct sequence spread spectrum (DSSS) and frequency hopping spread spectrum (FHSS) methods for secure communications. FDSS can be considered as a specific transmission system of the group of the so-called multicarrier code division multiple access (CDMA) systems.

Reported recently, FDSS has been shown to be superior to the classical alternatives, namely DSSS and FHSS, for combating partial time jamming [1,2,3,4]. The main advantages of frequency diversity spread spectrum are based on the repetition of the desired signal along all frequency diversity branches. Since the jammer cannot extend its bandwidth, yet preserving significant levels of interference density power, then several diversity components in the FDSS system, where the desired signal remains unjammed, may be used to provide optimum and suboptimum receivers with simple real-time implementations.

The basic architecture of the transmitter is shown in Figure 1. From this scheme, one can distinguish three stages, which represent the different procedures applied to spread the spectrum of the basic information signal. This general scheme, which is discussed in [3], describes in details the information framing in FDSS systems. The sequence $\{a_n\}$ contains the information symbols with signaling period equal to T_0. The information symbols are passed to a channel encoder which introduces the first spreading. For every information symbol, N sequences of coded symbols are generated at a rate equal to T_0. In order to permit symbol by symbol detection, we assume a pure repetition code. This implies that the information symbol is repeated in the N paths.

The second stage of spreading is formed by the N chip signal $c_i(t)$. At this stage, the spreading ratio depends on the number of chip symbols per coded symbol. Without loss of generality, we will assume that a single chip symbol γ_i is used for every coded symbol interval. In other words, no spreading of the signal bandwidth is generated at this stage. The chip symbol induces decorrelation among potential interferers or jamming signals contaminating different frequency replicas. This decorrelation is shown to be an essential part of the demodulation process.

* Correspondence: Email:moeness@ece.vill.edu; Telephone: 610 519 7305; Fax: 610 519 4436

The third stage is designated for generating the frequency diversity of the transmitted signal, as every branch contains a passband filter whose frequency response is disjoint with those of other filters. This non-overlapping frequency band property is a key feature that defines the difference between FDSS and OFDM systems. The orthogonality between the diversity components is a result of non-overlapping filters rather than using other linear orthogonal transformations like DFT. The filters are implemented by a polyphase network and the difference with OFDM traduces in the fact that, for a partial band jammer, some frequency bands can be considered entirely jammer-free. The presence of the desired signal free of jamming in several bands allows two important features of frequency diversity spread spectrum system, namely sub-optimum receiver and blind spatial processing.

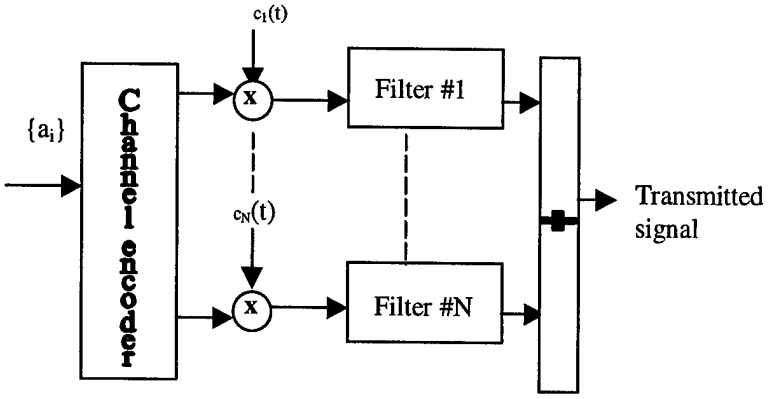

Figure 1. General scheme for FDSS transmitter.

There are several techniques devised in the literature to suppress narrowband interference or instantaneously narrowband jamming signals in broadband signal platforms. These techniques may implement adaptive filtering, linear transform-domain, and bilinear distribution methods. For detailed information on a variety of interference excision techniques, the reader should consult the articles by Milstein, [5], Poor and Rusch [6], and Laster and Reed [7], and Amin and Akansu [8]. These interference rejection and signal enhancement techniques do not find clear applications in frequency diversity schemes, as the jammer and the desired signal must have distinct frequency characteristics or time-frequency signatures over the frequency band of interest, an assumption that is not satisfied by the transmitter in Fig. 1.

This work describes the adaptive design of the optimum beamforming sets for FDSS in the presence of partial band jamming. The adaptive algorithm array coefficients forms the proper beamforming and for every diversity branch, achieving optimum receiver performance under different jamming conditions, without significant degradation of the desired signal. This includes the case of severe shadowing, when the jammer aperture signature coincides with that of the desired signal. The proposed adaptive algorithm provides a valuable alternative to the block design described by the same authors in reference [9]. The structure of the paper is as follows. Section 2 provides a brief summary of the work in references [1,2] concerning the optimum receiver for FDSS systems. Section 3 briefly discusses optimum spatial processing for the frequency diversity spread spectrum receiver detailed in [9]. It also includes the relationship between the above receiver and that implementing the cross-SCORE algorithm introduced in [10]. Section 4 presents the adaptive algorithm, which basically uses chip symbol modulation, without requiring adequate labeling of the received signal in every branch. Finally, section 5 provides a computer simulation example showing the performance of the FDSS uniform linear array receiver implementing the proposed adaptive algorithm.

2. OPTIMUM RECEIVER FOR FDSS SYSTEMS

After the chip demodulation, and matched filtering and sampling at the symbol rate, the decision variable Λ_i for the i^{th} symbol encompasses the signals $y_{m,i}$ in all frequency bands m =1,2,...,N, and is given by

$$\Lambda_i = \sum_{m=1}^{N} y_{m,i} F_m \tag{1}$$

The factor F_m accounts for the contribution of front-end noise $N_{o,m}$ as well as the jammer's or interference's contribution $J_{o,m}$ to the overall energy in the m^{th} frequency band. Note that if the bandwidth of each frequency band is made equal to the minimum bandwidth of the jammer, then the jammer within any frequency band appears as a wideband signal with uniform strength (see figure 2). With this assumption, F_m takes the following expression [9]

$$F_m = \begin{cases} 1/\left(1+\left(\frac{J_{o,m}}{N_o}\right)\right) & \text{for hit bands} \\ 1 & \text{otherwise} \end{cases} \tag{2}$$

Since it is typical that the front-end noise does not change from one band to another, it is assumed that N_o in (2) remains constant for all bands $1 \le m \le N$. Further, without loss of generality, it is also assumed that the jammer strength is fixed over all contaminated bands ($J_{o,m}=J_o$ for $m=1,2,\ldots,N$).

The optimal detection of the transmitted alphabet a_i maximizes $Re(a_i.\Lambda_i)$, where Re(.) denotes real part. The respective symbol error probability is given by [1,2],

$$P_e = Q\left(\sqrt{\left(\frac{2E_s}{N_o}\right)\beta}\right) \tag{3}$$

where E_s is the symbol energy and β is a loss factor established by the presence of the jammer. This loss factor depends on the relative strength of the jammer with respect to the front-end noise. It is also a function of the fraction η of the frequency bands hit by the jammer signal. If the jammer power is spread over all frequency replicas, then $\eta=1$, whereas the condition $\eta=0$ implies a jammer free communication channel. The loss factor is given

$$\beta = \left(\eta\left(1+\frac{J_o}{N_o}\right)^{-1}\right)+(1-\eta) \tag{4}$$

The above expression is testimonial to the superiority of FDSS over its counterparts; direct sequence spread spectrum and frequency hopping spread spectrum systems [1,2,4] under partial band jamming conditions. It is noteworthy that, unlike the optimum receiver given by equations (3,4), the sub-optimum receiver identifies the jammer replicas and then erases, them and as such, losing valuable desired signal energy. Accordingly, the corresponding loss factor for suboptimum receivers is $\beta=(1-\eta)$, and the respective bit-error probability increases to

$$P_e = Q\sqrt{2E_b(1-\eta)/N_o} \tag{5}$$

The aim of spatial processing, in essence, is to reduce, as much as possible, the factor η using potential differences between the spatial signatures of the desired signal and the jammer signal. In [9], a complete description of a block processing algorithm is reported, together with the control variable that take into account the jammer spatial shadowing of the desired source in the detection process.

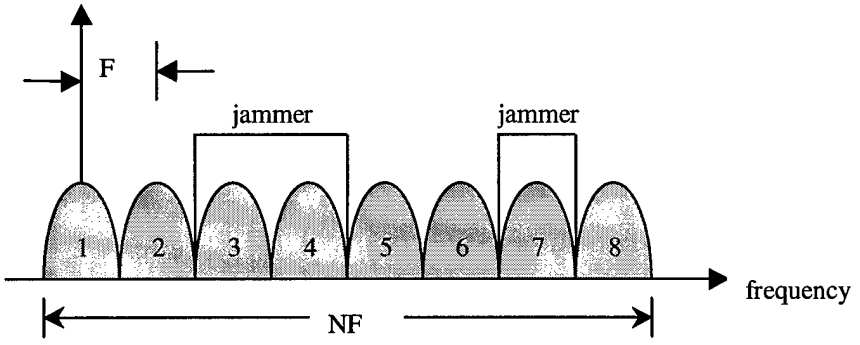

Free bands: 1,2,5,6,8
Hit bands: 3,4,7

Figure 2. Signal and interference spectrum, N = 8, η = 3/8, signal bandwidth = F

This work provides an adaptive algorithm that achieves block processing performance, but yet it is more suitable for rapidly time varying environments. The basic idea is to explore the two key advantages the receiver of the FDSS transmission system. These are: 1) the presence of the desired signal in all the frequency diversity components as a result of using a pure repetition code, 2) the uncorrelation of the jammer signals over different frequency bands, due to chip modulation. Note that the latter represents an added value to chip modulation, otherwise it becomes necessary to identify, at the receiver, the frequency bands that are hit by the jammer and those that are jammer free.

Finally, it is worthwhile mentioning that even though the FDSS system admits suboptimum receiver implementation as discussed above, which is independent of the jammer strength [1], the use of spatial diversity and beamforming in FDSS systems guarantees optimum receiver performance at all times [9].

3. OPTIMUM SPATIAL DIVERSITY FDSS RECEIVER

In order to describe the proposed algorithm we define $\underline{X}_{f,n}$ and $\underline{X}_{h,n}$ as the data snapshots received by the multi-sensor array receiver corresponding to any pair of the frequency replicas used by the FDSS system, and subindex n indicates time. The aperture is an array of N_q antennas. It is assumed that the snapshots are provided after chip demodulation, and as such, the jammer is uncorrelated between frequency bands f and h. The main goal is to exploit the redundancy of the desired signal present in the snapshots, corresponding to the two bands f and h, to provide adequate reference signal r(n). This signal is then used in the design of the digital beamformers for all other frequency bands in the diversity scheme.

Let us assume that the beamformer coefficients at time n for the respective frequency bands f and h are given by the vectors $\underline{w}_{f,n}$ and $\underline{w}_{h,n}$,and the corresponding signal outputs are denoted by $y_{f,n}$ and $y_{h,n}$. Since the jammer does not contribute to the data $\underline{X}_{f,n}$ in the free band and it is also uncorrelated with respect to the data $\underline{X}_{h,n}$ in the hit bands, a suitable procedure to allow $y_{f,n}$ to represent the desired reference signal r(n) is to minimize the mean square error (MSE) cost function defined as

$$\xi = E[|\, y_{f,n} - y_{h,n}\,|^2] \tag{6-a}$$

where

$$y_{f,n} = \underline{w}_{f,n}^H \underline{X}_{f,n} \quad and \quad y_{h,n} = \underline{w}_{h,n}^H \underline{X}_{h,n} \tag{6-b}$$

We stress the fact that although the minimization (6) is cast in terms of free and hit bands, any pair of signal frequency replicas can be used. The subscript 'i', identifying the transmitted symbol, is dropped in the sequel for simplicity. In order to avoid trivial solutions in achieving the above objective which traduce in simultaneous nulling of the desired signal and the jammer waveform, a constraint needs to be set throughout the minimization procedure. As pointed out in [9], one possible constraint is to enforce a pre-selected value ϕ for the cross-correlation between the two output signals which also serves as an automatic gain control for the desired signal,

$$\phi = 2\,\mathrm{Re}(E[y_{f,n} y_{h,n}^*]) \tag{7}$$

Denoting the array autocovariance matrices and cross-covariance matrix of the data in the two frequency channels as

$$\underline{\underline{R}}_f = E[\underline{X}_{f,n} \underline{X}_{f,n}^H],\ \underline{\underline{R}}_h = E[\underline{X}_{h,n} \underline{X}_{h,n}^H],\ \underline{\underline{P}}_{f,h} = E[\underline{X}_{f,n} \underline{X}_{h,n}^H] \tag{8}$$

The minimization problem can then be posed as:

$$\text{Minimize } \xi = \underline{w}_f^H \underline{\underline{R}}_f \underline{w}_f + \underline{w}_h^H \underline{\underline{R}}_h \underline{w}_h - \underline{w}_f^H \underline{\underline{P}}_{f,h} \underline{w}_h - \underline{w}_h^H \underline{\underline{P}}_{f,h} \underline{w}_f \tag{9}$$

$$\text{Constrained to } \quad \underline{w}_f^H \underline{\underline{P}}_{f,h} \underline{w}_h + \underline{w}_h^H \underline{\underline{P}}_{f,h} \underline{w}_f = \phi$$

Forming the Lagrangian and setting the partial derivatives with respect to the weight vectors equal to zero, the optimal spatial combiners are obtained as:

$$\underline{\underline{R}}_f \underline{w}_f = (1+\lambda)^2 \underline{\underline{P}}_{f,h} \underline{\underline{R}}_h^{-1} \underline{\underline{P}}_{f,h}^H \underline{w}_f \tag{10-a}$$

$$\underline{w}_h = (1+\lambda) \underline{\underline{R}}_h^{-1} \underline{\underline{P}}_{f,h} \underline{w}_f \tag{10-b}$$

where λ is the Lagrange multiplier. Since ξ is minimum for minimum λ, the optimum combiner for the jammer free band is the eigenvector of (10-a) associated with the minimum eigenvalue. After $\underline{w}_f$ is found, the combiner for the hit band is Just the weiner solution for the cross-correlation vector $\underline{\underline{P}}_{f,h}^{H}.\underline{w}_f$

The above optimum solution holds a great resemblance to the one obtained using the cross spectral self-coherence restoral (SCORE) algorithm derived in reference [10]. In the SCORE algorithm, it is assumed that the desired signal is spectrally self coherent at frequency separation γ if the correlation between the desired signal s(t) and s(t) frequency-shifted by γ is nonzero for some time-lag τ. In the underlying frequency diversity spread spectrum problem, the frequency shift represents the offset in the carrier frequency between two replicas of the signal frequency band, and the lag variable τ takes a zero value. That is, both parameters for the spectral coherence are known apriori and defined by the transmitter. In [10], however, the quadratic cost function minimization (5-a) is replaced by the maximization of the strength of the cross-correlation coefficient $\rho(\underline{w}_f,\underline{w}_h)$ between the outputs of two beamformers $y_{f,n}$ and $y_{h,n}$

$$\overline{\rho}(\underline{w}_f,\underline{w}_h)=\frac{\underline{w}_f^H\underline{\underline{P}}_{f,h}\underline{w}_h}{[\underline{w}_f^H\underline{\underline{R}}_f\underline{w}_f][\underline{w}_h^H\underline{\underline{R}}_h\underline{w}_h]} \tag{11}$$

Maximizing ρ with respect to $\underline{w}_h$ and $\underline{w}_f$ is interpreted in [10] as restoration of the spectral self-coherence to both beamformer $y_{f,n}$ and $y_{h,n}$. From the Cauchy-Schwarz Inequality, the optimum $\underline{w}_f$ for a fixed $\underline{w}_h$ is given by

$$\underline{w}_f^{opt} \propto R_f^{-1}P_{f,h}\underline{w}_h \tag{12}$$

Similarly, $\underline{w}_h$ is optimized for fixed $\underline{w}_f$ by

$$\underline{w}_h^{opt} \propto R_h^{-1}P_{f,h}\underline{w}_f \tag{13}$$

Substituting (13) in (11), the cross-correlation takes the form

$$\rho(\underline{w}_f,\underline{w}_h)=\frac{\underline{w}_f^H[\underline{\underline{P}}_{f,h}\underline{\underline{R}}_h^{-1}\underline{\underline{P}}_{f,h}^H]\underline{w}_h}{[\underline{w}_f^H\underline{\underline{R}}_f\underline{w}_f]} \tag{14}$$

Which is maximized by setting $\underline{w}_f$ equal to the dominant eigenvector corresponding to the maximum eigenvalue ν of

$$\nu\underline{\underline{R}}_f\underline{w}_f=[P_{f,h}\underline{\underline{R}}_h^{-1}P_{f,h}^H]\underline{w}_f \tag{15}$$

This is exactly the solution given in (10-a), where ν_{max} corresponds to $1/(1+\lambda_{min})^2$.

4. AN ADAPTIVE BEAMFORMING ALGORITHM FOR FDSS

The proposed adaptive scheme is blind in the sense that the knowledge of polarization and direction-of-arrival dependent antenna gains, cross-sensor phase mismatches, and near-field multipath and mutual coupling effects on the array is not required. The adaptive algorithm is based in the instantaneous gradient of the Lagrangian. In consequence, the updating terms are obtained from the partial derivatives with respect the beamformer coefficients. The parameter λ_n stands for the Lagrange multiplier corresponding to the cross-correlation constraint. Since the constraint serves as an automatic gain control, it can be used in the dynamic control requirements for the design of the baseband processor.

The constrained cost function is given by,

$$\begin{aligned}\xi_n &= \left|y_{f,n}-y_{h,n}\right|^2-(\lambda_n-1)2\,\mathrm{Re}\left(y_{f,n}y_{h,n}^*\right) \\ &= \left|y_{f,n}-y_{h,n}\right|^2-(\lambda_n-1)\phi_n\end{aligned} \tag{16}$$

The corresponding weight vector updates are given in (17), where $\mu_{f,n}$ and $\mu_{h,n}$ are the step-size parameters corresponding to the frequency bands f and h, respectively,

$$\begin{aligned}\underline{w}_{f,n+1} &= \underline{w}_{f,n}-\mu_{f,n}\underline{X}_{f,n}\left(y_{f,n}^*-\lambda_n y_{h,n}^*\right) \\ \underline{w}_{h,n+1} &= \underline{w}_{h,n}-\mu_{h,n}\underline{X}_{h,n}\left(y_{h,n}^*-\lambda_n y_{f,n}^*\right)\end{aligned} \tag{17}$$

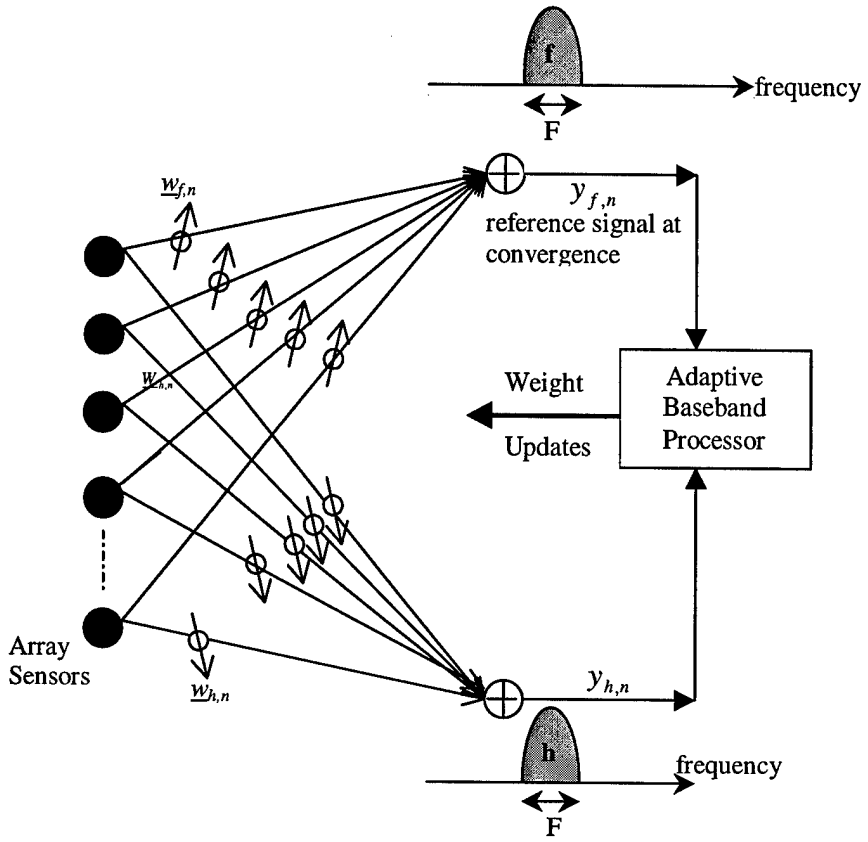

Figure 3. Adaptive Scheme for spatial diversity FDSS receiver

The step size parameters are selected according to the normalized version of the least mean square (LMS) algorithm,

$$\mu_{f,n} = \alpha / Q_{f,n} \;;\; \mu_{h,n} = \alpha / Q_{h,n} \tag{18}$$

where the denominators represent the instantaneous power of the corresponding snapshots,

$$Q_{f,n} = \underline{X}^{H}_{f,n} \underline{X}_{f,n} \;;\; Q_{h,n} = \underline{X}^{H}_{h,n} \underline{X}_{h,n} \tag{19}$$

The bounds for convergence of the missadjusment parameter α will be provided hereafter. In order to determine the value of the Lagrange multiplier, we need to define the instantaneous power of the output signal, as indicated below,

$$P_{f,n} = |y_{f,n}|^2 \;;\; P_{h,n} = |y_{h,n}|^2 \tag{20}$$

Since we adopted the instantaneous gradient updates, it seems adequate to force the updated weights to satisfy the constraint value of ϕ_n. Using this criteria and assuming that the previous two sets of weights satisfy the same constraint, we obtain the following equation which provides the value of the multiplier,

$$\lambda_n^2 \phi_n \alpha + 2\lambda_n (P_{f,n} + P_{h,n})(1-\alpha) + \phi_n (\alpha - 2) = 0 \tag{21}$$

A suitable approximation of the multiplier can be obtained by observing that the value of the parameter α is small compared to one. This often the case in practice, where α controls the missadjusment noise of the algorithm. Typical values of α are smaller than 0.05. Using this property, the Lagrange multiplier is approximately given by

$$\lambda_n = \frac{\phi_n}{(P_{f,n} + P_{h,n})} \tag{22}$$

This expression provides valuable insights to the role of the parameter λ_n in the proposed adaptive algorithm for the multi-sensor FDSS receiver. Note that the constraint, at the steady state will be equal to twice the value $P_{f,n}$. In consequence, ϕ_n serves as an automatic control gain, as previously announced. Once the constraint is set to the desired power level of the reference, the Lagrange multiplier measures the difference between $P_{f,n}$ and $P_{h,n}$. This parameter will

be very much different from one at the start-up of the algorithm and increases, as time goes on, until it reaches approximately a unit value upon convergence. In summary, the algorithm weights the outputs of the beamformers to produce the proper error correction to the beamformers updates. Furthermore, assuming the steady state condition with λ_n close to one, and substituting the updated weights in the instantaneous MSE, then the relationship between the iterated error and the original (without updates) sets the convergence bounds for parameter α,

$$\xi_n^{iter.} = (1-2\alpha).\xi_n \text{ -----> } 0<\alpha<0.5 \tag{23}$$

Table 1 summarizes the adaptive algorithm.

Set ϕ=1 and β>0.8
1. Get $\underline{X}_{f,n}$ and $\underline{X}_{h,n}$
2. Compute beamformer outputs $y_{f,n}$ and $y_{h,n}$ (see (6))
3. Update powers with forgetting factor β $Q_{f,n}=\beta.Q_{f,n-1}+(1-\beta).\underline{X}_{f,n}^H.\underline{X}_{f,n}$ $Q_{h,n}=\beta.Q_{h,n-1}+(1-\beta).\underline{X}_{h,n}^H.\underline{X}_{h,n}$ $P_{f,n}=\beta.P_{f,n-1}+(1-\beta).y_{f,n}^*.y_{f,n}$ $P_{h,n}=\beta.P_{h,n-1}+(1-\beta).y_{h,n}^*.y_{h,n}$
4. Compute step-sizes (see (18))
5. Compute parameter λ_n (see (21))
6. Update weights (see (17))
7. Use $y_{f,n}$ as time reference for the rest of the FDSS bands (m=1,2,..,N and m $\neq$ h)

Table 1

The key difference between the proposed algorithm and the Maxmin algorithm lies in the signal and the jammer frequency bands simultaneously used in the adaptive algorithm to enhance the signal to interference-plus noise ratio in the band of the interest. This difference is a product of using two different transmitters, namely frequency hopping and frequency diversity. We note that the adaptive scheme shown in Table 1 is simpler than that introduced for the frequency hopping systems in [11].

5. SIMULATION

The simulation example used to demonstrate the performance of the algorithm was formed by a uniform linear array (ULA) array of 5 sensors. The FDSS system was formed using seven diversity branches, where the desired signal was included with SNR equal to 0 dB per branch, BPSK modulated. The repetition code was applied in the channel encoder and one chip symbol per branch was used in the second stage of the FDSS modulator. The jammer was included in three non-successive diversity components (bands 2, 3 and 6). The SNR of the jammer was set equal to 10 dB. The parameter α, controlling the misadjusment, was given the value 0.01, and the smoothing parameter β was set for a memory factor of 10 snapshots. The direction of arrivals (DOAs) of the desired and the jammer signals were 10 degrees and 15 degrees from the broadside, respectively.

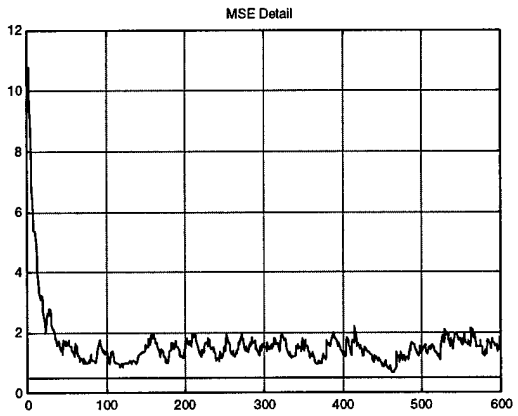

Figure 4. Learning curve of the adaptive algorithm

Figure 4 depicts the details of the learning curve associated with the proposed adaptive technique highlighted in table1. Proper convergence of the algorithm is evident with a steady state reached after 80 snapshots.

The algorithm was evaluated for three different jamming percentage η, ranging from 42.85% up to 85.71% and the results showed insignificant changes in both convergence rate and missadjusment.

CONCLUSIONS

An adaptive scheme for multi-sensor reviver operating on frequency diversity spread spectrum signals is presented. The jammer is present over some of the signal frequency replicas and is treated in each contaminated replica as a broadband signal. The adaptive algorithm implements the optimum spatial diversity receiver for FDSS communication signals, and allows the use of the desired signal in the jammed frequency bands to improve the probability of error. The proposed adaptive algorithm incorporates the data snap shots from two frequency bands and strives to generate upon convergence, a desired signal that can be used to eliminate the jammer in other hit bands. It is shown that the adaptive spatial diversity FDSS receiver can be simply implemented using a modest number of computations.

ACKNOWLEDGMENTS

This work is been supported by CICYT TIC96-0500-C10-01, TIC98-0412, CIRIT: 1996SGR-00096, and the Office of Naval Research, ONR grant #N00014-98-0176.

REFERENCES

[1] G. K. Kaleh, "Frequency diversity spread spectrum communications system to counter bandlimited Gaussian interference," IEEE Transactions on Communications, Vol. 44, No. 7, pp. 886-893, July 1996.

[2] G. K. Kaleh, "Performance comparison of frequency diversity and frequency hopping spread spectrum systems," IEEE Transactions on Communications, Vol. 45, No. 8, pp. 910-912, August 1997.

[3] R. Prasad and S. Hara, "An overview of Multicarrier CDMA," Proc. IEEE IV International Symposium on Spread Spectrum Techniques and Applications, pp. 107-113, Mainz, Germany, December 1996.

[4] E. Lance and G. K. Kaleh, "A diversity scheme for a phase- coherent frequency- hopping spread spectrum system," IEEE Transactions on Communications, Vol. 45, No. 9, pp. 1123-1129, September 1997.

[5] L. Milstein, "Interference rejection techniques in spread spectrum communications," Proceedings of the IEEE, vol. 76, no. 6, pp. 657-671, June 1988.

[6] H. V. Poor and L. A. Rusch, "Narowband interference suppression in spread spectrum CDMA," IEEE Personal Comm. Magazine, vol. 1, pp. 14-27, August 1994.

[7] J. D. Laster and J. H. Reed, "Interference rejection in digital wireless communications," IEEE Signal Processing Magazine, pp. 37-62, May 1997.

[8] M. Amin and A. Akansu, " Time-frequency for interference excision in SS communications," Highlights of Signal Processing for Communications, ed. G. Giannakis, Vol. 16, No. 2, March 1999.

[9] M. A. Lagunas, A. I. Perez, and M. G. Amin, J. Vidal, "Spatial Processing for Frequency Diversity Schemes," submitted, Transactions on Signal Processing, August 1998.

[10] B. Agee, S. Schell, and W. Gardner, "Spectral self-coherence restoral: A new approach to blind adaptive signal extraction using antenna arrays," Proceedings of the IEEE, Vol. 78, No.4, pp. 753-767, April 1990.

[11] D. Torrieri and K. Bakhru, "Frequency Compensation in an adaptive antenna system for frequency-hopping communications," IEEE Transactions on Aerospace and Electronic Systems, Vol. AES-23, No. 4, pp. 448-467, July 1987.

Time-Frequency MUSIC

Adel Belouchrani, *Associate Member, IEEE,* and Moeness G. Amin, *Senior Member, IEEE*

***Abstract*— A new method for the estimation of the signal subspace and noise subspace based on time-frequency signal representations is introduced. The proposed approach consists of the joint block-diagonalization (JBD) of a set of spatial time-frequency distribution matrices. Once the signal and noise subspaces are estimated, any subspace based approach, including the multiple signal classification (MUSIC) algorithm, can be applied for direction of arrival (DOA) estimation. Performance of the proposed time-frequency MUSIC (TF-MUSIC) for an impinging chirp signal using three different kernels is numerically evaluated.**

I. Introduction

In THIS letter, we introduce a new subspace-based method with a geometrical relation not involving the exact moments of the data, as is commonly the case [1]–[3], but rather the data *spatial time-frequency distribution.* The spatial time-frequency distribution (STFD) is a generalization of the time-frequency distribution to a vector signal. In a previous contribution [4], we have successfully used the notion of STFD to solve the problem of blind source separation for nonstationary signals. In this letter, we apply this new tool to solve the problem of direction of arrival (DOA) estimation.

II. Spatial Time-Freuqency Distributions

Consider an array of M sensors receiving waveforms of N sources ($M > N$). The data snapshot, representing the sensor output vector $\boldsymbol{x}(t)$, is assumed to obey the following model:

$$\boldsymbol{x}(t) = \boldsymbol{A}(\theta)\boldsymbol{s}(t) + \boldsymbol{n}(t) \tag{1}$$

where $\boldsymbol{n}(t)$ is an additive noise, $\theta^T = [\theta_1, \theta_2, \cdots, \theta_N]$, and $\boldsymbol{A}(\theta) = [\boldsymbol{a}(\theta_1), \boldsymbol{a}(\theta_2), \cdots, \boldsymbol{a}(\theta_N)]^T$. The signal vector at time t is $\boldsymbol{s}(\theta) = [s_1(t), \cdots, s_N(t)]^T$, with the superscript "$T$" denoting the transpose operator, and $\boldsymbol{a}(\theta_k)$ is the transfer vector between $s_k(t)$ and $\boldsymbol{x}(t)$. The parameter vector θ defines the DOA's.

The STFD matrix is defined [4] by

$$\boldsymbol{D}_{xx}(t,f) = \sum_{\ell=-\infty}^{\infty}\sum_{m=-\infty}^{\infty} \cdot \phi(m,\ell)\boldsymbol{x}(t+m+\ell)\boldsymbol{x}(t+m-\ell)e^{-4j\pi f\ell} \tag{2}$$

where m and f represent the time index and the frequency index, respectively. The kernel $\phi(m,\ell)$ characterizes the TFD and is a function of both the time and the lag variables (m,ℓ). Under the linear data model of (1) and assuming noise-free environment, the spatial time-frequency matrix takes the following simple structure:

$$\boldsymbol{D}_{xx}(t,f) = \boldsymbol{A}\boldsymbol{D}_{ss}(t,f)\boldsymbol{A}^H \tag{3}$$

where $\boldsymbol{D}_{ss}(t,f)$ is the signal TFD matrix whose entries are the auto and cross-TFD's of the sources, and the superscript "H" denotes matrix transpose conjugation. We note that $\boldsymbol{D}_{xx}(t,f)$ is a matrix of dimension $M \times M$, whereas $\boldsymbol{D}_{ss}(t,f)$ is of $N \times N$ dimension. Expression (3) is similar to that which has been commonly used in blind source separation and DOA estimation problems, relating the signal correlation matrix to the data spatial correlation matrix. The two subspaces spanned by the principle eigenvectors of $\boldsymbol{D}_{xx}(t,f)$ and the columns of $\boldsymbol{A}$ are, therefore, identical. Since the off-diagonal elements are cross-terms of $\boldsymbol{D}_{ss}(t,f)$, then this matrix is diagonal for all $(t\text{-}f)$ points that correspond to a true power concentration, i.e., the signal autoterms. In the sequel, we consider the $t\text{-}f$ points that satisfy this property.

III. Subspace Estimation

By performing the SVD of the steering matrix, we obtain

$$\boldsymbol{A}(\theta) = [\boldsymbol{E_s} \quad \boldsymbol{E_n}][\boldsymbol{D} \quad \boldsymbol{0}]\boldsymbol{V}^H. \tag{4}$$

Incorporating the above equation in (3), it is easily shown that

$$\boldsymbol{D}_{xx}(t,f) = [\boldsymbol{E_s} \quad \boldsymbol{E_n}]\boldsymbol{D}(t,f)[\boldsymbol{E_s} \quad \boldsymbol{E_n}]^H \tag{5}$$

where $\boldsymbol{D}(t,f)$ is a block-diagonal matrix given by $\boldsymbol{D}(t,f) = \text{diag}[\boldsymbol{D}\boldsymbol{V}^H\boldsymbol{D}_{ss}(t,f)\boldsymbol{V}\boldsymbol{D}\ \boldsymbol{0}]$. Since $\boldsymbol{E_s}$ and $\boldsymbol{E_n}$, which span the signal subspace and the noise subspace, respectively, are fixed and independent of the time-frequency point $(t\text{-}f)$, relation (5) reveals that any matrix $\boldsymbol{D}_{xx}(t,f)$ is block-diagonalized by the unitary transform $\boldsymbol{E} = [\boldsymbol{E_s}\boldsymbol{E_n}]$.

A simple way to estimate $\boldsymbol{E_s}$ and $\boldsymbol{E_n}$ is to perform the SVD on a single matrix $\boldsymbol{D}_{xx}(t,f)$. But indeterminacies arise in the case where $\boldsymbol{D}_{ss}(t,f)$ is singular. To avoid this problem, we propose to perform a joint block-diagonalization (JBD) of the combined set of $\{\boldsymbol{D}_{xx}(t_k,f_k)/\boldsymbol{k} = \boldsymbol{1}\cdots\boldsymbol{K}\}$ by exploiting the joint structure (5) of the STFD matrices. This joint block-diagonalization is achieved by the maximization under unitary transform of the following criterion [5]:

$$C(U) = \sum_{k=1}^{K}\sum_{i.j=1}^{n} |\boldsymbol{u}_i^*\boldsymbol{D}_{xx}(t,f)\boldsymbol{u}_j|^2 \tag{6}$$

over the set of unitary matrices $\boldsymbol{U} = [\boldsymbol{u}_1, \cdots, \boldsymbol{u}_m]$. In [5], an efficient algorithm for solving (6) is presented. Once the signal and the noise subspaces are estimated, one can use any subspace-based technique to estimate the DOA's. Herein, the MUSIC algorithm [9] is applied to the noise subspace

Manuscript received March 16, 1998. This work was supported by the Office of Naval Research under Grant N0014-98-1-0176. The associate editor coordinating the review of this manuscript and approving it for publication was Prof. D. L. Jones.

The authors are with the Department of Electrical and Computer Engineering, Villanova University, Villanova, PA 19085 USA (e-mail: moeness@ece.vill.edu).

Publisher Item Identifier S 1070-9908(99)03110-7.

matrix $\hat{E}_n$, estimated from (6). The time-frequency MUSIC (TF-MUSIC) algorithm estimates the DOA's by finding the N largest peaks of the localization function $f(\theta) = |\hat{E}_n^H a(\theta)|^{-2}$.

IV. Conditions on Time-Frequency Kernels

It is clear from (6) that from a perspective of the JBD technique, attractive time-frequency distributions are those that allow the formation of nonsingular diagonal matrices $D_{ss}(t, f)$ at the prospective time-frequency points. This property should be viewed in light of the following observations.

1) Since the off-diagonal elements of $D_{ss}(t, f)$ in the key equation (5) should be zeros, distributions that mount the cross-terms on the top of autoterms may not be so desired in the context of the underlying application.
2) Time-frequency distributions that spread cross-terms over the entire time-frequency plane [7] should, using the same argument, lead to improved performance over those distributions which localize the cross-terms in the auto-term regions.
3) Time-frequency distributions that reduce, but still localize the cross-terms away from the auto-term regions, appear to be most applicable to the diagonal matrix requirements [8].
4) The time-frequency signature of the sources, although remain distinct, should intersect as often as possible, producing a large number of candidate points.

V. Numerical Simulations

The purpose of this example is to show that the TF-MUSIC based on joint diagonalization gives good angle estimation performance for various time-frequency kernels. The performance of the conventional MUSIC [9] is compared to that of the proposed TF-MUSIC using 1) the Wigner kernel, 2) the Choi–Williams kernel [10], and 3) the Born–Jordan kernel [1]. Consider a uniform linear array of four sensors separated by half a wavelength. The impinging signal is a chirp of unit variance arriving at $\theta_1 = 10$ degrees. The chirp's signal start and end frequencies are $\omega_1 = 0.17\pi$ and $\omega_2 = 0.67\pi$, respectively. The noise used in this simulation is zero-mean, Gaussian distributed, and temporally white. The noise power or σ^2 is adjusted to give the desired SNR$= 10\log_{10}(\sigma^{-2})$. Fifty STFD matrices are considered. The variance in dB of the estimated DOA's are computed over 500 independent trials. Fig. 1 displays the variance of the estimated DOA $\hat{\theta}_1$ versus SNR for 100 samples. The solid line presents the conventional MUSIC algorithm. The dashed line, the dash-dot line, and the dotted line correspond to the TF-MUSIC using the Choi–Williams kernel, the Born–Jordan kernel, and the Wigner kernel, respectively. According to this plot, the conventional MUSIC and TF-MUSIC based on the above three kernels give similar results over the specified range of SNR in Fig. 1.

VI. Conclusions

A new DOA estimation approach using time-frequency distributions (STFD) is introduced. The new approach is based on the joint block-diagonalization of a set of spatial time-frequency distribution matrices. The TFD matrices of the data and the sources appear in place of the covariance matrices commonly used under stationary environment. We have focused on the time-frequency distributions of Cohen's class, however, one can use other bilinear time-frequency signal representations [10], [11].

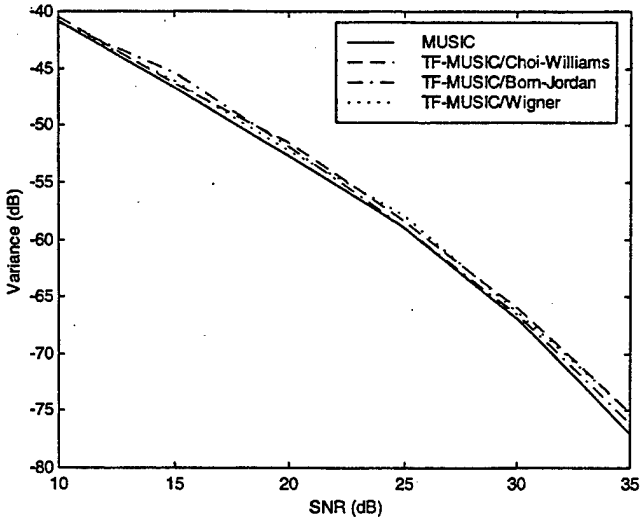

Fig. 1. Variance of estimated DOA versus SNR.

For the purpose of introducing this new technique, we have provided one simulation example. The offerings of the TF-MUSIC to direction finding will become evident upon examining it performance under low SNR's and by conducting extensive analysis of both its structural and statistical properties.

References

[1] R. Schmidt, "Multiple emitter location and signal parameter estimation," *IEEE Trans. Antennas Propagat.*, vol. AP-34, pp. 276–280, 1986.
[2] M. Viberg and B. Ottersten, "Sensor array processing based on subspace fitting," *IEEE Trans. Signal Processing*, vol. 39, pp. 1110–1112, 1991.
[3] R. Degroat, E. Dowling, and D. Linebarger, "The constrained MUSIC problem," *IEEE Trans. Signal Processing*, vol. 41, pp. 1445–1449, 1993.
[4] A. Belouchrani and M. G. Amin, "Blind source separation based on time-frequency signal representations," *IEEE Trans. Signal Processing*, vol. 46, pp. 2888–2897, Nov. 1998.
[5] A. Belouchrani, M. G. Amin, and K. Abed-Meraim, "Direction finding in correlated noise fields based on joint block-diagonalization of spatio-temporal correlation matrices," *IEEE Signal Processing Lett.*, vol. 4, pp. 266–269, 1997.
[6] Y. Zhu, L. Atlas, and R. Marks II, "The use of cone-shaped kernels for generalized time-frequency representations of nonstationary signals," *IEEE Trans. Acoust., Speech, Signal Processing*, vol. 38, pp. 1084–1091, 1990.
[7] H. Choi and W. Williams, "Improved time-frequency representation of multicomponent signals using exponential kernels," *IEEE Trans. Acoust., Speech, Signal Processing*, vol. 37, pp. 862–871, 1989.
[8] M. Amin, "Minimum variance time-frequency distribution kernels for signals in noise," *IEEE Trans. Signal Processing*, vol. 44, pp. 2352–2356, 1996.
[9] L. Cohen, *Time-Frequency Analysis*. Englewood Cliffs, NJ: Prentice-Hall, 1995.
[10] J. Bertrand and P. Bertrand, "A class of affine Wigner functions with extended covariance properties," *J. Math. Phys.*, vol. 33, pp. 2515–2527, July 1992.
[11] A. Papandreou, F. Hlawatsch, and G. F. Boudreaux-Bartels, "The hyperbolic class of quadratic time-frequency representations—Part I: Constant-Q warping, the hyperbolic paradigm, properties, and members," *IEEE Trans. Signal Processing*, vol. 41, pp. 3425–3444, Dec. 1993.

List of All Publications

Papers Under Review

1. "Spatial Averaging of Time-Frequency Distributions for Source Separations," Under Review. IEEE Transactions on Signal Processing. Co-author: Yimin Zhang.

2. "Subspace analysis of spatial time-frequency distributions matrices." Under Review. IEEE Transactions on Signal Processing. Co-author: Yimin Zhang and Weifeng Mu.

3. "The spatial ambiguity function and its applications." Under Review. IEEE Signal Processing Letters. Co-author: Yimin Zhang.

4. "Direction finding based on spatial time-frequency distribution matrices." Under Review. DSP: A Review Journal

5. "Time-frequency maximum Likelihood methods." Under Review. Journal of the Franklin Institute

Papers Accepted/Appeared

1. "Time-frequency MUSIC," IEEE Signal Processing Letters, May 1999. Co-author: Adel Belouchrani.

2. "Spatial processing for frequency diversity schemes." Accepted. To appear in the IEEE Transactions on Signal Processing. Co-authors: Miguel Lagunas, Ana Perez, and J, Vidal.

3. "Spatial evolutionary spectrum for DOA estimation and blind signal separation." Accepted. To appear in the IEEE Transactions on Signal Processing. Co-authors: Salim Kayhan.

Conference Papers

1. "Spatial averaging of time-frequency distributions," Proceedings of the IEEE International Conference on Acoustics, Speech, and Signal Processing, March 1999. Co-author: Yimin Zhang.

2. "Maximum Likelihood methods for array processing based on time-frequency distributions," SPIE, Conference on Advanced algorithms and Architectures for Signal Processing, Denver, CO, July 1999. Co-author: Yimin Zhang and Weifeng Mu.

3. "Spatial evolutionary spectrum for DOA estimation and blind source separation," SPIE, Conference on Advanced algorithms and Architectures for Signal Processing, Denver, CO, July 1999. Co-author: Salim Kayhan.

4. "Direction finding based on spatial time-frequency distribution matrices," Joint USA/Australia Workshop in Defense Applications of Signal Processing, Starved Rock State Park, Illinois, August 1999.

5. "Spatial bilinear transformations for superresolution and blind source separation," Proceedings of the High Resolution Radar Techniques, North Atlantic Treaty Organization (NATO), Granada, Spain, March 1999.

6. "A subband MUSIC technique for direction finding" Proceedings of the IEEE Sarnoff Symposium, March 1999. Co-authors: Weifeng Mu and Yimin Zhang.

7. "Beamspace time-frequency MUSIC with application to airborne antenna array," Proceedings of the Asilomar Conference on Signals, Systems, and Computers, Pacific Grove, CA, November 1998. Co-author: Yimin Zhang.

8. "Nonstationary interference excision in spread communications using projection filtering methods," Proceedings of the Asilomar Conference on Signals, Systems, and Computers, Pacific Grove, CA, November 1998. Co-author: Govind Mandapati.

9. "Spatial time frequency distributions for direction finding and blind source separation," SPIE AeroSense Symposium, Wavelet Applications, Orlando, FL, April 1999.

10. "Adaptive blind spatial processing for frequency diversity spread spectrum communications," SPIE AeroSense Symposium, Digital Wireless Communication, Orlando, FL, April 1999. Co-author Miguel Lagunas and A. Perez.

REPORT DOCUMENTATION PAGE

Form Approved
OMB No. 0704-0188

PLEASE DO NOT RETURN YOUR FORM TO THE ABOVE ADDRESS.

1. REPORT DATE (DD-MM-YYYY)	2. REPORT DATE	3
1-10-1999	Interim	October 1998-September 1999

4. TITLE AND SUBTITLE

BLIND TIME-FREQUENCY ANALYSIS FOR SOURCE DISCRIMINATION IN MULTISENSOR ARRAY PROCESSING

5a. CONTRACT NUMBER

5b. GRANT NUMBER

G-N00014-98-1-0176

5c. PROGRAM ELEMENT NUMBER

6. AUTHOR(S)

Moeness G. Amin

5d. PROJECT NUMBER

5e. TASK NUMBER

5f. WORK UNIT NUMBER

7. PERFORMING ORGANIZATION NAME(S) AND ADDRESS(ES)

Villanova University
800 Lancaster Ave
Villanova, Pa 19085

8. PERFORMING ORGANIZATION REPORT NUMBER

Acc: 527616

9. SPONSORING/MONITORING AGENCY NAME(S) AND ADDRESS(ES)

Office of Naval Research
Ballston Center Tower One
800 North Quincy Street
Arlington VA 22217-5660

10. SPONSOR/MONITOR'S ACRONYM(S)

11. SPONSORING/MONITORING AGENCY REPORT NUMBER

12. DISTRIBUTION AVAILABILITY STATEMENT

Approved for Public Release; distribution is Unlimited

13. SUPPLEMENTARY NOTES

14. ABSTRACT

This report includes results on the applications of time frequency distributions in blind source separation and direction finding problems. The major contributions in this area over the fiscal year ending September 30th 1999 are: 1) Regress analysis of eignestructure methods employing time-frequency distributions which has demonstrated their superiority over those used in conventional high resolution methods based on data covariance matrices, 2) Evaluating the performance of the spatial time-frequency distributions in low SNR and coherent signal environments, and introducing maximum likelihood techniques based on the sources' time-frequency signatures, 3) Identifying the role of time-frequency cross-terms in spatial signal processing, and presenting a prudent way to use those terms for enhanced performance, 4) Providing a novel approach for incorporating the revolutionary power spectra into source discrimination and DOA estimation, and examining their advantages over quadratic time-frequency distributions.

15. SUBJECT TERMS

Blind Source Separation, Direction Finding, Time-Frequency Distributions, Subband Arrays, Spatial Diversity Spread Spectrum Communications

16. SECURITY CLASSIFICATION OF:			17. LIMITATION OF ABSTRACT	18. NUMBER OF PAGES	19a. NAME OF RESPONSIBLE PERSON
a. REPORT	b. ABSTRACT	c. THIS PAGE			19b. TELEPONE NUMBER (*Include area code*)
U	U	U	UU	210	

Standard Form 298 (Rev. 8-98)
Prescribed by ANSI-Std Z39-18